DEVELOPMENT AND IMPLEMENTATION OF PIV SYSTEMS WITH SELECTIVE PARTICLE SEEDING FOR PRODUCTION WIND TUNNEL TESTING

A Thesis

by

EDWARD JAMES LEBER

Submitted to the Office of Graduate and Professional Studies of
Texas A&M University
in partial fulfillment of the requirements for the degree of

MASTER OF SCIENCE

Chair of Committee,	Edward White
Committee Members,	Nathan Tichenor
	Reza Sadr
Head of Department,	Rodney Bowersox

May 2020

Major Subject: Aerospace Engineering

ABSTRACT

This thesis presents designs and implementations of 2-D Particle Image Velocimetry (PIV), stereo-PIV, and selective seeding that enable application of PIV in large-scale, production-type wind tunnels. The PIV systems use conventional tools and methods to capture flow characteristics in the 7 foot x 10 foot test section of the Oran W. Nicks Low Speed Wind Tunnel at Texas A&M University (LSWT). The systems are designed to measure velocity fields non-invasively to prevent affecting flow quality. Validation tests demonstrate that in-plane velocity measurements obtained using the 2-D PIV system have measurement uncertainty below 0.5% which meets industry standards. Validation tests of stereoscopic PIV produced a similar result with a measurement uncertainty below 0.5% for in-plane velocities and below 5% for the out of plane velocity. Both values also meet their corresponding standards. A selective seeding system is implemented as a proof of concept for a method to overcome particle seeding challenges associated with very large-scale facilities. Velocity deficit measurements show the system does not significantly impact flow quality in the test section. Stereo PIV measurements captured behind a model demonstrate that the seeding column produced provides PIV data of equivalent quality to traditional, flooded-tunnel approaches.

ACKNOWLEDGEMENTS

There are so many people that I want to thank for helping me reach this point. I am incredibly grateful to Drs. Edward White and Nathan Tichenor, Lisa Brown, Rick Warren, John Kochan, Doug Kutz, and all the undergraduate and graduate students at the LSWT. Special recognition also goes to Joel White and Madeline McMillan, students outside the LSWT who made significant contributions during data processing and analysis. Finally, this thesis could not have been completed without the financial backing of National Aerospace Solutions LLC through subcontract 407039, monitored by David Plemmons. Without all of your hard work, guidance, and assistance this project would never have been possible. I am also beyond grateful for my incredible peers outside the lab, who have made the experience of graduate school better than I could have ever hoped.

DEDICATION

This thesis is dedicated to my loving parents, Jill and James Leber, who have always pushed me to chase my dreams and pursue the impossible. No matter the challenges I’ve faced in life, you have encouraged me to tackle them head on with poise and confidence. You have both been an inspiration to me, and I would not be the person I am today without your love and support.

TABLE OF CONTENTS

Page

LIST OF FIGURES

Page

LIST OF TABLES

Page

1. INTRODUCTION

1.1 Motivation for Research

This research is intended to solve challenges associated with implementation of Particle Image Velocimetry (PIV) in large-scale, production-type wind tunnel facilities. Researchers and test engineers at the National Full Scale Aerodynamic Complex (NFAC) and the Arnold Engineering Development Complex (AEDC) seek to implement PIV measurements in a routine way in their subsonic facilities but PIV in those facilities is hindered by a variety of challenges not present in smaller-scale research facilities. Both AEDC and NFAC facilities are operated by National Aerospace Solutions (NAS) under contract to the U.S. Air Force. To address these challenges, the Oran W. Nicks Low-Speed Wind Tunnel (LSWT) at Texas A&M University is being used to develop and test solutions to large-scale PIV challenges especially those relevant to production wind tunnels. In particular for this thesis, development of an alternative seeding method for large scale facilities was selected by NAS as a key objective.

The LSWT was selected as a test facility for large-scale PIV implementation tests because it is sufficiently large to face some of the same issues as larger-scale production facilities operated by NAS. However, the LSWT can be operated at sufficiently lower costs to enable inexpensive proof-of-concept testing. The LSWT is a large-scale wind tunnel facility (by university standards) that regularly conducts aerodynamic tests for research and commercial applications. While these tests vary greatly in length and complexity, each seeks to understand the aerodynamic effects experienced by wind tunnel models. LSWT instrumentation includes both a high-capacity external balance and multiple internal balances that measure loads experienced by wind tunnel models. In many wind-tunnel tests, a balance provides the engineering result of an aerodynamic design: the aerodynamic forces and moments produced by a given configuration. However, the loads above are only part of what can be of value in a wind tunnel test. It can also be of value to measure the velocity field about a model. Particle Image Velocimetry (PIV) provides that capability.

1.2 Facility Overview

Texas A&M’s Low Speed Wind Tunnel (LSWT) began construction in the 1940s and evolved into a closed-loop tunnel in the 1950s. The tunnel has continued to upgrade its systems and develop its capabilities. An automatic external balance was installed in the 1970s that eventually transitioned to a fully digital system. Forays into a 2-D PIV system were made during the late 2000s and early 2010s but only for a single project. Currently, flow field measurements at the LSWT can be taken using a multi-hole probe on a traverse mechanisms or on a wake rake. These techniques capture flow characteristics at discrete points or arrays of discrete points. Each of these methods capture data in the form of dynamic pressure which can be used to calculate local velocity. However, these systems are limited. First, both systems can only capture data at discrete points rather than entire fields. Second, the placement of the instruments could alter the flow about the model and change what the systems are attempting to measure. Finally, the probe and wake rake cannot capture data close to or in front of models due to how the instruments are mounted. As a result, it can be difficult to measure flow fields over individual features on a model which is usually the goal of flow field measurements.

In contrast to the conventional pressure-based systems in use at the LSWT, a PIV system would significantly improve the capacity for flow-field measurements. Unlike the probe and wake rake, a PIV system is able to simultaneously capture data in a defined field of view. Additionally, using a PIV system removes the need for physical hardware inside the tunnel and does not risk aerodynamic interference caused by the mounting arrangements of other methods of flow field measurement. Finally, PIV allows for data capture at any point in the test volume. The cameras in a PIV system can be moved and manipulated as necessary to capture flow over virtually any feature of a model which allows for velocity measurements over critical components and regions of interest. This can be significant for both research and commercial applications and represents a significant improvement in the capabilities of the LSWT.

1.3 Review of PIV

PIV has been widely used since the 1980s. The method allows researchers to non-intrusively measure instantaneous velocity fields at many points (10^3 to 10^5) across a field of view (Adrian 2005). The method consists of capturing high-resolution images of illuminated seed particles that move with a flow then using computer software to determine the movement of each particle between subsequent images. PIV can be advantageous compared to traditional, intrusive measurement techniques because it captures the instantaneous velocities in an entire region of interest without disturbing the flow itself. This region can either be a plane or a volume within the flow, depending on the type of PIV used. Two-dimensional (2-D) PIV is the simplest application of the method and is able to capture 2-D velocity components in the illuminated plane (Adrian 2005, Scarano 2013). Stereoscopic and tomographic PIV are more complicated. These are able to produce three-dimensional velocity components. Stereoscopic PIV (SPIV) uses multiple cameras angled at an illuminated plane to measure both the in-plane and out-of-plane velocities. Tomographic PIV uses multiple cameras that image an illuminated volume to produce 3-D velocity data in that volume flow data (Scarano 2013).

PIV systems usually use the combination of a laser to illuminate the particles in a flow and cameras with over 1 million CCD pixels and the ability to capture image pairs within 1 μs. Depending on the orientation of the system, a set of mirrors and lenses convert the pulsing laser beam into a thin light sheet in the test section where it illuminates seed particles. Seed particle selection is important; each particle must be small enough to follow the flow without substantial deviation while also reflecting sufficient light to be visible in images (Zhang et al. 2003). A synchronizing system is used to ensure the cameras collect data when the laser pulses.

After data is collected, image pairs are individually processed using image-analysis software. For this thesis, all data is processed using DaVis 8.4.0. For the analysis, each monochrome image pair is overlaid with a mesh of square elements. The program iterates through each square element, searching the second image of the pair for the nearby region that has the highest correlation to the first image. This results in a pixel shift vector that, when divided by the time between the images, produces a velocity field with one vector for each individual square element. A relatively coarse initial grid is analyzed first and a higher resolution grid is analyzed second using the coarse-grid result as an initial estimate to accelerate the subsequent fine-resolution analysis.

DaVis 8.4.0 software is used for data processing in this thesis. It's approach is similar to any PIV processing software and is important to document because it informs later discussion of PIV measurement uncertainty. The overall approach is similar for 2-D and Stereoscopic PIV data but user inputs have small variations that are discussed below. In both cases, images are taken of a calibration plate in the region of interest using each camera (one for 2-D and two for stereo) and processed using the DaVis calibration function. An image of the calibration plate used for this thesis can be seen in Fig 1. It is 5 inches wide by 3 inches tall and includes an array of 40 × 31 calibration dots on a 0.12-inch spacing.

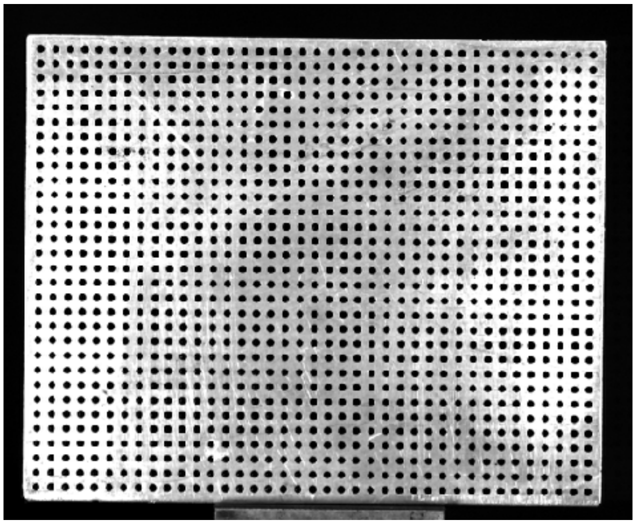

Figure 1: Calibration Plate

The DaVIS software scans the calibration image and calculates the pixel scale. For stereoscopic PIV, the software additionally uses the distortion of the plate in the calibration images to determine the each camera's offset angle from the line normal to the calibration plate.

Data analysis for both methods of PIV begins with the import of pairs of "A" and "B" images captured during testing. These images are greyscale light-intensity maps captured from the illuminated particle field. The image pairs captured by each camera are processed using a cross correlation function that breaks image A into a grid of square interrogation regions. Starting with the interrogation region in the top right corner of image A, the software scans image B for a region of equal size that has the highest correlation value. This produces a vector on the vector field moving from the center of the interrogation region in image A to the center of the best-correlated region of the same size in image B. This process is repeated until every interrogation region in image A has been assigned a corresponding correlated region in image B and this results in a full vector field over the region of interest. This process can then be repeated with a sequence of decreasing interrogation sizes. All PIV calculations for this thesis consist of an initial vector calculation with mesh elements 64 pixels × 64 pixels, followed by three subsequent passes with mesh elements of 32 pixels × 32 pixels. A smaller final interrogation size would give a denser vector field but results in poor correlation quality.

Stereoscopic PIV completes an additional processing step to generate in-plane and out-of-plane velocities. Once an instantaneous vector field is obtained for both cameras, the software uses the calibrated offset angles and the individual vector fields to produce the full 3-component vector field. This is accomplished using the vector projection of the results of both cameras onto the plane of the laser sheet. Because particles near the edges of the image are somewhat out of focus because the cameras' optical axes are not exactly normal to the image plane, data quality degrades near the edges of the image. This phenomenon is discussed at length in Section 3.2.

Especially when the camera offset angle is large, schiempflug adaptors are used to provide consistent image focus across the inclined field of view. Using these adaptors, each camera is focused on the center of the calibration card and the variation in image focus from the center towards the edges of the image is reduced relative to not using the adaptors. This reduces the measurement uncertainty at the image edges. Because the focus of this thesis was not optimizing stereoscopic measurement quality, schiempflug adaptors were not purchased for this work. They will be recommended for future use.

A typical experimental setup and data processing flowchart for a PIV system can be seen in Fig. 2 from Westerwheel et al. (2013).

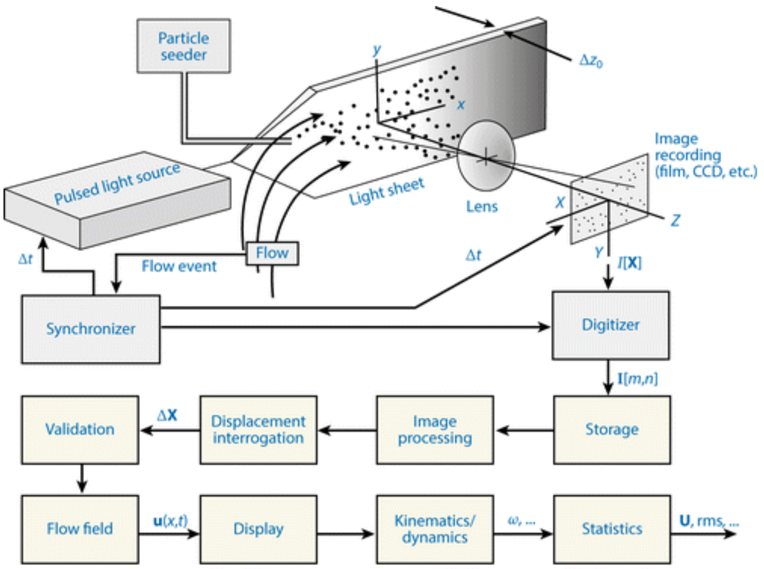

Westerweel J, et al. 2013.
Annu. Rev. Fluid Mech. 45:409–36

**Figure 2: PIV Setup & Data Processing
(Reprinted from Westerweel et al. 2013)**

1.4 Synopsis of Large-Scale PIV Challenges

While PIV is a well-established method of measuring velocity in small-scale wind tunnels, using PIV in large-scale wind tunnel tests produces a wide array of challenges (Towers et al. 1991, Westerwheel et al. 2013). Many of the complications stem from the necessity of high-resolution imaging in the experimental location of interest. In small-scale tests, cameras and laser sources may be arranged fairly close to the region of interest and can capture individual particles with relative ease. However, large-scale tunnels require the cameras and laser to be located much further from the region of interest. While these elements can be moved, seeding particles cannot be larger than in small-scale tunnels as they would no longer properly follow the flow. As a result, a complex optical setup is needed to properly illuminate the particles in the flow and capture sufficiently detailed images for analysis. Depending on the setup around the test section, the laser may require additional mirrors and lenses to properly align the beam with the test section. This can be problematic, as the additional optics decrease the power of the beam entering the test section of the tunnel. This decrease in power can lead to less illumination of the particles, resulting in increased measurement error or a failure to capture sufficient data for processing.

Additionally, the region of interest in large-scale tests is much larger than in traditional PIV applications. Currently, cameras with sufficiently high resolution to capture the entire field of interest without increasing individual pixel size can be difficult and expensive to obtain. And, at the scale envisioned for use in NFAC facilities, may not even exist. As a result, large-scale PIV systems often require a set of multiple cameras operating in parallel to photograph the entire region of interest. Each camera must be carefully aligned to capture a unique section of the experimental region. During data reduction, images from the various cameras can be stitched together to produce a single depiction of the flow in the region of interest. While this is a theoretically simple process, dedicated testing is required to prove the efficacy of image stitching in large-scale PIV setups.

Particle seeding also becomes particularly challenging in large-scale applications. In small-scale tests, the amount of particulate utilized for any given test is fairly small and the entire tunnel can be filled to a selected particle density. This would not be cost effective for large-scale tests. Furthermore, flooding a large facility with seed particles may have major health and safety concerns. Regular particle choices such as silicon carbide or titanium dioxide are impractical due to their cost and the increased number of particles required to maintain sufficiently dense particle seeding. Researchers also caution against such particles due to the adverse health effects of these particles in large doses (Raffel et al. 2018).

A different seeding challenge is that tracking errors can occur when particles fail to follow the flow without slip. This is problematic in large scale facilities where larger particles are often used to compensate for the larger pixel scales associated with larger fields of view. While this keeps particles visible in PIV images, it also increases the likelihood that particles will slip in regions with strong fluid accleration. Additionally, the likelihood of inhomogeneous particle seeding grows with increased wind tunnel size. Inhomogeneous particle seeding can force data analysis programs to extrapolate results for sparsely seeded sections of an image which decreases accuracy.

Large scale facilities also introduce unique challenges for optical alignment because of mechanical vibrations and flexures in the test section. At small scale, vibrations and flexure of the test section are small enough that a PIV system is not affected. However, large scale tests can often experience vibrations and flexure that can significantly affects the alignment of cameras and the laser optics during tests. These distortions often degrade the alignment of the PIV system such that the data produced must be corrected mathematically in post-processing. In particular, this affects more complicated PIV systems such as tomographic and holographic PIV. 2-D PIV systems are easier to set up but can be more tedious in operation because more system alignment runs are required to capture the needed data. For example, if researchers are trying to capture both the flow over a wing and the wingtip vortices, the PIV system will need to be moved and recalibrated for multiple measurement planes. This operation is less of an issue in small-scale tests, where equipment can be easily moved around the test section. However, in large scale tests this operation can include designing and implementing different optical setups and mounting considerations, making the change both time consuming and difficult to accomplish.

1.5 Objective

The objective of this thesis is to develop procedures and support infrastructure that enable accurate and efficient use of PIV at the Oran W. Nicks Low Speed Wind Tunnel. This includes the validation of 2-D and stereoscopic PIV that can be used during future research and customer projects to enhance the quality of data produced. These systems will include operational procedures and checklists that are found in Appendices A and B. These procedures and support infrastructure are expected to be representative of the work needed to achieve the same ends in larger-scale production facilities such as NFAC and AEDC subsonic wind tunnels. In addition, this thesis seeks to demonstrate a method of selective seeding for large scale wind tunnels that meets the data quality of traditional seeding methods. This proof of concept will be a gateway to future work with other large-scale facilities seeking to implement PIV. The end product of this thesis includes a detailed procedural guide for both 2-D and stereoscopic PIV setup, optical alignment, data collection, data analysis and reporting, as well as a successful proof of concept for a selective seeding system.

2. REVIEW OF LITERATURE

2.1 History of PIV

The earliest iterations of PIV began in the late 1970's with three independent research groups. Adrian (2005) writes that each of these teams sought to demonstrate the use of a laser speckle to measure the velocity of a fluid flow. In 1977, Barker and Fourney, Dudderar and Simpkins, and Grousson and Malick each successfully measured the parabolic velocity profile in a laminar tube flow. The experimental setup was similar to a modern PIV system. The experiments used double-exposure photographs and a laser light sheet to capture the movement of particles in the flow. In 1983, Meynart achieved the first use of laser light to measure flow velocities for laminar and turbulent flows in both liquids and gasses. This work was given the term Laser Speckle Velocimetry (LSV), but the images produced usually depicted individual particles in a flow, rather than a laser speckle. Continuing efforts led to the modern concept of PIV (Adrian 1984, 2005).

In the mid 1980's, many researchers began using PIV as a means of studying turbulent flow. This focus on turbulence significantly impacted the development of the PIV method. Researchers needed a measurement technique that could capture a wide, dynamic range of velocities within the same flow. They also needed a system that could handle randomness, didn't rely on a set direction of flow, and could operate accurately at high Reynolds numbers (Adrian 2005). All of these needs combined with the necessity of small particles (a few microns in diameter) led to the use of high intensity, pulsing lasers for particle illumination.

As PIV continued to develop as a reliable measurement technique, the challenges began to shift from the data analysis to optimization of the image capture systems. The transition from film to digital imaging we especially helpful for PIV, as the rate of image (and subsequently data) capture was far beyond anything achievable with traditional film cameras. When digital imaging was first used by Nishino et al. (1989), a recording of 19,200 image pairs produced the most statistically significant PIV data for turbulent flows to that date. Furthermore, digital imaging allowed image pairs to be recorded with less time between images, allowing data collection in higher velocity flows. It was this advancement that pushed PIV into mainstream usage in the research community, and made it into the measurement method that it is today (Adrian 2005).

2.2 Types of PIV

This review focuses on the most commonly used PIV methods: 2-D PIV (or simply PIV), stereoscopic PIV, tomographic PIV, and holographic PIV. All variations of the technique share certain components. These include a double-oscillating Nd:YAG laser, double-exposure cameras with at least 1 million pixels (1000 by 1000 pixel capture), and an external timing device that synchronizes the laser pulses with each exposure for the camera(s). A graphic depicting the capabilities of each system can be seen in Fig. 3 from Scarano (2013):

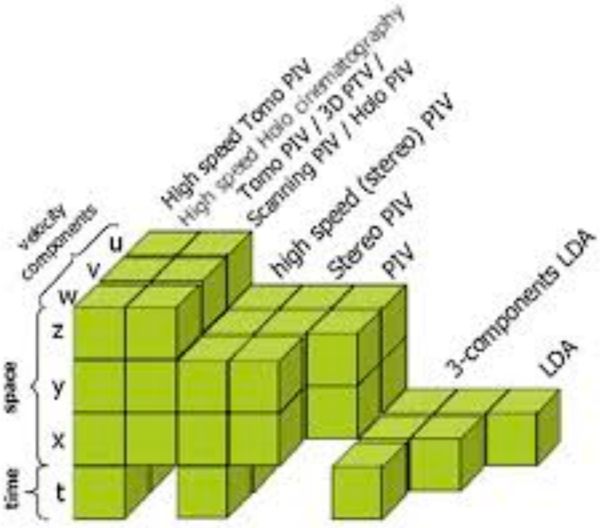

Figure 3: Capabilities of PIV Methods (Reprinted from Scarano 2013)

The ability to measure flow velocities based on space rather than time allows for a wide array of flow measurements that were previously difficult and/or impossible to measure, particularly in turbulent flows. Depending on the flow being analyzed, it is even possible for some PIV systems to capture the material derivative of velocity in a flow, thereby incorporating the benefits of systems such as LDA into a non-intrusive method of flow measurement (Scarano 2013).

2.2.1 2-D PIV

2-D PIV is the simplest form of PIV and has been well-established since the 1980's. A standard 2-D system uses a single camera aligned normal to a pulsing laser sheet that illuminates seed particles (Wereley 2010). The exact laser power required to achieve sufficient illumination depends on the type of particle and the distance between the laser head and the region of interest.

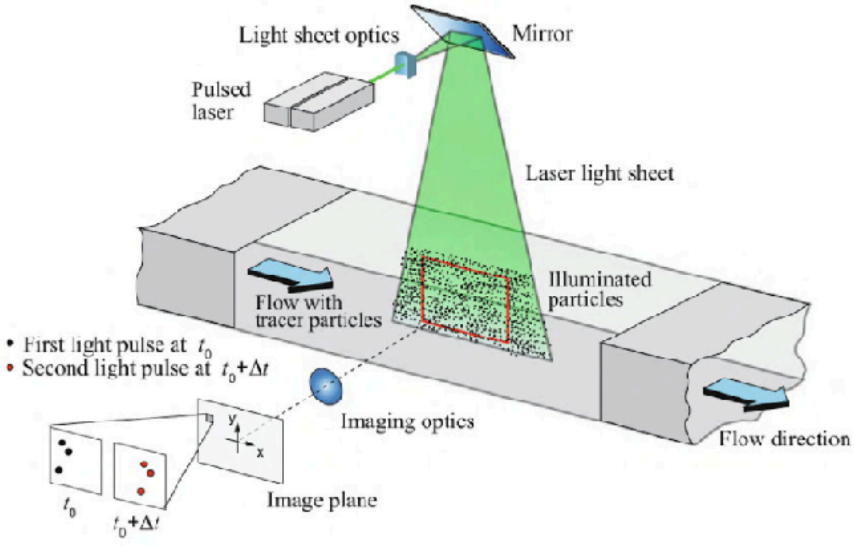

As such, researchers must optimize the laser power for each experiment. A standard 2-D PIV setup can be seen in Fig. 4:

Figure 4: 2-D PIV Setup (Reprinted from Raffel et al. 2018)

While Fig. 4 provides a standard setup, the optics used are specific to each facility. It is important to note that the field of view (outlined in red) must be smaller than the laser sheet so that the entire image field produces data. If the images taken have voids or inhomogeneous seeding, bias errors are introduced into the data analysis (Westerwheel 2000). The imaging optics shown in Fig. 4 are usually simply the camera lens optics. In general, imaging systems that include additional optical lenses lead to larger perspective distortions, which can skew results in 2-D PIV. Thus, most systems use fixed-zoom camera lenses without additional optics to minimize the distortions incurred for each image.

2.2.2 Stereoscopic PIV

Stereoscopic PIV (SPIV) is a more advanced style of PIV measurement that provides the out-of-plane velocity in addition to the the two in-plane velocities provided by 2-D PIV. This is accomplished using a pair of cameras installed at an angular offset from a plane normal to the illuminated plane. The two cameras produce two different simultaneous image pairs that are use to calculate the three-dimensional flow field in the experimental region of interest (Prasad 2000). Because the angle between the cameras and a plane normal to the laser sheet are known, the out-of-plane velocities can be determined based on the vector projections of each particle's velocity in both images. The results from each set of pictures are then analyzed and combined to produce the velocity field in the experimental region of interest. A comparison image of 2-D and stereoscopic PIV setups can be seen in Fig. 5:

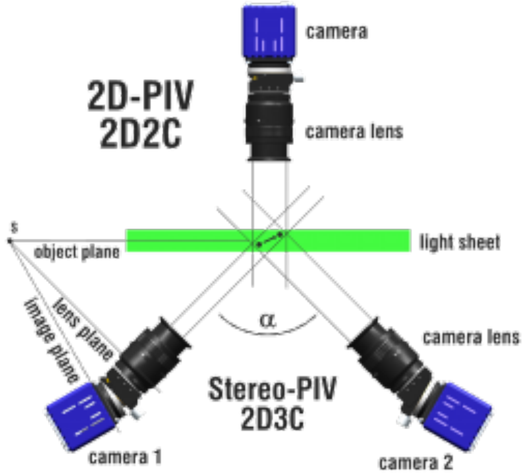

Figure 5: Comparison of 2-D and Stereoscopic PIV
(Reprinted from LaVision https://www.smart-piv.com/en/products/flowmaster/2d-stereo-piv/ 2019)

The SPIV system shown in Fig. 5 includes schiempflug mounts that offset the camera CCD planes from the lens planes. This is not required for successful SPIV. However, schiempflug mounts can significantly expand the system's usable field of view and region of data accuracy by maintaining focus across the entire object plane (i.e. the illuminated laser sheet). Without these mounts, basic SPIV systems using a narrow depth of focus will produce images that are slightly out of focus because the subject of the image varies in distance from the camera. To remedy these issues, SPIV setups without schiempflug mounts use a smaller aperture to produce a large depth of focus and ensure the entire image remains in focus. This can be effective but smaller apertures result in less light capture which can lead to poor particle illumination.

Regardless of the lens setup, SPIV systems must be calibrated with specialized calibration targets to ensure the flow is accurately represented (Wieneke 2005). Calibration targets include dimensioned marks and/or features that are used to calculate the pixel scale (pixels per unit length) in the recorded images. Using calibration plates, multiple images must be obtained at different locations. Alternatively, stepped blocks or volumes with other dimensioned 3-D characteristics can be sued to calibrate the system without having to capture multiple images or move calibration instruments (Soloff et al. 1997).

While stereoscopic PIV is capable of measuring out-of-plane velocities, the out-of-plane component is known with substantially lower accuracy than the in-plane components. This is because SPIV operates with a thin laser sheet rather than an illuminated volume. With this planar setup, SPIV systems calculate the out-of-plane velocity based on the angles between the cameras and normal to the laser sheet and the in-plane velocities. Because the out-of-plane velocity results, essentially, from the difference of the two camera's results, measurement uncertainties are larger than the in-plane velocities which are essentially the mean of the two camera's results. The out-of-plane measurements accentuate measurement uncertainties while the in-plane measurements reduce measurement uncertainty.

2.2.3 Tomographic PIV

If all three components of velocity require equivalently high accuracy, 3-D PIV systems such as tomographic PIV are necessary (Buchner et al. 2011). This produces a tradeoff between the accuracy of results versus the amount of time spent in system setup and data analysis. Thus, the decision to use stereoscopic or tomographic PIV must be made for each experiment, depending on the level of detail needed and the amount of time available for data reduction. Tomographic PIV is a much more complicated version of PIV that uses multiple cameras surrounding an illuminated volume that captures three-dimensional flow characteristics with equivalent accuracy across the entire volume in all three directions. The major distinction between stereoscopic and tomographic PIV is the evolution from a laser sheet to an illuminated volume of interest in the flow. Work by Elsinga et al. (2005), Scarano (2012), and Buchmann (2012) suggests that the illuminated volume requires a depth at least 1/4th the width of the field of view. This is accomplished by a combination of optics that either expand a pulsing laser beam into a laser sheet and subsequently into a rectilinear volume or expand a pulsing laser beam directly into a cylindrical laser volume. The optical setup used is largely dependent on the phenomena being measured and the capabilities of the facility conducting the experiment. In order to capture sufficient data for each particle in the flow, tomographic systems are equipped with at least four synchronized cameras that capture double-exposure images of the volume of interest at the same time. A depiction of a typical tomographic PIV setup can be seen in Fig. 6:

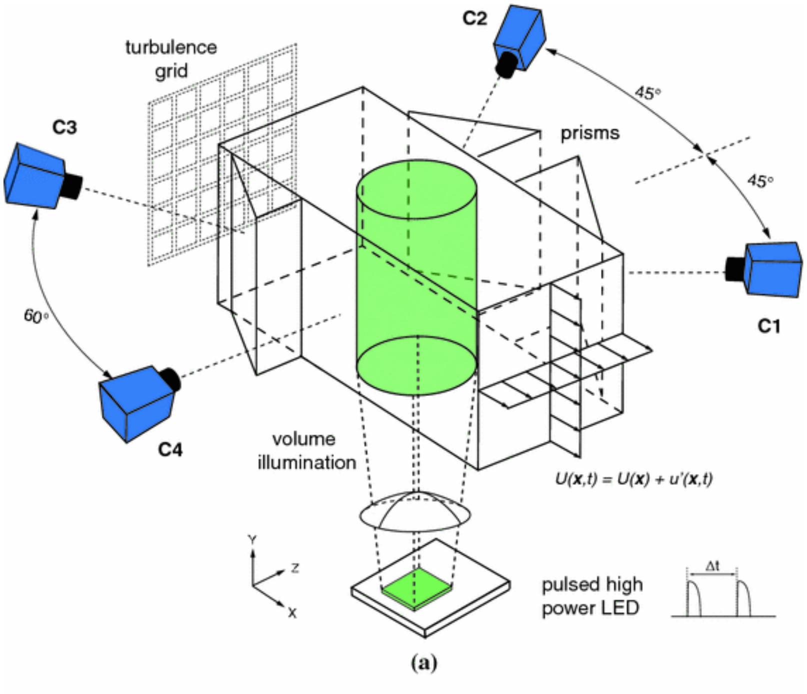

Figure 6: Tomographic PIV Setup (Reprinted from Buchmann et al. 2012)

Figure 6 shows the complexity of a tomographic PIV system is far higher than a 2-D or stereoscopic system. Alignment of each camera is critical for successful data collection and this makes application to large-scale facilities particularly challenging. As described above, large-scale tunnels inherently produce stronger vibrations and mechanical flexure than smaller-scale tunnels and these effects can significantly alter the alignment of the cameras when the tunnel is in operation. In small-scale environments, this can be alleviated by attaching the tomographic PIV setup to a fixed frame that ensures the relative positioning of the cameras and optics remain constant. However, such fixed frames aren’t feasible in large-scale facilities, as the test section is too large to accommodate a single frame that is sufficiently rigid to ensure a common, fixed frame for the entire PIV system.

In addition to setup challenges, tomographic PIV also has a significantly more complicated and time consuming data reduction requirements. The major bottleneck is the number of voxels (3-D pixels) to be analyzed. The exact number can vary depending on the cameras being used, but it is not uncommon to process billions of voxels in each iteration (Scarano 2012). Oftentimes, weeks or months of data processing are required after a test before results can be obtained. As a result, researchers are working to develop new algorithms to expedite the process (Worth and Nickels 2008, Atkinson et. al 2008, Atkinson and Soria 2009).

2.2.4 Holographic PIV

Holographic PIV is the newest and most complicated version of PIV. Similar to tomographic PIV, the holographic PIV is capable of resolving 3-D flow characteristics and Meng et al. (2004) claim is the most accurate method of doing so. However, this accuracy comes at a cost. Various complexities make the system much more difficult to set up and use compared to other techniques (Schäfer and Schröder 2011). A diagram of a typical holographic PIV setup can be seen in Fig. 7:

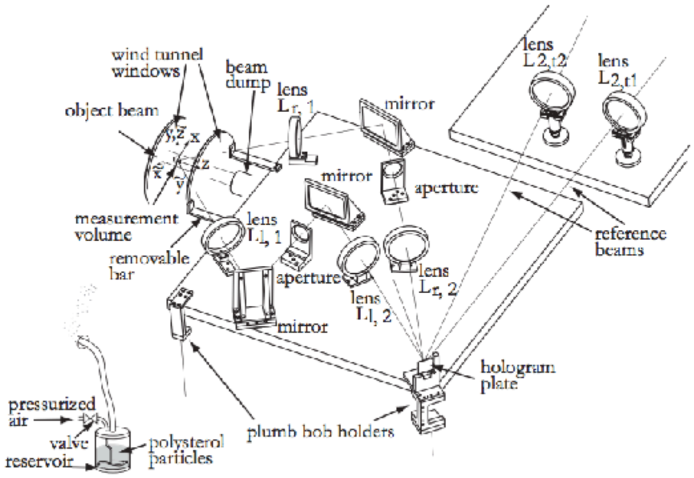

Figure 7: Holographic PIV Setup (Reprinted from Schäfer and Schröder 2011)

The key difference between Figs. 6 and 7 is the increase in complexity within the optical system. Holographic PIV captures images of a holographic projection of the region of interest rather than directly imaging particles in the flow. The system uses a complex array of optics to replicate the region of interest in a scaled hologram which is then analyzed normally. This enables deeper experimental volumes to be studied than tomographic PIV. However, Schäfer and Schröder (2011) explain that in addition to the method's inherent complexity, holographic PIV lacks the ability for online measurements, meaning that image focus and data validity cannot be assessed for hours after an experiment, a challenge that is also present with tomographic PIV setups. This can limit test cadence because the best experimental practice would be to verify successful data capture before adjusting the setup to make additional test runs.

2.3 Challenges of Large-Scale PIV

The principal concern of this thesis is application of PIV methods to large-scale, production-type wind-tunnel testing. Thus the continuing focus of this review will be 2-D and stereoscopic PIV that are currently most realistic for application in that context. Some of the challenges detailed here are solvable at the cost of time in calibration, alignment, or data reduction. This time can be a deterrent to PIV use in production environments where testing is often tightly constrained by schedule and the cost of tunnel occupancy.

2.3.1 Physical Setup

One of the inherent challenges to scaling PIV systems for use in large-scale facilities is hardware implementation. Small-scale tunnels enable cameras and laser sources to be placed relatively close to the region of interest which makes measurements fairly easy to capture (Westerwheel et al. 2013). Implementing a PIV system in a large-scale facility forces hardware to be much farther from the region of interest and this leads to several issues. First, higher zoom lenses are required to capture particle flow. When the camera is moved farther from the experimental region of interest, either a variable-zoom lens or a lens with a higher fixed magnification is required. In either case, the additional optics within the lens lead to image distortions. Alvarez et al. (2012) show that these distortions can be modeled and corrected, a functionality that has since been added into most standard PIV computing softwares. Variable-zoom lenses in particular produce significant distortion due to the additional optics contained within the lens (Li & Lavest 1996).

PIV systems in large-scale environments must also contend with increased mechanical vibrations and mechanical flexture. In small-scale wind tunnels, most components are essentially rigid because of their small size. However, large-scale wind tunnels tend to be more flexible because of the longer lengths of the various structural members. This leads to larger steady mechanical flexure when the tunnel is in operation and there is a static pressure difference between the test section and the surroundings. The more-flexible structures can also have lower natural frequencies that are more apt to vibrate during testing. These two effects present a major challenge for PIV because precise alignments are critical to accurate data collection. Vibrations can influence the alignment of the PIV cameras, laser, and optics, and this makes the calibration scheme for large scale facilities much more complex (Raffel et al. 2004). Specifically, vibrations encountered in large scale facilities can change the location of the camera during image capture, changing the field of view for the first and second exposure. This results in an incorrect velocity measurements because particles appear to have all shifted due to the vibration, not just because of the actual motion of the flow. Similarly, vibrations can move the optics generating the laser sheet and change the plane of the flow being observed. This introduces a particle shift between images and can also illuminate particles outside the depth of focus for the camera. If this occurs, data analysis either cannot be completed or produces data that is unreliable. In either case, vibrations can be minimized through mechanical damping and/or be accounted for in data analysis. However, there will always be an additional error not present in small-scale tests (Raffel et al. 2004).

Another concern in large-scale PIV implementation is the selection and use of proper seeding particles. In small-scale applications seeding can be straightfoward as there are a wide variety of usable tracer particles and only small amounts of tracer are typically needed. The traditional approach is to flood the wind tunnel with these particles to create a homogeneous distribution of particles that properly follow the flow (Towers et al. 1991, Westerwheel et al. 2013). However, saturating large-scale wind tunnels with particles can be impractical due to the amount of particulate required. Depending on the particle selected, flooding the tunnel may be prohibitively expensive and could potentially have adverse health effects (Raffel et al. 2018). Extra attention must also be paid to the size of the individual particles in relation to the individual pixel size of the camera. If the particles are smaller than the dimensions of the pixels, the positions of each particle are approximated to the closest pixel which leads to significant errors. Moreover, very small particles will often not be adequately illuminated for reliable imaging. Kähler et al. (2012) shows that the best practice is for individual particles to have a diameter of 2.5 pixels or larger. This is possible in small-scale configurations with small regions of interest but large scale applications cannot attain this ratio while using particles that are sufficiently small to follow the flow. The two of these size constraints create a bounded region where the seeding particle selected must be sufficiently large to appear in the image pairs and receive sufficient illumination, while remaining small enough to accurately follow the flow.

2.3.2 Image Capture and Analysis

The relationship between camera resolution and the large field of view in a large-scale wind tunnel introduces a significant challenge to successful use of PIV. As the desired field of view increases, either the resolution of the cameras being used for PIV must increase or the size of the seed particles must increase. As discussed previously, increasing the seed particle size is not feasible, as the particles must be small enough to accurately follow the flow (Zhang et al. 2003). Therefore, increasing the resolution of the camera is the best way to achieve a larger field of view. However, this can be somewhat difficult and expensive to accomplish with a single camera because resolution must be increased while keeping the dimensions of each pixel as low as possible (Kähler et al. 2012). Previous experiments with increasing PIV field-of-view at NASA Langley have used high resolution cameras to take images that are 4008 x 2672 pixels, and capture approximately half the model used (Jenkins et al. 2009). These cameras have square pixels that are 9.0 microns by 9.0 microns, and represented some of the more cutting edge cameras at the time. An approximated field of view can be seen in figure 8, where lengths are normalized by vehicle wingspan, b:

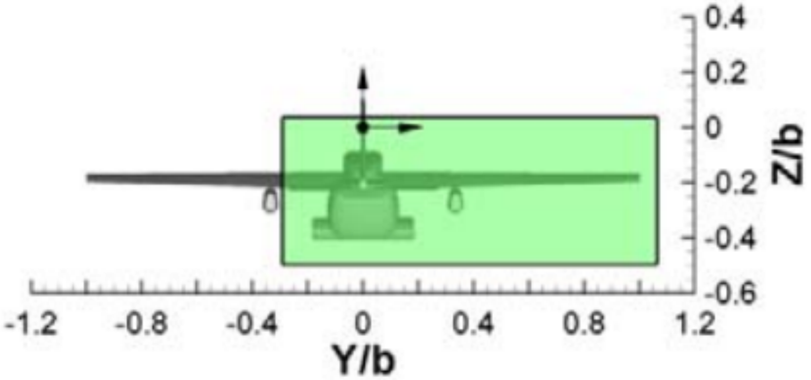

Figure 8: 14 x 22 Foot Test Section Field of View (Reprinted from Jenkins et al. 2009)

The largest field of view captured in this experiment was 1.5 meters by 0.9 meters, which is much larger than most PIV applications. Based on this experiment, it appears that increasing camera resolution is a viable strategy for large-scale PIV implementation. However, it should be noted that increasing camera resolution is somewhat limited by the technology currently available. One possible solution is the implementation of multiple cameras capturing individual images that can be stitched together during data analysis to artificially capture a larger field of view, but there have not been enough attempts at this method to confirm its efficacy.

3. SYSTEM DESIGN, VERIFICATION, AND TESTING

Chapter 2 provided an in-depth review of PIV as a measurement technology, and outlined the major issues facing PIV implementation in large-scale facilities. This chapter details the design, manufacture, and validation of systems to overcome these challenges and implement PIV in a large-scale production environment.

3.1 PIV Frame Design and Manufacture

Repeatability is critical to the successful implementation of PIV in a production testing environment. As discussed in the Chapter 2, there are a variety of physical setup concerns that can decrease the repeatability of measurements in large scale wind tunnels, especially when operating at high speeds. Mechanical vibrations in large scale tunnels make unanchored mounting systems insufficient, as cameras are not anchored in a fixed position throughout the test. Furthermore, temporary mounting systems such as tripods cannot be reliably located in the same position relative to the test section on every setup, and can be accidentally bumped or moved by operators during testing. As a result, a method for rigidly locating the PIV cameras relative to the test section as deemed critical for the success of PIV in a production wind tunnel testing environment. At first, a list of requirements for the mounting system was developed. To be deemed effective, the system must:

1. Be removable when not in use
2. Provide rigid and repeatable positions for the PIV cameras
3. Allow configuration of camera height, yaw, and streamwise position

To meet these requirements, a mounting frame design was selected, manufactured, and implemented at the LSWT. A photograph of the system installed on the test section front window is given in Figure 9.

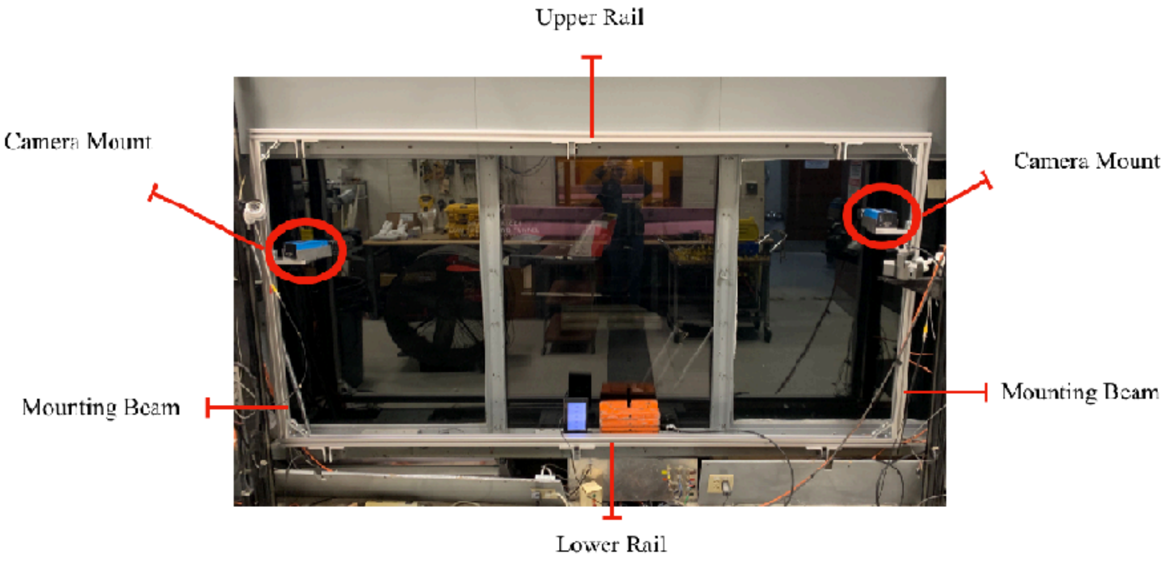

Figure 9: PIV Mounting Frame

The frame is made of extruded aluminum with T-slots along all sides. The upper and lower rails are fixed to the outer wall of the test section with aluminum angle brackets and bolted in place to ensure a rigid connection. The mounting beams on the left and right sides may be moved along the rails in the streamwise direction to allow image capture at any point in the test section. This can be easily done by loosening bolts connecting the interior gussets to the T-slot nuts and sliding the mounting beams into the desired position. Tightening the bolts ensures that camera position in the streamwise direction remains fixed relative to the test section, as long as the frame does not become detached from the tunnel.

The camera mounts are machined of stock aluminum. A detailed image of the mount design can be seen in Figure 10. The camera mounts are made entirely of machined aluminum and assembled with standard english fasteners. The locating pocket and walls ensure the camera position within the mount remains fixed. Discrete angle selection holes allow rapid selection of standard camera angles depending on the holes used to bolt the camera mount together. Additionally, the system has a central bolt hole that may be used to set each camera at a custom angle if needed. The full mounting bracket is attached to the mounting beams with bolts that run into T-slot nuts in the inside grooves of both beams. Holes along the height of the mounting beams allow for a locating pin that sets a discrete height for the cameras. It is important to note that these pins are optional, and the camera mounts can be fixed at any point along the mounting beams by tightening the bolts when the mount is at the desired height. Overall, this system ensures that camera position remains fixed relative to the test section, ensuring repeatability between subsequent runs and tests. Flexibility of camera position is also maintained should other camera positions be needed.

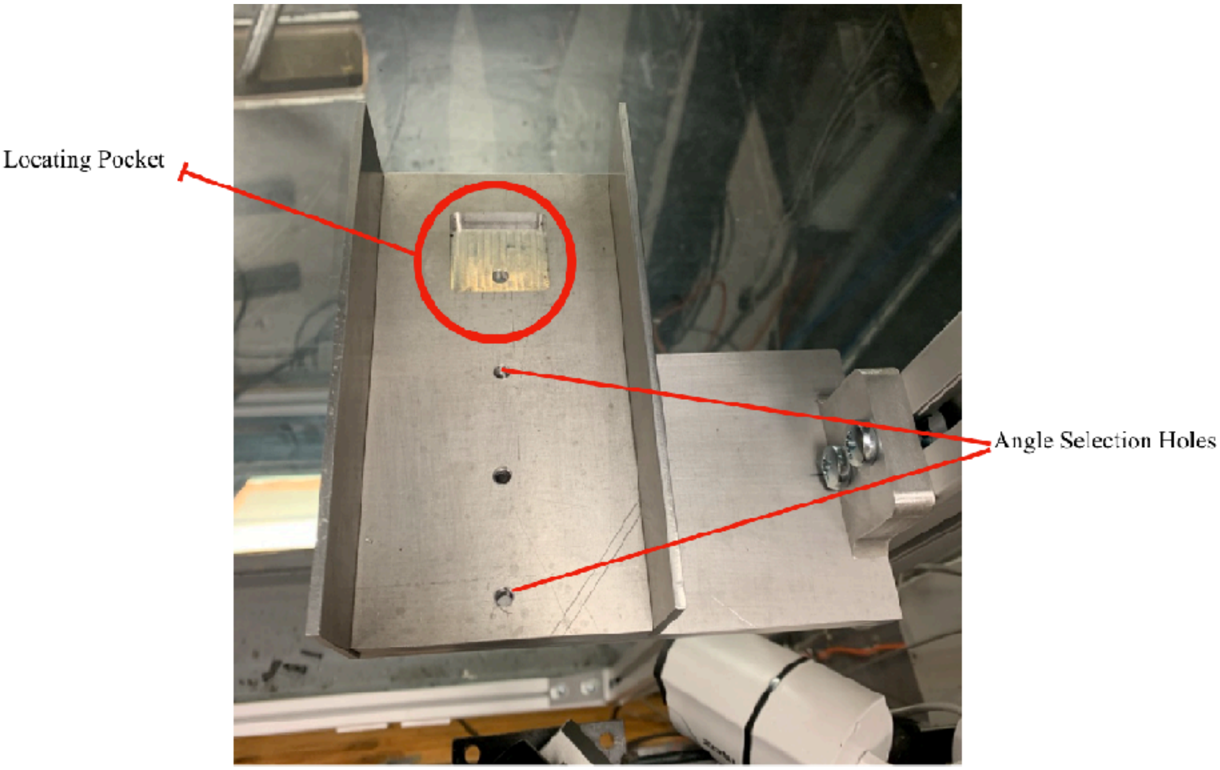

Figure 10: PIV Camera Mount

3.2 PIV Uncertainty Maps and Post-Processing Explanation

Upon completion of post-processing, a time-average vector field was computed from all image pairs at each nominal velocity. DaVis 8.4.0 calculates the standard deviation of the measured *x* and *y*-direction velocity at each point in field using the sequence of instantaneous velocity values measured at each point. The standard deviations are then used to compute the uncertainty of the time-average velocity at each point in the field as the standard error of the mean:

$$S_{\bar{x}} = \frac{\sigma_x}{\sqrt{N}}$$

in which *S* is the uncertainty of the mean velocity value, σ_x is the standard deviation at a given point, and *N* is the number of velocity vectors measured at that point. It should be noted that *N* can vary from point to point because every image pair does not necessarily capture an instantaneous velocity vector at every single point in the region of interest. Moreover, some instantaneous vectors are rejected during post processing. When the calculation is completed across the full average vector field, an uncertainty plot based on position within the region of interest can be produced. Plots for the 100 mph nominal freestream case with the 2-D and Stereoscopic PIV systems can be seen in figures 11 and 12. Additionally, Figures 13 and 14 break down the uncertainty for in-plane and out-of plane velocities captured during 100 mph run of the out-of-plane velocity validation test discussed in section 3.4.

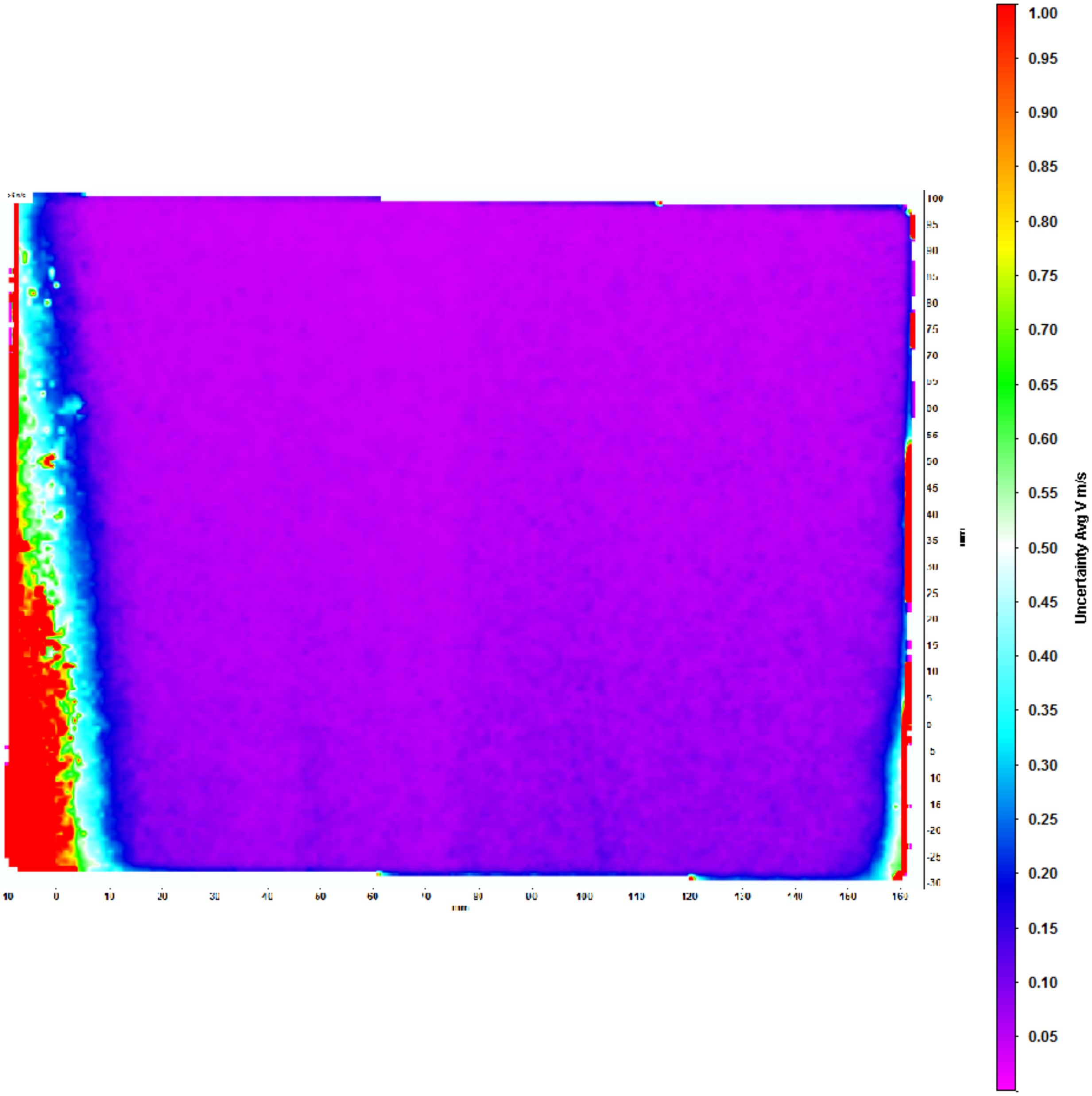

Figure 11: 100 mph 2-D freestream Velocity Uncertainty Field

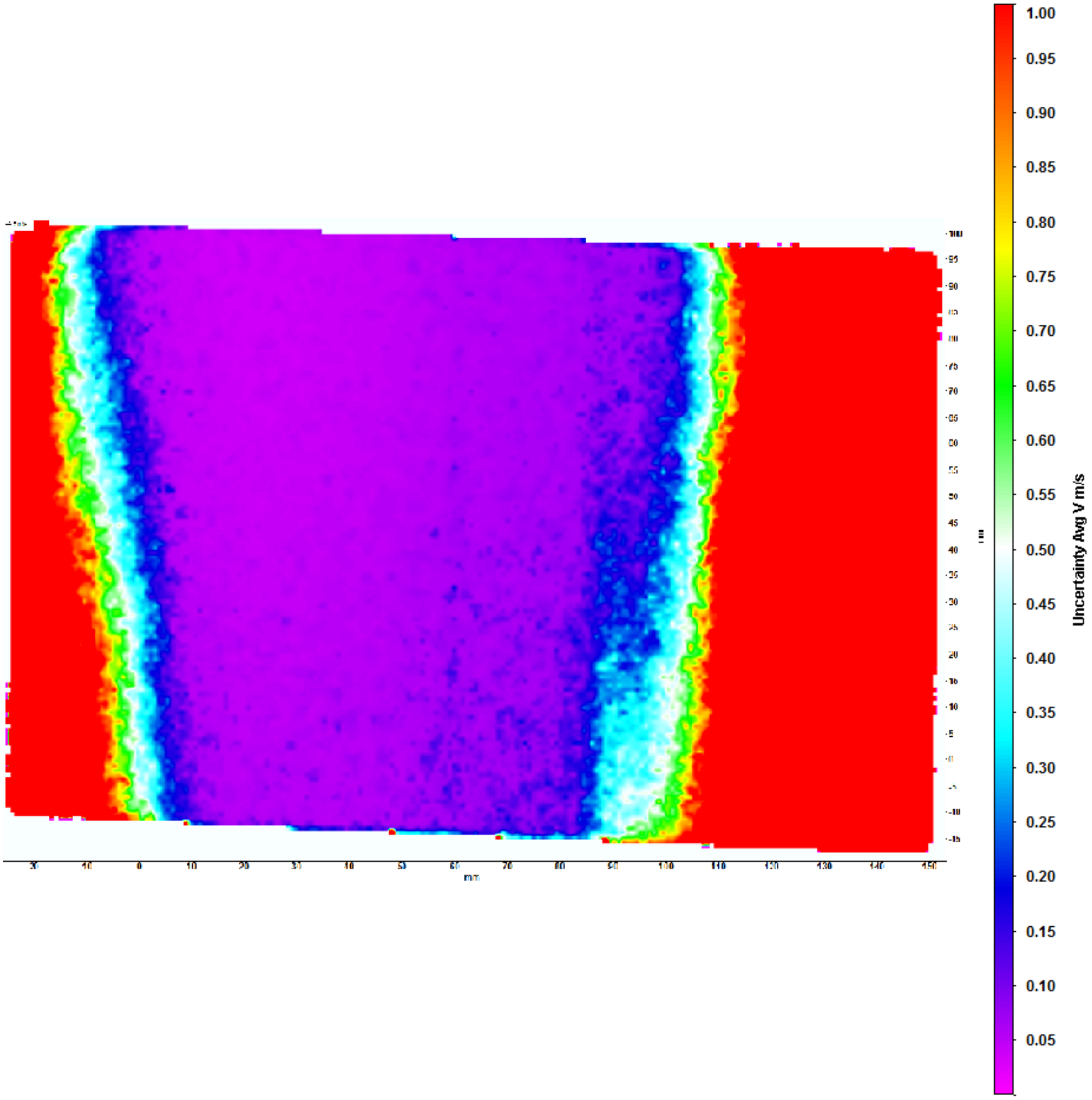

Figure 12: 100 mph Stereoscopic PIV freestream Velocity Uncertainty Field

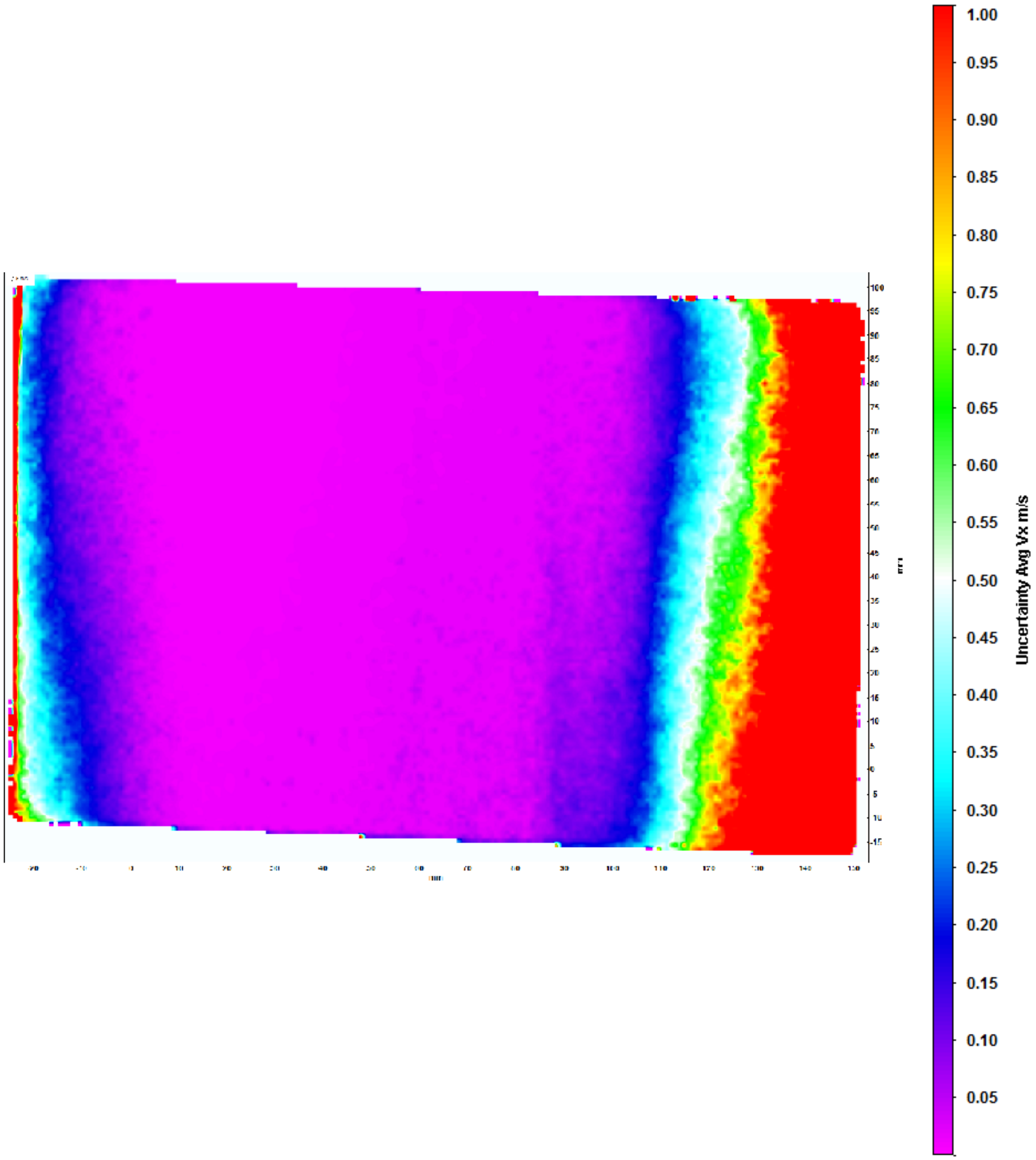

Figure 13: 100 mph Stereoscopic PIV In-Plane Velocity Uncertainty Field

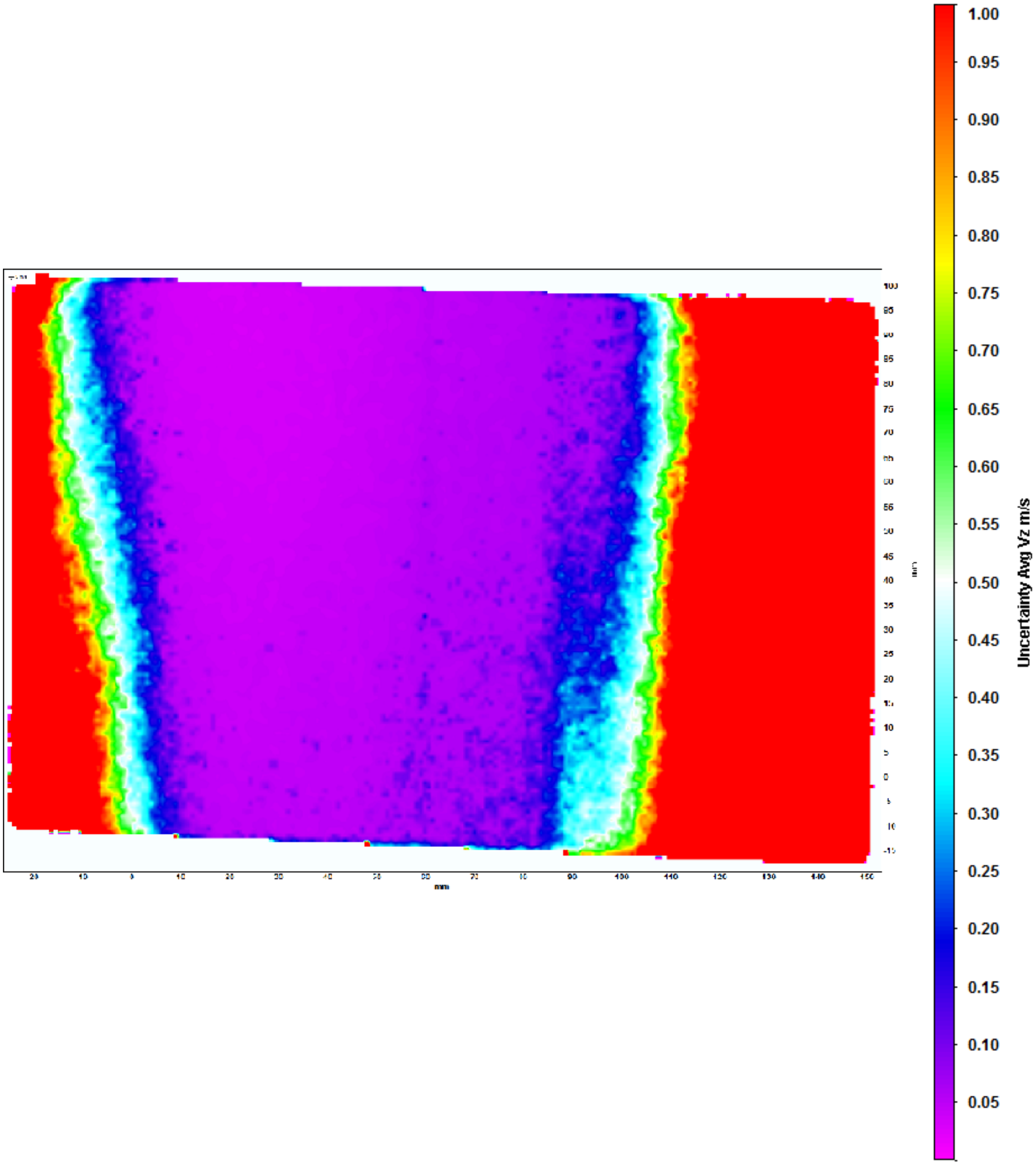

Figure 14: 100 mph Stereoscopic PIV Out-Of-Plane Velocity Uncertainty Field

Once all image pairs were processed, each individual vector field went through two rounds of post processing with the application of consistency filters. First, a filter to eliminate spurious vectors was applied. The vector field for each image pair was scanned for spurious vectors whose magnitude fell outside a specified tolerance band. A significant degree of trial and error was used to determine the final tolerance band size, with the wake rake measured velocity ± 5 m/s eliminating a majority of the most extreme errors. Erring towards a large tolerance band was preferable, as the inclusion of some spurious vectors was far better than the omission of non-spurious results. This operation produced vector fields with small holes or gaps in data which were then backfilled via interpolation. The vector fields for all image pairs were then averaged together to produce a single average vector field.

After averaging the vector fields together, a second post-processing step was applied to eliminate the effects of particles entering or leaving the region of interest between image frames. This produces a small region of invalid data near the edges of the region of interest that must be removed in order to properly determine the efficacy of the PIV system. This was accomplished by the addition of a bounding box that cut all edge effects from the final average vector field. The bounding box was individually tailored to the dataset analyzed, and was sized to eliminate the edge effects with minimal elimination of viable data. Figures 15 and 16 show the before and after effects of post processing on measurement uncertainty for the 100 mph freestream stereoscopic PIV case.

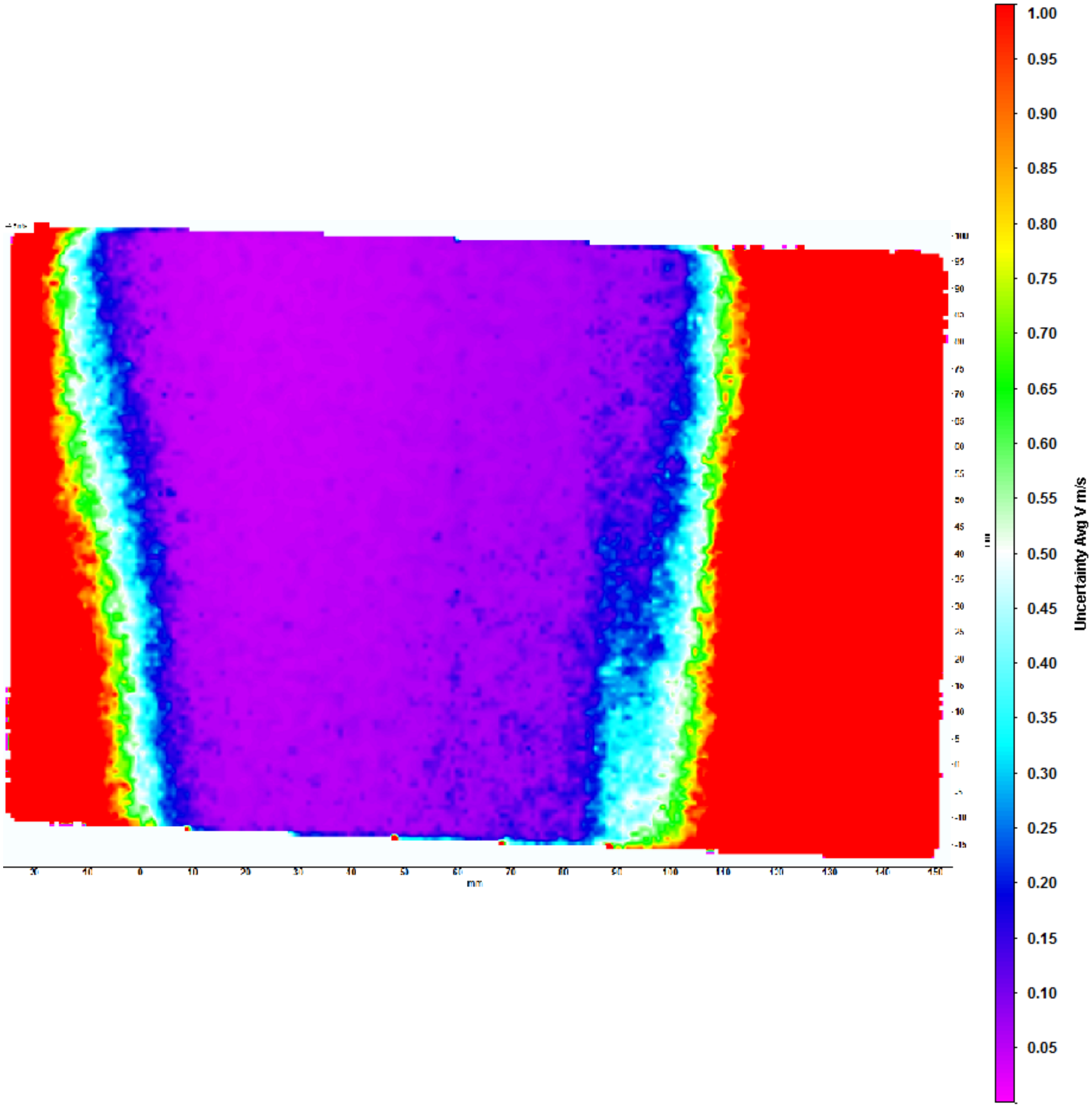

Figure 15: 100 mph Stereoscopic PIV Out-Of-Plane Velocity Uncertainty Field

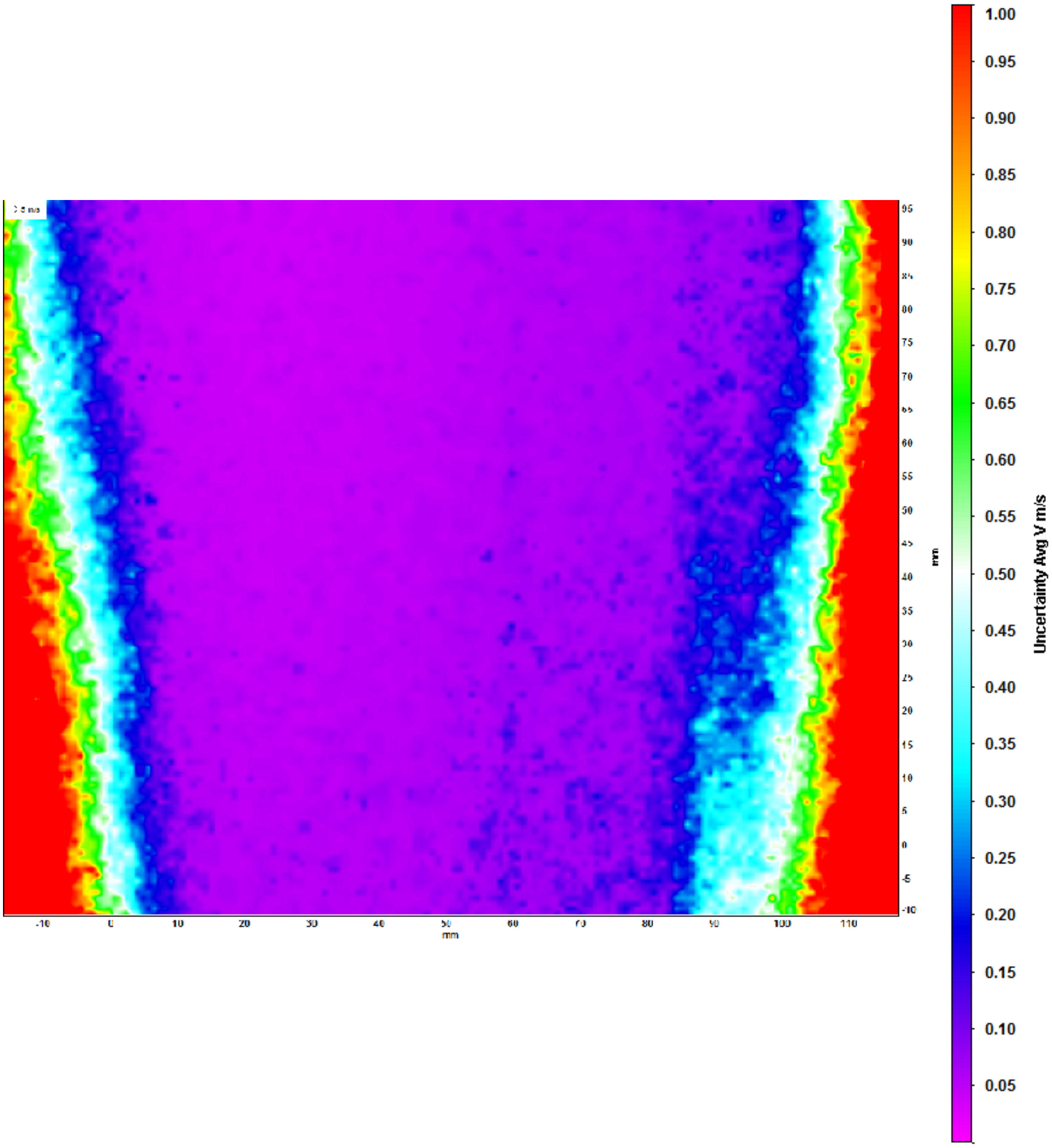

Figure 16: 100 mph Stereoscopic PIV freestream Velocity Uncertainty Field

This capability is incredibly helpful when determining the appropriate bounding region or elimination of spurious values, as it provides a clear depiction of what data is highly accurate and what data must be disregarded during data analysis. The 2-D PIV velocity Uncertainty field shows that measurement uncertainty is relatively constant across the full image, with an increase in error at the left and right sides of the image. This increase is expected for any PIV system due to particles entering and leaving the field of view between images. Applying a bounded region to the dataset that omits the edges of each vector field eliminates these regions of higher uncertainty, providing the final data. In cases where the edges of the frame must remain in the image (i.e. to show the trailing edge of a wing or tail as done in the WB-57 tests in chapter 4), researchers must be mindful that measurements near the edges of the image will have a higher uncertainty due to these edge effects.

The Stereoscopic PIV uncertainty fields provide similar insight to the 2-D PIV velocity field, showing the increase in measurement uncertainty moving out from the center of the image. While some of the uncertainty at the edges of the image is still due to edge effects, the major cause of uncertainty in this setup is the variation in image focus from the center to the edges of each image. Without schiempflug adapters, focus will naturally vary slightly from the center of the images to the other, increasing the uncertainty of individual particle positions. This carries over into the processed data, where less focused areas within the image produce data with higher uncertainty. Similar to the 2-D case, the application of a bounding region eliminates the regions of high uncertainty and produces the final data. Once again, in cases where the edges of the frame must remain in the image (i.e. to show the trailing edge of a wing or tail as done in the WB-57 tests in chapter 4), researchers must be mindful that measurements will be most accurate at the center of the image, with increasing uncertainty moving towards the left and right extremes of the vector field.

Of course, these uncertainty maps do not provide a comparable uncertainty to the values measured by the wake rake in this experiment. In order to determine the uncertainty of the PIV system measurement as a whole, the uncertainty equation from Schiacchitano and Wieneke (2016) must be used again to produce a single uncertainty for the full vector field. This is accomplished by using the mean velocity, standard deviation, and number of vectors within the average velocity field to produce a single uncertainty value for the full field. This method was used to produce the uncertainty values for the PIV systems catalogued in Tables 1-3.

3.3 2-D PIV System Validation

After the selective seeding system performance was verified, the 2-D PIV system was validated against conventional wind-speed measurements to validate the PIV system. In order to minimize the number of systems tested, all PIV system validation was conducted with a flooded test section. The PIV system captured data in the center of the test section at a height of 45 inches. This ensured the freestream velocity was unaffected by any possible flow anomalies caused by the wake rake or traversing mechanism and also minimized any wall effects experienced in the test section. During each run, PIV and pressure data were simultaneously collected in 12 second cycles and converted to velocities. Pressure data was collected with a wake rake and converted to velocity measurements. An example test setup can be seen in figure 17, with the red rectangle denoting the region of interest location and the red oval outlining the wake rake.

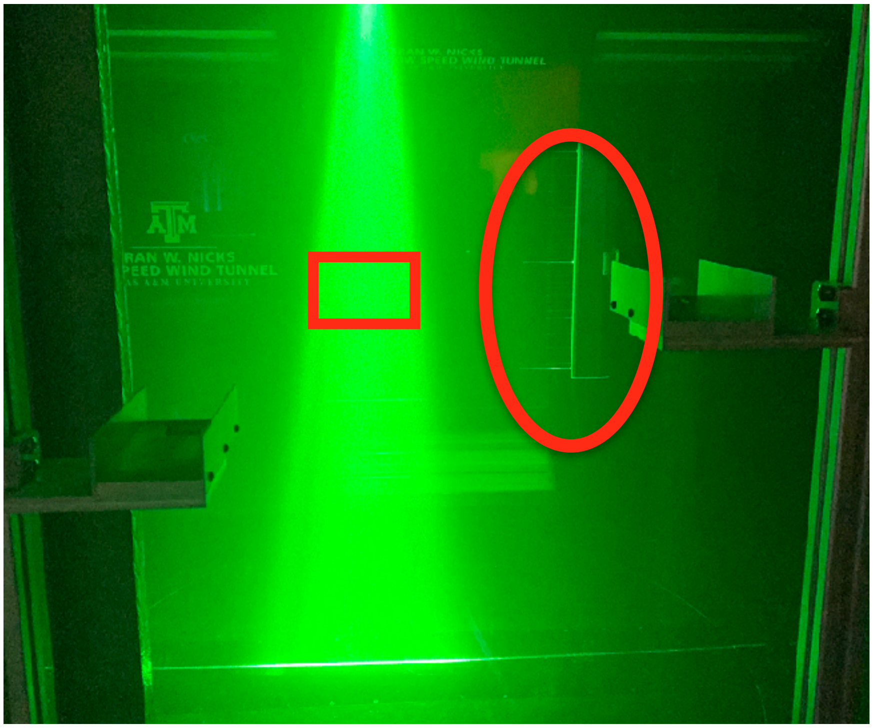

Figure 17: Example Validation Test Setup

During collection, one image pair was processed immediately to ensure image quality, with the remaining image pairs being stored for later processing. Validation data was collected for at 25 mph, 50 mph, and 100 mph to verify the system's accuracy at a wide range of velocities. A total of 1035 image pairs were captured across 3 runs and analyzed using DaVis 8.4.0 software. The data for each run was first analyzed with a cross correlating PIV scheme, beginning with a 64 pixel x 64 pixel interrogation window. After the initial pass, three passes with a 32 pixel x 32 pixel interrogation window were made to achieve higher measurement detail.

All data was post-processed using the methodology detailed in section 3.2. The changes to the average velocity field with the discussed post-processing steps can be seen in Figures 18-20:

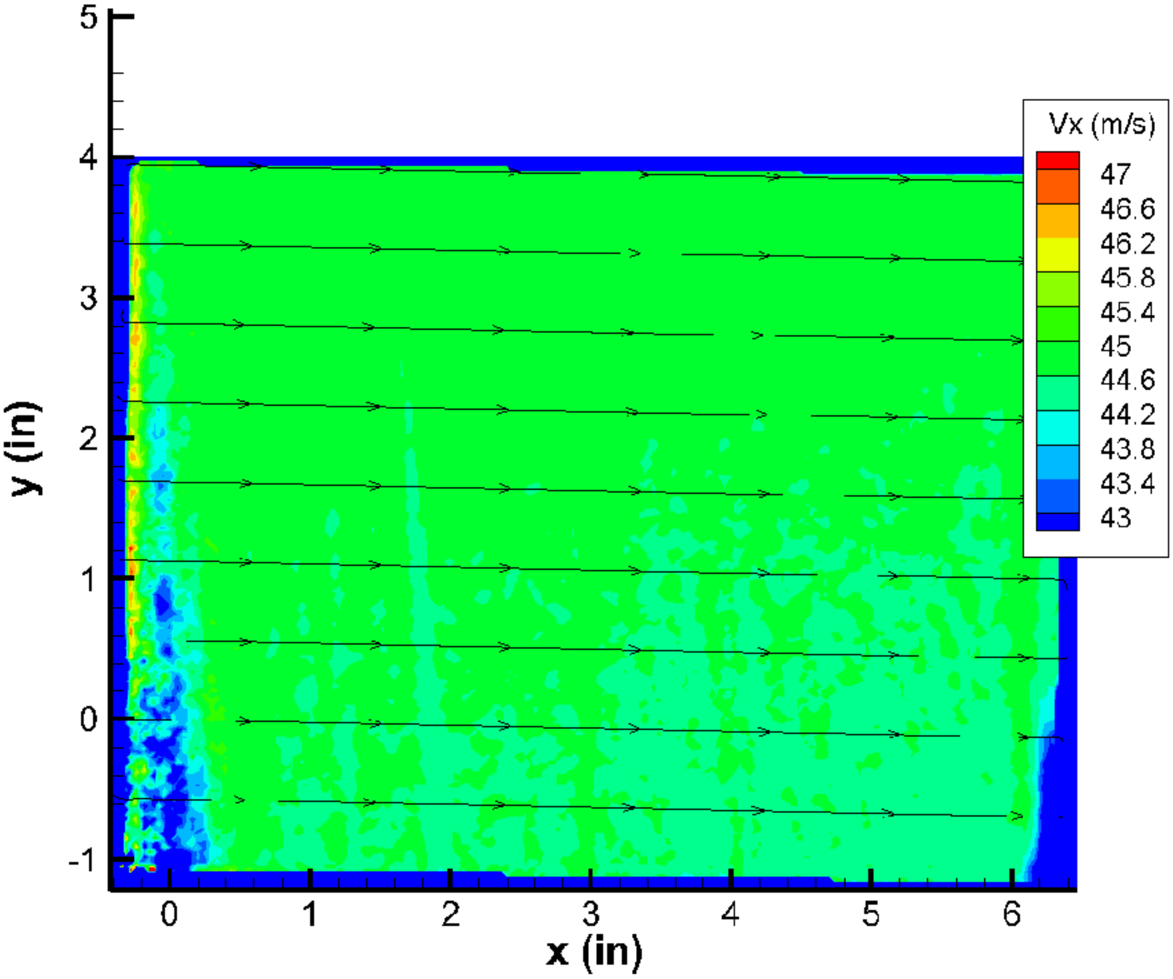

Figure 18: 2-D PIV 100 mph Average Vector Field before Post-Processing

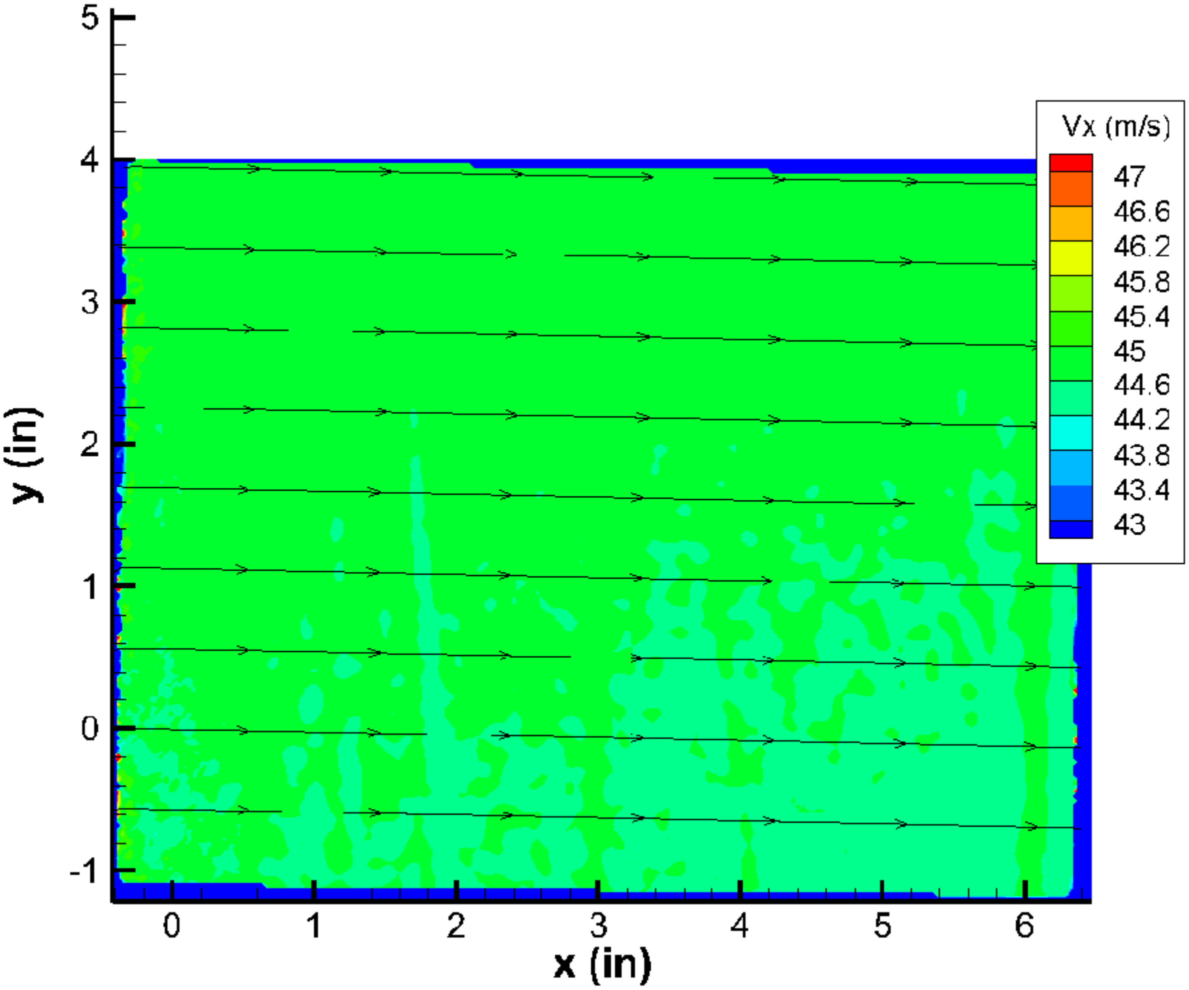

Figure 19: 2-D PIV 100 mph Average Vector Field with Consistency Filter

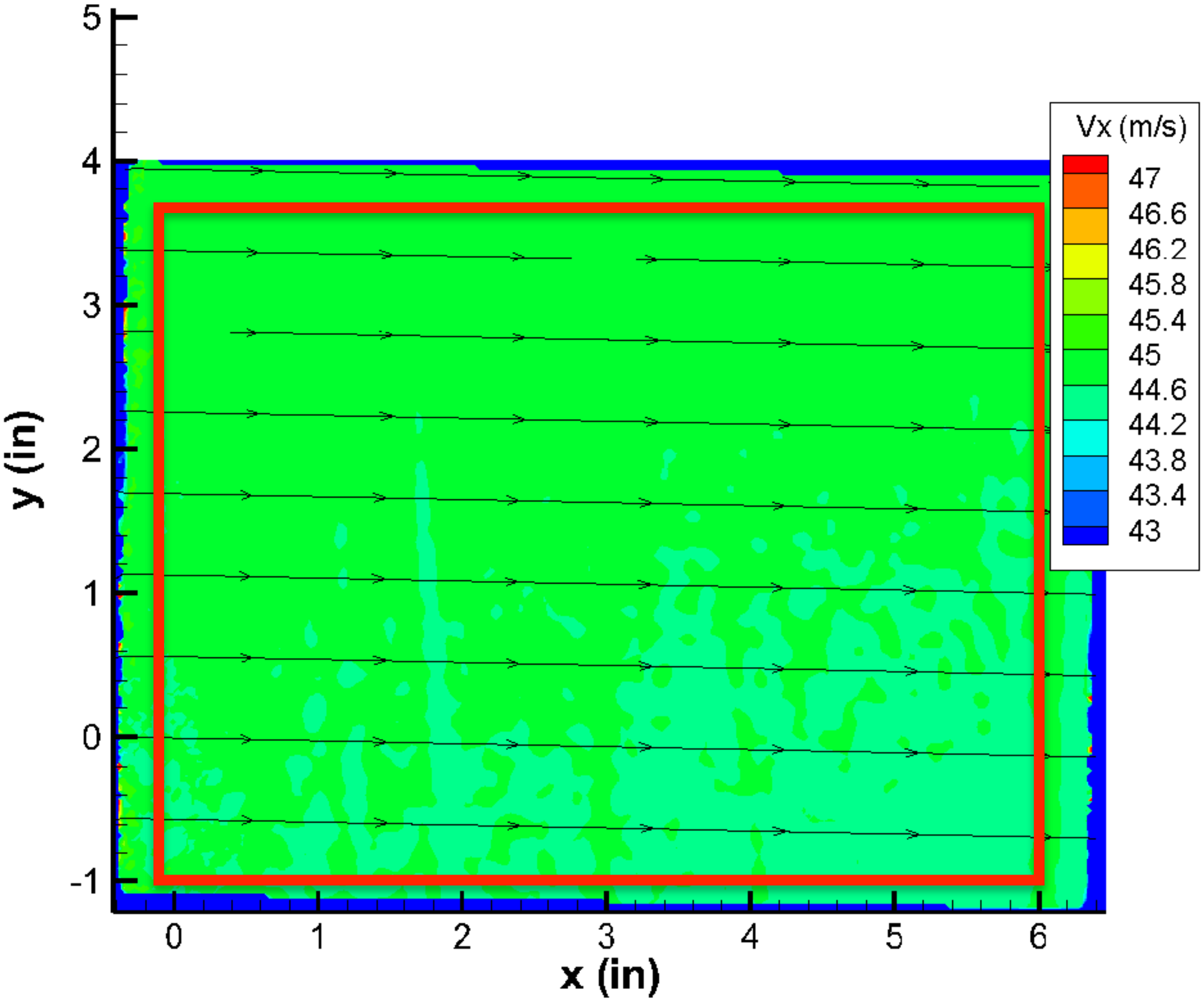

Figure 20: 2-D PIV 100 mph Average Vector Field with Bounding Box

These plots show that during the 100 mph test, the velocity measured by the 2-D PIV system varies by approximately ± 0.2 m/s (0.4%). Figures 18 and 19 show this variation with the slight change in color in the green regions of the plots. It should be noted that values located on the edges of each figure are spurious results due to particles entering or leaving the region of interest between images. A full breakdown of the measurement uncertainty for the 2-D PIV system can be seen in Table 1:

Nominal Operating Velocity	Wake Rake Velocity (mph)	2-D PIV Velocity (mph)
25 mph	11.5 ± 0.2	11.5 ± 0.1 (0.4%)
50 mph	22.6 ± 0.2	22.6 ± 0.1 (0.1%)
100 mph	44.8 ± 0.2	44.7 ± 0.2 (0.4%)

Table 1: 2-D PIV System Percent Error

This data shows that the error of the 2-D PIV system implemented at the LSWT is below 0.5%. Depending on the source, the average uncertainty for PIV is usually cited at or slightly below 1% (Wilson and Smith 2013), demonstrating that the system produced through this thesis meets or exceeds the current technology standards for PIV as a measurement technique. Thus, implementing PIV will be advantageous for the elevated standards for data accuracy and precision curated at the LSWT.

3.4 Stereoscopic PIV System Validation

The Stereoscopic PIV system was also validated against data from the wake rake and the 14-hole probe to determine its measurement accuracy. As before, the PIV system captured data in the center of the test section at a height of 45 inches and used 12-second pressure samples. Also as before, one image pair was processed during data collection to ensure image quality, with the remaining image pairs being stored for later processing. Validation data was collected for at 25 mph, 50 mph, and 100 mph. Data collection during the out of plane verification runs followed a similar format, but used the angle of the laser sheet to calculate in-plane and out-of-plane velocity components to compare with the results of PIV. After data was collected, DaVis 8.4.0 was again used for analysis and post-processing. The data for each run was first analyzed with a cross correlating PIV scheme, beginning with a 64 pixel x 64 pixel interrogation window. After the initial pass, three passes with a 32 pixel x 32 pixel interrogation window were made to achieve higher measurement detail.

All data was post-processed using the methodology detailed in section 3.2. The changes to the average velocity field with the discussed post-processing steps can be seen in Figures 21-23.

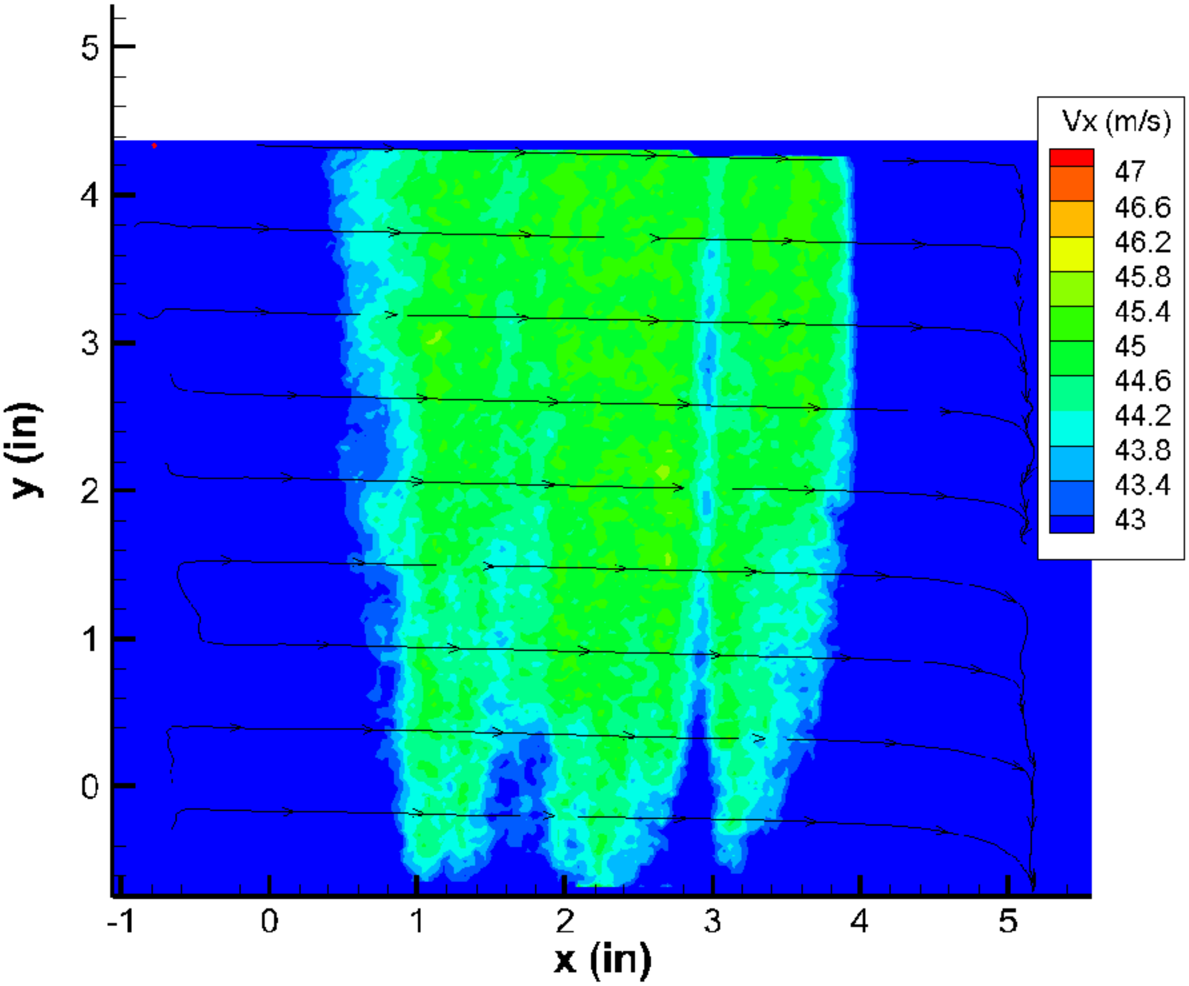

Figure 21: Stereoscopic PIV 100 mph Vector Field before Post-Processing

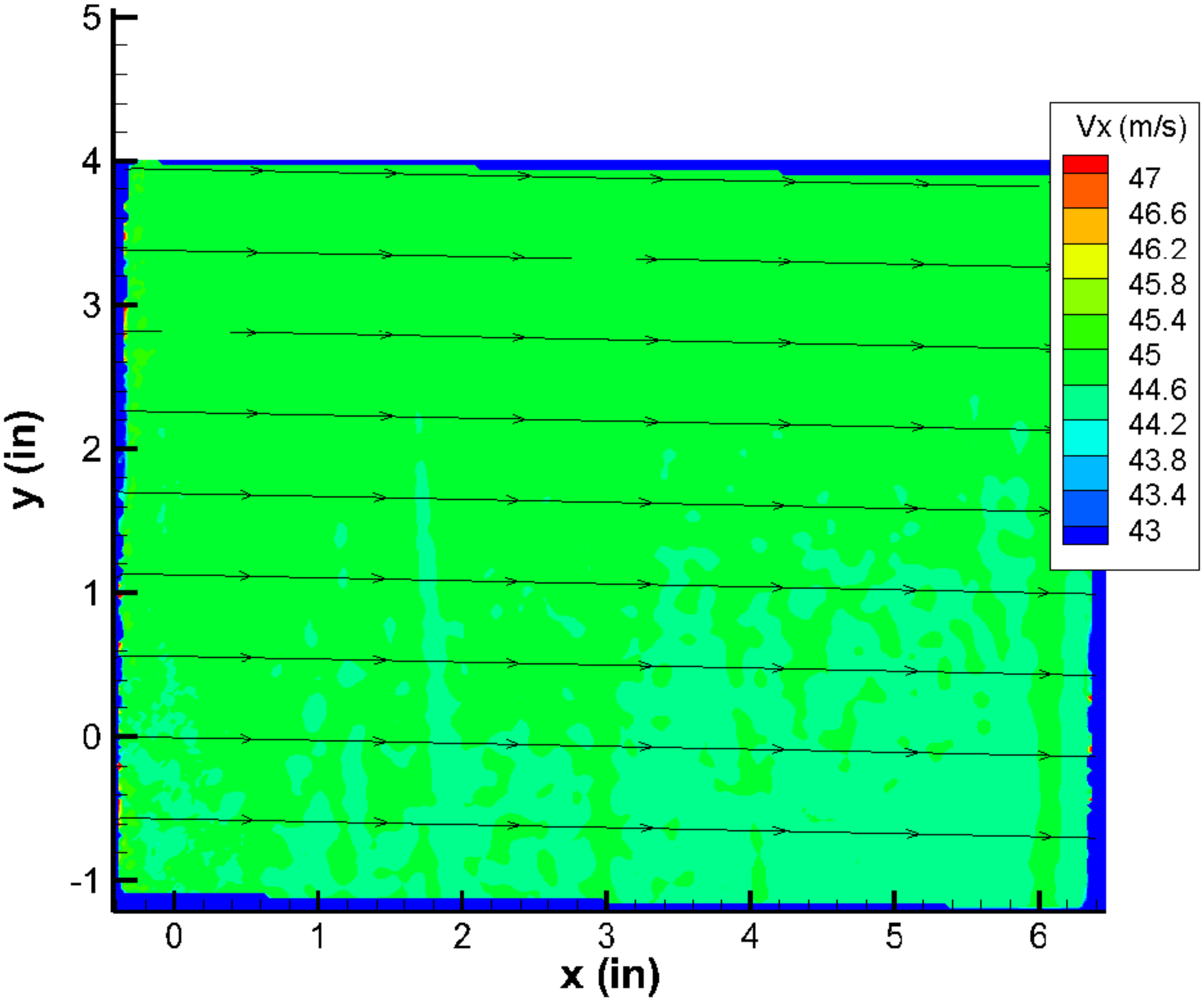

Figure 22: Stereoscopic PIV 100 mph Vector Field After Consistency Filter

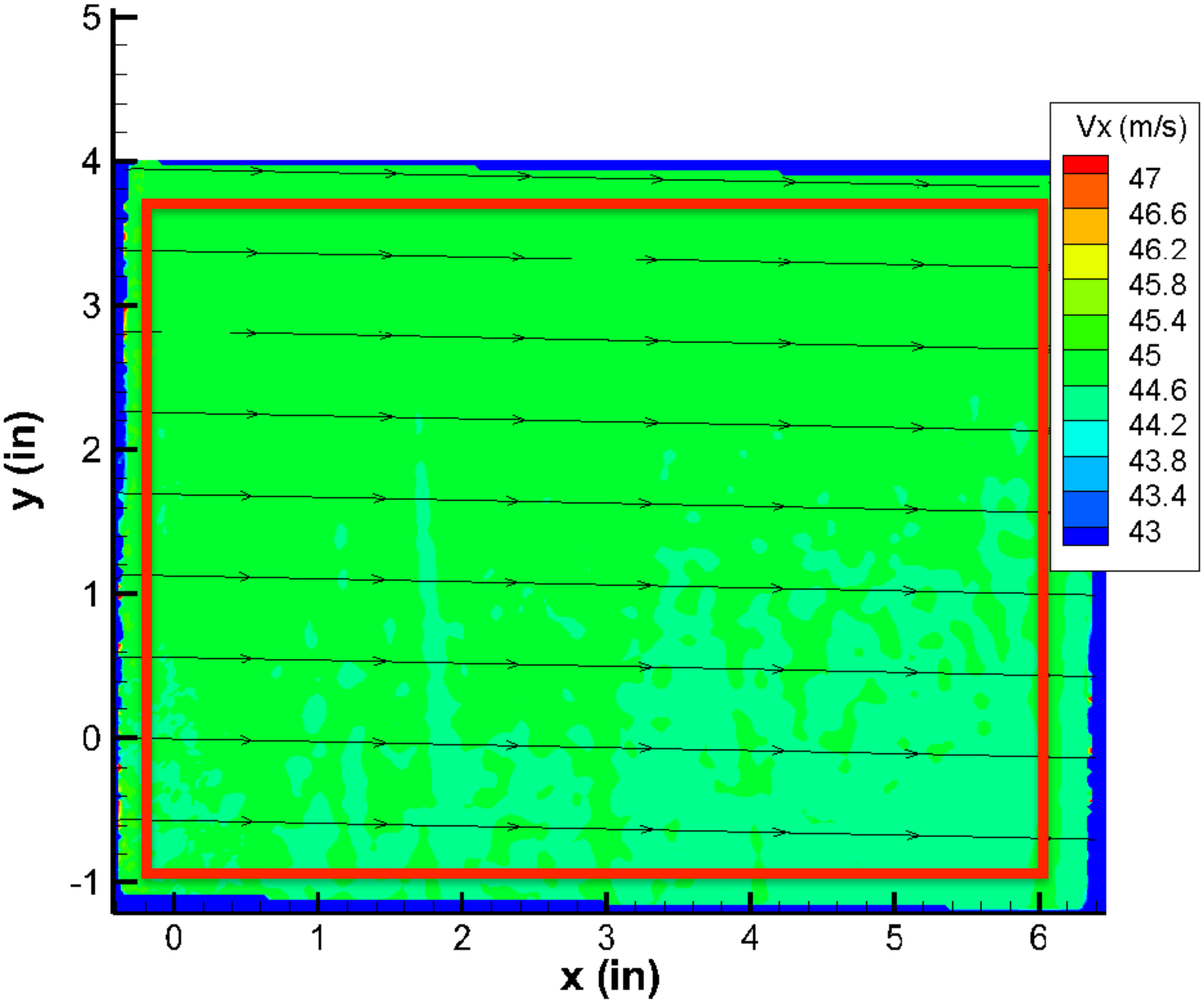

Figure 23: Stereoscopic PIV 100 mph In-Plane Vector Field With Bounding Box

These plots show that during the 100 mph test, the velocity measured by the SPIV system varies by approximately ± 0.2 m/s (0.4%). Figures 21-23 show this variation with the change in color in the green sections of the plot. It should be noted that values located on the edges of the post-processed image are spurious results due to particles entering or leaving the region of interest between images. The dramatic improvement in data quality from figure 21 to figure 23 demonstrates the importance of effective post-processing for PIV data analysis. Consistency filters effectively removed erroneous values that were altering the velocity field and produce a much more accurate velocity field in the region of interest. These erroneous vectors can be attributed to two main factors. First, particles entering and leaving the region of interest create an edge effect of spurious results around the full image. This phenomenon is consistent with the challenges experienced with 2-D PIV, and can be seen in the SPIV vector field in figure 22 after the consistency filter has been applied. Second, the large regions of spurious vectors in figure 21 are caused by the variation of focus from left to right for each camera. Since SPIV uses angled cameras to capture the out-of-plane velocity, the subject of each image has a varying distance from the camera. As such, each camera is most focused at the center of the image, with slightly degraded focus towards the edges. This can be alleviated with the addition of schiempflug mounts to the camera setup as discussed in Chapter 2, an addition that would decrease system dependence on the consistency filter and increase accuracy. A full breakdown of the measurement uncertainty for the SPIV system can be seen in Table 1.

Upon completion of post-processing, an average vector field was computed from all image pairs at each velocity. The average velocity across this field was then obtained and compared against the average freestream velocity reported by the wake rake to determine the percent error of the in-plane velocity measured by the stereoscopic PIV system. The data comparisons for the in plane velocities can be seen below:

Nominal Operating Velocity	Wake Rake Velocity (mph)	Stereoscopic PIV Velocity (mph)
25 mph	11.5 ± 0.2	11.5 ± 0.1 (0.1%)
50 mph	22.7 ± 0.2	22.7 ± 0.1 (0.2%)
100 mph	44.9 ± 0.2	44.8 ± 0.1 (0.3%)

Table 2: Stereoscopic PIV System In Plane Velocity Percent Error

To quantify the accuracy of out of plane velocity measurements made by the stereoscopic PIV system, the laser sheet was angled across the freestream direction at a defined angle. This allowed a decomposition of the freestream velocity in the test section to in-plane and out of plane components. A diagram of the test setup can be seen in figure 24.

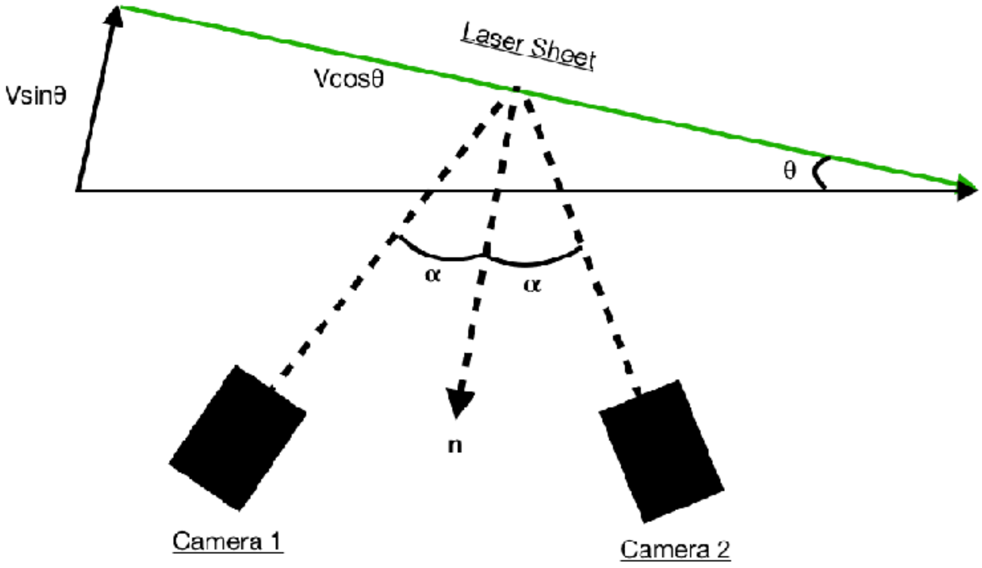

Figure 24: Stereoscopic PIV Out of Plane Velocity Test Setup

A theoretical value for the out of plane velocity was calculated from the average freestream velocity measured by the wake rake during each run. This result was used as the baseline expected value and compared against the output of the stereoscopic PIV system to determine a percent error of the out of plane velocity measurement. The inputs and resulting uncertainties can be seen in table 3, and an example of the out of plane velocity field can be seen in figure 25.

Nominal Operating Velocity	Laser Sheet Angle (deg)	Wake Rake Velocity (m/s)	Stereo In-Plane Velocity (m/s)	Out of Plane Velocity (m/s)	Stereo PIV Out of Plane Velocity (m/s)
25 mph	17.6	11.5 ± 0.2	11.5 ± 0.1 (0.3%)	3.5 ± 0.2	3.4 ± 0.1 (2.9%)
50 mph	17.6	22.6 ± 0.2	22.6 ± 0.1 (0.2%)	6.8 ± 0.2	6.6 ± 0.3 (4.7%)
100 mph	17.6	44.9 ± 0.2	44.8 ± 0.1 (0.2%)	13.6 ± 0.2	13.2 ± 0.4 (3.0%)

Table 3: Stereoscopic PIV Out of Plane Velocity Percent Error

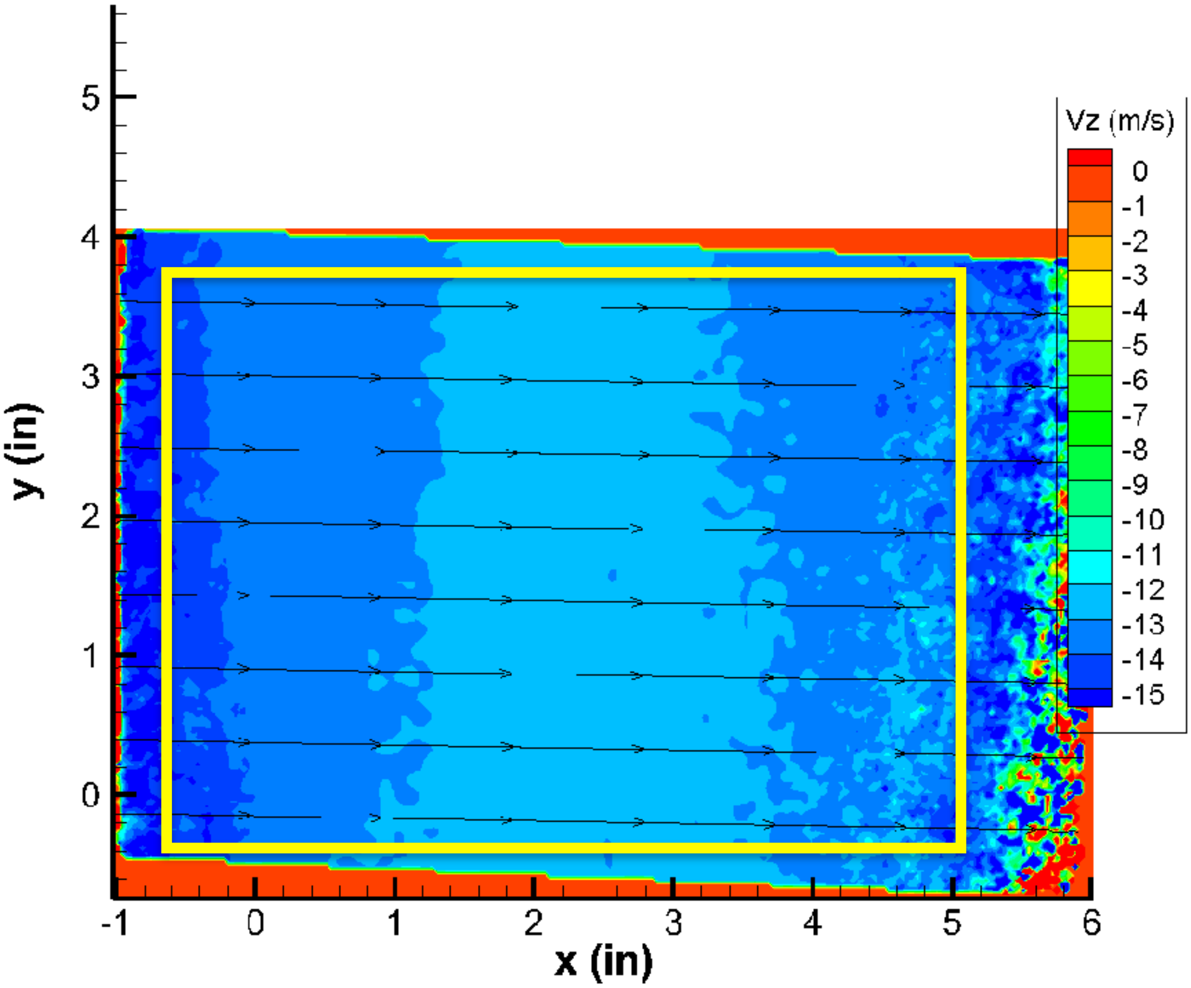

Figure 25: Stereoscopic PIV 100 mph Out-of-Plane Velocities With Bounding Box

This data coupled with the freestream error analysis in Table 3 demonstrates the efficacy of the Stereo PIV system produced through this thesis. All in-plane velocity errors are below 0.5%, maintaining the accuracy standard set with the 2-D PIV system. In fact, the average in-plane velocity error for the Stereo PIV system is slightly lower than the error of the 2-D system. This is largely due to the dual camera aspect of Stereo PIV, which allows for correlation between the image pairs produced by each camera to decrease the error of the method.

The out-of-plane velocity error of the Stereo PIV system also meets the accepted standard for measurement accuracy, maintaining an error below 5%. As discussed in Chapter 2, the out of plane velocity error of Stereo PIV is inherently larger than capturing the same measurement with a fully 3-D method (such as tomographic PIV) due to the planar nature of the light source used in a Stereo setup. However, out of plane measurements in wind tunnel tests are almost always dominated by the flow characteristics in the streamwise direction, making an error below 5% in out of plane measurements sufficient for most wind tunnel applications. Figure 21 also provides a strong example of the effect of varied focus on data quality in SPIV measurements. As discussed with the SPIV in-plane velocity fields, the variation of focus across images captured with SPIV introduces a degree of error that must be eliminated with either post-processing or additional hardware. Figure 25 shows the out-of-plane measurements are significantly impacted by the variation in focus, further demonstrating the importance of schiempflug adapters. With the current system available at the LSWT, the accuracy of out-of plane measurements is highest in the center of the image, with decreasing fidelity towards the edges of the region of interest. As discussed with figures 21-23, this can be mitigated with the inclusion of schiempflug adapters in the SPIV system, allowing the full image to be focused evenly.

3.5 Seeding System Design and Manufacture

As discussed in Chapter 2, effective particle seeding is a tremendous challenge in large scale wind tunnel tests. To achieve effective seed particle density for PIV in large scale environments, selective particle seeding was a necessity. A list of system requirements were developed and discussed with researchers at Arnold Air Force Base in the Engineering Design Complex (AEDC). The resulting list of requirements is as follows:

1. Create a particle column at least 1 foot wide x 0.5 inch deep of sufficient density for successful PIV measurements
2. Deliver the particle column anywhere from floor level to 5 feet above the floor and anywhere across the middle 5 feet of the test section
3. Be configurable such that the particle column may be oriented vertically or horizontally in the test section OR deliver a 1 foot wide x 1 foot deep column
4. Be sufficiently robust to safely enable q = 75 psf operation in the test section and provide a steady particle column position
5. Be capable of installation and removal in less than 1 day (each) OR be sufficiently robust to remain permanently installed and enable operation up to q = 125 psf in the test section
6. Create no more than a 1% wake velocity deficit in the test section
7. Inject particles downstream of any screens or honeycomb to avoid fouling those flow-quality devices

Based on these requirements, a proof of concept particle seeding system was designed and implemented at the LSWT. The seeding system consists of a MDG Touring 5000 APS fog generator, a custom blower, and a custom seeding tube. The seeding tube matches the contour of a symmetric airfoil with a 3” diameter PVC pipe for the leading edge. Particles from the fog generator are piped into the seeding tube with the custom blower, and ejected from the leading edge through 0.25” holes. This produces a curtain of particles that travels downstream from the settling chamber and through the region of interest to provide seeding without flooding the entire test section. Pictures of these components and a diagram of the full assembly can be seen in Figures 26-29.

Figure 26: MDG Fog Generator

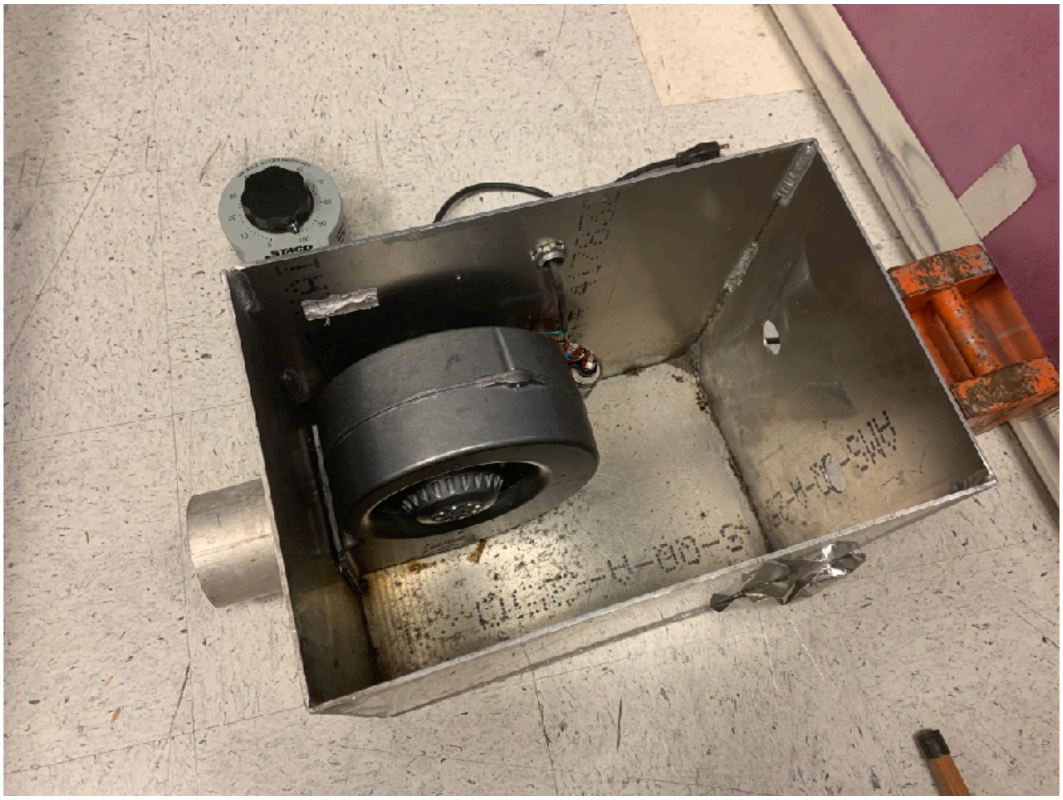

Figure 27: Custom Blower Box (Lid Removed)

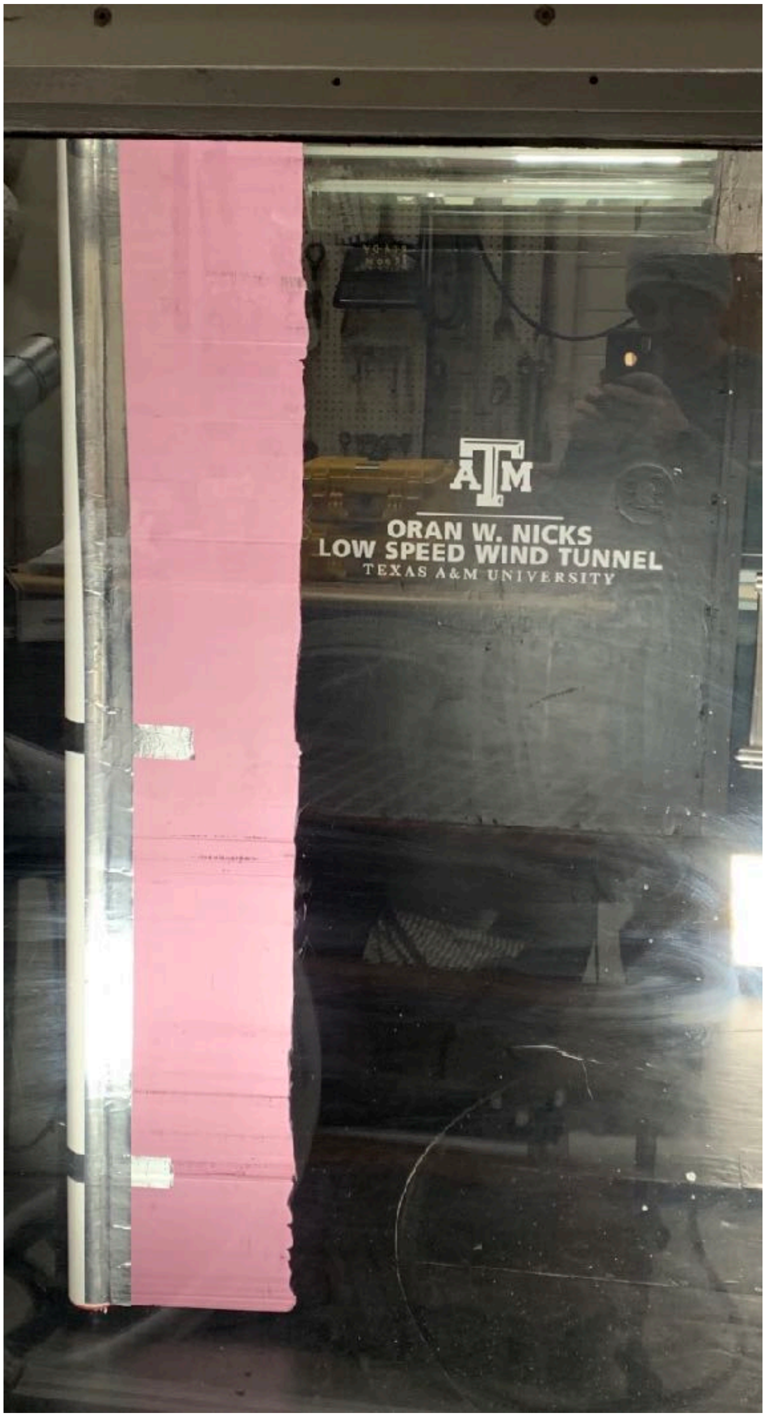

Figure 28: Custom Seeding Tube Center Section (Proof of Concept Test)

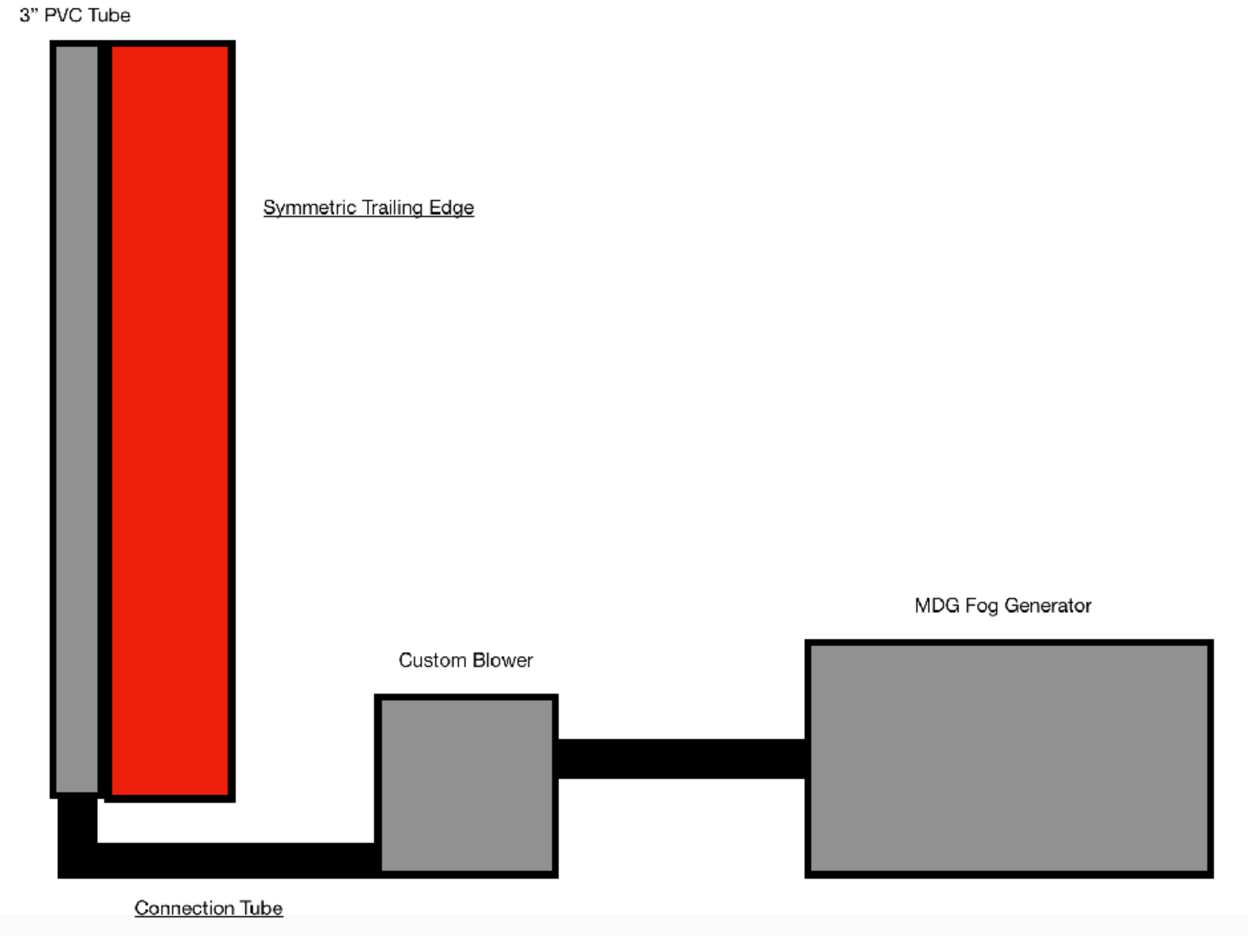

Figure 29: Selective Seeding System Diagram

All components for the seeding system were manufactured on-site at the LSWT. The custom blower box is made of aluminum sheets and angle brackets. A blower fan is bolted inside of the box and is controlled with a variable transformer. The MDG fog generator is connected to the blower box via two 1 inch diameter pipes that are slip fit to the input holes on the box and taped to form a seal. A 2 inch PVC flex pipe connects the blower box output to the custom seeding tube, which consists of a 3 inch PVC pipe and a trailing edge of foamular 250 high density insulation foam. This section is connected to the the settling chamber with two specially designed connections for the floor and ceiling, as seen in Figures 30 and 31.

Figure 30: Selective Seeding System Ceiling Connection

Figure 31: Selective Seeding System Floor Connection

The ceiling connection has three holes spaced 1 inch apart on the top of the PVC end cap. The center hole allows the attachment of a steel cable to an internal pin which allows the system to be lifted to the top of the tunnel via a winch system. The cable is inserted through a hole in the top of the settling chamber and lowered to the floor, where it can be attached to the seeding system. The outer two holes are used to bolt the seeding system to the roof of the tunnel, with bolts originating inside the cap. When the seeding system is lifted into place, the bolts align with holes in the top of the settling chamber where they are each locked into place with a nut. The floor connection is designed to admit the PVC flex pipe and improve the configurability of the design. During installation, the two aluminum support blocks at the bottom of the system are removed to allow the assembly of the full seeding system. Once the ceiling connection is secure, the support blocks are bolted to the bottom of the system and then to the bottom of the tunnel. When coupled with the pinned connections between each section of PVC pipe, this design puts the full system in tension, helping to eliminate any vortex induced vibrations that could occur during testing.

The trailing edge foam of the seeding system was cut into a symmetric airfoil using a hot wire cutter. A wedge with a 140˚ interior angle was cut into the leading edge of the foam to provide two points of contact along the PVC pipe, and the foam was fastened into place with aluminum tape. Aluminum tape was used in place of a more permanent bond to allow testing with and without the trailing edge, as well as testing with particle distribution holes at varying angles relative to the trailing edge. The preliminary design can be seen in figure 32.

Figure 32: Preliminary System Check Smoke Sheet

Based on the performance of the selective seeding system during preliminary system checks, the system was evaluated for performance against the requirements listed in table 2.

3.6 Seeding System Validation

To verify that the selective seeding system met its flow quality requirements the velocity deficit caused by the system and the quality of seeding was evaluated. Its velocity deficit was measured with the seeding system installed and operating in the test section with a 10 mph flow.

This velocity was selected to simulate the anticipated velocity in the settling chamber during a standard 100 mph test. This installation was captured in figure 28. The wake rake was used to measure the velocity across the test section 3 feet behind the trailing edge of the seeding system. Multiple rake positions were combined to create the velocity deficit plot seen in figure 33.

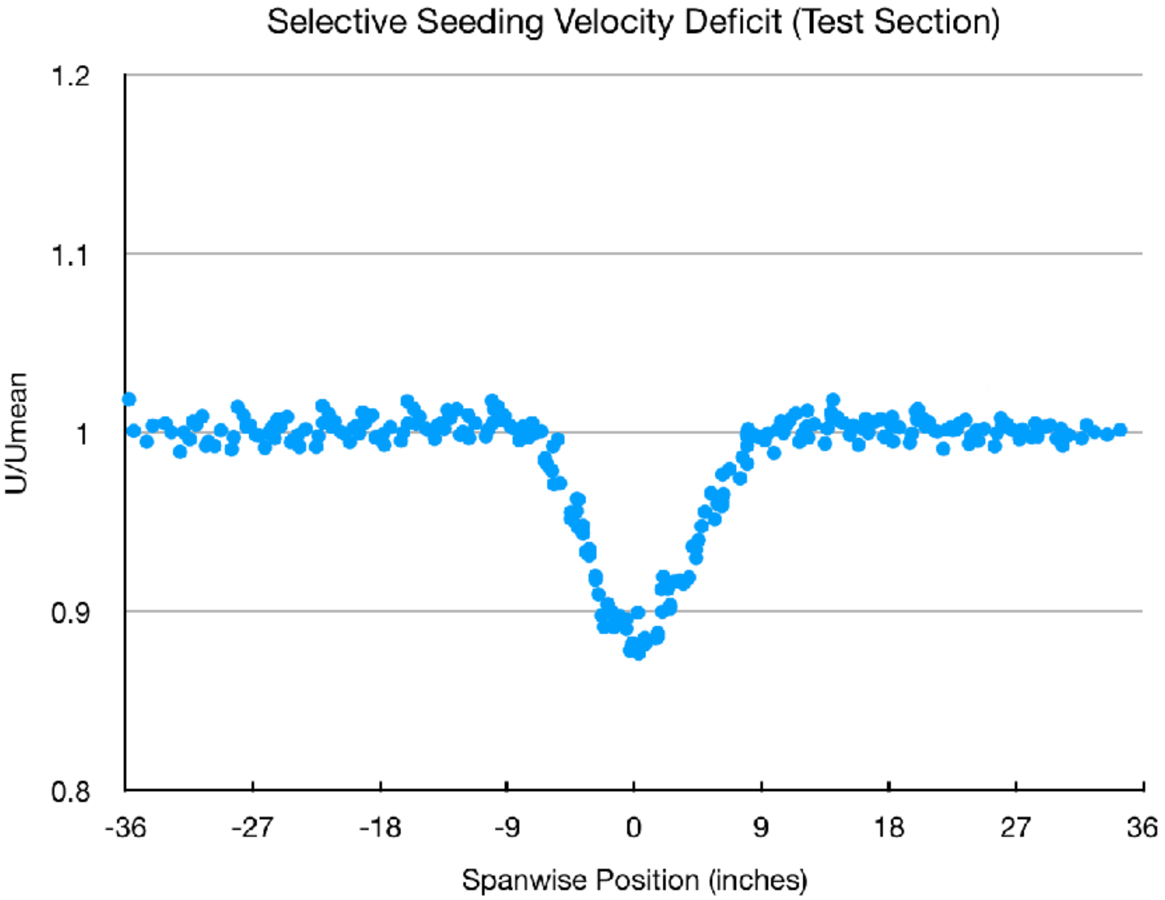

Figure 33: Selective Seeding System Velocity Deficit 3 ft Downstream

This plot shows the velocity behind the seeding system is approximately 90% of the freestream velocity. When the system is moved upstream of the contraction, the expected velocity deficit would significantly decrease due to transition upstream to the settling chamber. The increased distance from the seeding system to the region of interest coupled with the effects of the 10:1

contraction were estimated as sufficient to bring the wake velocity deficit in the region of interest below 1% of the freestream velocity in the test section. Based on this result, the design was moved to the settling chamber for further testing and evaluation.

To verify the structural stability of the system when installed in the 30-ft diameter settling chamber, a full model of the selective seeding system was designed and tested using the FEA package in Solidworks 2019. A drag coefficient of 0.2 was determined using the wake integral for the seeding system, and a lift coefficient of 0.1 was estimated based on the worst case alignment of the system during installation. These values were used to calculate expected loads for the selective seeding system at 10 mph and 20 mph. Both velocities were selected based on the design of the LSWT, which has a 10:1 contraction between the settling chamber and the test section. This means that a 10 to 20 mph flow experienced by the seeding system in the settling chamber corresponds to a 100 mph to 200 mph flow in the test section. No PIV tests would be conducted above 200 mph. The foam portion of the airfoil was included in the drag and lift estimates, but was not included in the FEA analysis. This is because the bond between the foam and the PVC pipe is not sufficient for a good transfer of stress. Thus, all loading on the system will be experienced by the PVC pipe in the leading edge of the seeding system. The connection between the seeding system and the floor of the settling chamber was modeled as a fixed connection, and the connection between the seeding system and the ceiling was modeled as a hinged connection. These particular interactions were selected based on the connections designed for each location. In total, four load cases were simulated as seen in Table 4. An example deflection plot for the 10 mph drag load case can be seen in figure 34.

Load Case	Applied Load (N)	Maximum Deflection (mm)	Maximum Von Mises Stress (MPa)	Maximum Strain
10 mph Drag	1.7	3.1	1.4	4.4E-04
10 mph Lift	3.9	7.0	3.2	9.9E-04
20 mph Drag	6.9	12.5	5.7	1.8E-03
20 mph Lift	15.7	28.1	12.9	3.9E-03

Table 4: Seeding System Structural Evaluation

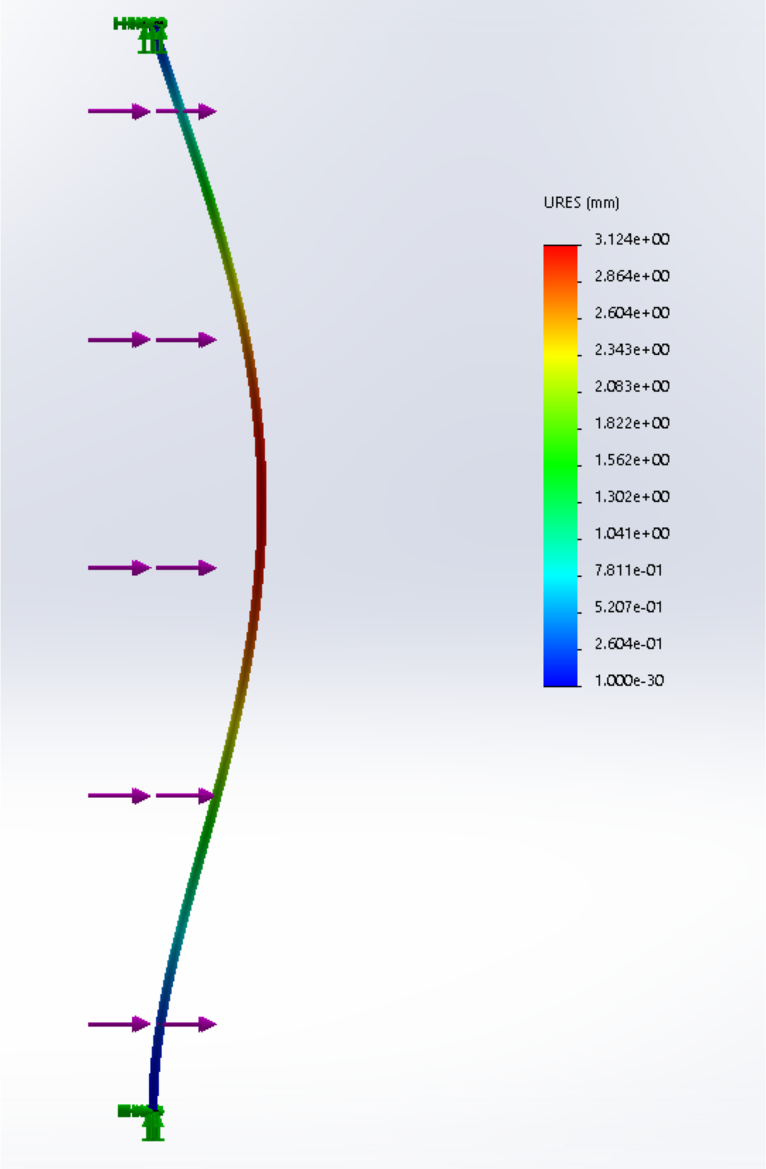

Figure 34: 10 mph Drag Load Case: Deflection

This structural analysis confirmed the structural viability of the selective seeding system. PVC is commonly cited as having a yield stress of 55 MPa, well above the maximum yield stress experienced by the system. Furthermore, the maximum deflection of the system under any simulated load condition was 14 mm in the middle of the system. This deflection is small in comparison to the size of the system, so the aerodynamic properties behind the system are not expected to change under load. This all suggests the system is sufficiently rigid without additional support.

In addition to capturing the wake velocity deficit and estimating the loads on the selective seeding system, stereoscopic PIV data was taken behind the seeding system to verify the quality of smoke produced by the system. Seed particles were injected into the flow in short bursts, which were captured with the stereoscopic PIV system. All data was compiled and analyzed with DaVis 8.4.0 to ensure the seeding density was high enough to produce quality PIV data. An example set of images for the smoke quality test and the corresponding flow field can be seen in figures 35 and 36.

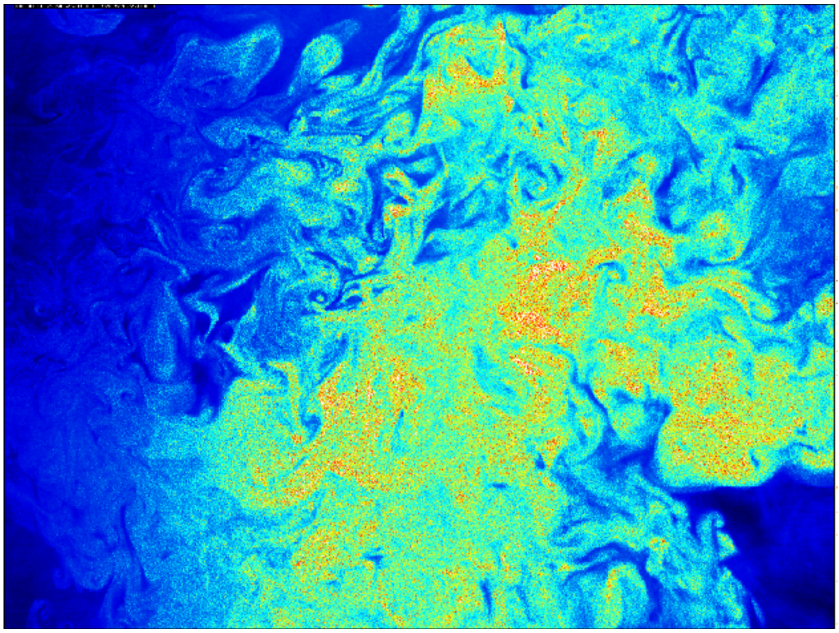

Figure 35: Selective Seeding Smoke Quality Example

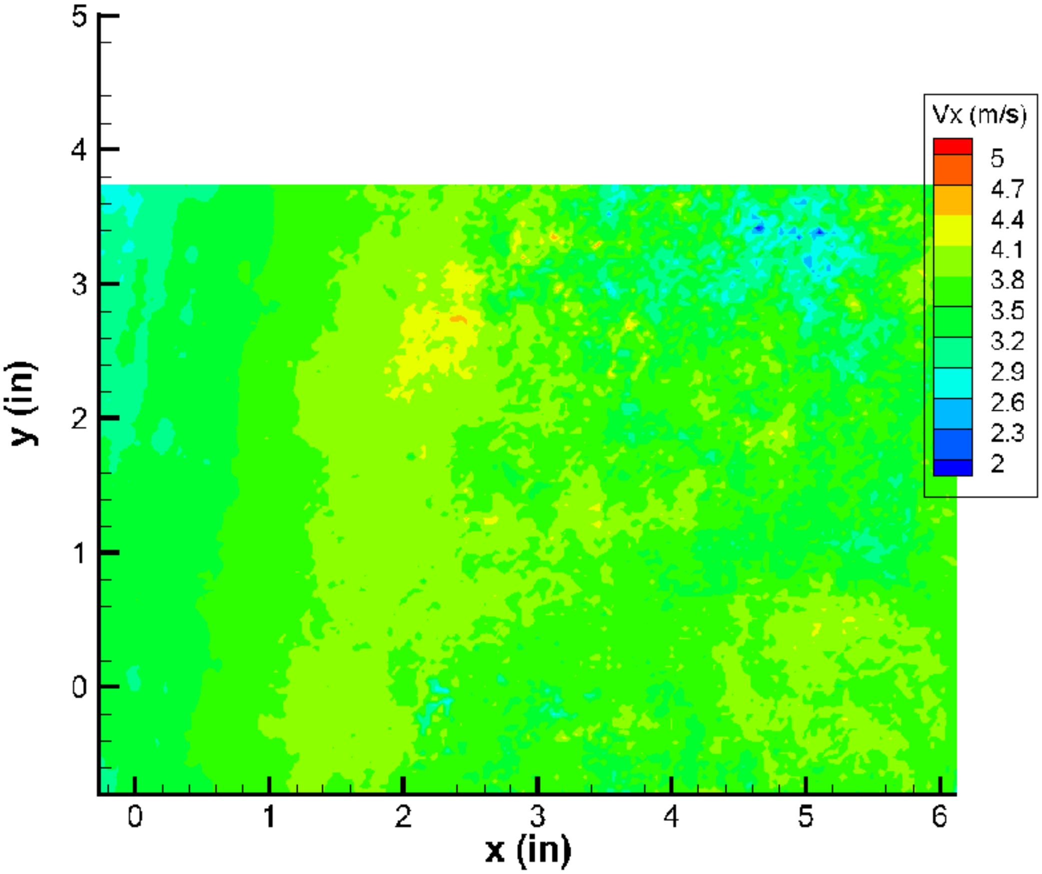

Figure 36: Selective Seeding Smoke Quality Example Flow Field

This data shows the smokescreen generated by the system is of a sufficient quality to produce successful PIV data. Figure 35 shows a dense set of particles in the the region of interest that can be analyzed by the PIV software. This image can be taken as a best case image for selective seeding with the current system. During testing, it was noted that particle density in each image varied due to the non-homogeneous nature of the smoke column produced. As such, larger datasets are required to ensure the average velocity fields produced are accurate. The average velocity field produced from the smoke quality test in Figure 36 shows the flow accelerating as it moves away from the trailing edge (located 1 foot upstream of the depicted velocity field). This is expected near the trailing edge of an airfoil, demonstrating the selective seeding system's ability to produce smoke sufficiently dense for successful PIV measurements.

After verifying the velocity deficit and smoke quality of the seeding system, the full design was implemented in the settling chamber of the LSWT. Based on the configurable design of the system, the seeding section may be placed in the either the upper, middle, or bottom 10 feet of the settling chamber during installation. An installation with the seeding section in the middle 10 feet of the settling chamber can be seen in figure 37.

Figure 37: Selective Seeding System (Installed)

In total, the full installation of the selective seeding system took 6.5 hours from start to finish during its first installation. This satisfies meeting requirement 7 as listed on page 55. The configurable nature of the system ensures that smoke can be delivered at any vertical position in the tunnel, satisfying requirement 2, and the placement of the system downstream of the vanes and screen in the settling chamber satisfies requirement 7. Additionally, due to the approximately constant diameter of the settling chamber, this system can be installed in either a vertical or horizontal orientation, satisfying requirement 3. It is important to note that horizontal installation in the LSWT necessitates the use of scaffolding both inside the settling chamber and outside the tunnel to fasten the system into place. Furthermore, each installation orientation requires a unique set of holes in the shell of the settling chamber. As such, the data for this thesis focuses solely on data collected from a vertically-oriented installation, to minimize the number of holes created in the settling chamber and the acquisition of additional equipment.

After the system installation was complete, a second velocity deficit was taken with the system installed to ensure the velocity deficit met the 1% tolerance outlined in requirement 6. The validation was run at 75 mph, and produced the deficit plot in figure 38.

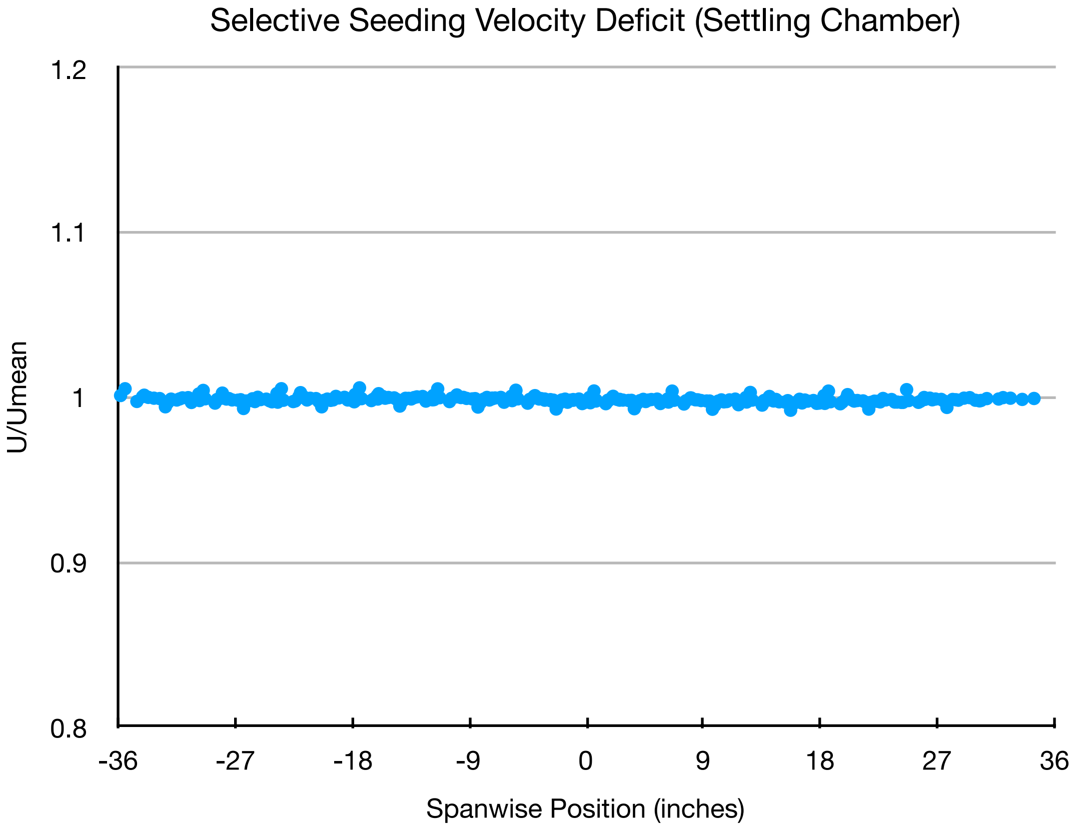

Figure 38: Velocity Deficit With Seeding System Installed in the Settling Chamber

This plot is very significant, as it confirms the expectation that the contraction between the settling chamber and the test section eliminates any measurable velocity deficit produced by the seeding system.

Finally, the smoke column produced by the seeding system had to be evaluated to ensure the smoke sheet generated was at least 1 ft tall by 0.5 in thick at any point in the test section.

This was accomplished by running the tunnel at 25 mph and capturing images of the seed particles passing over dimensioned instruments in the test section. The resulting images can be seen in figures 39-42.

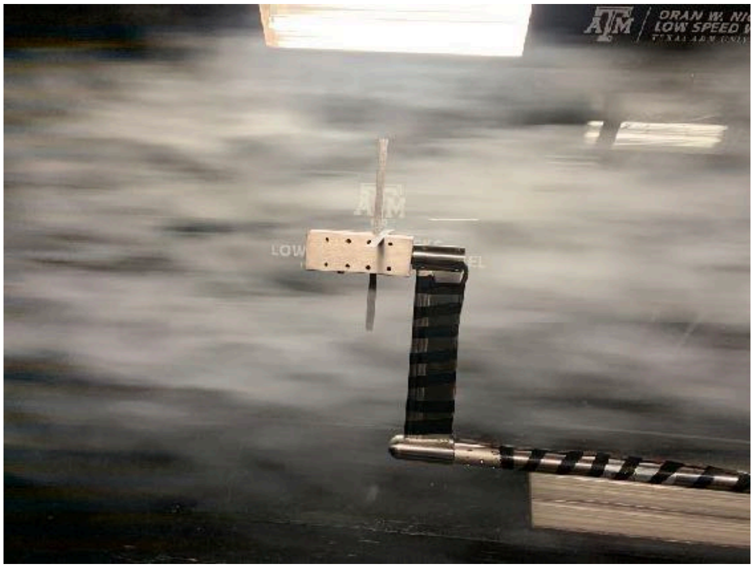

Figure 39: Selective Seeding Column Height (Centered Particles)

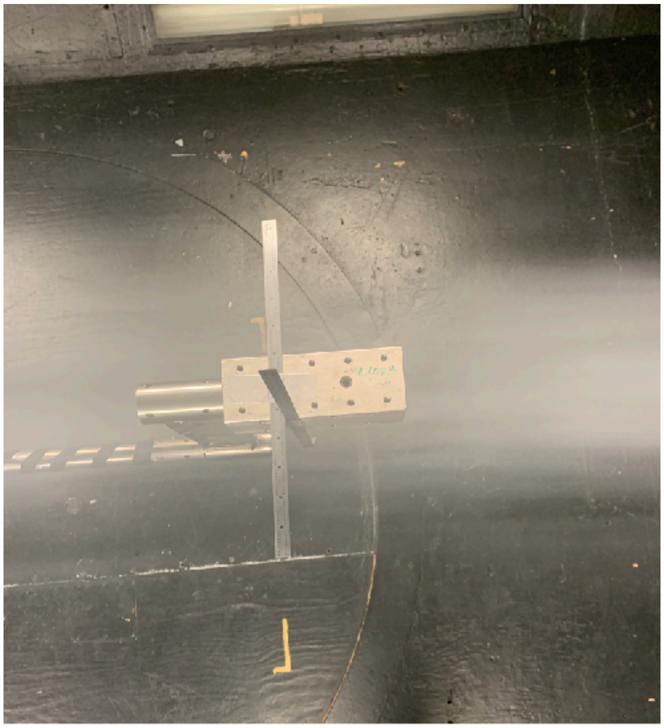

Figure 40: Selective Seeding Column Thickness (Centered Particles)

Figure 41: Selective Seeding Column Height (Particles at Floor Level)

Figure 42: Selective Seeding Column Thickness (Particles at Floor Level)

These images demonstrate the ability of the selective seeding system to produce a sufficiently large column of particles to effectively conduct PIV measurements in a large scale environment. The centered particle column has a height well above the desired 1 ft measurement, and a thickness of approximately 8 inches. When the particle column is located near the floor, the height decreases slightly but remains at approximately 1.5 ft, with the thickness increasing to 1.5 ft. In both cases, the seeding column produced by the system is well beyond the minimum dimensions listed in requirement 1 on page 55.

4. APPLICATION EXAMPLES

Chapter 3 detailed the design, production, and validation of each individual system produced for this thesis. After completion of all validation steps, the systems were used for multiple tests at the LSWT to demonstrate viable use cases for the systems in future production level tests. Chapter 4 details the results of these application tests.

4.1 HARS Flow Quality Test

This test serves as an application example for 2-D PIV with a fully seeded tunnel at the LSWT. In order to demonstrate effective implementation of 2-D PIV at the LSWT, the system was used to measure and evaluate the improvement in flow quality over the bullet of the High Attitude Robotic Sting (HARS). This system is used to mount a wide variety of models at the LSWT, and was recently redesigned to decrease the aerodynamic impact of the bullet on the tail end of models tested at the LSWT. Images of the old and new designs can be seen in figures 43 and 44.

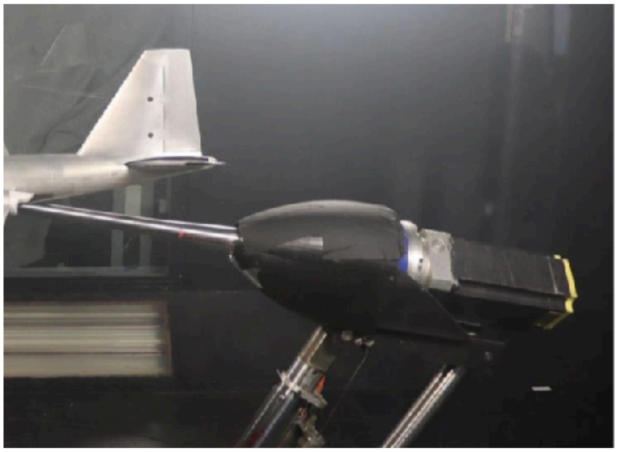

Figure 43: Old HARS Bullet

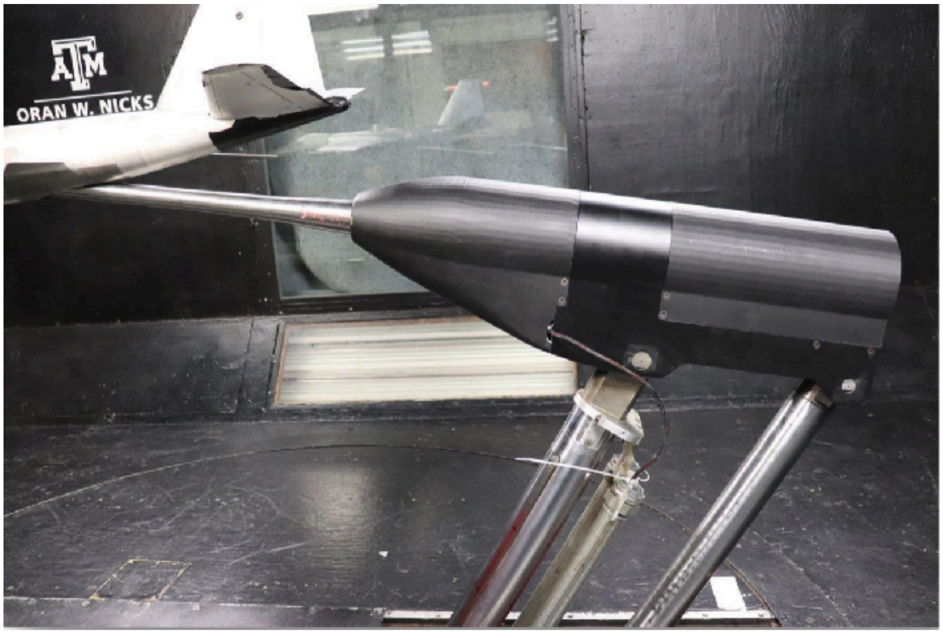

Figure 44: New HARS Bullet

The lower profile of the new design is intended to decrease the upflow angle near the tail of the model visible in figures 43 and 44. PIV data is intended to test this hypothesis. Capturing this data would be nearly impossible with the standard equipment at the LSWT due to the location of the region of interest, making the test an ideal application for 2-D PIV. Data was captured in a square region of interest aligned with the nose of the old HARS bullet design, two inches above the sting. This placement was selected to eliminate reflections from the sting in the final images, as well as capture the impact of each design on upflow angle near the location of the WB-57 tail when installed. A diagram of region of interest placement for both the old and new HARS bullet designs can be seen in figures 45 and 46.

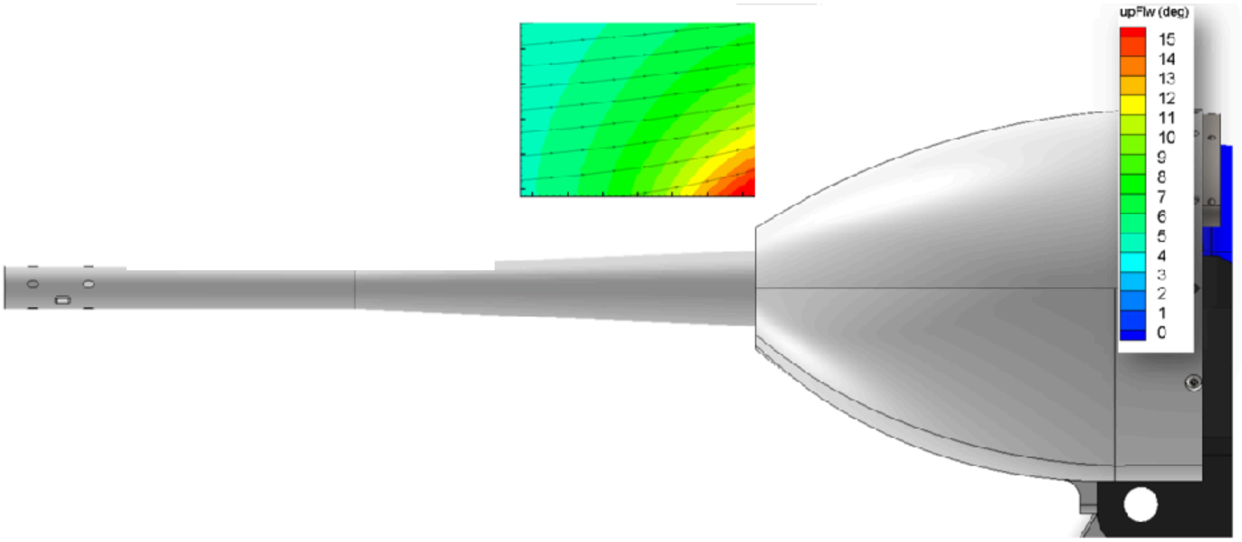

Figure 45: Old Bullet Region of Interest Placement

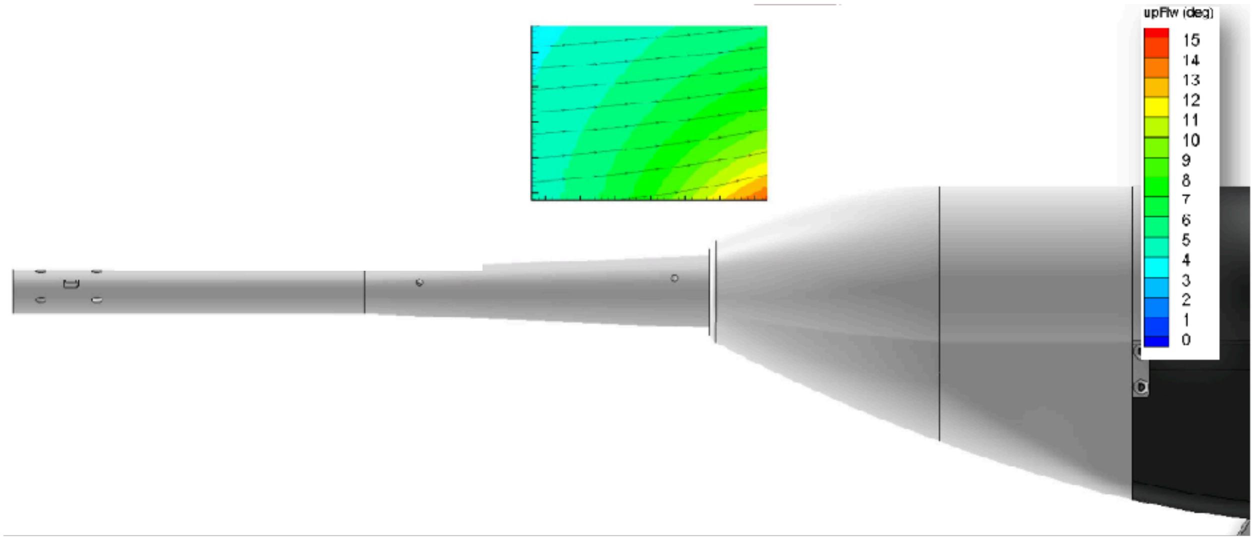

Figure 46: New Bullet Region of Interest Placement

Larger versions of the inset PIV data plots near the bullet are shown in figures 47 and 48, and corresponding velocity uncertainty plots can be seen in figures 49 and 50. These plots show a clear decrease in upflow angle with the design change, confirming the efficacy of the new design. In addition, this experiment demonstrates that the PIV system developed for use at the

LSWT can usefully quantify a 2-D velocity field in a region of interest, a capability that has been previously lacking at the LSWT. Additional information about these tests is given by Miller, Leber, Brown and White (2020).

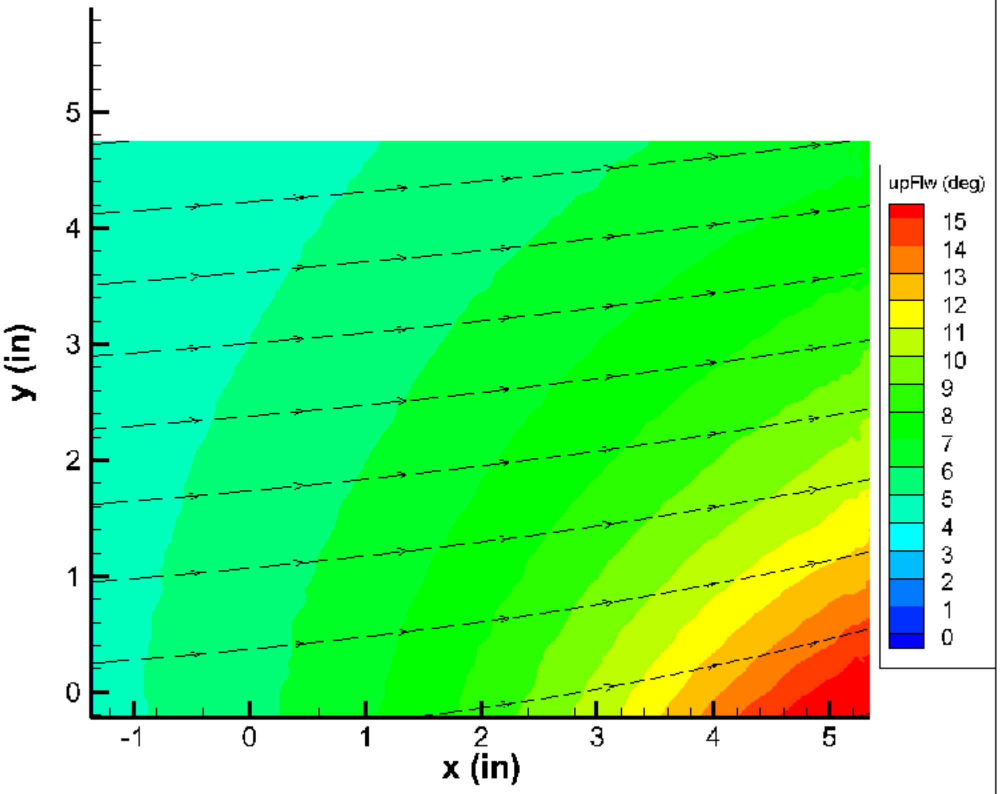

Figure 47: Old Bullet Nose Upflow Angle

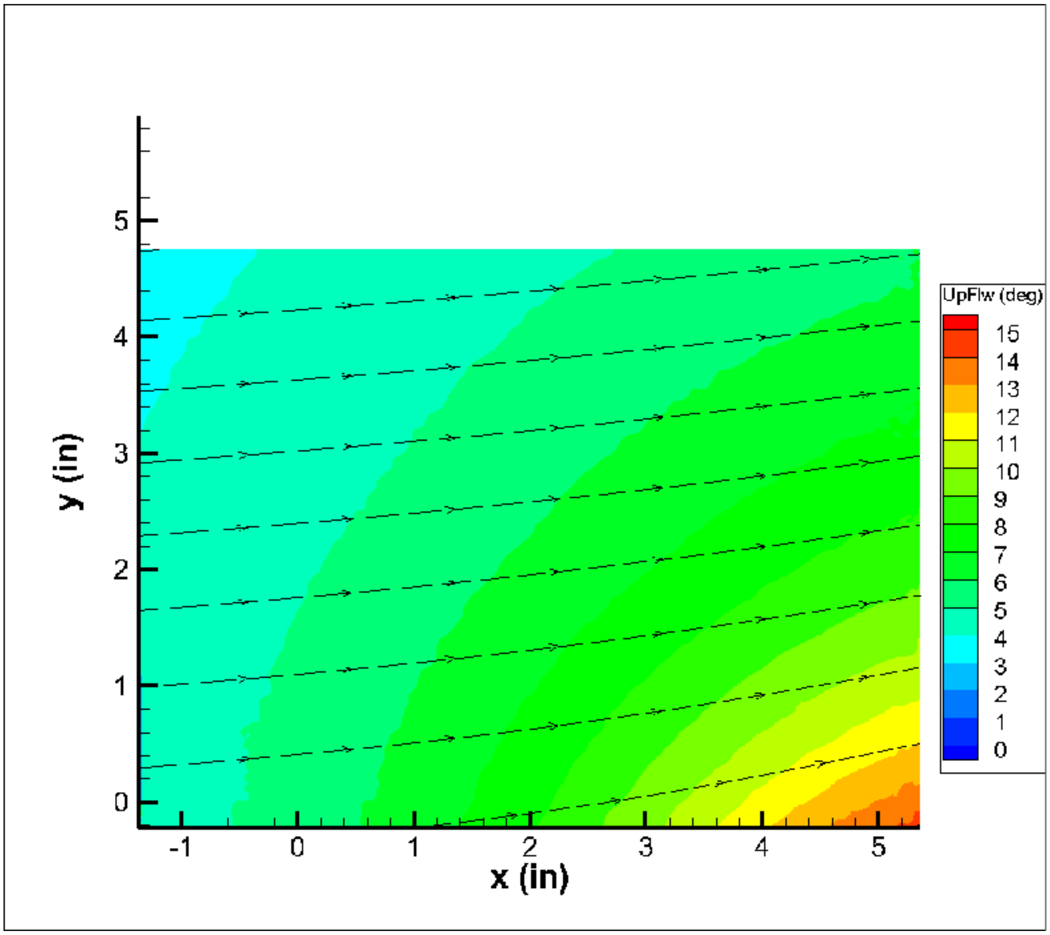

Figure 48: New Bullet Nose Upflow Angle

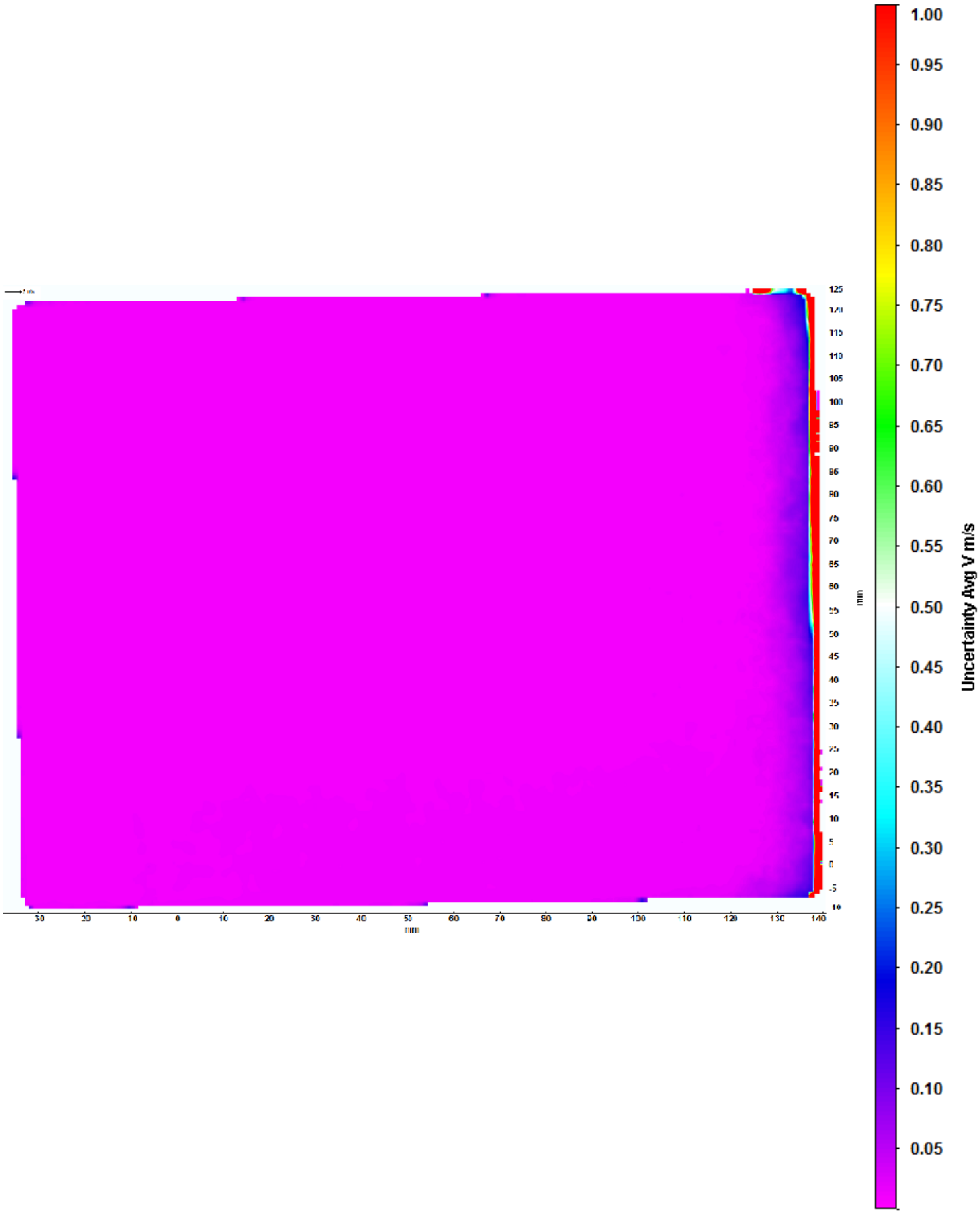

Figure 49: Old Bullet Velocity Uncertainty Plot

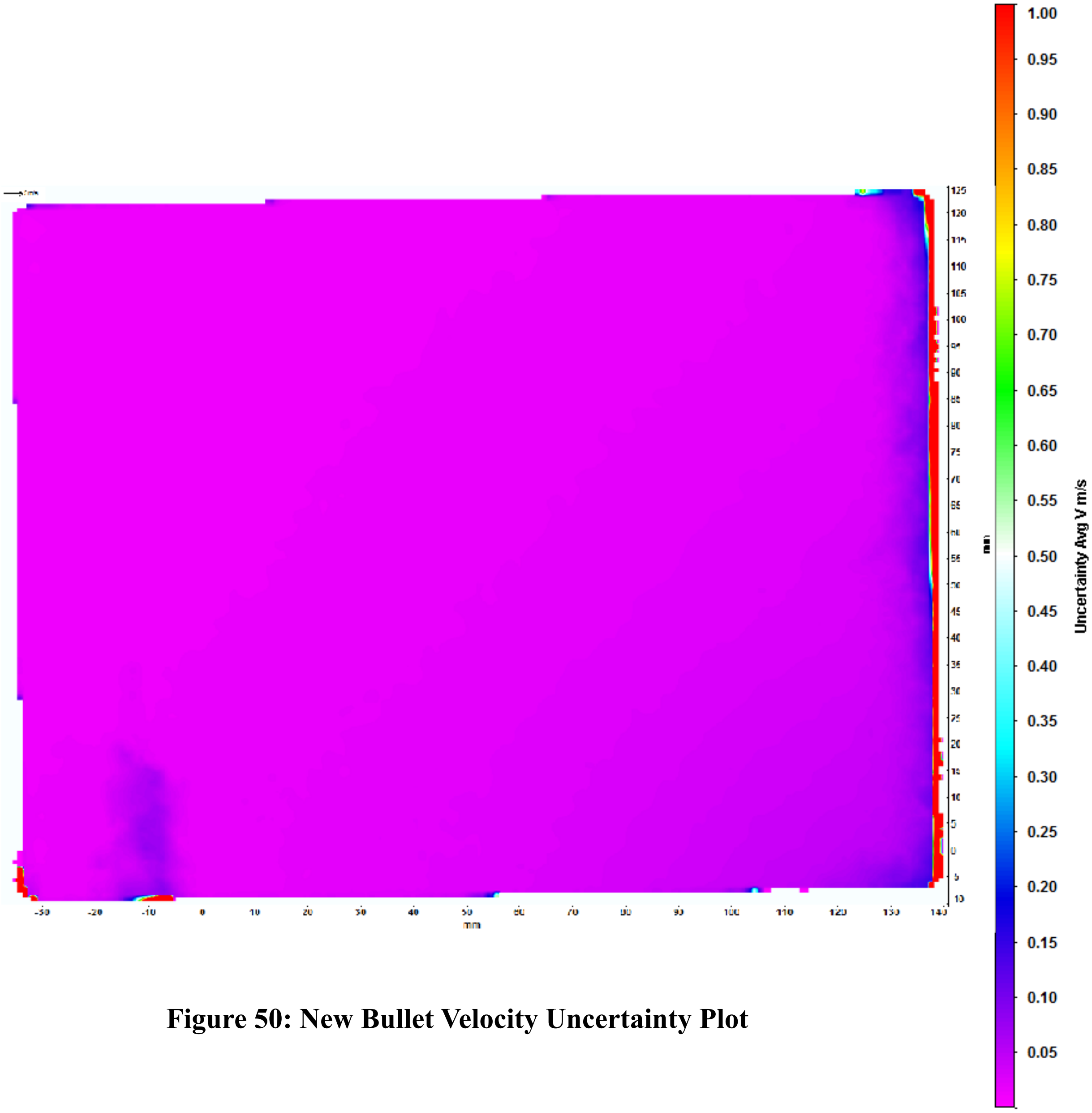

Figure 50: New Bullet Velocity Uncertainty Plot

Figures 47 and 48 show a clear decrease in upflow angle near the nose of the bullet with the implementation of the new bullet design.

4.2 WB-57 3-D Flow Field Test

The second application example demonstrates Stereoscopic PIV using selective seeding. During normal operation, PIV measurements of both in-plane and out of plane velocities could be a desired output of the system. As such, stereoscopic PIV data was captured for both an angle of attack (alpha) sweep and a sideslip (beta) sweep to demonstrate the efficacy of the system.

The WB-57 is an aluminum model produced by the LSWT for a previous NASA test. The model is representative of many of the tests conducted at the LSWT. Images of the model can be seen in Figures 51 and 52.

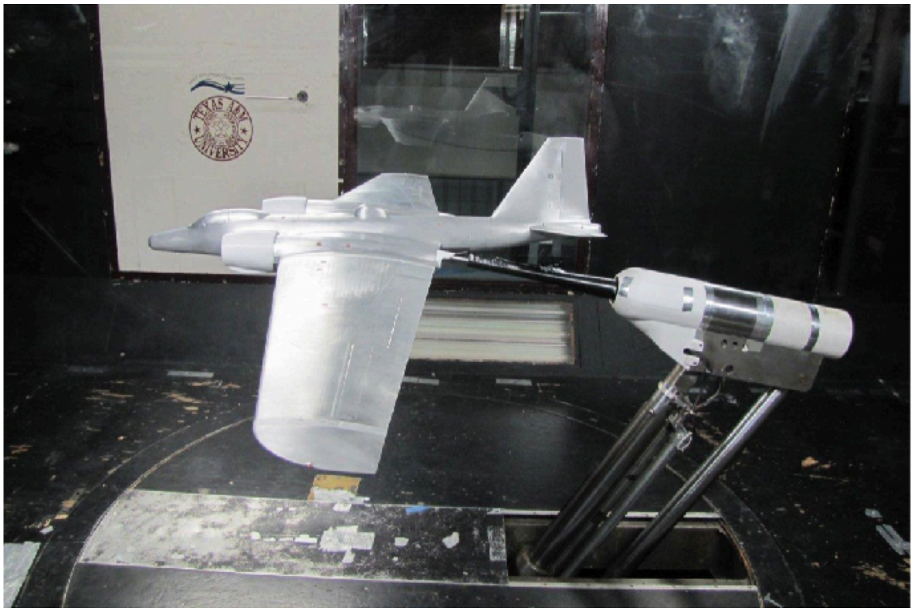

Figure 51: WB-57 Model (Side View)

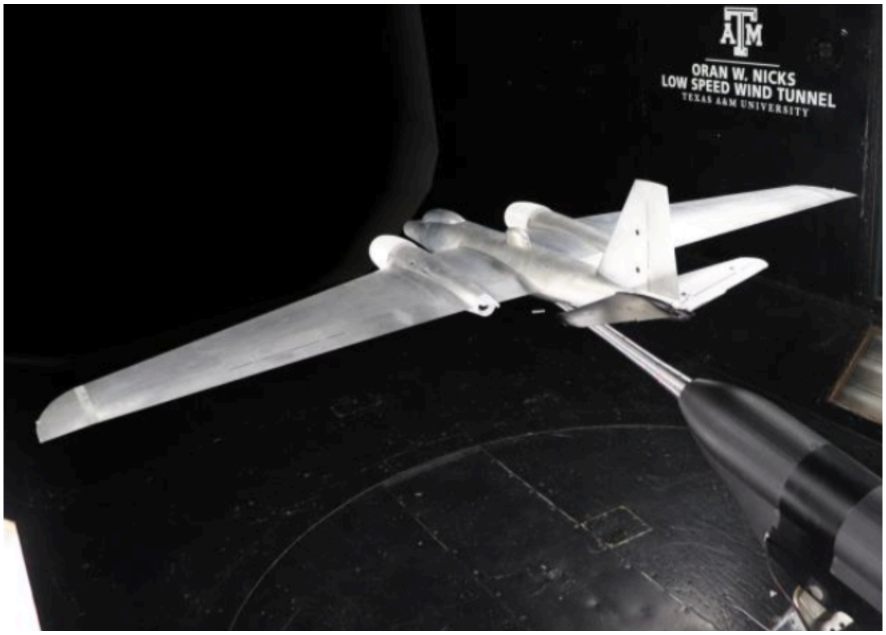

Figure 52: WB-57 Model (Rear View)

For this thesis, the WB-57 model was selected for the stereoscopic PIV application example to simulate a standard LSWT production level test. As discussed in Chapter 1, customers are often interested in the aerodynamic causes for loads output by the internal and external balances during tests. Conducting PIV for an alpha and beta sweep of the WB-57 provides insight into the aerodynamics of the model as it approaches stall conditions.

The alpha sweep test was used to measure velocities above and behind the trailing edge of the WB-57 wing. Measurements were taken sufficiently close to the top surface of the wing such that data acquisition with existing equipment at the LSWT would not have been possible without disrupting the flow characteristics in the region of interest. To begin, an alpha sweep without PIV data was used to produce a lift coefficient versus alpha plot to determine the stall angle of the WB-57 model. The plot can be seen in figure 53.

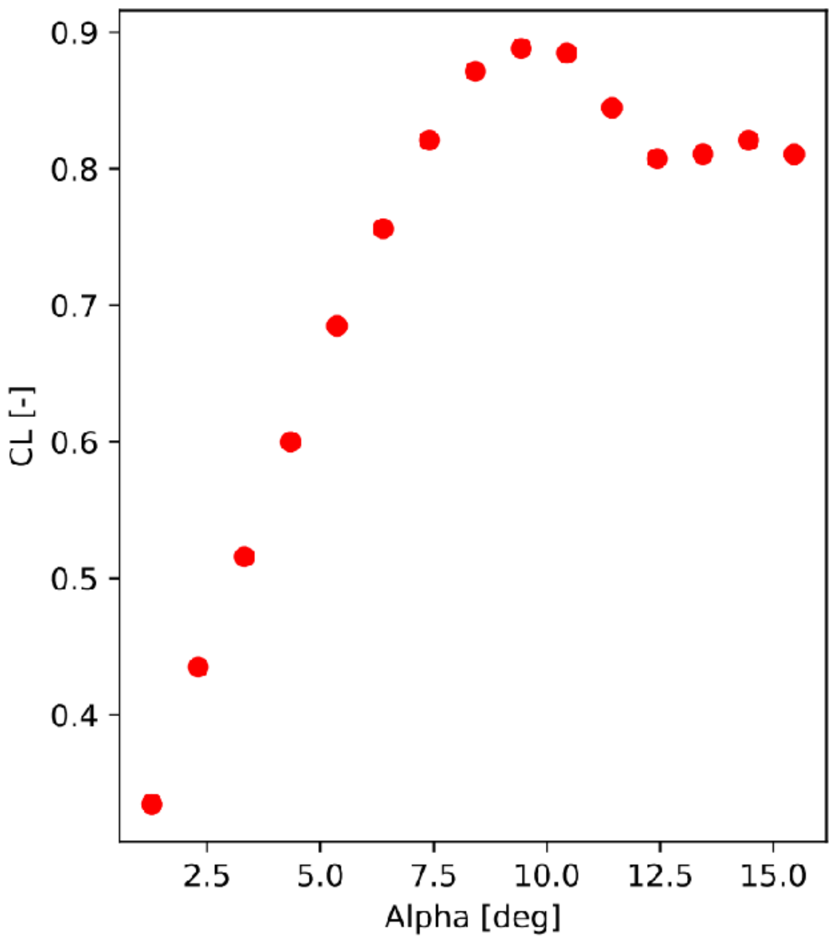

Figure 53: Lift Coefficient versus alpha for WB-57

Based on this data, five discrete angles of attack were chosen that corresponded with five distinct flight conditions level flight (0˚ angle of attack), low angle of attack (2.5˚), moderate angle of attack (5˚), Stalled flight (10˚ angle of attack) and well beyond stall (15˚ angle of attack). These conditions were selected to provide insight into how the flow characteristics behind the WB-57 wing change as the aircraft approaches and passes through stall. A diagram of region of interest placement can be seen in figure 54, and an approximate region of interest location on the real-world model can be seen in figure 55.

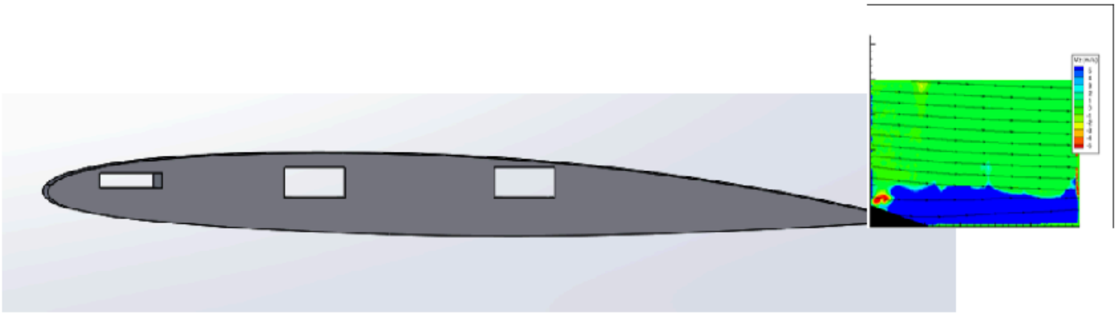

Figure 54: WB-57 Alpha Sweep Region of Interest Placement

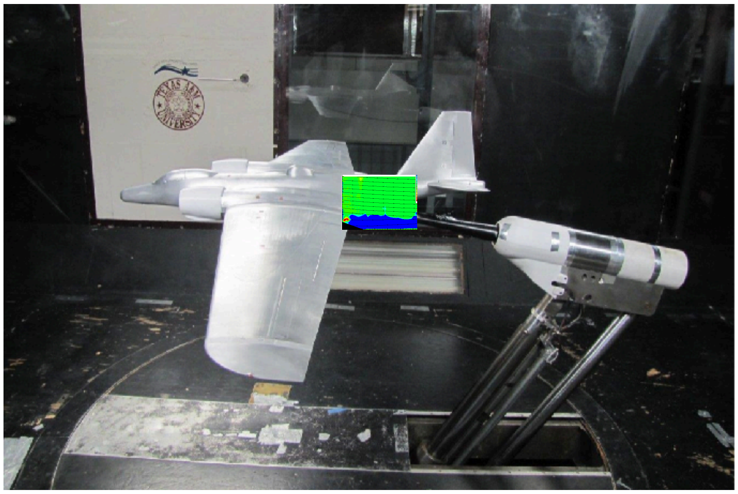

Figure 55: Alpha Sweep Region of Interest on Real-World Model

Each plot contains a black triangle the lower left corner that outlines the placement of the WB-57 wing. The trailing edge of the wing intersects with the x-axis in each plot. Figures 56-60 give the progression through the alpha sweep, while figures 61-65 provide the corresponding velocity uncertainty fields. Streamlines are generated from streamwise (Vx) and vertical (Vy) velocities. Spanwise velocity (Vz) is depicted with a color contour, with positive Vz out of the page.

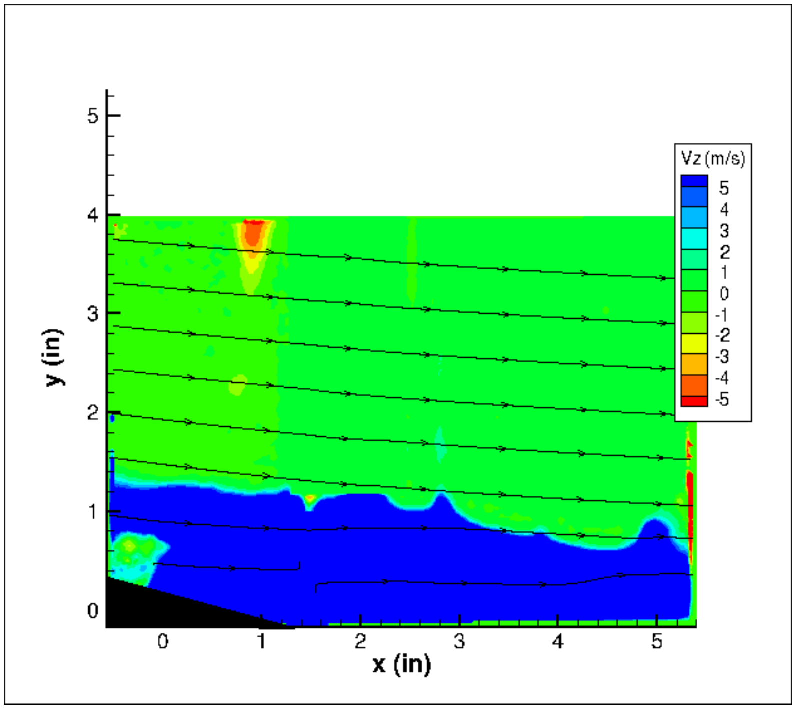

Figure 56: WB-57 0° AOA PIV Results

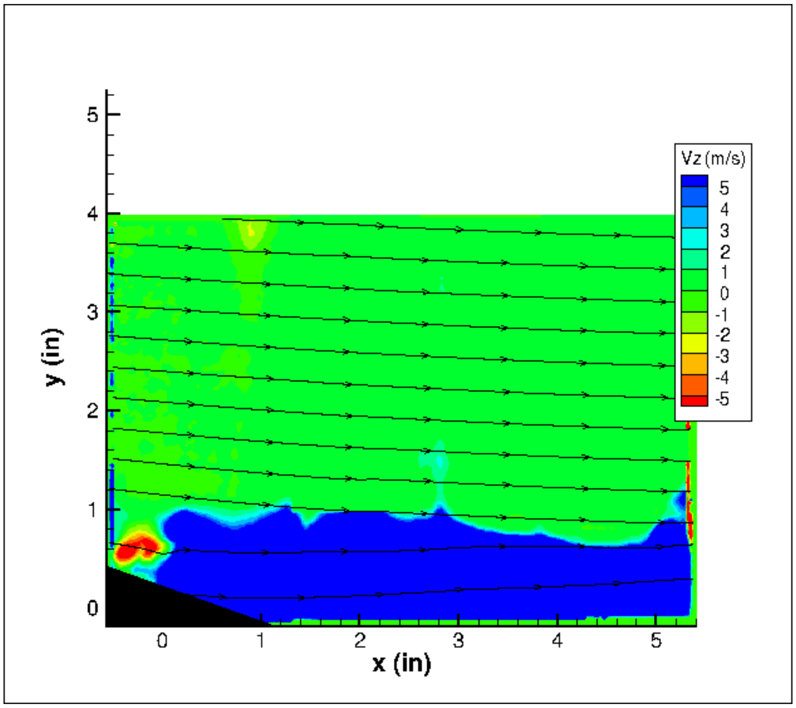

Figure 57: WB-57 2.5° AOA PIV Results

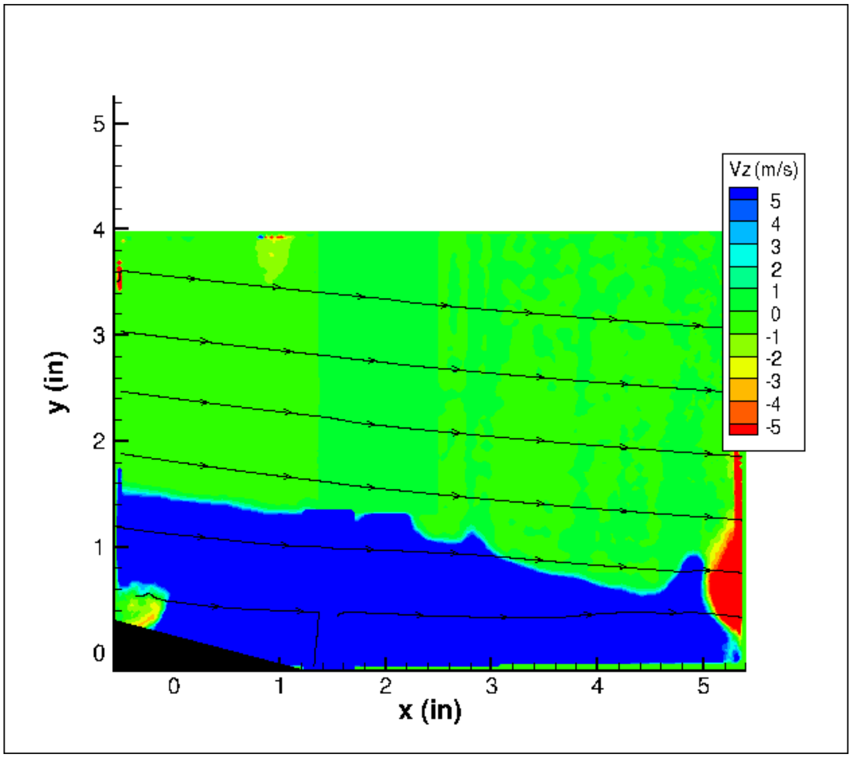

Figure 58: WB-57 5° AOA PIV Results

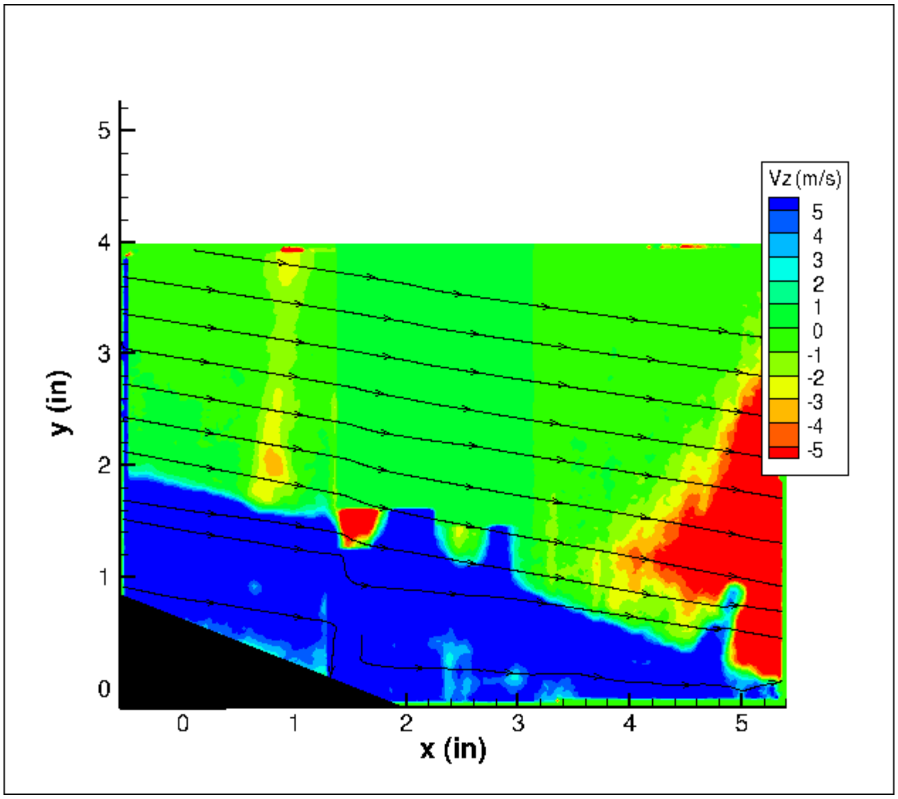

Figure 59: WB-57 10° AOA PIV Results

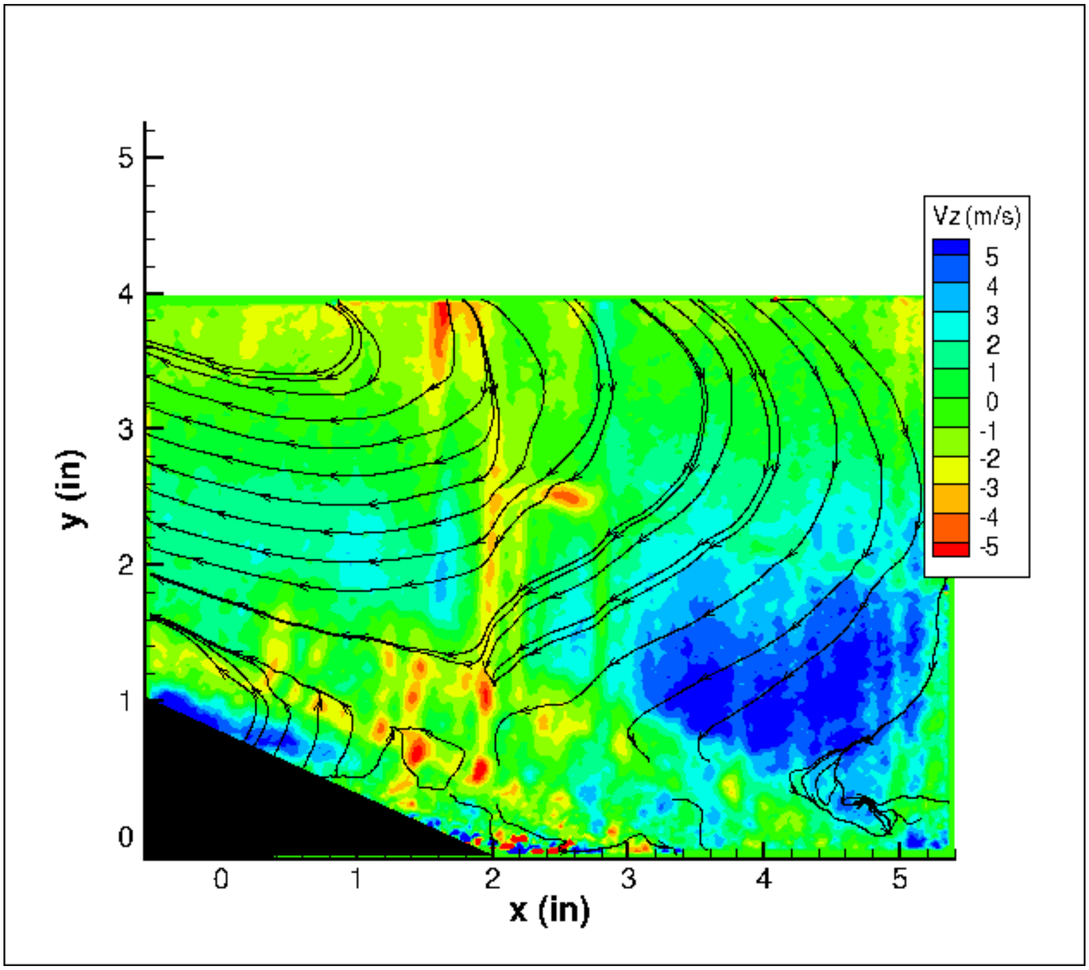

Figure 60: WB-57 15° AOA PIV Results

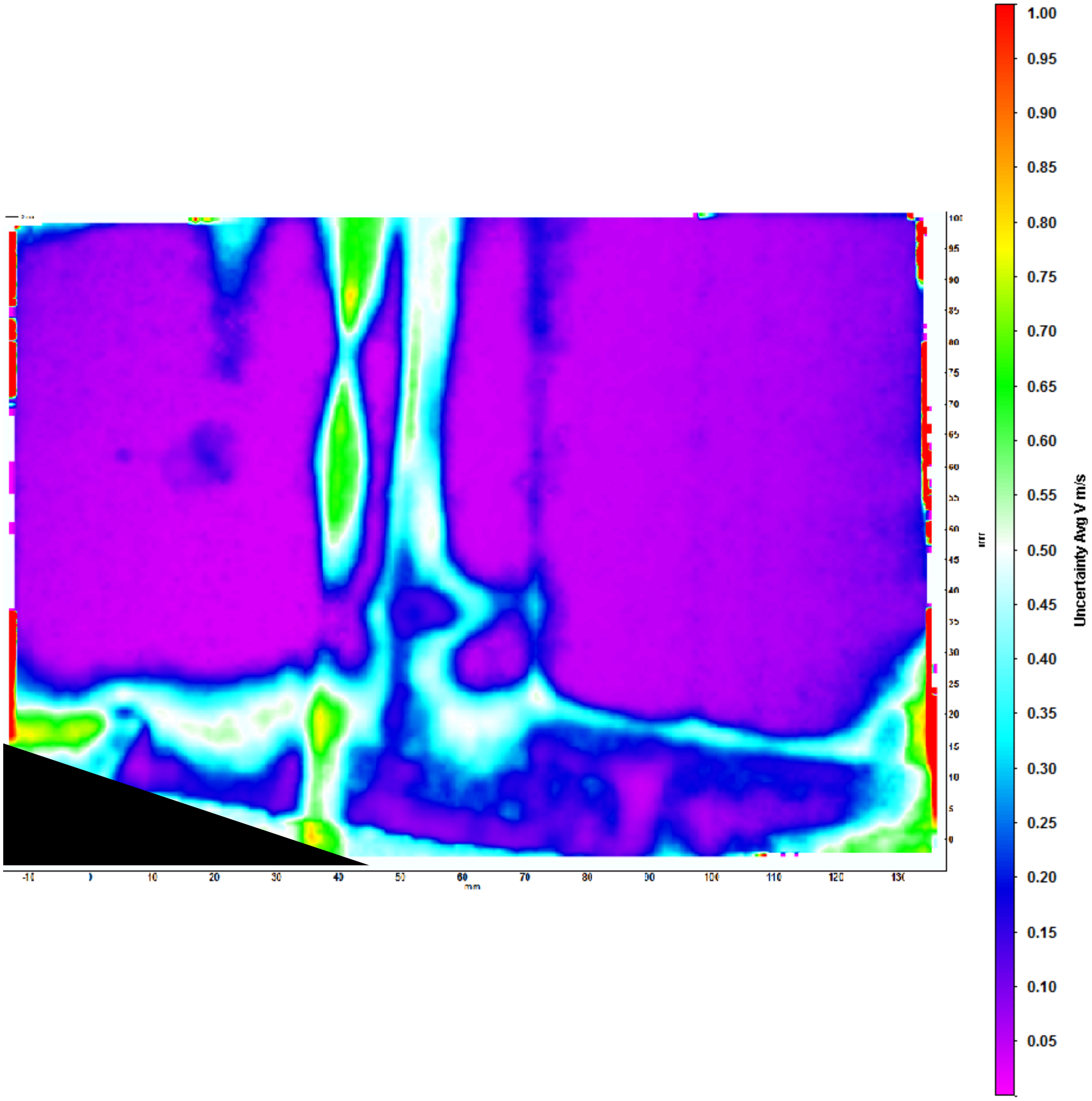

Figure 61: WB-57 0° AOA Velocity Uncertainty Plot

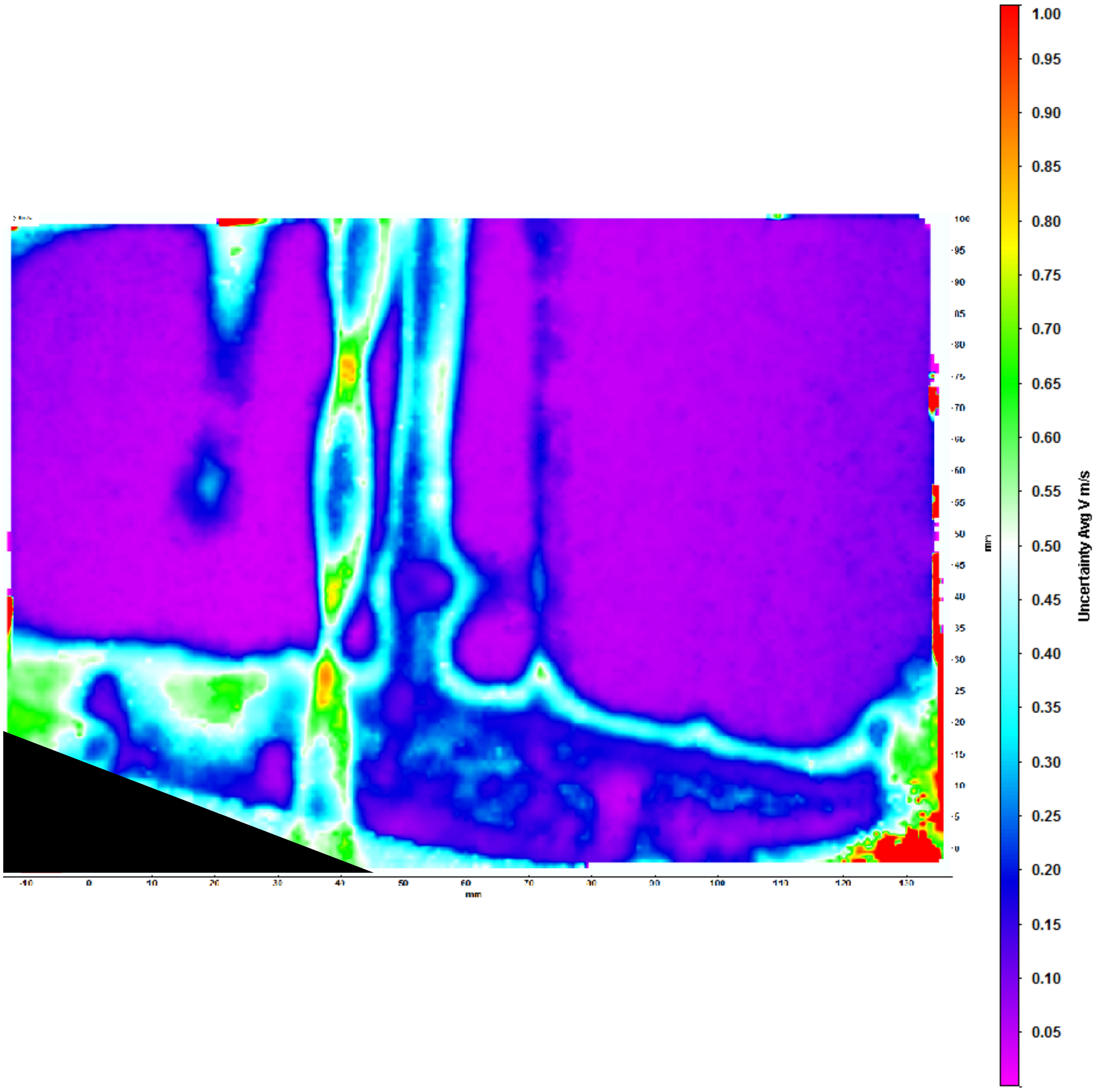

Figure 62: WB-57 2.5° AOA Velocity Uncertainty Plot

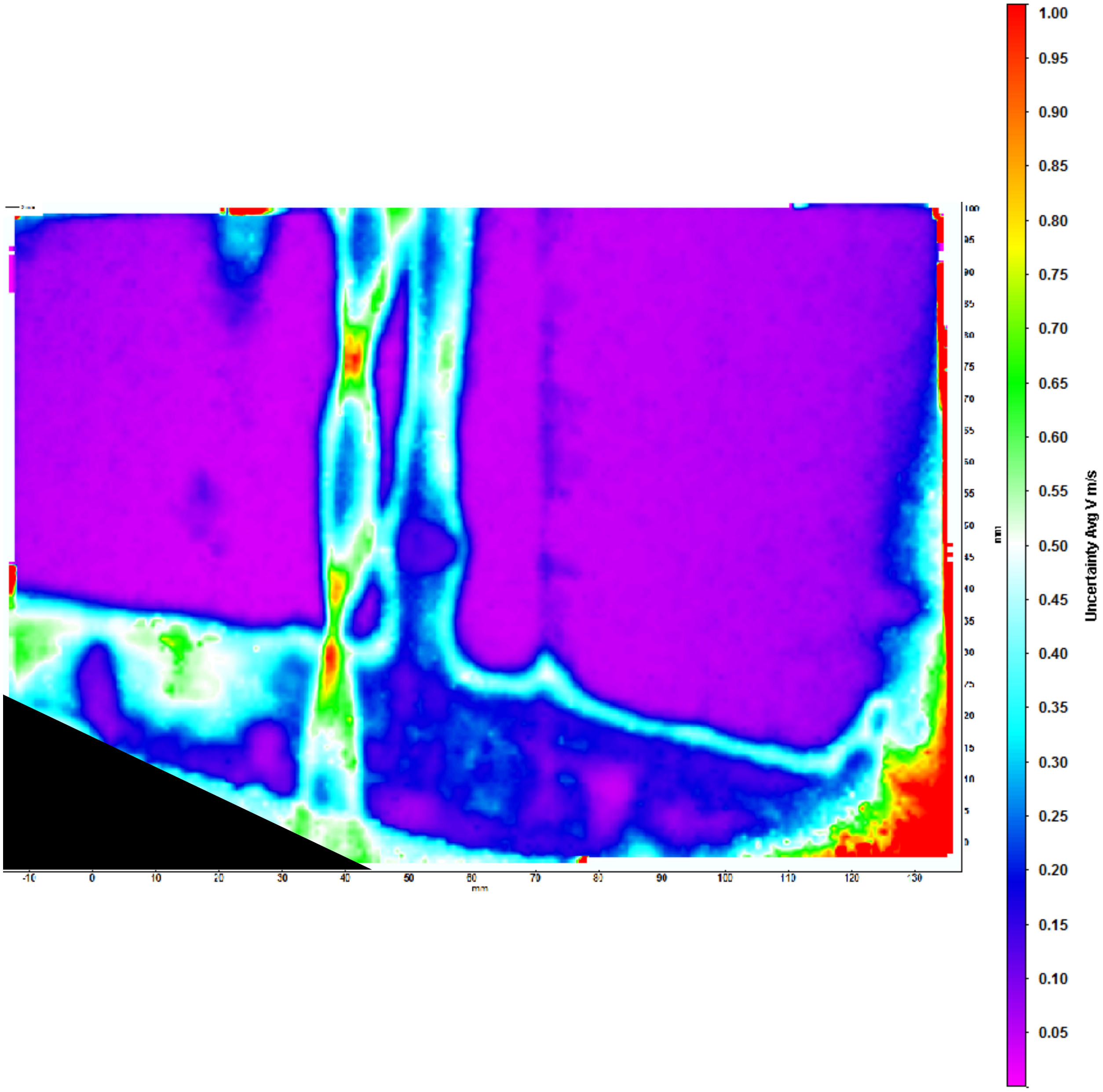

Figure 63: WB-57 5° AOA Velocity Uncertainty Plot

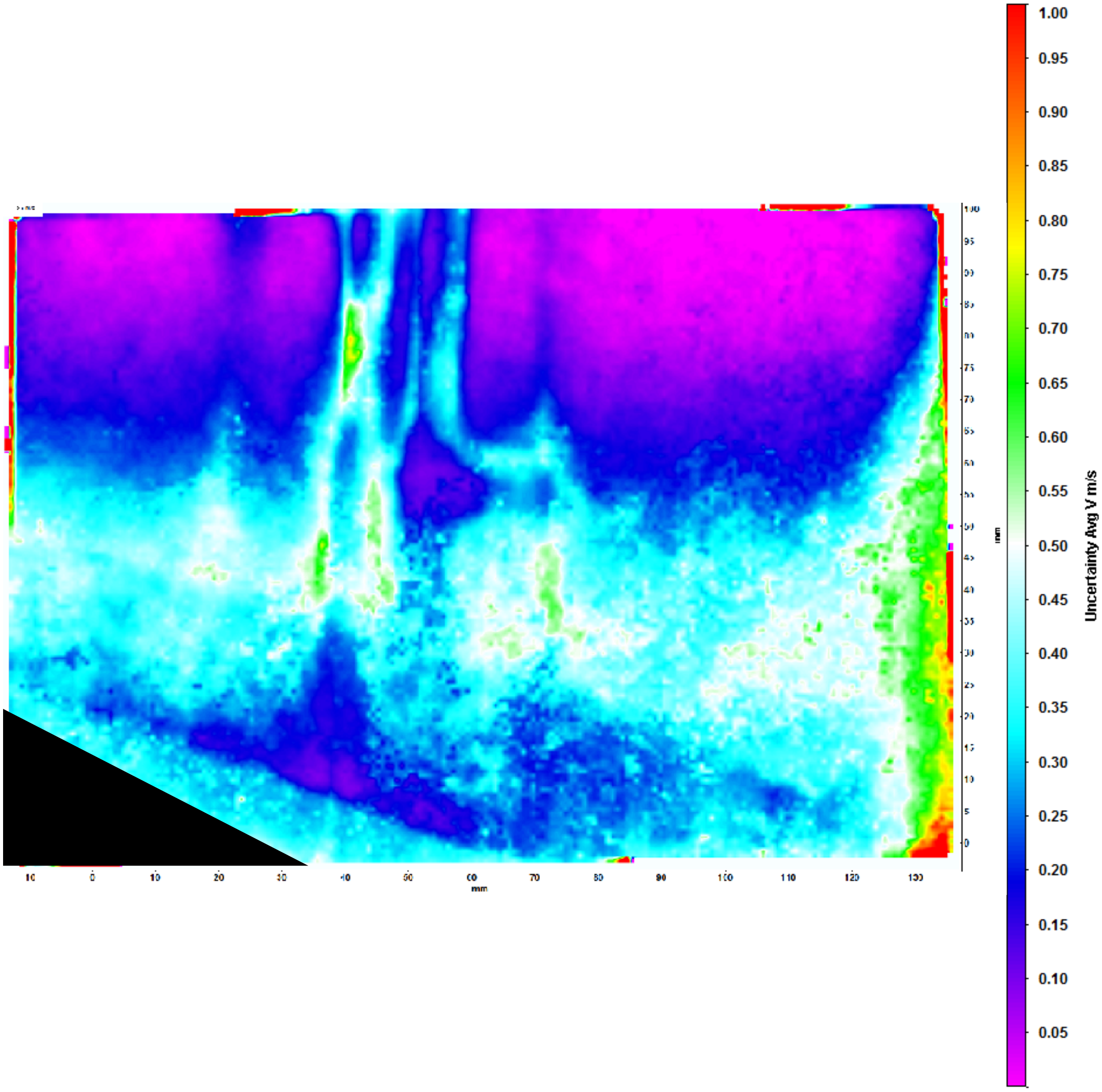

Figure 64: WB-57 10° AOA Velocity Uncertainty Plot

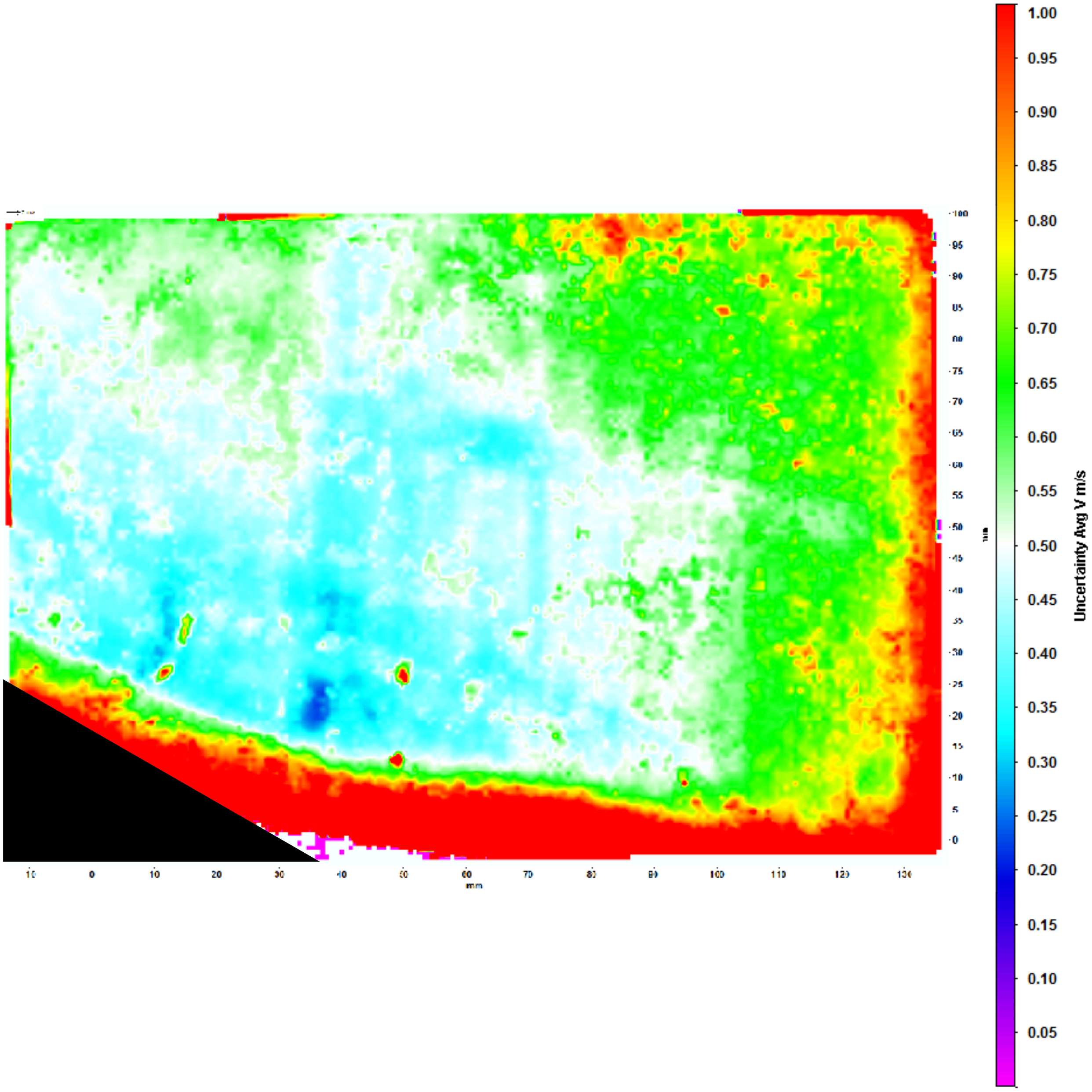

Figure 65: WB-57 15° AOA Velocity Uncertainty Plot

As the model proceeds through the alpha sweep, PIV data provides two key insights. First, Vy becomes more negative over the trailing edge and behind the wing until stall is reached. This is consistent with the physics of how wings generate lift, with the flow following the curvature of the wing's upper surface as closely as possible. Secondly, PIV data provides insight into how and when the flow separates from the upper surface of the wing. The PIV data shown above depicts the gradual growth of separated flow region with increasing angle of attack. When the model is beyond stall (the 15˚ angle of attack case), clear vortex structures behind the wing dominate the flow, representing full separation and turbulent flow behind the wing, all of which aligns with the currently accepted understanding of how flow separation occurs with increased angle of attack and aircraft stall. This is mirrored in the Vz measurements for each plot, which show a nominally 0 out-of-plane velocity far from the surface of the wing. This value drastically changes when entering the turbulent section of the flow, depicted by the positive out of plane velocity near the wing. At a 15º angle of attack, the out of plane velocities are much less uniform, which is characteristic of flow behind a fully stalled wing.

Streamlines depicted in the 2.5˚, 5˚, and 10˚ plots have a slight discontinuity in the separated flow region near x = 1.5 inches. This is due to a scratch in the glass roof of the LSWT test section that blocked the portion of the laser sheet corresponding to this x location. The blocked portion of the data provided erroneous data, and was therefore removed in post-processing and filled with the average of the values on either side of the gap. In the laminar flow regime, this did not significantly affect the streamlines or measured velocities, as the flow was largely continuous. However, the effects of the scratches can still be seen in the uncertainty plots, where higher uncertainty values near the center of the region of interest appear and then return to the expected uncertainty of the system. This did not significantly impact the data collected in this particular test, but could negatively impact results in future tests. It should also be noted that as flow behind the wing becomes more turbulent, the overall uncertainty of measurements increases. This is due to the increase in the Vz component of the flow, which has a higher uncertainty than Vx and Vy due to the planar nature of Stereoscopic PIV measurements. Thus, as the magnitude of Vz grows at any point, the uncertainty of the velocity measured at that point increases. Regardless, the data produced by the PIV system provides valuable insight into the separation behind the trailing edge of the WB-57, and is a valuable application of the system for the LSWT.

The beta sweep test was used to measure velocities above and behind the trailing edge of the WB-57 vertical tail. Measurements were taken sufficiently close to the tail that data acquisition with existing equipment at the LSWT would not have been possible without disrupting the flow characteristics in the region of interest. Similar to the alpha sweep test, a preliminary run was conducted without PIV data to determine the sideslip angle corresponding to stalling the vertical tail of the WB-57. This was determined from the yawing moment coefficient versus beta plot shown in figure 66.

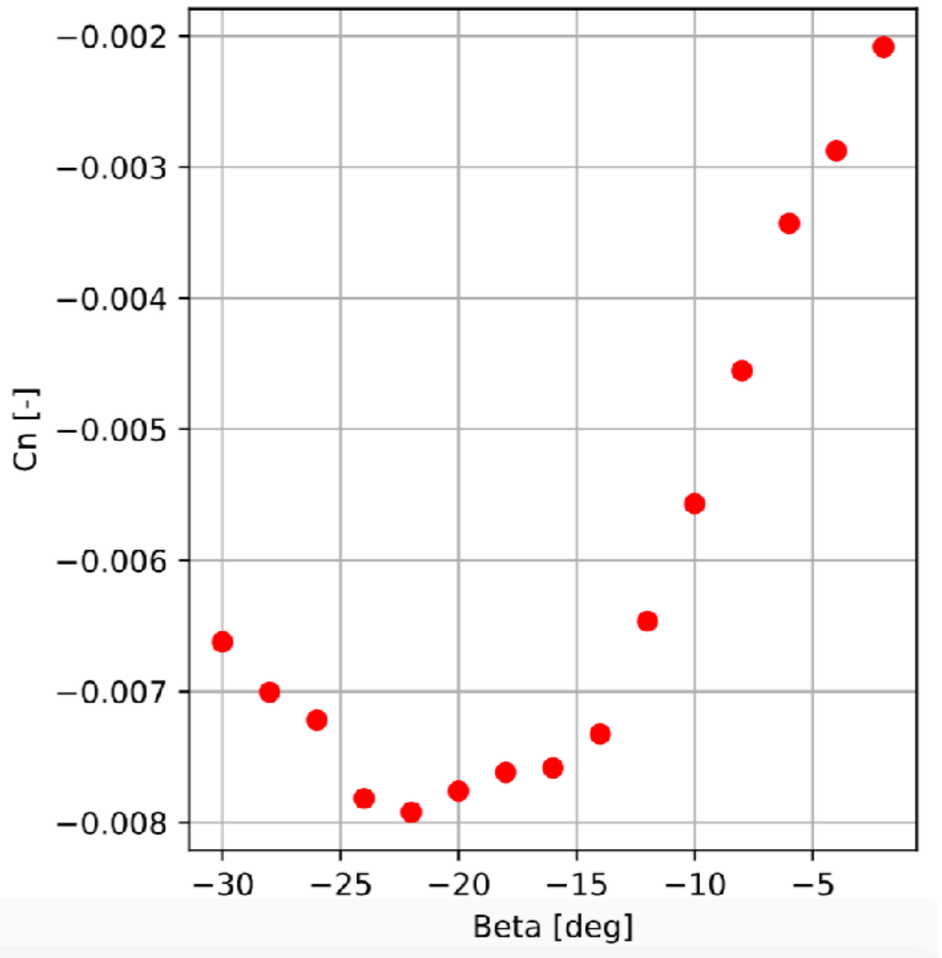

Figure 66: Yawing Moment Coefficient vs Beta for WB-57

This plot shows that the vertical tail of the WB-57 stalls at a sideslip of approximately 15 degrees. Based on this data, five discrete sideslip angles were chosen that corresponded with five distinct flight conditions level flight (0˚ sideslip), low sideslip (5˚), moderate sideslip (10˚), vertical tail stall (15˚ sideslip) and well beyond stall (25˚ sideslip). These conditions were selected to provide insight into how the flow characteristics behind the WB-57 vertical tail change as the aircraft approaches and passes through vertical tail stall. A depiction of the region of interest on the real world model can be seen in figure 67.

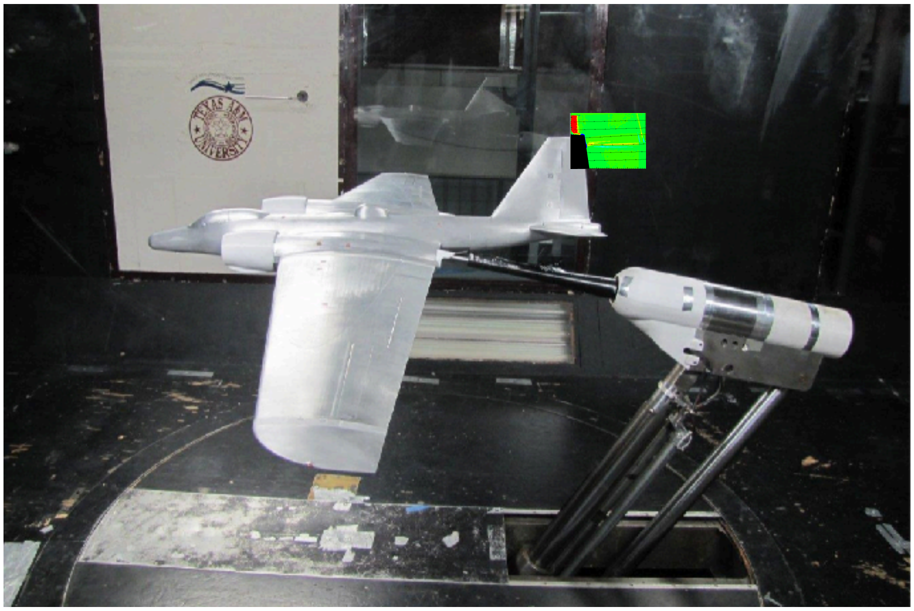

Figure 67: Beta Sweep Region of Interest on Real-World Model

Measurements for each flight condition were captured with both a traditional flooded tunnel approach and a selectively seeded approach to demonstrate the efficacy of both methods. Figures 68-73 give the progression through the beta sweep, and figures 74-79 provide the corresponding velocity uncertainty plots. Streamlines are generated from streamwise (Vx) and vertical (Vy) velocities. Spanwise velocity (Vz) is depicted with a color contour, with positive Vz out of the page. It should be noted that data located directly above the vertical tail is not accurate, due to reflections off the upper surface of the vertical tail. These reflections oversaturate the images in the region over the tail, leading to spurious values of Vz.

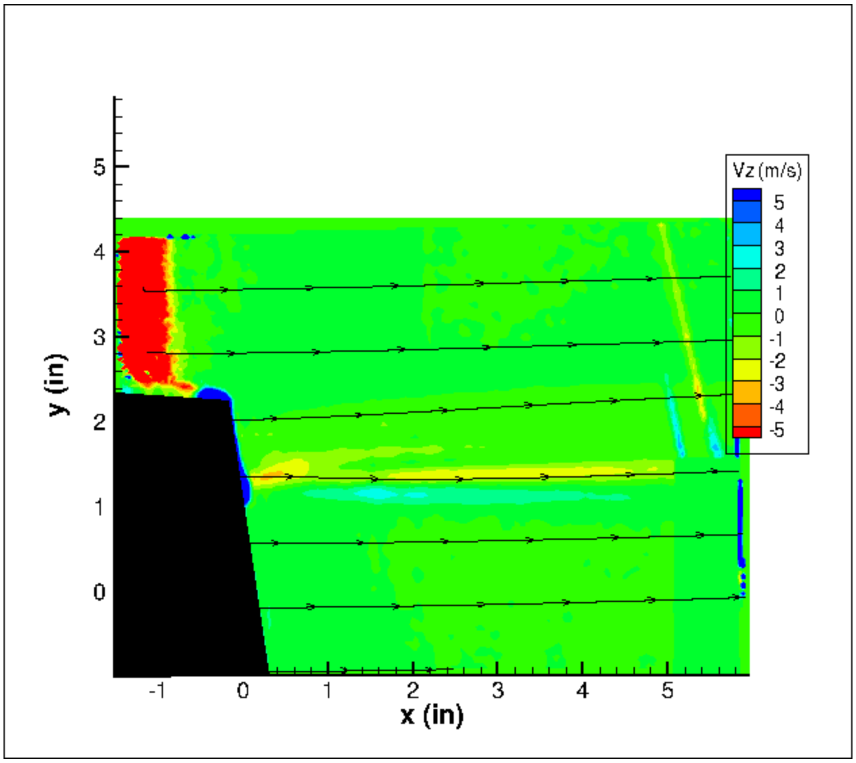

Figure 68: WB-57 0˚ Sideslip Flooded PIV Results

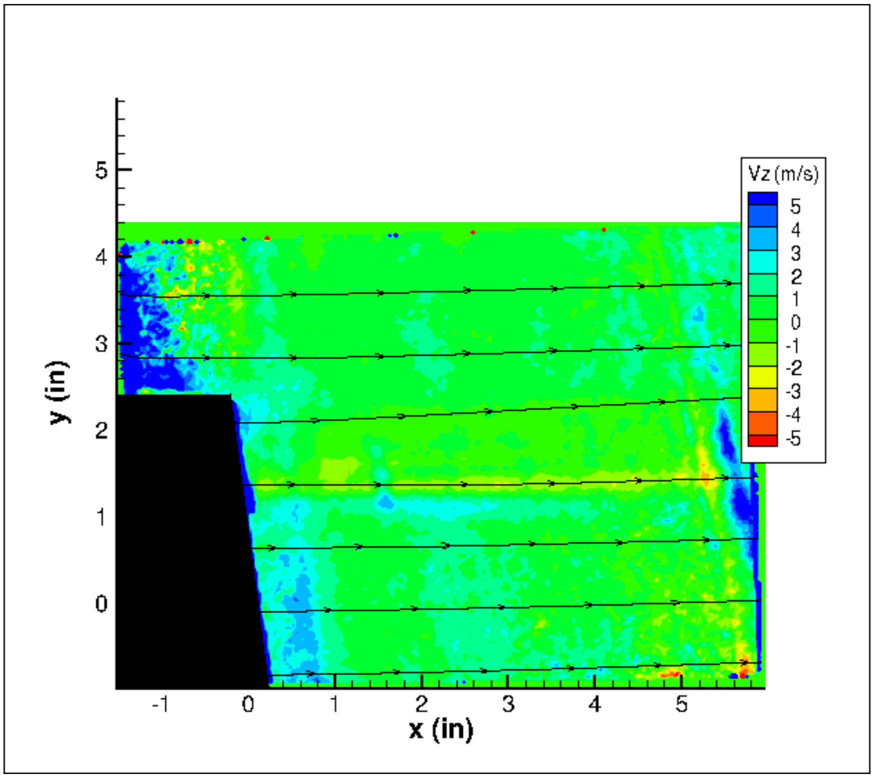

Figure 69: WB-57 0˚ Sideslip Selective Seeding PIV Results

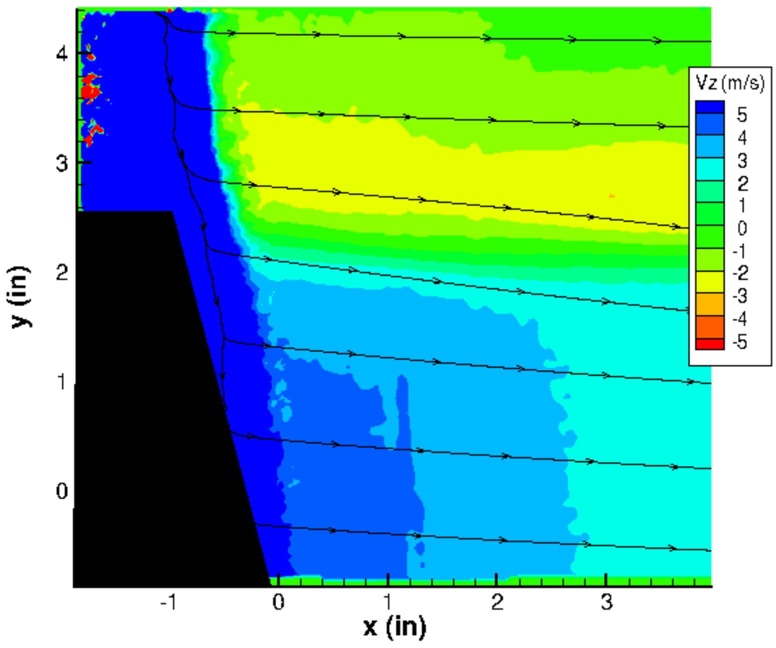

Figure 70: WB-57 5° Sideslip Flooded PIV Results

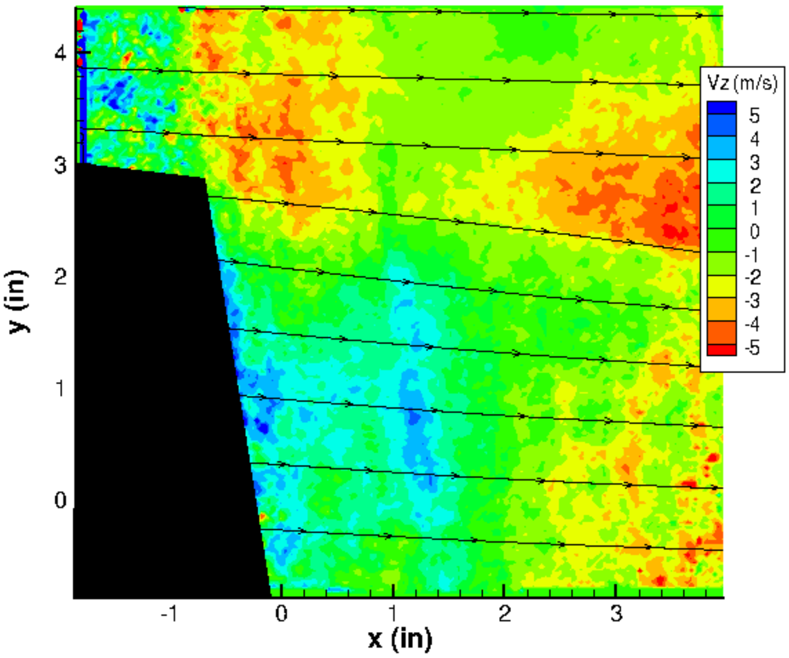

Figure 71: WB-57 5° Sideslip Selective Seeding PIV Results

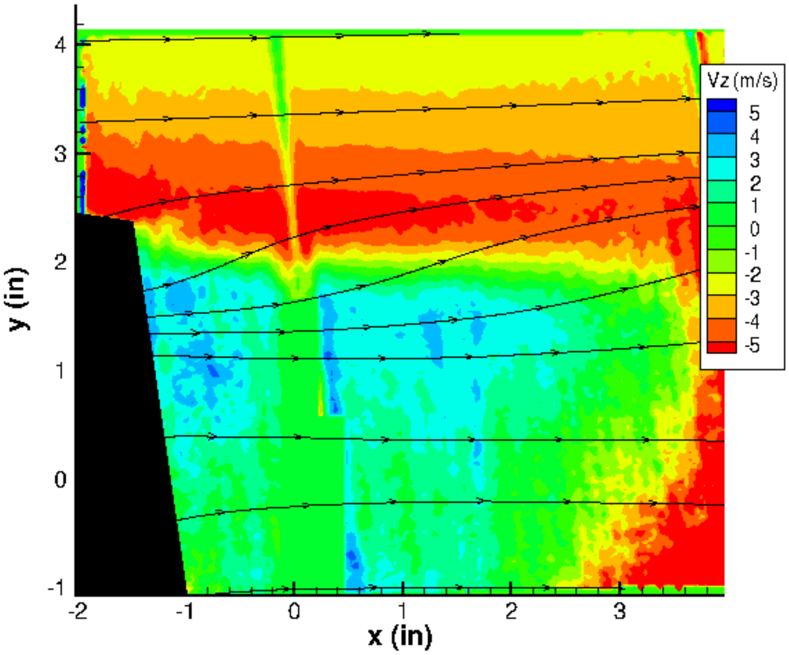

Figure 72: WB-57 10° Sideslip Flooded PIV Results

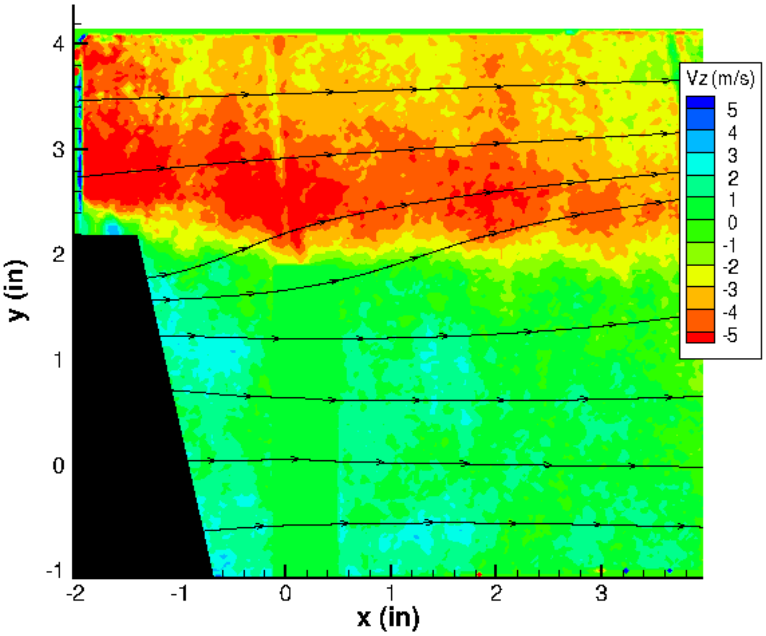

Figure 73: WB-57 10° Sideslip Selective Seeding PIV Results

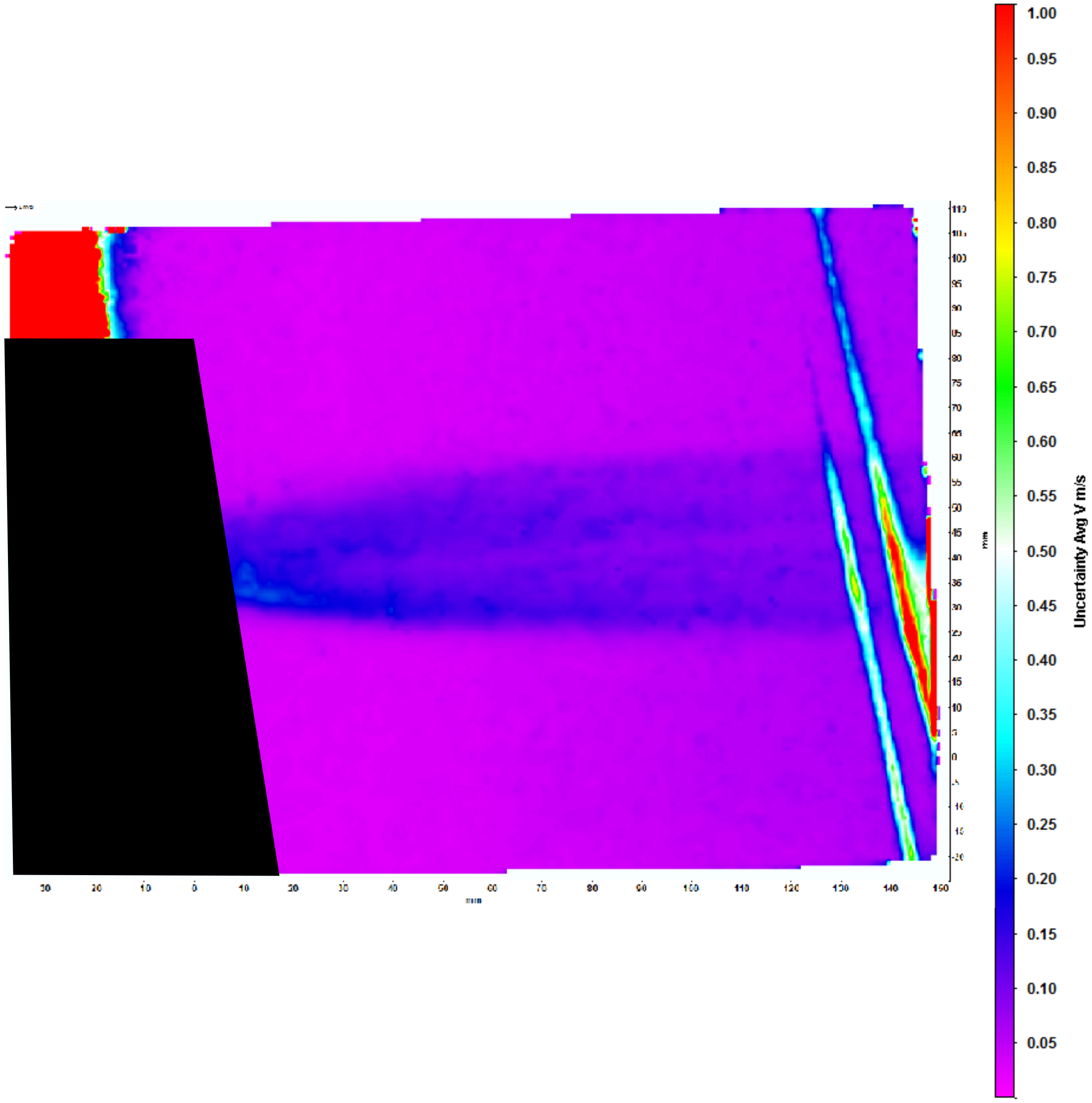

Figure 74: WB-57 0° Sideslip Flooded PIV Results

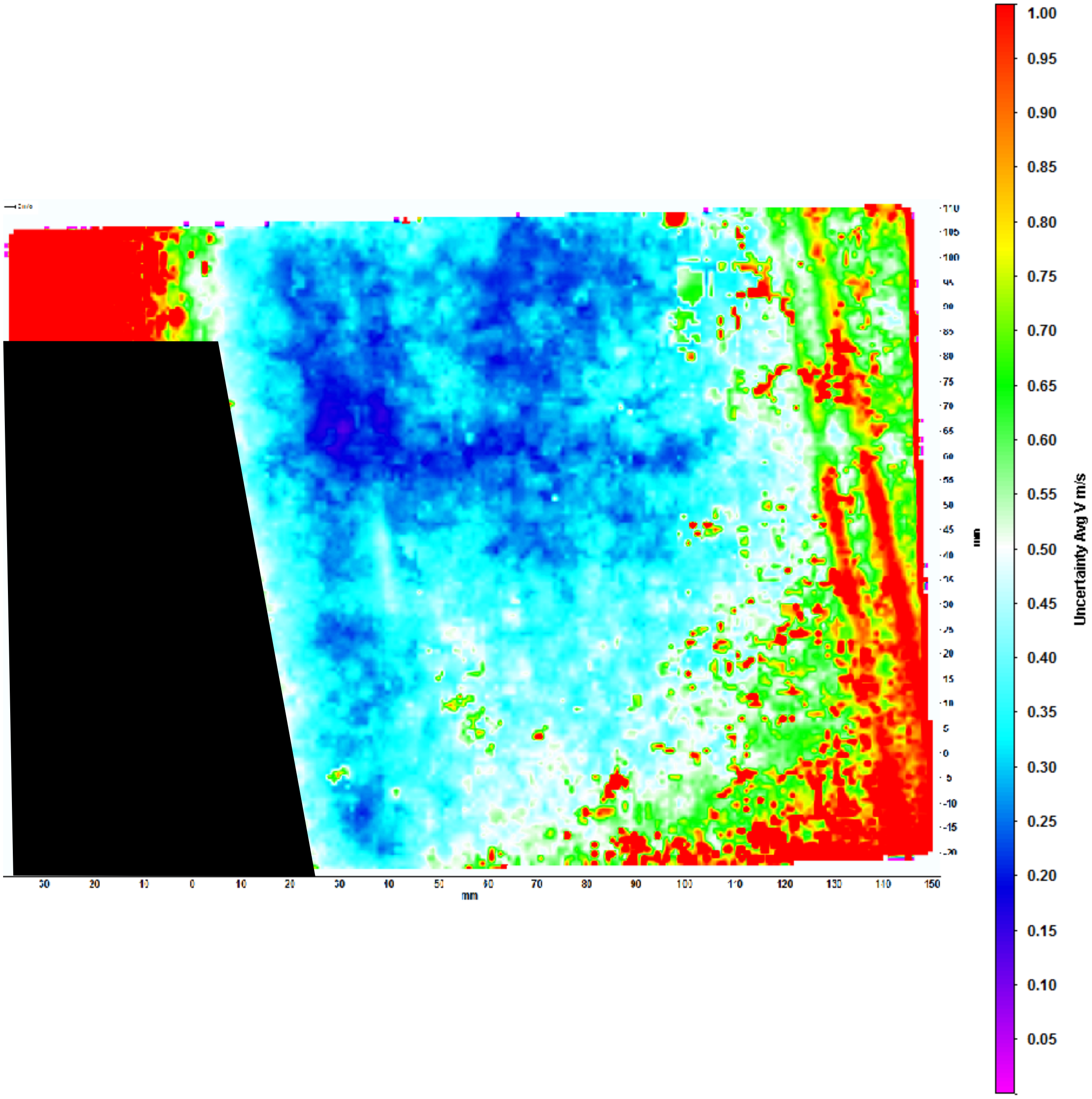

Figure 75: WB-57 0° Sideslip Selective Seeding PIV Results

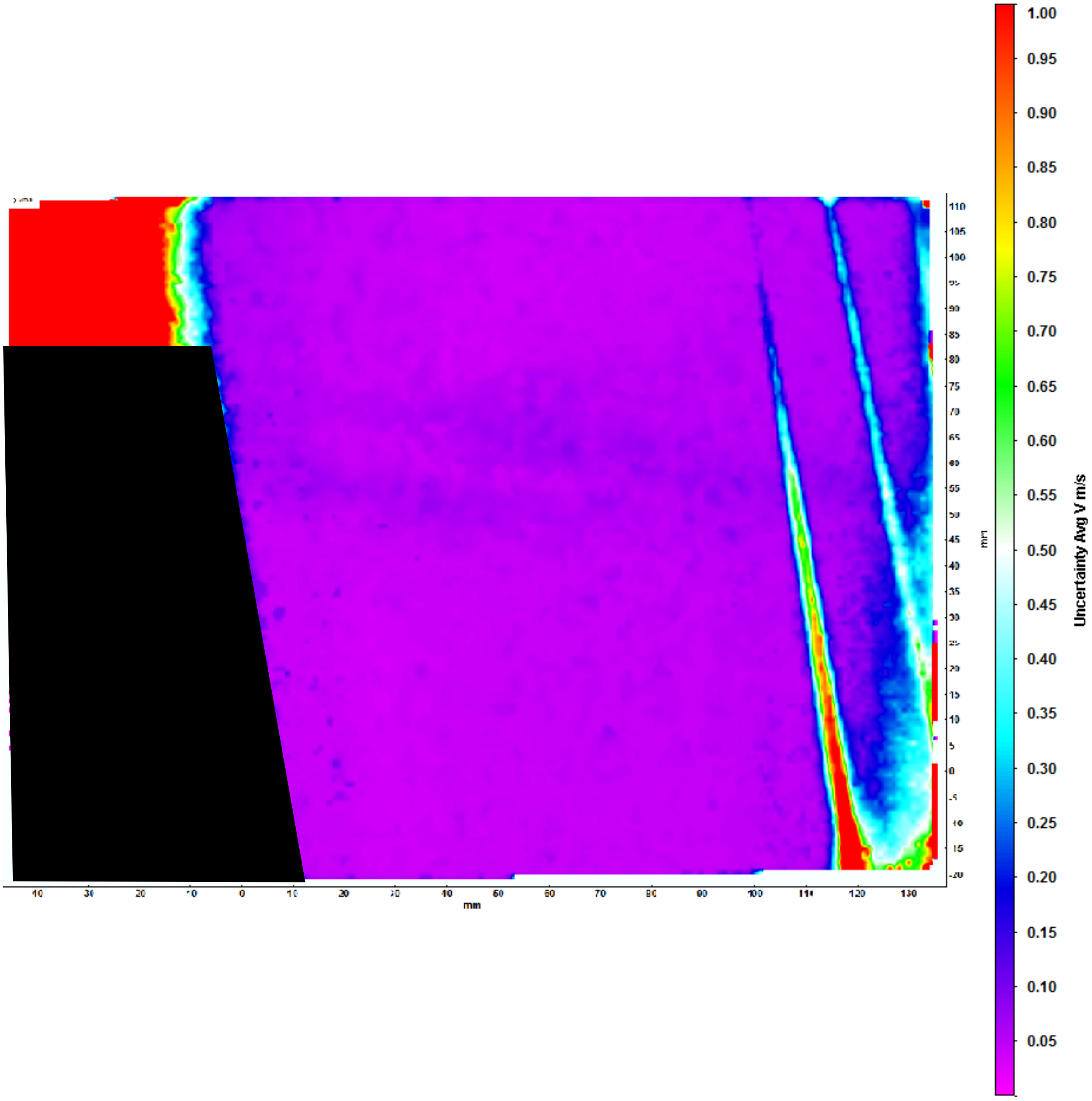

Figure 76: WB-57 5° Sideslip Flooded PIV Results

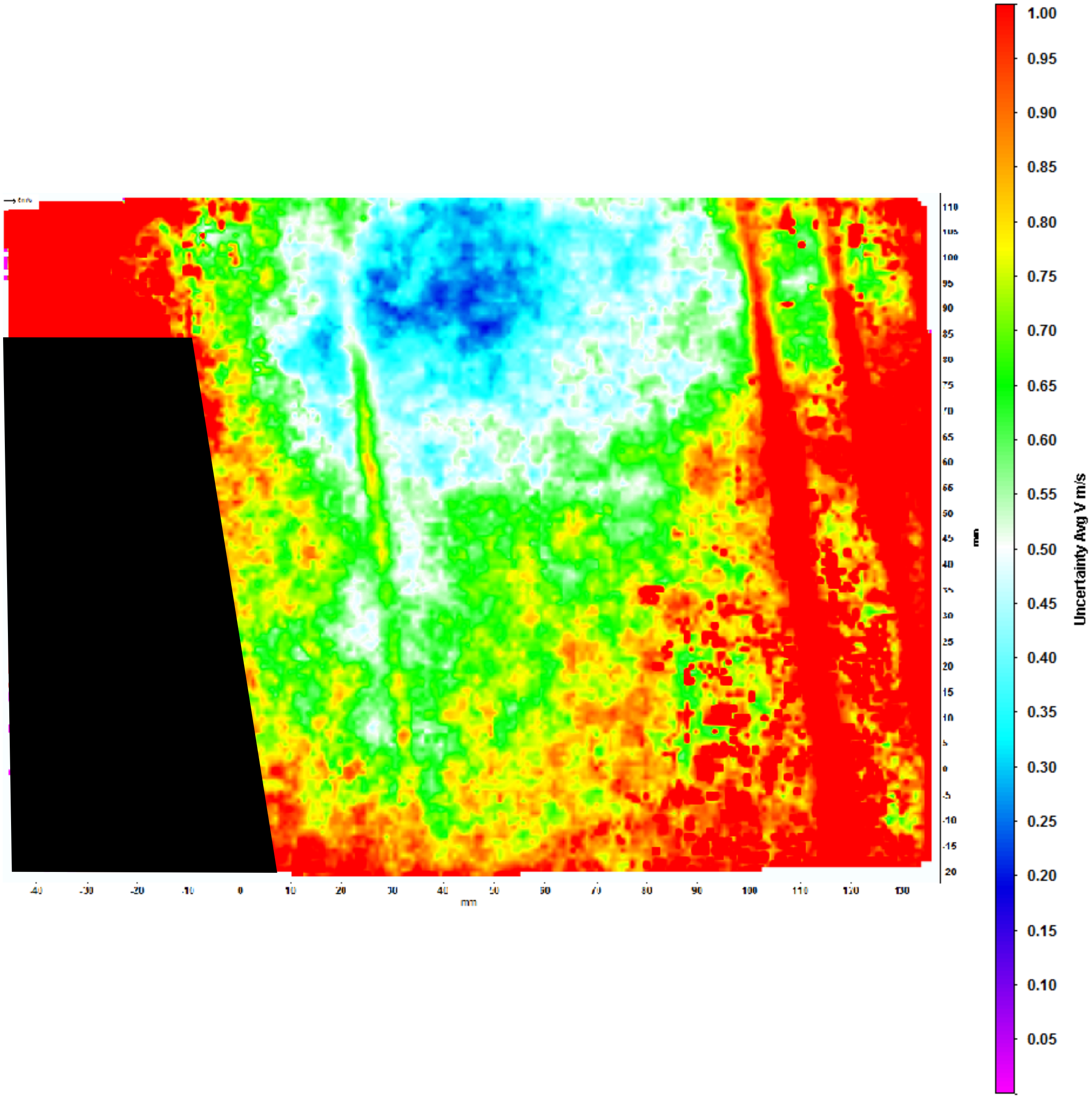

Figure 77: WB-57 5° Sideslip Selective Seeding PIV Results

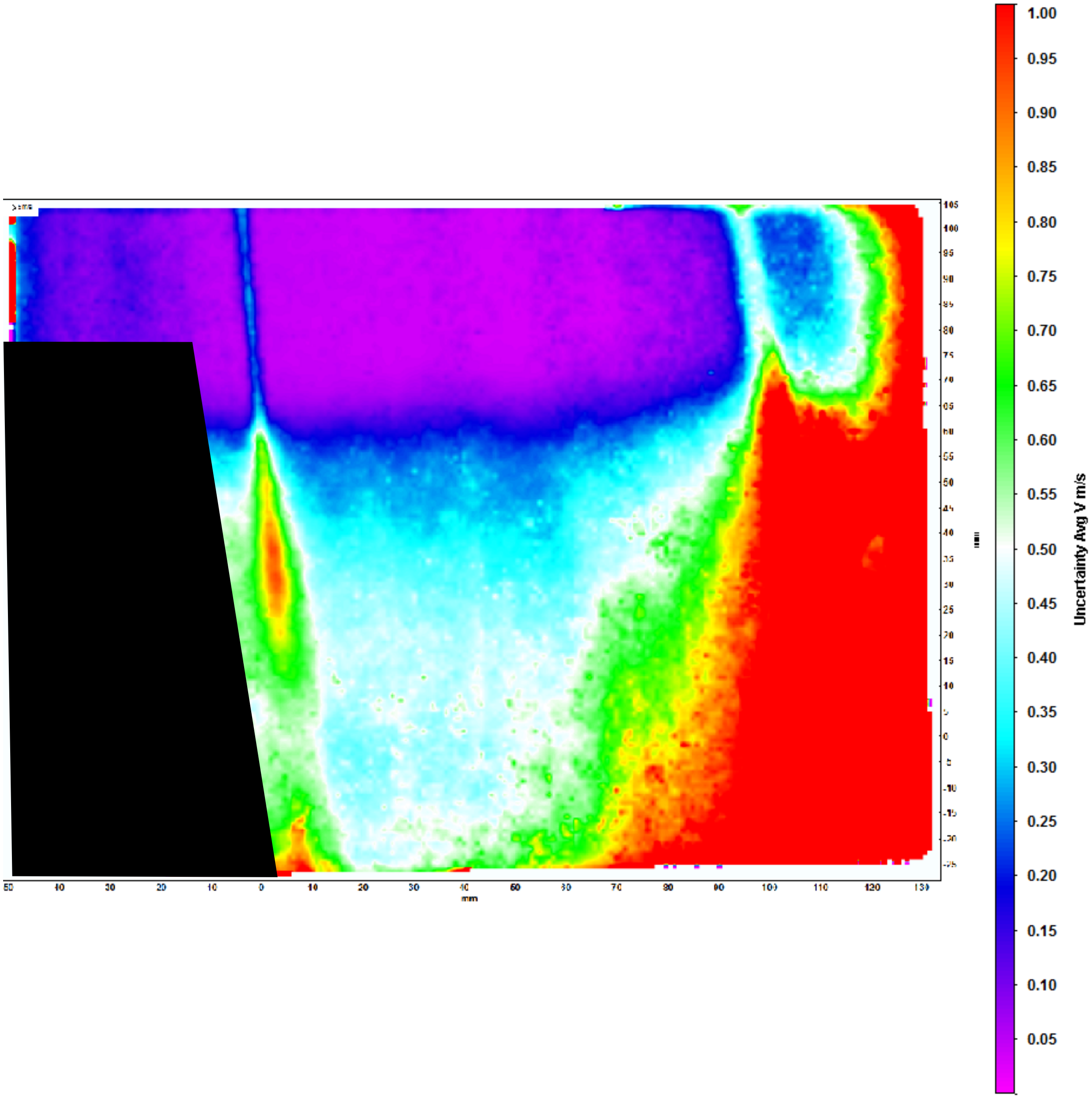

Figure 78: WB-57 10˚ Sideslip Flooded PIV Results

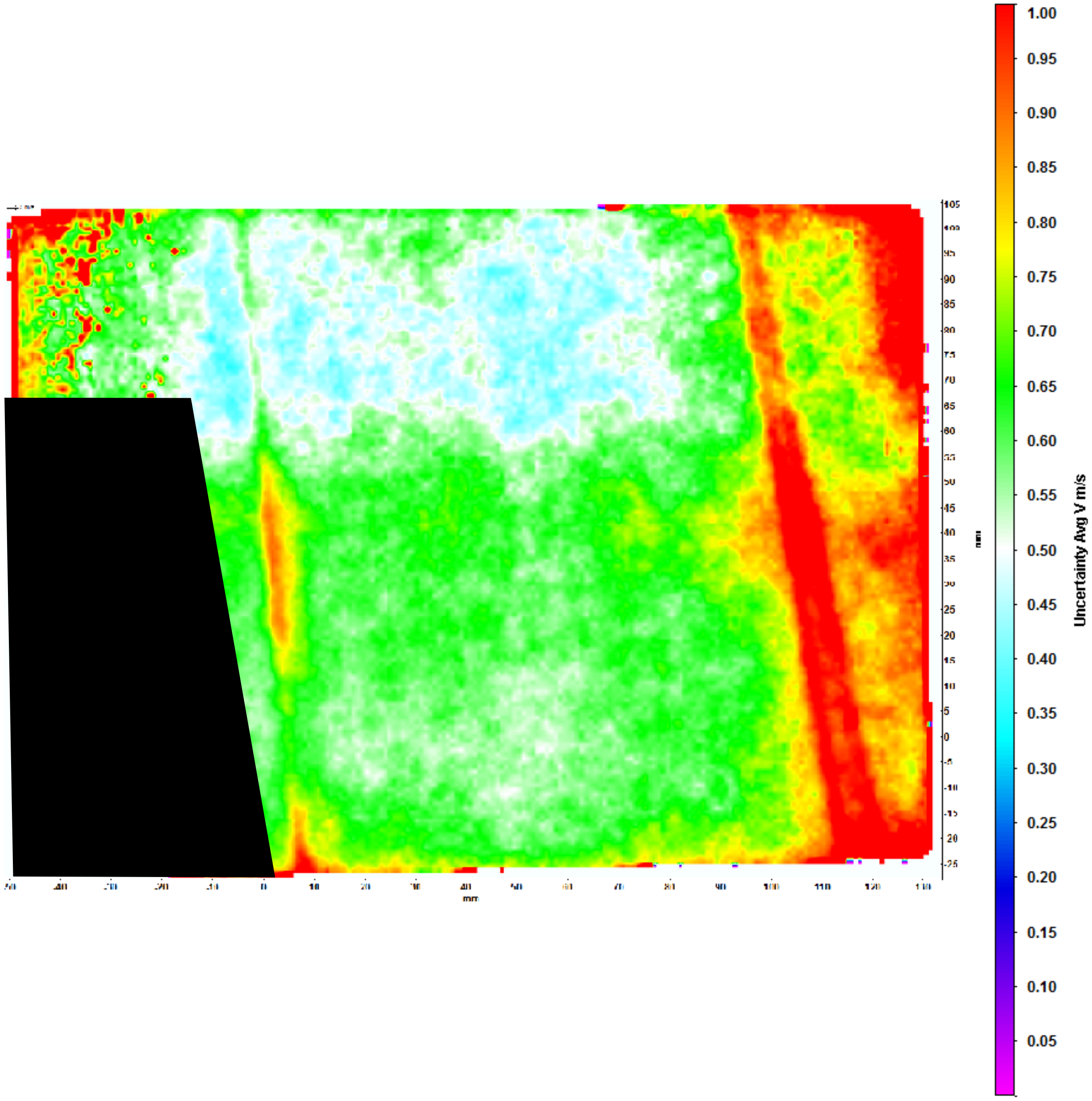

Figure 79: WB-57 10˚ Sideslip Selective Seeding PIV Results

Each plot was aligned such that the top of the vertical tail of the WB-57 could be easily identified on the left side of the image. The exact placement of the vertical tail varies slightly, as the region of interest was shifted and recalibrated for each new sideslip angle. At low sideslip angles (0˚, 5˚ and 10˚), results closely match the expected flow characteristics behind the tail of the WB-57. The 0˚ cases depict linear flow with horizontal streamlines and a minimal Vz component which is expected when the tail is producing no sideforce. One interesting phenomena visible in both the flooded and selectively seeded cases is the presence of a small vortex along the streamline at y = 1.5 in. This small vortex lines up with the edge of the tape used on the aluminum model to prevent reflections, and its capture shows the sensitivity of the stereo-PIV system developed through this thesis. The 5˚ cases also provide a realistic depiction of flow coming off the tail, with a positive Vz component coming off the tail of the model that trends towards zero moving downstream from the model. Looking at the flooded case, the beginnings of a vortex at the top of the vertical tail can also be seen, with Vz moving into the page above and behind the top of the vertical tail. The selectively seeded image for this case differs substantially from the flooded case, depicting one of the potential pitfalls of selective seeding. In reviewing the dataset, the number of image pairs with sufficient smoke density was found to be lower in these images than the more successful selectively seeded runs at 0º and 10º sideslip. This shows that selective seeding is not perfect, and must be more carefully observed during testing to ensure smoke density is sufficient in each run.

In the 10˚ case, the vortex caused by the top of the vertical tail becomes more pronounced, while flow directly behind the tail maintains its positive Vz that trends towards zero downstream. At the right side of the flooded image, spurious vectors from another scratch in the glass roof of the LSWT test section lead to a very negative Vz near the edge of the image. The same issue was present in the selectively seeded result, but was more effectively filtered out in post-processing. This suggests that to a point, higher particle densities help decrease the impact of minor system defects.

The 15˚ and 25˚ sideslip measurements were made but did not result in useful data. At both angles, the vertical tail is stalled and there is a large out-of-plane Vz. As such, a large number of particles leave the laser sheet between the first and second exposure of the cameras, resulting in a much lower fidelity dataset. This points towards a well-known issue with stereoscopic PIV as a measurement technique more than anything specific about the system developed through this thesis. As out of plane velocities in stereoscopic PIV setups approach the magnitude of the in-plane measurements, data accuracy drastically decreases due to the lost particles mentioned above. In these cases, a tomographic PIV setup would be preferable if a true 3-D depiction of flow behind the tail was desired. Alternatively, a 90˚ rotation of both the laser sheet and the cameras about the x-axis would allow stereoscopic PIV to more effectively capture the vortices behind the vertical tail when it moves beyond stall. A more extensive explanation of future system improvements and suggestions can be found in Chapter 5.

The uncertainty plots also provide interesting insights into the efficacy of the selective seeding system. Each uncertainty plot demonstrates an increase in uncertainty with increased Vz in accordance with the WB-57 alpha sweep. However, these plots also show that uncertainty is higher in runs with selectively seeded PIV. This makes sense, as the lack of homogeneity during seeding means that there are fewer image pairs with seed particles available at any single point for the average velocity at that point. As a result, there are fewer vectors being used to calculate the velocity uncertainty at any one point in the region of interest. Thus, the uncertainty for non-homogenous, selectively seeded PIV will always be higher than flooded PIV datasets.

Overall, the results are sensible and consistent between the selectively seeded and traditionally flooded runs. This is very significant from a proof of concept standpoint for the selective seeding system, as it demonstrates that selective seeding can replace traditional seeding methods in large scale PIV setups. Accordingly, it is worthy of continuing development for use in large scale wind tunnels at facilities such as the Arnold Engineering Development Complex (AEDC) or the National Full-Scale Aerodynamics Complex (NFAC). In particular, the selectively seeded 5º sideslip case illuminates a path for future development of a new iteration of selective seeding that produces a smoke column of continuous homogeneous density.

5. CONCLUSIONS AND RECOMMENDATIONS

5.1 Conclusions

This thesis reports on the design, implementation, and use of hardware and procedures for both 2-D and stereoscopic PIV in the Texas A&M Low Speed Wind Tunnel. This includes the development of specially designed mounting hardware that facilitates the rapid and repeatable installation and execution of PIV that is vital to successful usage in a production environment. While these factors are already important in research applications, they may be more important in production environments where external customers run on a tight testing schedule and trust the data produced for critical design decisions. As such, the successful validation of the PIV system to an uncertainty of 0.5% in plane and 5% out of plane was a critical threshold for data quality. The PIV systems produced for the LSWT are fully validated and available for use upon conclusion of this thesis.

The selective seeding system has also performed well in proof of concept testing, meeting all design requirements. The lack of velocity deficit in the test section seen during the validation stages of testing and the comparable data to traditionally seeded data produced during the WB-57 beta sweep are particularly encouraging because it suggests facility flow quality can be maintained in the presence of a selective seeding system. Furthermore, the relatively equivalent results from the selective seeding and flooded tunnel runs in the WB-57 beta sweep suggest that selective seeding in large wind tunnels is a viable alternative to traditional seeding methods. In some cases, selective seeding was even found to be more effective in eliminating spurious vectors due to the higher particle density produced by selective seeding. That being said, it appears important to collect more image pairs when using selective seeding configurations than under flooded conditions, as the lack of seeding homogeneity remains a concern. Nevertheless, the method demonstrates a clear step forward for large scale facilities seeking to implement any type of PIV system.

5.2 Recommendations

Looking ahead, continuing effort should address a few key development needs. First and foremost, improvements to selective seeding uniformity should be made as soon as possible. The implementation of the system is currently effective, but requires more image pairs and processing effort than a flooded tunnel approach. This is largely due to the lack of uniformity in the smoke column that is being generated which can produce datasets with insufficient particle density, leading to higher velocity measurement uncertainties. While this was not a hinderance in this particular thesis, continued implementation in production level environments necessitates further system improvement.

Second, image stitching to create larger fields of view should be investigated. With the current setup, PIV data can only be captured in a region of interest approximately 4 inches x 6 inches. This could be somewhat expanded by acquiring higher resolution cameras or a large calibration card, but results with this method would be limited. The best avenue to a large field of view lies in stitching individual regions of interest together into a larger field of view. Of course, this could be accomplished by shifting the camera positions multiple times throughout a single test, but such an approach would be highly time consuming. Depending on the desired field of view, acquisition of additional cameras to simultaneously capture multiple regions of interest that could then be stitched together could be the most viable approach.

The third incremental improvement for the LSWT would be the acquisition of schiempflug mounts for each camera used in the stereoscopic PIV system. These mounts offset the lens plane of the camera from the image plane, allowing cameras to capture focused images with a narrower depth of field. This will eliminate the need for extensive taping of reflective components behind the laser sheet, as the cameras can be more narrowly focused during calibration to capture exclusively the region directly illuminated by the laser sheet. At the LSWT this is particularly significant, as most models are made of either metals or 3-D printed materials, both of which are reflective surfaces. As such, taping is currently necessary to prevent data interference, making the process of PIV data acquisition longer than it should be. Additionally, schiempflug mounts would allow researchers to position the cameras at larger off-normal angles relative to the laser sheet. The current system is capped at a 20˚ off angle mount, as larger angle values decrease the fidelity of in-plane measurements. This improvement would significantly expand the capabilities of the LSWT, and enable data acquisition over a wider array of theoretical configurations.

Fourth, it will be important to implement a mounting system to conduct stereoscopic PIV in the xz plane. A rotated stereoscopic configuration is needed to capture flows with significant Vz components. This would enable the study of situations such as the 15º and 25º sideslip configurations discussed in chapter 5, where out-of-plane velocity accuracy was a hinderance to data collection.

Fifth, replacement of the glass panel in the roof of the LSWT test section will significantly decrease the effort required in post-processing by removing scratches and imperfections that can block portions of the laser sheet during data collection. While the effects of these imperfections were fairly minimal, they did slightly reduce data quality in both stereoscopic PIV application examples as discussed in Chapter 4.

REFERENCES

Adrian, R.J. (1984). Scattering Particle Characteristics and Their Effect on Pulsed Laser Measurements of Fluid Flow: Speckle Velocimetry vs Particle Image Velocimetry. *Applied Optics, 23*(11), 1690-1691.

Adrian, R.J. (2005). Twenty Years of Particle Image Velocimetry. *Experiments in Fluids, 39*(01), 159-169.

Alvarez L., Gómez L., & Henríquez P. (2012). Zoom Dependent Lens Distortion Mathematical Models. *Journal of Mathematical Imaging and Vision 44*(03), 480-490.

Atkinson C.H., Dillon-Gibbons C.J., Herpin S., Soria J. (2008). Reconstruction Techniques for Tomographic PIV of a Turbulent Boundary Layer. *14th International Symposium on Applications of Laser Techniques to Fluid Mechanics*, Lisbon, Portugal.

Atkinson C.H., Soria J. (2009). An Efficient Simultaneous Reconstruction Technique for Tomographic Particle Image Velocimetry. *Experiments in Fluids 47*, 553-568.

Buchmann N.A., Willert C.E., Soria J. (2012). Pulsed, High-Power LED Illumination For Tomographic Particle Image Velocimetry. *Experiments in Fluids 53*(05), 1545-1560.

Buchner A.J., Buchmann N., Kilany K., Atkinson C., Soria J. (2011). Stereoscopic and Tomographic PIV of a Pitching Plate. *Experiments in Fluids 52*, 299-314.

Elsinga G.E., Scarano F., Wieneke B., van Oudheusden B.W., (2005). Tomographic Particle Image Velocimetry. *Experiments in Fluids 41*(6), 933-947.

Jahanmiri, M. (2011). *Particle Image Velocimetry: Fundamentals and Its Applications* (Report No. 2011:03). Göteborg, Sweden: Chalmers University of Technology.

Jenkins L.N., Yao C., Bartram S.M., Harris J., Allan B., Wong O., & Mace W.D. (2009). Development of a Large Field-of-View PIV System for Rotorcraft Testing in the 14- x 22-Foot Subsonic Tunnel. AHS International 65th Forum and Technology Display. Grapevine, TX, 27-29 May 2009.

Kang C., Liu H., Mao N., Zhang Y. (2019). A Brief Overview of Research Methods. In: Methods for Solving Complex Problems in Fluids Engineering. Springer, Singapore.

Kähler C.J., Scharnowski S., & Cierpka C. (2012). On the Resolution Limit of Digital Particle Image Velocimetry. *Experiments in Fluids 52*, 1629-1639.

Kumashiro K., Steinberg A., Yano M. (2019). High Spatial Resolution 3D Fluid Velocimetry by Tomographic Particle Flow Velocimetry. University of Toronto, Canada.

LaVision (Retrieved 2019, April 3). *2D & Stereo PIV*. Retrieved from https://www.smart-piv.com/en/products/flowmaster/2d-stereo-piv/

Li, M. & Lavest, J.M. (1996). Some Aspects of Zoom Lens Camera Calibration. *IEEE Transactions on Pattern Analysis and Machine Intelligence 18*(11), 1105-1110.

Meng H., Pan G., Pu Y., Woodward S. (2004). Holographic Particle Image Velocimetry: from Film to Digital Recording. *Measurement Science and Technology 15*(04), 673-685.

Miller M. Q., Leber E., Brown L., & White E.B. (2020). Redesign of a Sting Mount Pitch Actuator for Improved Data Quality. *AIAA 2020-1355.*

Nishino K., Nobuhide K., Masaru H. (1989). Three-Dimensional Particle Tracking Velocimetry Based on Automated Digital Image Processing. University of Tokyo, Japan.

Pickering C.J.D., & Halliwell N. A. (1984). Laser Speckle Photography and Particle Image Velocimetry: Photographic Film Noise. *Applied Optics 23*(17), 2961-2969.

Prasad A.K. (2000). Stereoscopic Particle Image Velocimetry. *Experiments in Fluids*

Raffel M., Willert C., Scarano F., Kähler C., Wereley S. & Kompenhans, J. (2018). *Particle image velocimetry: A Practical Guide*. Cham: Springer.

Raffel M., Richard H., Erhenfried K., Van der Wall B., Burley C., Beaumier P., McAlister K., & Pengel K. (2004). Recording and Evaluation Methods of PIV Investigations on a Helicopter Rotor Model. *Experiments in Fluids 36*, 146-156.

Scarano F. (2013). Tomographic PIV: Principles and Practice. *Measurement Science and Technology 24*(01), 1-28.

Schäfer L., Schröder W. (2011). Comparison of Holographic and Tomographic Particle Image Velocimetry Turbulent Channel Flow Measurements. *Journal of Physics: Conference Series 318.*

Schiacchitano, A. & Wieneke, B. (2016). PIV Uncertainty Propogation. *Measurement Science Technology 27.*

Soloff SM., Adrian RJ., Liu ZC (1997). Distortion Compensation for Generalized Stereoscopic Particle Image Velocimetry. *Measurement Science Technology 8*,1441-1454.

Towers C.E., Bryanston-Cross P.J., Judge T.R. (1991). Application of Particle Image Velocimetry to Large-Scale Transonic Wind Tunnels. *Optics & Laser Technology, 23*(05), 289-295.

Wereley S.T., Meinhart C.D. (2010). Recent Advances in Micro-Particle Image Velocimetry. *Annual Review of Fluid Mechanics, 42*, 557-576.

Westerwheel J. (2000). Analysis of PIV Interrogation for Inhomogeneous Image Fields. *Proc. 10th Int. Symp. on Application of Laser Techniques to Fluid Mechanics (Lisbon, Portugal)* ed R. Adrian *et al*, Paper 13:1.

Westerwheel J., Elsinga G., Adrian R. (2013). Particle Image Velocimetry for Complex and Turbulent Flows. *Annual Review of Fluid Mechanics, 45*, 409-436.

Wieneke B. (2005). Stereo-PIV Using Self-Calibration on Particle Images. *Experiments in Fluids 39*(02), 267-280.

Willert C. (1997). Stereoscopic Digital Particle Image Velocimetry For Application in Wind Tunnel Flows. *Measurement Science and Technology, 8*, 1465-1479.

Wilson B.M. & Smith B.L. (2013). Uncertainty of PIV Mean and Fluctuating Velocity Due to Bias and Random Errors. *Measurement Science and Technology, 24*(03)*,* 1-15.

Worth N.A., Nickels T.B. (2008). Acceleration of Tomo-PIV by Estimating the Initial Volume Intensity Distribution. *Experiments in Fluids, 45*, 847.

Zhang T., Celik D., & Van Sciver S.W. (2003). Tracer Particles for Applications to PIV Studies of Liquid Helium. *Journal of Low Temperature Physics 134*(314), 985-1000.

APPENDIX A: 2-D PIV SOP

2-D PIV Setup, Operation, and Analysis Checklist (Current as of 2/6/2020)

Physical System Setup

1. __ Bolt in PIV Laser Mounting Frame to top of Tunnel

2. __ Bolt camera mounting frame to side of Tunnel

3. __ Clamp Optics table to PIV Mounting Frame

4. __ Bolt Laser Head to Optics Table

5. __ Connect Laser Head to Laser Power System

6. __ Bolt Connection Rail 1 to Optics Table

7. __ Attach Mirror to Optics Table

8. __ Attach Mirror, Focusing Lens and Cylindrical Lens to Connection Rail 2

9. __ Clamp Connection Rail 2 to Connection Rail 1

10. __ Attach Calibration Plate to desired Region of Interest

11. __ Turn on Laser at low power (Flip Power Switch on Back > Turn Key to on > Hold Down Start > press Laser 1 and Laser 2)

12. __ Angle/move mirrors to center beam on the calibration plate

13. __ Angle/move lenses to achieve desired beam width and thickness

14. __ Stop Laser (Press Stop)

15. __ Open Smoke Port inside Tunnel

16. __ Put Smoke tubes through smoke port and attach tubes to smoke generator

17. __ Plug Foot Pedal into Smoke Generator and Plug Smoke Generator into power

18. __ Attach Regulator to Smoke Generator

19. __ Attach Compressed Air to Regulator

20. __ Set Regulator to 30 Psi

21. __ Attach Camera to mounting bracket

22. __ Attach Lens to Camera

23. __ Connect Camera to Power Box and Connect Power box to power

24. __ Connect Camera to Computer with USB 3.0 port

25. __ Turn On Camera

26. __ Open PCO Camware 64

27. __ Remove Lens Cap

28. __ Open Exposure View windows (View > B/W Window > Image A+Image B)

29. __ Align Camera with Calibration Plate

***Calibration Plate Should fill image field of view**

Data Collection

30. __ Set Image Capture to Auto Sequence (Camera Control > Auto-Sequence > Accept)

31. __ Record Calibration Images of Calibration Plate (Red Record button to start, white square to stop)

32. __ Export Recorder Sequence (File > Export Recorder Sequence > select desired save destination > Select Split doubleshutter > Save)

33. __ Open Calibration Image and check focus and alignment (Move Camera and recapture images as necessary)

34. __ **ONCE FOCUSED CALIBRATION IMAGES ARE CAPTURED:** Measure Pixels Per Inch on Calibration Card and write down result

35. __ Use Pixels per Inch and desired tunnel run speed to calculate the time for something to move 20 pixels in the image

36. __ Attach Laser to Quantum Composer (Fire Lamp 1 to T1, Fire Lamp 2 to T4, Fire Q-Sw 1 to T6, Fire Q-Sw 2 to T7)

37. __ Attach Camera to Quantum Composer (Control In Exp Trig to T8)

38. __ Turn On Quantum Composer

39. __ Set Laser and camera Timings (T6 delay = T1 + 190 μs, T7 Delay = T4 + 190 μs, T8 delay = T0 + 0 s)

40. __ Set time between laser pulses to the time for something to move 20 pixels with the Quantum Composer (T4 delay= T1 + X seconds)

41. __ Set time between laser pulse cycles (T1 delay = T0 + X sec)*

This step Varies based on the exposure time set in PCO Camware64. This time must be less than the exposure time in PCO Camware 64, but greater than the exposure time minus T4.* *(AKA: PCO Exposure Time - T4 < T1 < PCO Exposure Time)***

42. __ In PCO Camware64: Set Image Capture to External Exposure start (Camera Control > External Exp. Start > Accept)

43. __ Start Laser firing (hold start > press Laser 1 and Laser 2)

44. __ Turn Laser to external control (press Q-SW and Flashlamp buttons to illuminate EXT)

45. __ Turn Laser To High Power (Toggle Low/High Button, Turn Energy Dial to display 999)

46. __ Put on Laser Safety Goggles

47. __ **TURN ON LASER WARNING LIGHT!!! DO NOT PROCEED WITHOUT DOING THIS STEP!**

48. __ Turn on Smoke Generator (On Switch and on button on foot pedal)

49. __ Once Ready light on smoke generator foot pedal is illuminated, Start the tunnel

50. __ Generate Smoke until smoke is sufficiently dense by hitting start on pedal (no measurement for this, just use best judgement)

51. __ Turn all lights in the ready room, control room, and test section off

52. __ Press Run on Quantum Composer (if laser doesn’t turn on, hit Laser 1 and Laser 2 Buttons on Laser Power Box)

53. __ Press Record in PCO Camware64

54. __ Once 168 image pairs have been recorded, press stop in PCO Camware64

55. __ Export Recorder Sequence (File > Export Recorder Sequence > select desired save destination > Select Split doubleshutter > Save)

Data Analysis

56. __ Open DaVis 8.4.0

57. __ Start a new PIV Project (New button in top left > type of project is PIV)

58. __ Click Import in top Left

59. __ Use Directory on left to navigate to the desired images and select image A of the first image pair

60. __ Define time between frames as T4 and time between images as PCO Exposure time

61. __ Click Add to List

62. __ Select the image from the import list in the bottom left

63. __ Verify the file range to be imported includes the full range of images captured

64. __ Click Import Data

65. __ Click Exit

66. __ Select imported dataset, then click Processing

67. __ Add Group Vector Calculation - Double Frames, Operation PIV (particle image velocimetry)

68. __ Under Vector Calculation parameter, select Cross correlation, leave all other settings

69. __ Select Test Processing and verify result matches expected flow characteristics

70. __ Repeat steps 53-55 for remainder of test

71. __ Once All Points have been Captured, Shut Down Tunnel

72. __ Press Stop on Quantum Composer

73. __ To process all data, follow steps 58 - 69, but select Start processing instead of test processing

<u>1.</u>

Frame should be bolted in at each corner, with 1/4-20 bolts.

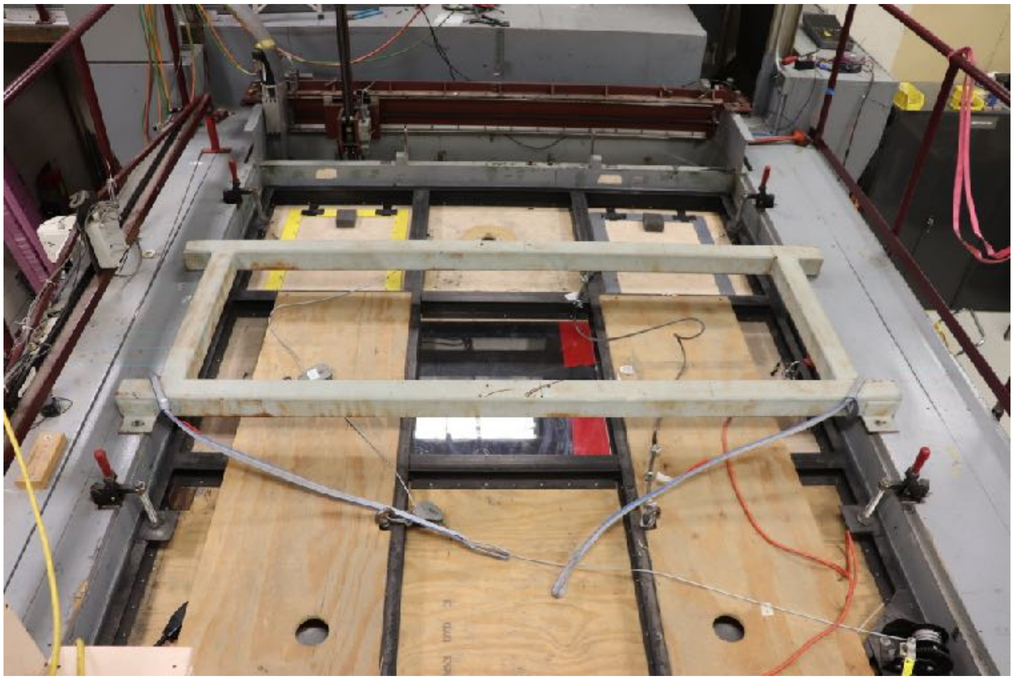

<u>2.</u>

Frame is bolted into the 6 steel mounting blocks on the side of the test section. A close-up of the mounting bracket can be seen below:

3.

The optics table should be clamped to the PIV frame on the roof of the tunnel in such a way that it will not vibrate or move independently from the frame.

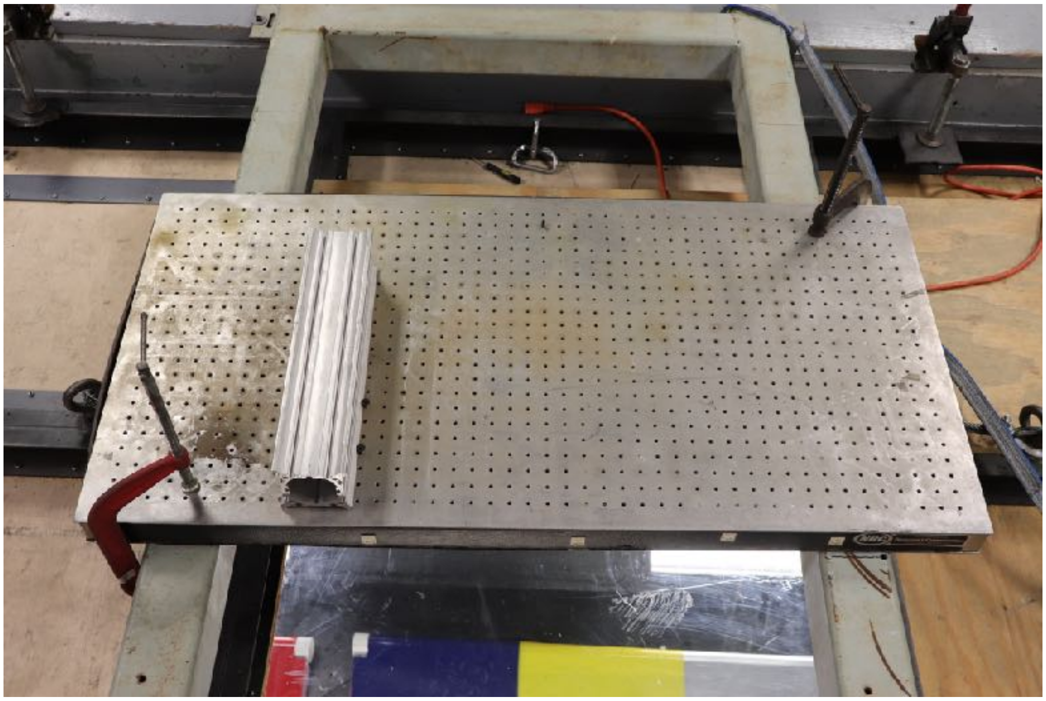

4.

Laser head should be bolted into a corner position such that it minimizes the area of the mounting table occupied.

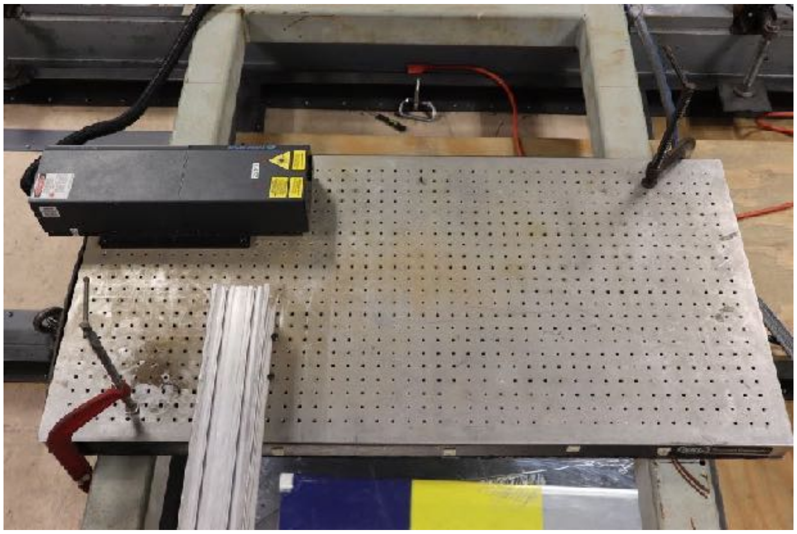

5.

The laser head has 4 connections which must be made to ensure proper operation. The water routing is color coded to ensure proper flow direction.

6.

Connection rail 1 should be bolted onto the laser table with at least 3" of overhang to facilitate the attachment of Connection rail 2. Connection rail 1 can be shifted as needed to accommodate connection rail 2 during the installation step.

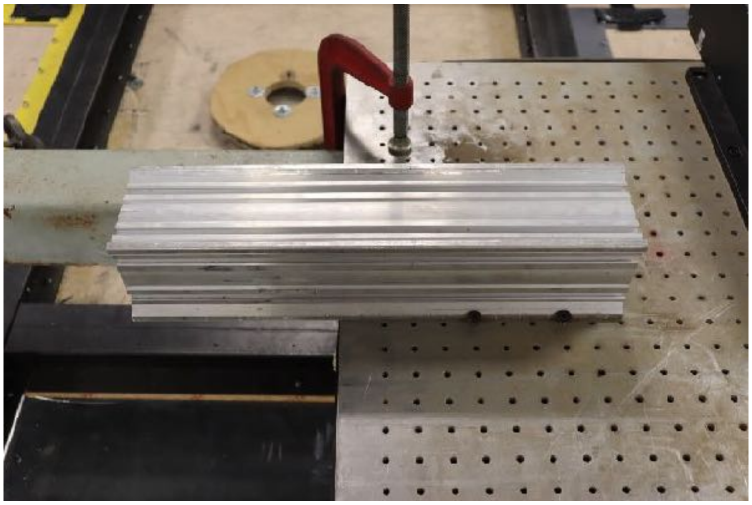

7.

The first mirror should be attached directly to the optics table with a 1” tall aluminum post using an insert that screws directly into the holes on the optics table. Be sure to align the mirror with the laser such that the beam can be turned at a 90 degree angle to run parallel with connection rail 1.

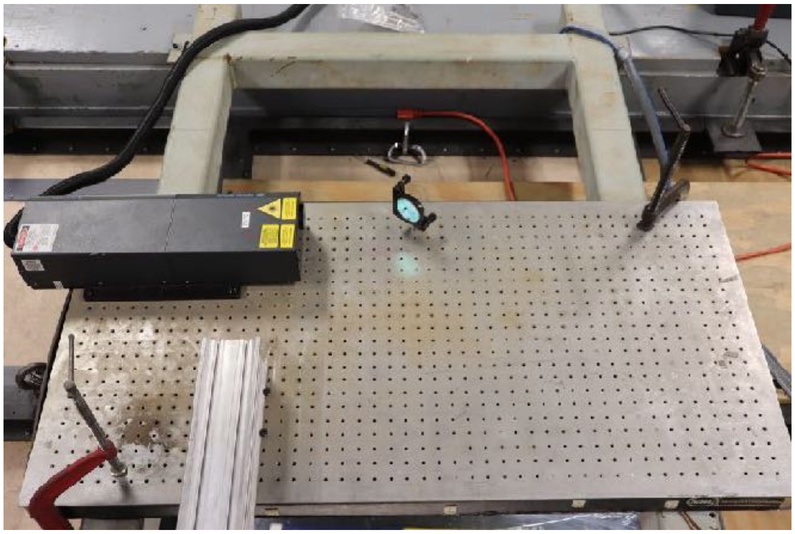

8.

The mirror, focusing lens, and cylindrical lens must be spaced such that the mounts will not interfere with one another, and the beam will be as focused as possible going into the cylindrical mirror. The exact distance changes depending on the lens used, but the distance between the focusing lens and the cylindrical lens should be equal the focal length of the focusing lens. Be sure the flat side of the cylindrical lens points towards the focusing lens. Exact placement of the mirror can be changed to angle the laser into the focusing lens.

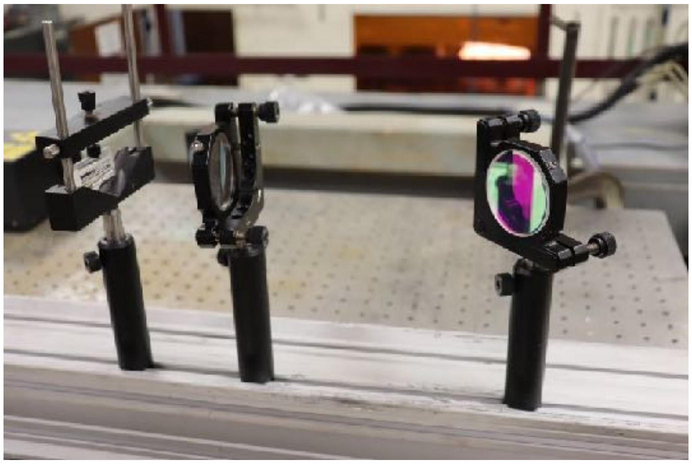

9.

Connection rail 2 should be clamped to connection rail 1 in such a way that the mirror will angle the beam off the laser table and down into the focusing lens.

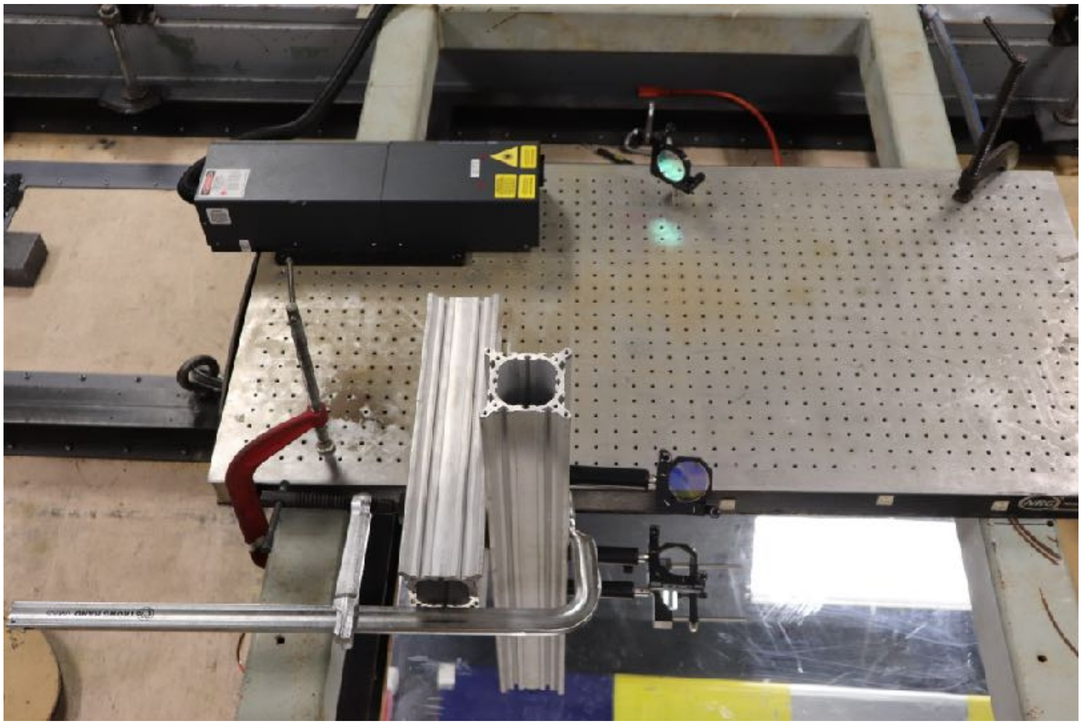

10.

The calibration plate should be set at the region of interest in the tunnel. For freestream tests and/or measurements around a model, this requires the use of a tripod or other support structure to locate the calibration plate in the desired area. For model tests, the plate can be placed directly on the model in the region of interest. It is highly recommended to secure the plate with a strip of aluminum tape on the back side so that it does not fall through gaps in the floor plate and into the balance room.

11.

When powering the laser on, it takes a few seconds after hitting start before the lasers will actually be able to turn on. There is a change in the frequency of the sound made by the laser which tells the user it is ready to be activated.

12.

Coarse movements of the beam can be made by moving the mirror and its optical post within the mount. Fine movements can be made using the knobs on the lens holder, with the target being the front edge of the calibration plate.

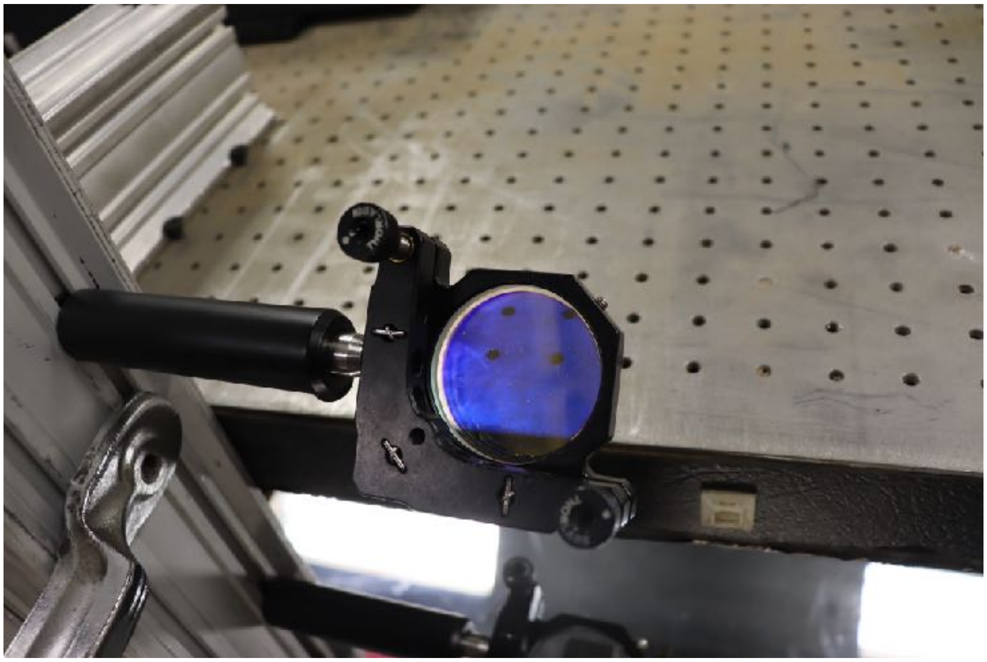

13.

The focusing lens may be moved up and down connection rail 2 to change the width and thickness of the laser sheet. For 2-D PIV, the sheet should be made as thin as possible.

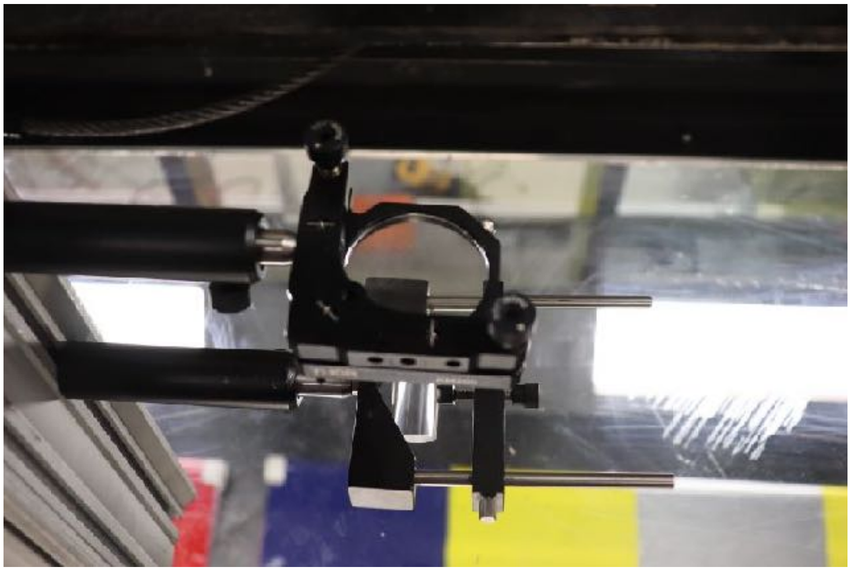

14.

This step is self explanatory. To stop the laser, press the stop button on the control box.

15.

Remove the smoke port by unscrewing the two bolts holding the plate into the wall of the tunnel.

16.

The smoke tubes are friction fit to slide together, and should not require tightening. If excess smoke is being released from the system during operation, slightly tighten the tubing using the screws located at each joiner.

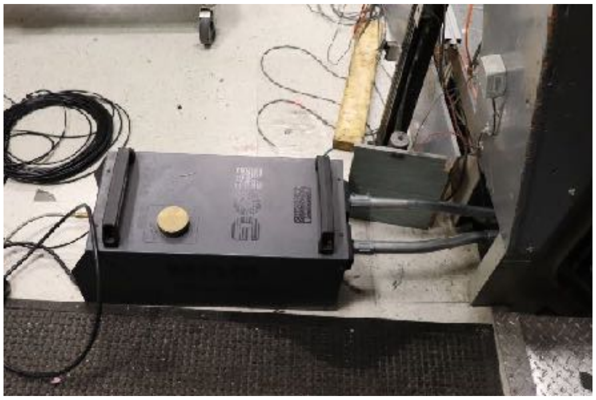

17.

The foot pedal plugs into the back of the smoke generator, and the smoke generator power plugs into an extension cord that runs into the corresponding plug below the 208V AC power switch on the left side of the ready room.

18.

The regulator can be attached to the smoke generator with a wrench. Be sure to tighten the connection with one wrench on the regulator input and one on the smoke generator input port to seal the connection as fully as possible.

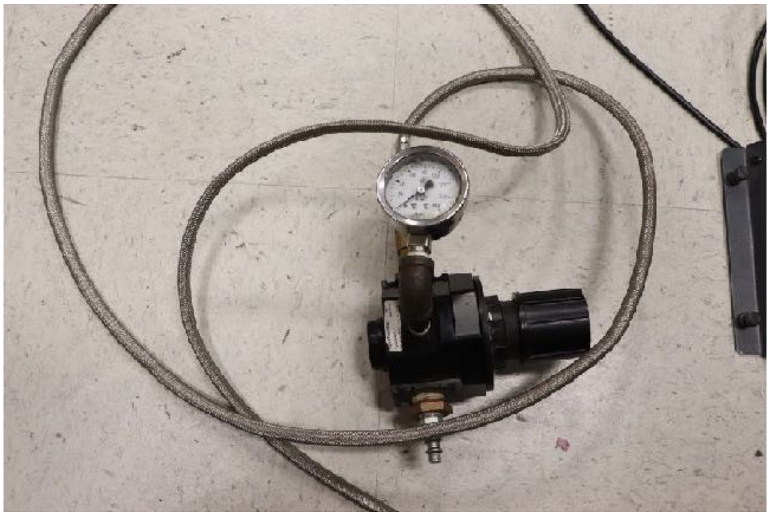

19.

A compressed air line can be pulled from next to the tunnel entry door and attached to the regulator.

20.

Depending on the regulator used, exact operation will vary, but setting the regulator to 30 psi is vital to the successful operation of the smoke generator. If the pressure is too low, the fog fluid will not be released into the heating element of the system, failing to produce any smoke. If the pressure is too high, the fluid will not spend enough time near the heating coil, shooting fog liquid into the test section of the tunnel without ever producing smoke.

21.

The camera should fit into the mounting bracket such that the back of the camera is flush with the back side of the mounting bracket, and the bottom of the camera mates flush with the inside surface of the mounting bracket.

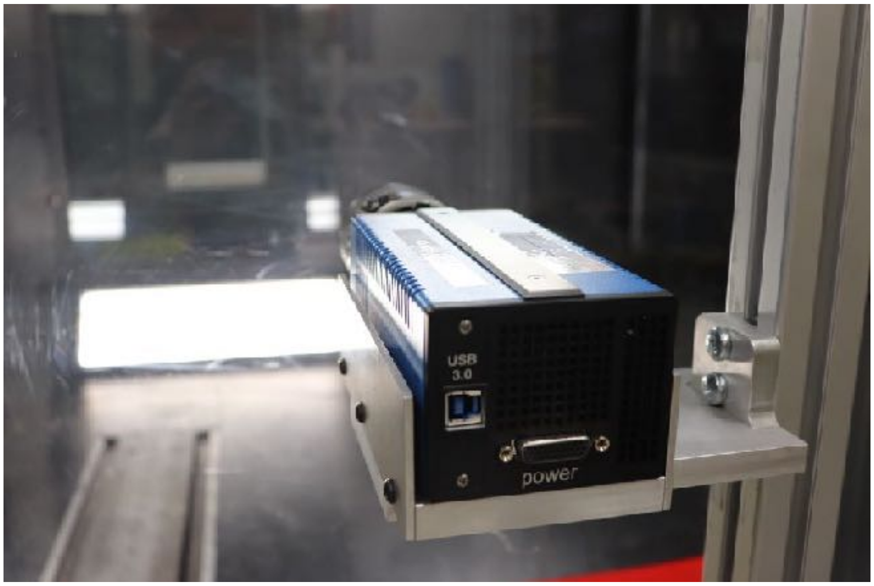

22.

If pulling the camera out from storage, attach the lens to the front of the camera by lining up the grooves on the lens and carmera base and twisting the lens until it clicks into place.

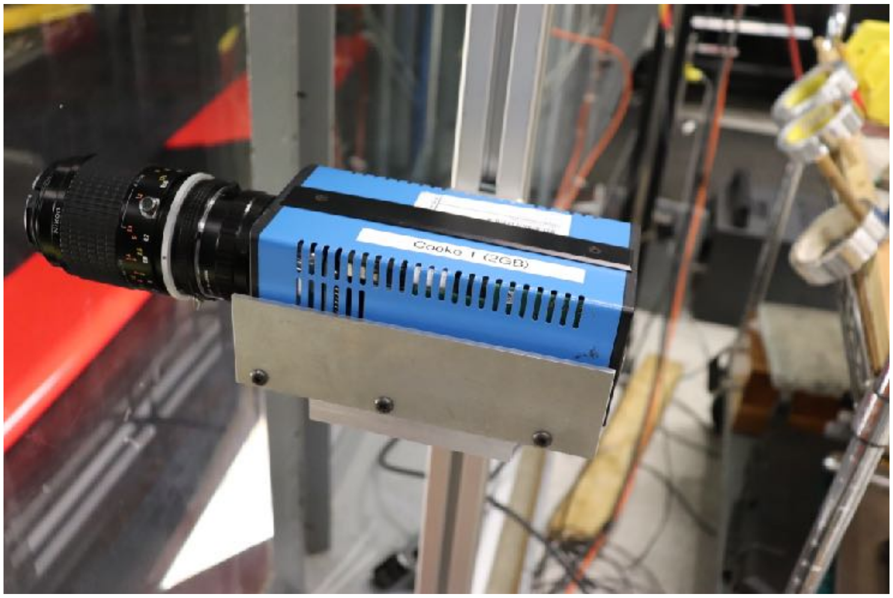

23.

The camera and power box are connected with a specific pinned adapter that must be screwed in with a flathead screwdriver. The camera power box is powered with a standard plug that is included in the yellow storage case.

24.

Each yellow storage case also includes a USB 3.0 cord that can be used to plug the camera into the computer. This allows for data transfer between the camera and the computer, and is necessary for the images to show up in the PCO camware64 software.

25.

The camera is powered on by flipping the power switch on the front of the power box. Once both lights on the front of the box have a steady green light, proceed to the next step.

26.

Use the start menu or desktop shortcut to navigate to PCO camware64. This program is what we use to capture all PIV image pairs, and is critical for all PIV data collection.

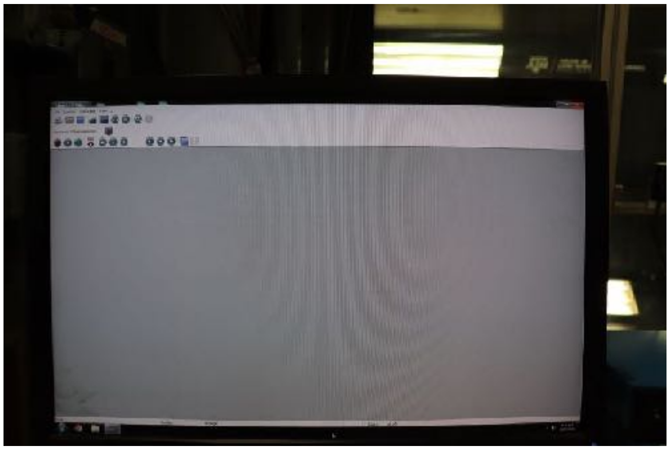

27.

Remove the lens cap on the camera to allow proper imaging of the region of interest.

28.

Exposure view windows can be opened by selecting the view tab, then selecting B/W window and clicking on image A + image B. This will produce two new windows that display the current view of image A and image B.

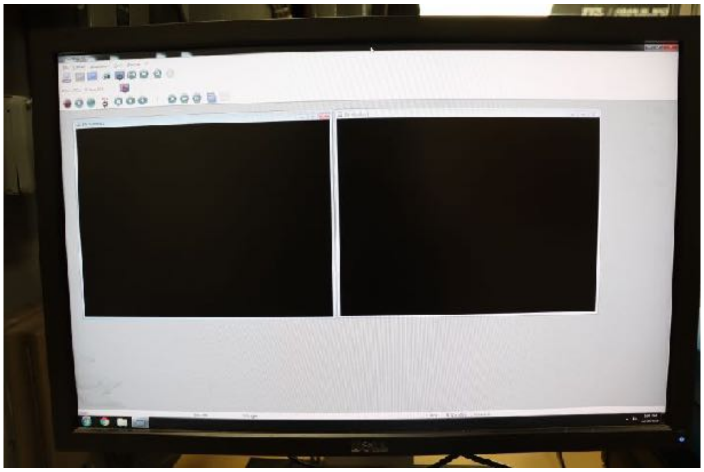

29.

Align the camera with the calibration plate by moving the vertical support of the mounting frame in the streamwise direction and moving the mounting bracket up and down on the vertical support. It is important to note that the calibration plate must fill the majority of the image frame in order for DaVis to produce a good calibration, so the zoom might need to be adjusted depending on the lens being used. A good camera placement can be seen below:

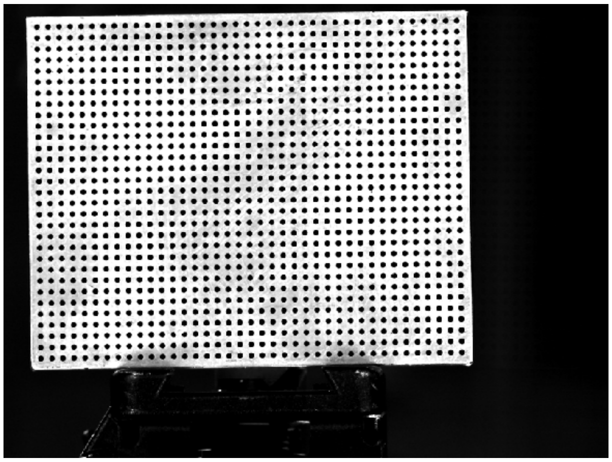

30.

Image capture settings can be changed by selecting Camera control, then clicking auto sequence in the new window and accept. If done correctly, the window should look like the picture below:

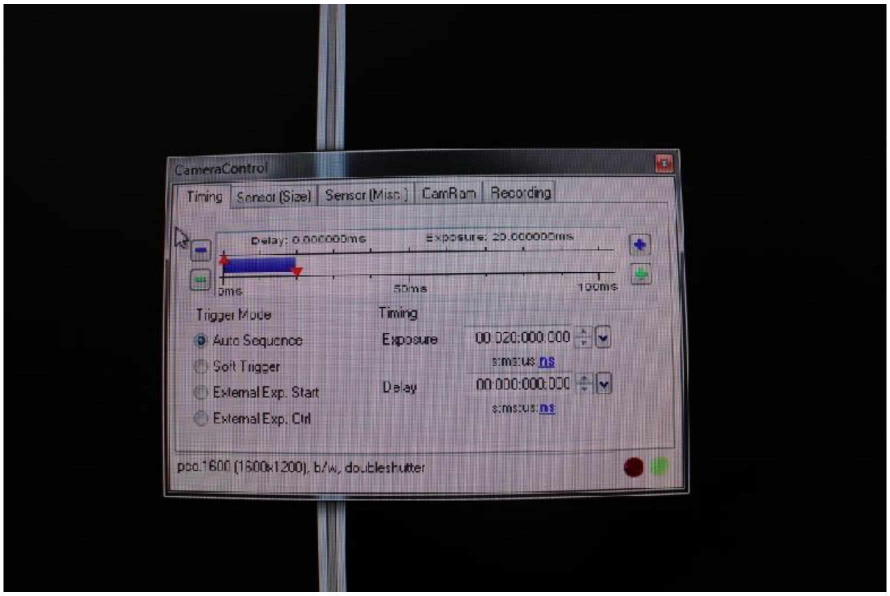

Delay: 0.000000ms

Exposure: 20.000000ms

Trigger Mode
- ● Auto Sequence
- ○ Soft Trigger
- ○ External Exp. Start
- ○ External Exp. Ctrl

Timing

Exposure 00:020:000.000 s:ms:us:ns

Delay 00:000:000.000 s:ms:us:ns

pco.1600 (1600x1200), b/w, doubleshutter

31.

To record images, click the red record button in the top left corner of the screen. The progress bar in the bottom left will begin to turn blue, and the recorder sequence can be stopped at any point with the white square next to the record button.

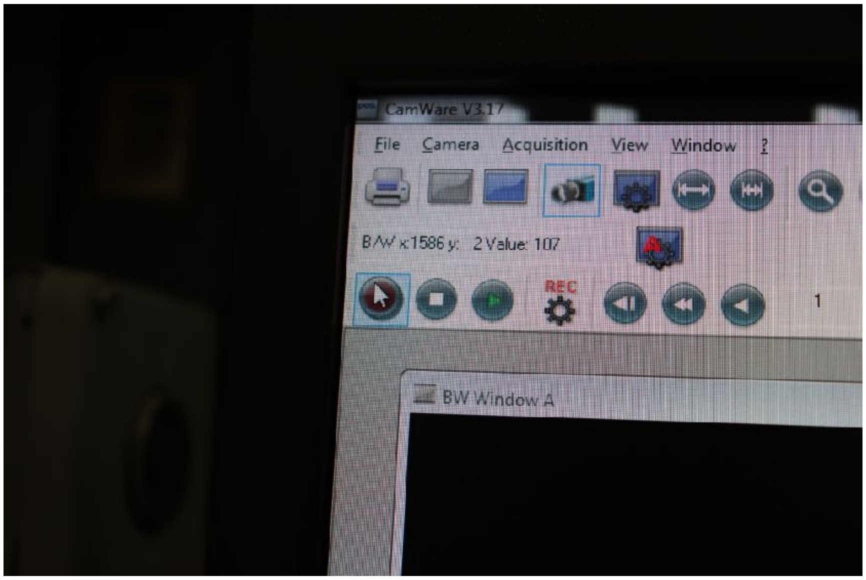

B/W x:1586 y: 2 Value: 107

32.

To export the images, click file, then export recorder sequence. Use the navigation menu to select the desired save destination, check the split double shutter box and click save.

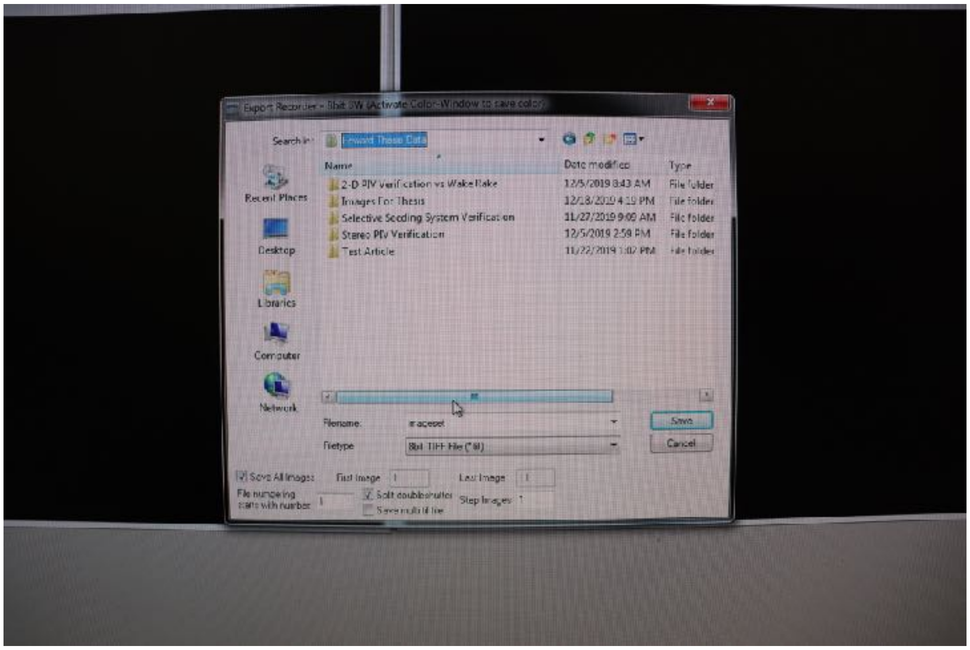

Search in: Forward These Data

Name	Date modified	Type
2-D PIV Verification vs Wake Rake	12/5/2019 8:43 AM	File folder
Images For Thesis	12/18/2019 4:19 PM	File folder
Selective Seeding System Verification	11/27/2019 9:09 AM	File folder
Stereo PIV Verification	12/5/2019 2:59 PM	File folder
Test Article	11/22/2019 1:02 PM	File folder

Filename: traceset
Filetype: 8bit TIFF File (*.tif)
☑ Save All Images First Image 1 Last Image 1
File numbering starts with number 1
☑ Split doubleshutter
☐ Save multi tif file
Step Images 1

33.

Navigate to the save destination of the calibration images and open one of the images to check the focus and alignment of the image. It is vital that the image is well-focused, otherwise the particles will not be easily identified by DaVis during image processing, resulting in incorrect measurements. Below is an example of a well-focused and aligned calibration image. You don't have to worry about any in-plane rotations of the plate, as these will be corrected during the calibration regime in DaVis.

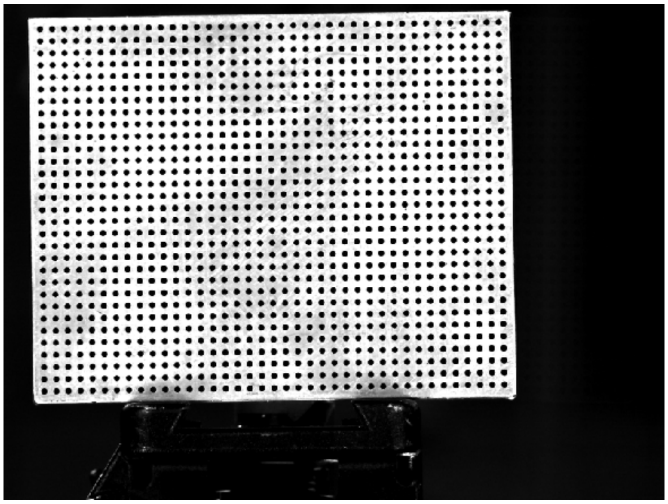

34.

To measure the pixels per inch, draw a volume from one side of the calibration plate to the other, with the corners of the box as close to the edges of the plate as possible. This will produce a pixel measurement for the calibration plate, which can be used to determine the conversion for pixels to inches. This will become relevant during setup of the quantum composer, so write the pixels per inch value down.

35.

To calculate the time for a particle to move 20 pixels in the image, one must determine a desired run speed in inches per second, and then use the pixels per inch value obtained in step 34 to convert the run speed into pixels per second. From there, calculate the time for each particle to move 20 pixels in the image with the following formula:

20 ÷ (pixels per second) = Time for a particle to move 20 pixels

36.

Use BNC cables to attach the laser power system to the quantum composer, attaching Fire Lamp 1 to T1, Fire Lamp 2 to T4, Fire Q-Sw 1 to T6, and Fire Q-Sw 2 to T7. It helps to have the cables color coded to make setup easier.

37.

The camera can be attached to the quantum composer with another BNC cable, running camera external exp trig to T8.

38.

Turning on the quantum composer is as simple as hitting the power button on the quantum composer. If it doesn't turn on, ensure that it is plugged in.

39 - 41.

To set the laser and camera timings, use the next button to navigate to the time delay for a given channel, and use the arrow keys on the quantum composer to change the time delay and reference time for that channel. For the reference time, T0 refers to the moment the run button is pressed, while all other TX values set the reference to another channel. To shift between channels (T1 to T2, etc.), press function and then channel.

42.

To set the camera control to external control in PCO camware64, select camera control, then click external exposure start and then accept.

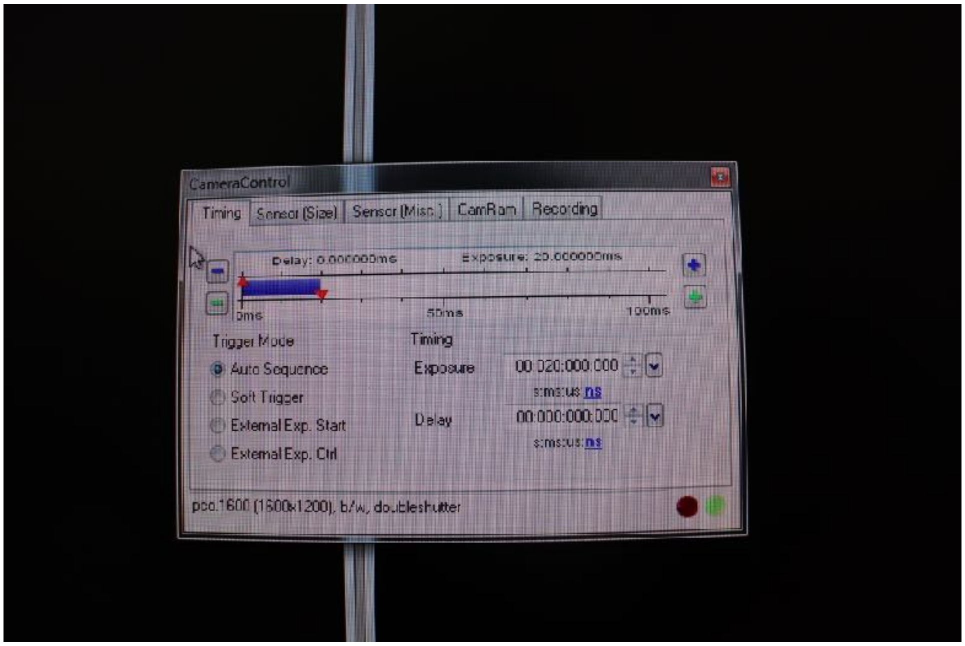

Delay: 0.000000ms
Exposure: 20.000000ms

Trigger Mode
● Auto Sequence
○ Soft Trigger
○ External Exp. Start
○ External Exp. Ctrl

Timing
Exposure 00:020:000:000 s:ms:us:ns
Delay 00:000:000:000 s:ms:us:ns

pco.1600 (1600x1200), b/w, doubleshutter

43.

To start the laser firing, press and hold start on the laser for approximately 2 seconds. Once the whirring of the laser decreases in frequency (clear audio cue), then press the laser 1 and laser 2 buttons to start the laser firing.

44.

Switch the laser to external control by pressing the Flashlamp and Q-SW buttons so that the light under EXT is illuminated.

45.

Turn the laser to high power by pressing the pressing the low/high button so that the light under high is illuminated, and turn the energy dial clockwise until the digital readout displays 999.

46.

Before proceeding, it is imperative that all personnel that will be in the ready room while conducting PIV are wearing laser safety goggles. The LSWT has multiple pairs that can be worn, including two that can be worn over normal glasses. At high power, this laser can do permanent damage to the naked eye, so it is vital that you are wearing proper safety attire prior to use of the laser at high power.

47.

It is also vital that you turn on the laser warning light. The switch may be found on the shelf in the front right corner of the control room on the shelf. This will illuminate the red lights above each entry to the ready room so that everyone in the facility will know the laser is in use and will take the necessary safety precautions.

48.

Turn on the smoke generator by flipping the switch on the generator and then pressing the on button on the foot pedal.

49.

This step is fairly self explanatory, there is a light on the foot pedal of the smoke generator that is labeled ready. When the generator is sufficiently warm, the ready light will turn green. When this happens, start the tunnel and get up to the desired speed.

50.

To generate smoke sufficiently dense for PIV measurements, press the start button on the foot pedal and allow the system to generate smoke until you see smoke coming from the settling chamber and into the test section. When that occurs, press the start button again and move to the next step.

51.

This step is also self explanatory. Turn off all lights in the ready room, control room, and test section. The goal is to eliminate as much light as possible to maximize the contrast between the particles illuminated by the laser sheet and the background of the image. Thus, making the room as dark as possible is ideal.

52.

Press the run button on the quantum composer to start the laser. Sometimes the laser will not start up on the first press of Run for reasons unknown. If this happens, leave the quantum composer running and press the laser 1 and laser 2 buttons on the laser power box.

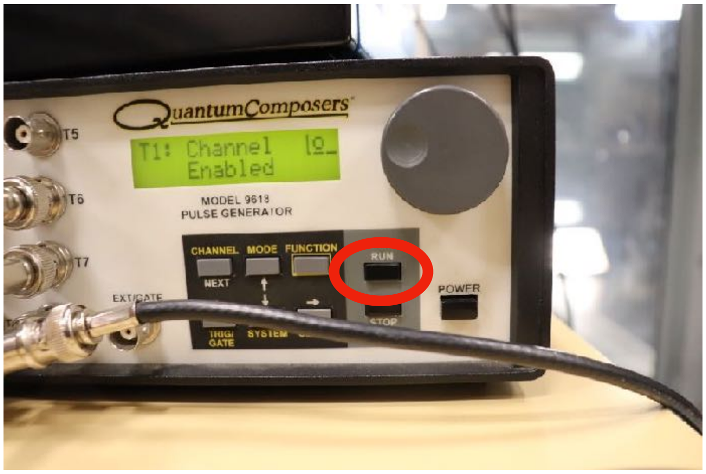

53.

To record image pairs, click the red record button in the top left corner of PCO camware64.

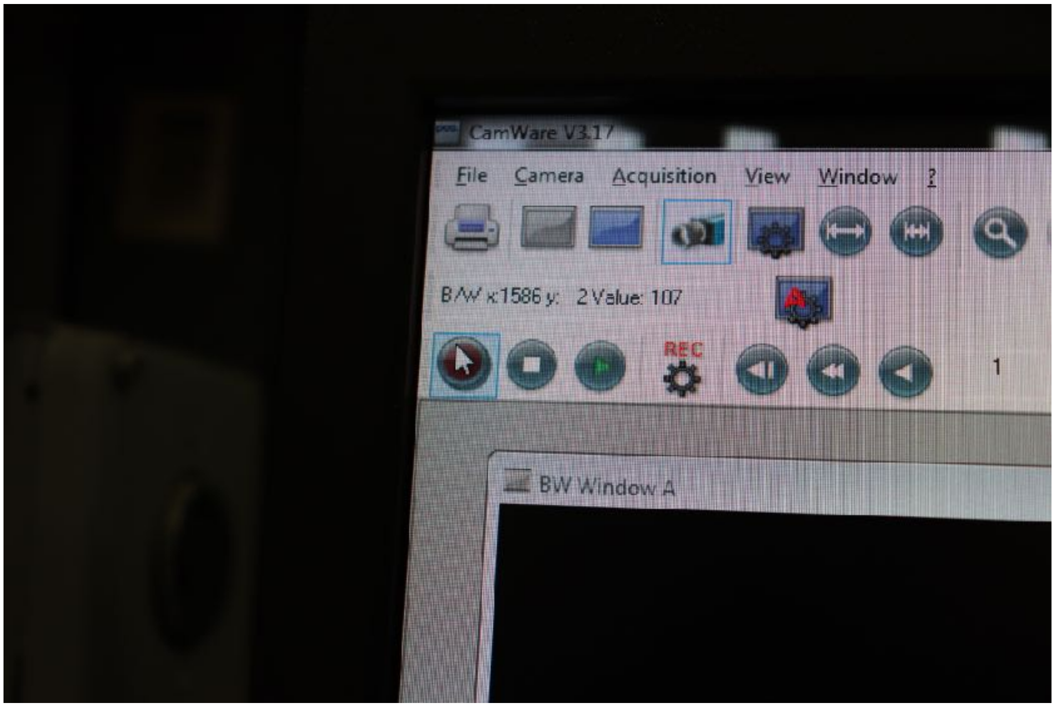

54.

Once the blue progress bar in the lower left portion of the screen is full, press stop in the upper left corner of PCO camware 64.

B/W x: 138 y: 50 Value: 112

55.

To export the images, click file, then export recorder sequence. Use the navigation menu to select the desired save destination, check the split double shutter box and click save.

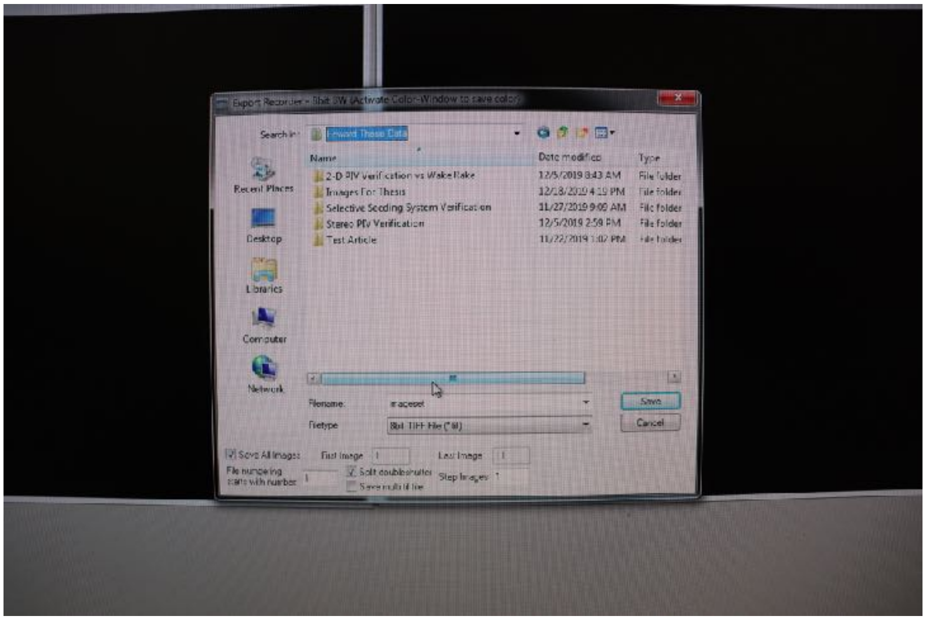

Search in: Forward These Data

Name	Date modified	Type
2-D PIV Verification vs Wake Rake	12/5/2019 8:43 AM	File folder
Images For Thesis	12/18/2019 4:19 PM	File folder
Selective Seeding System Verification	11/27/2019 9:09 AM	File folder
Stereo PIV Verification	12/5/2019 2:59 PM	File folder
Test Article	11/22/2019 1:02 PM	File folder

Filename: traceset

Filetype: 8bit TIFF File (*.tif)

☑ Save All Images

First Image: 1

Last Image: 1

File numbering starts with number: 1

☑ Split doubleshutter

☐ Save multi tif file

Step Images: 1

56.

Now that a dataset has been captured, it must be analyzed to ensure the image pairs captured produce reasonable data. To do this, DaVis 8.4.0 must be opened. It is important to note that the license dongle must be inserted into one of the USB ports on the computer in order for the program to open.

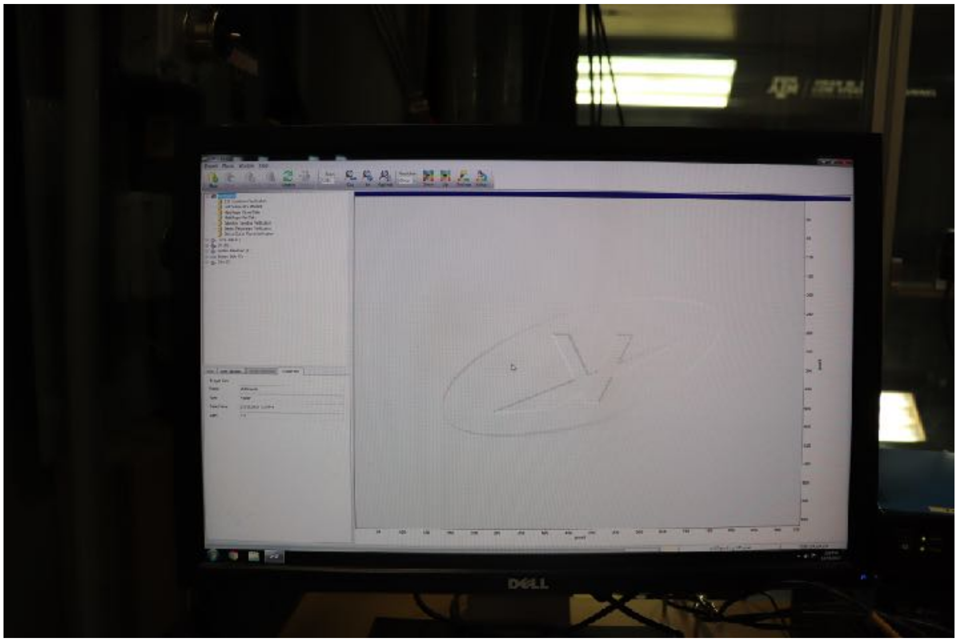

57.

To start a new PIV project, select the new icon in the top left corner of the screen. Select specify and input the desired project name, and be sure to designate the type of project as PIV before hitting ok.

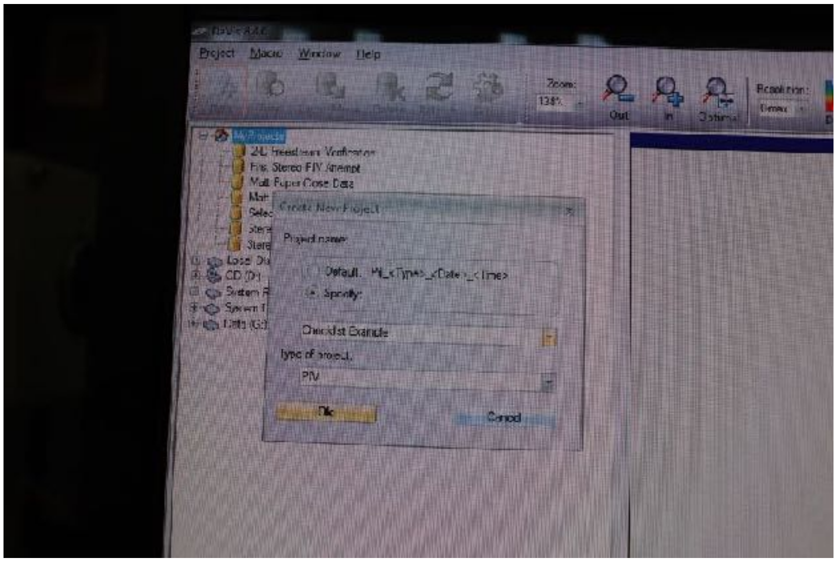

Project name:

○ Default: PIV_<Type>_<Date>_<Time>

● Specify:

Checklist Example

Type of project:

PIV

58.

To import the desired image pairs, select the import icon in the top left corner of the screen. This should send you to the screen shown below:

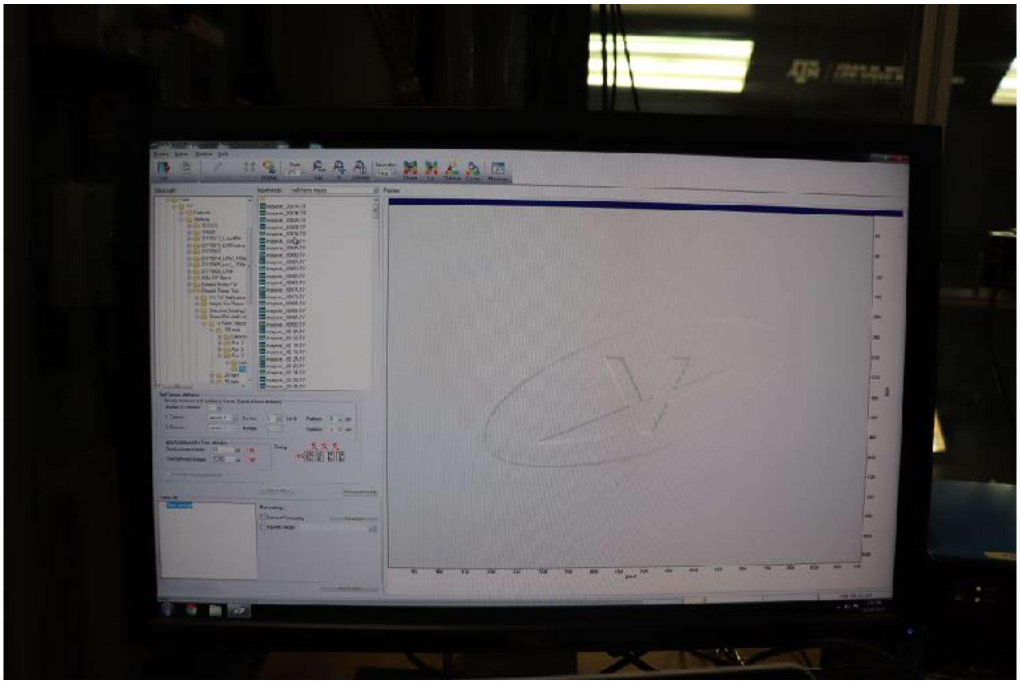

59.

Use the directory to navigate to the desired set of images for importing, and select image A from the first image pair of the dataset.

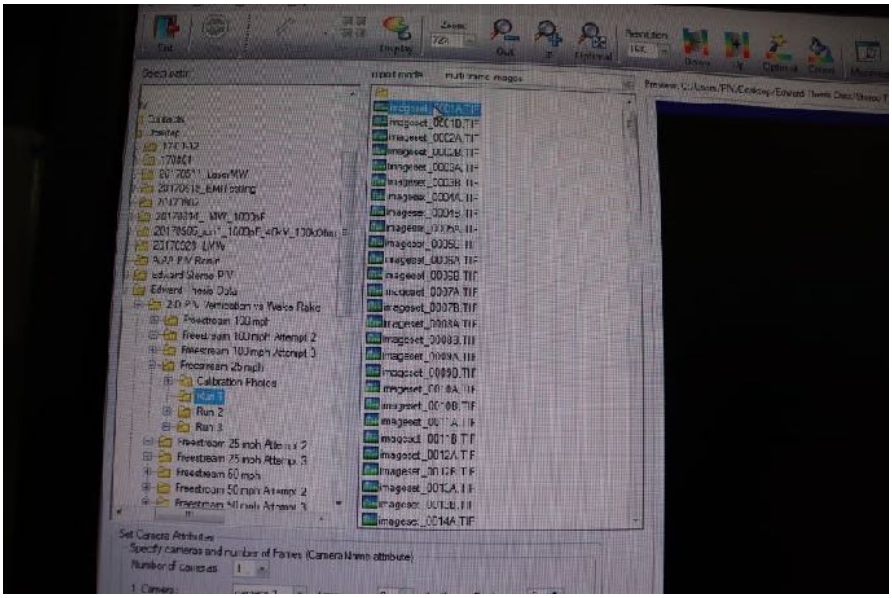

60.

In the import menu, define the time between frames as the delay on T4 in the quantum composer and the time between images as the exposure time defined in PCO camware64.

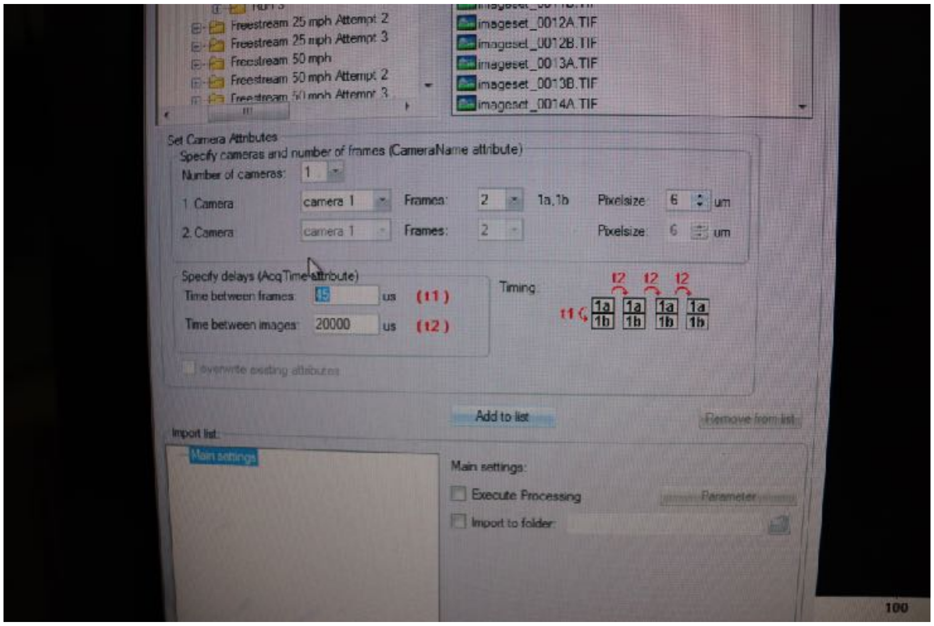

Set Camera Attributes

Specify cameras and number of frames (CameraName attribute)

Number of cameras: 1

1. Camera: camera 1 Frames: 2 1a,1b Pixelsize: 6 um

2. Camera: camera 1 Frames: 2 Pixelsize: 6 um

Specify delays (AcqTime attribute)

Time between frames: 15 us (t1)

Time between images: 20000 us (t2)

☐ overwrite existing attributes

Main settings:

☐ Execute Processing

☐ Import to folder:

61.

Click the add to list button on the left side of the screen to prepare the images for importing.

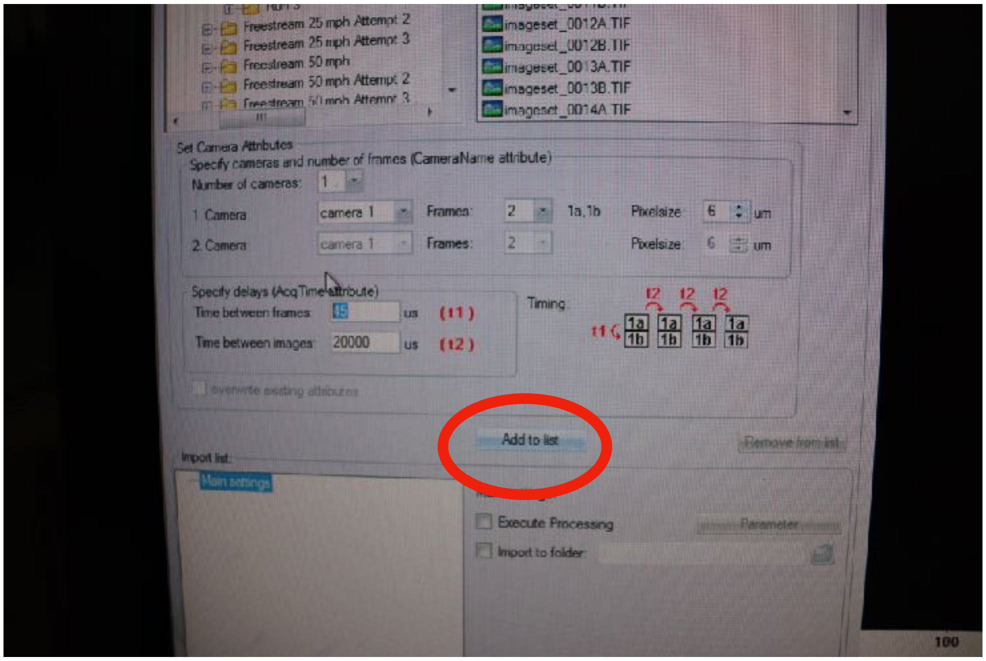

Set Camera Attributes

Specify cameras and number of frames (CameraName attribute)

Number of cameras: 1

1. Camera: camera 1 Frames: 2 1a,1b Pixelsize: 6 um

2. Camera: camera 1 Frames: 2 Pixelsize: 6 um

Specify delays (AcqTime attribute)

Time between frames: 15 us (t1)

Time between images: 20000 us (t2)

☐ overwrite existing attributes

☐ Execute Processing

☐ Import to folder:

62.

Now that Add to list has been clicked, the desired image should appear in the import list on the lower left corner of the screen. To view the import details for the desired dataset, select the image from the import list.

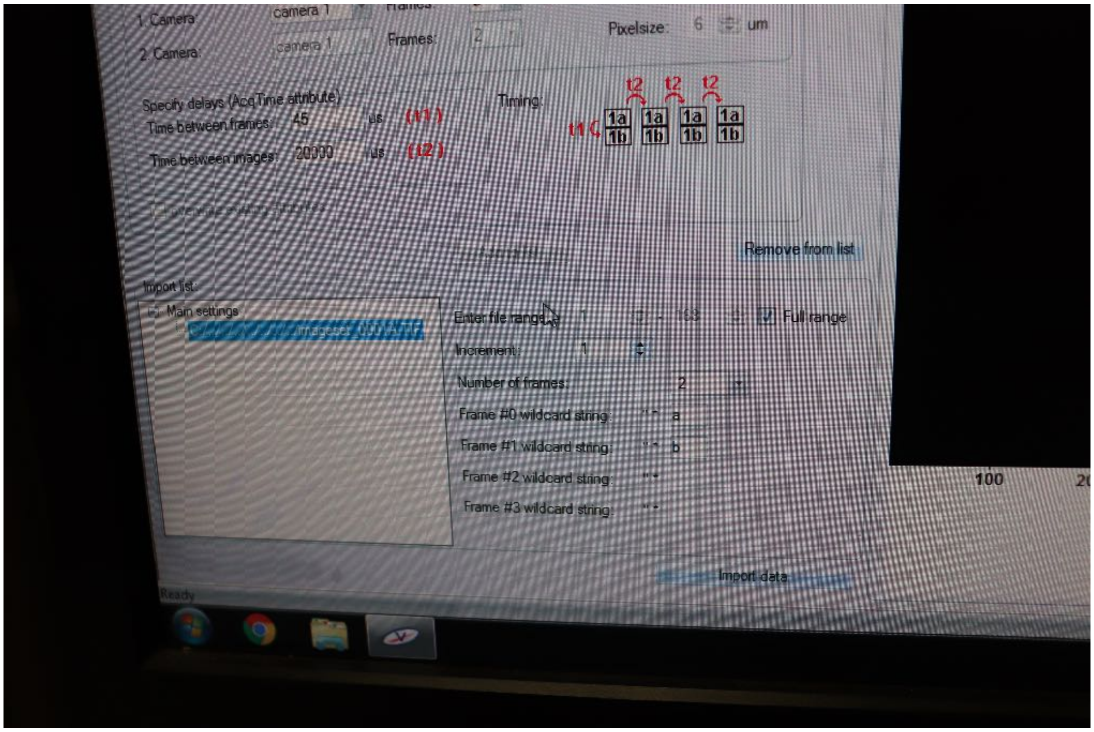

1. Camera: camera 1
2. Camera: camera 1
Frames: 2
Pixelsize: 6 um
Specify delays (AcqTime attribute)
Time between frames: 45 us (t1)
Time between images: 20000 us (t2)
Enter file range: 1 - 168 ☑ Full range
Increment: 1
Number of frames: 2
Frame #0 wildcard string: a
Frame #1 wildcard string: b
Frame #2 wildcard string:
Frame #3 wildcard string:

63.

Verifying the full range of images is imported by verifying the full range box is checked under the import details for the desired dataset. This range is located on the bottom left side of the screen, next to the import list.

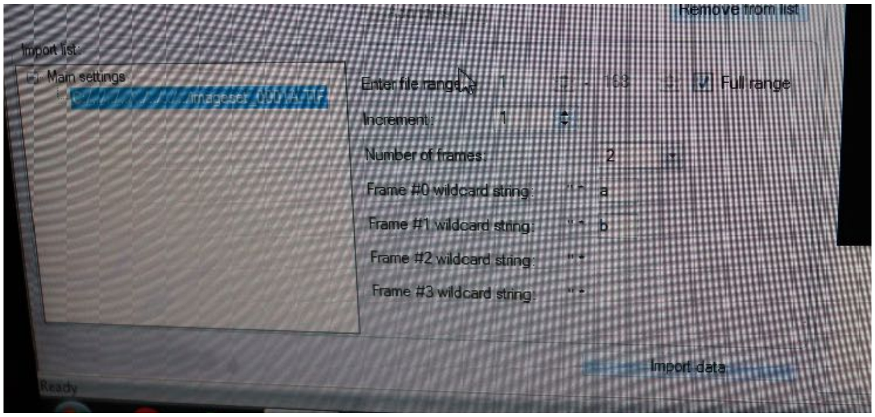

Enter file range: 1 - 168 ☑ Full range
Increment: 1
Number of frames: 2
Frame #0 wildcard string: a
Frame #1 wildcard string: b
Frame #2 wildcard string:
Frame #3 wildcard string:

64.

The import data button can also be found on the lower left side of the screen, beneath the import details and import list prompts. Clicking this button will import all image pairs from the import list into DaVis for processing.

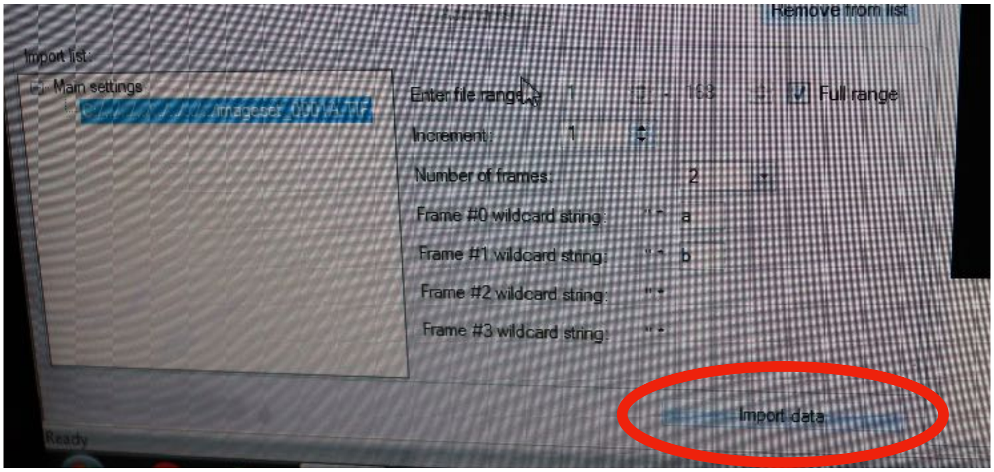

Import list:

Main settings

Enter file range: 1 - [illegible] ☑ Full range

Increment: 1

Number of frames: 2

Frame #0 wildcard string: "*" a

Frame #1 wildcard string: "*" b

Frame #2 wildcard string: "*"

Frame #3 wildcard string: "*"

65.

Once the exit icon in the top left corner becomes selectable, click exit to return to the project home screen.

66.

To process data, select the newly imported data and click processing in the top toolbar. This will navigate you to the data processing screen.

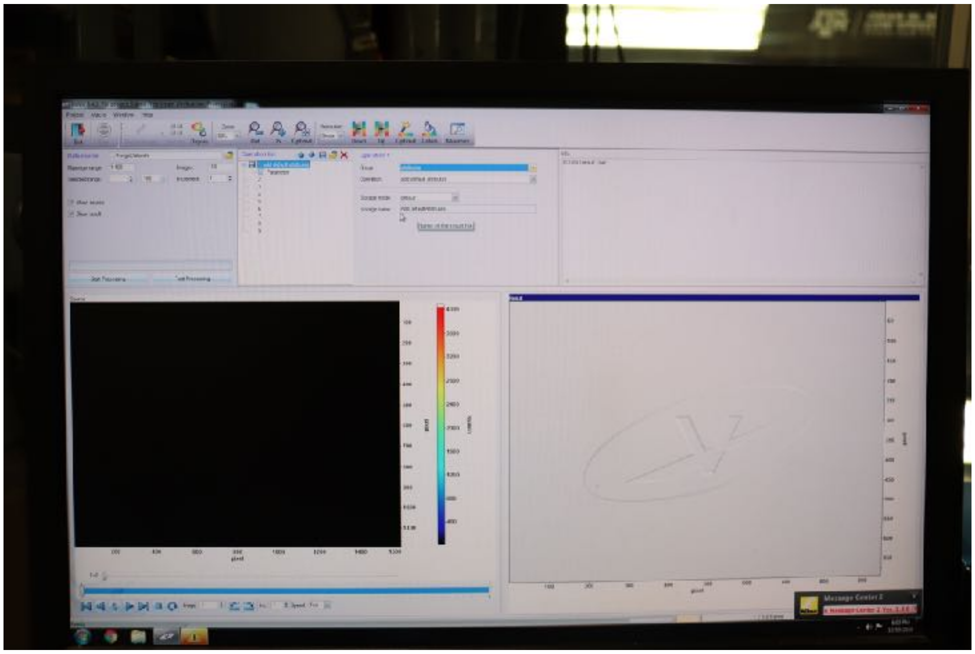

67.

To add a new processing step, clear the operation list with the red x in the upper right corner of the list, and then add a new operation. Under group, select Vector Calculation - Double Frames, and under operation select PIV (particle image velocimetry). Storage mode and storage name should be left alone.

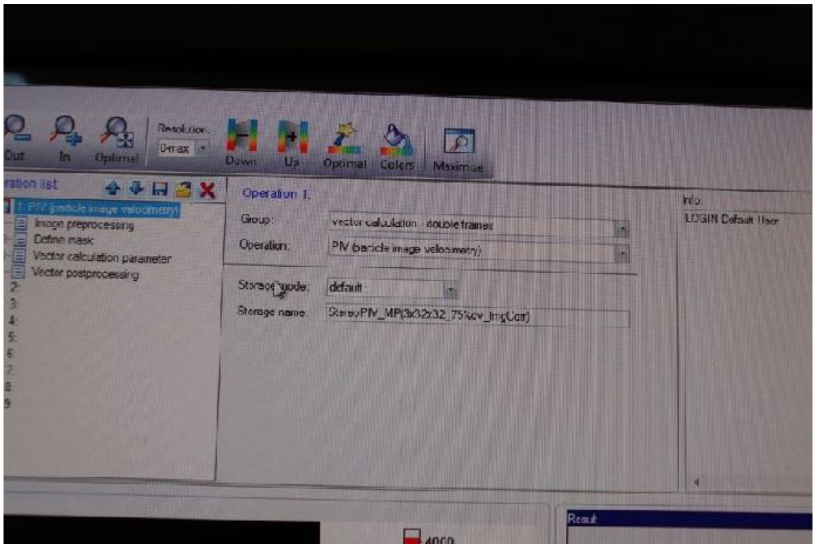

Operation 1.

Group: vector calculation - double frames

Operation: PIV (particle image velocimetry)

Storage mode: default

Storage name: StereoPIV_MP(3x32x32_75%ov_ImgCorr)

68.

Select Vector calculation parameter in the operation list, and then click cross correlation. All other settings should be left in their defaults. You can verify that the settings match the image shown below:

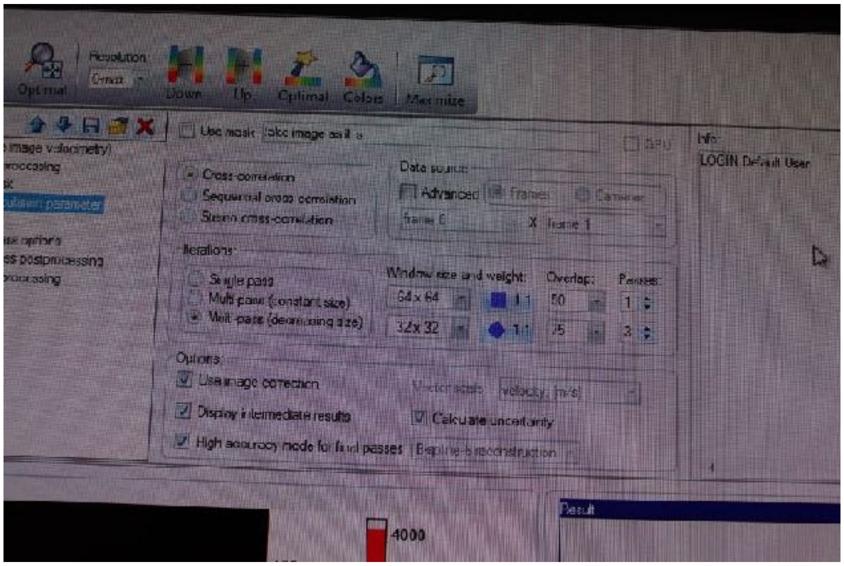

☐ Use mask
☐ GPU

● Cross-correlation
○ Sequential cross correlation
○ Stereo cross-correlation

Data source:
☐ Advanced
frame 0 X frame 1

Iterations:
○ Single pass
○ Multi pass (constant size)
● Multi pass (decreasing size)

Window size and weight:		Overlap:	Passes:
64 x 64	1:1	50	1
32 x 32	1:1	75	3

Options:
☑ Use image correction
Vector scale: velocity [m/s]
☑ Display intermediate results
☑ Calculate uncertainty
☑ High accuracy mode for final passes
B-spline-6 reconstruction

LOGIN Default User

69.

Select test processing and allow DaVis to process the first image pair. The results will show up in the results box on the lower right side of the screen. Once this is complete, verify the flow directions and values are reasonable by using the relevant vector filters under the vector length option in the upper toolbar. The test processing button can be seen in the lower portion of the image below, and the vector length selection can be seen greyed out in the top center of the image below.

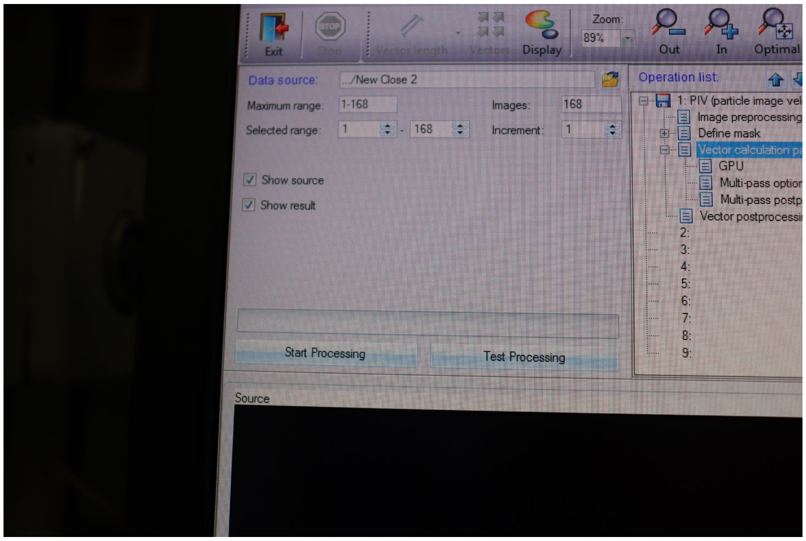

Data source: .../New Close 2
Maximum range: 1-168
Images: 168
Selected range: 1 - 168
Increment: 1

☑ Show source
☑ Show result

1: PIV (particle image vel
- Image preprocessing
- Define mask
- Vector calculation pa
  - GPU
  - Multi-pass optior
  - Multi-pass postp
- Vector postprocessi

2:
3:
4:
5:
6:
7:
8:
9:

70.

Repeat steps 53- 55 as many times as necessary to capture all requested data for the test. Depending on the customer, you may want to capture multiple datasets at each point, this is something that is by no means required, and only affects the amount of data that is taken.

71.

Once all data has been captured for a given run, shut down the tunnel.

72.

Press stop on the quantum composer to stop the laser pulses in the tunnel. This is imperative before removing safety glasses or turning off the laser warning light.

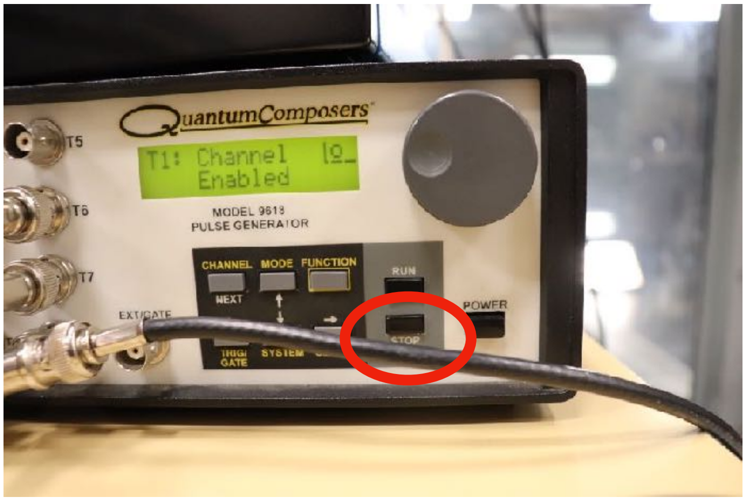

73.

To process all data for a specified point, follow steps 58 - 69, but select Start processing instead of test processing to batch process all the image pairs for that run.

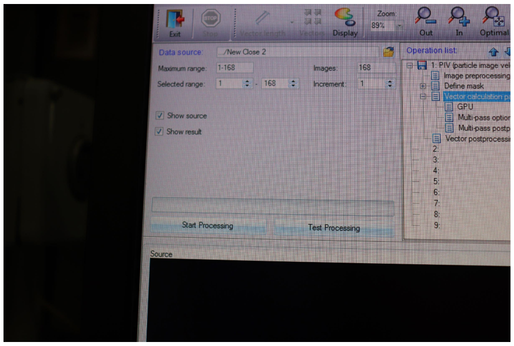

Zoom: 89%

Data source: .../New Close 2

Maximum range: 1-168

Images: 168

Selected range: 1 - 168

Increment: 1

☑ Show source

☑ Show result

APPENDIX B: STEREO-PIV SOP

Stereo PIV Setup, Operation, and Analysis Checklist (Current as of 2/6/2020)

Physical System Setup

1. __ Bolt in PIV Laser Mounting Frame to top of Tunnel

2. __ Bolt camera mounting frame to side of Tunnel

3. __ Clamp Optics table to PIV Mounting Frame

4. __ Bolt Laser Head to Optics Table

5. __ Connect Laser Head to Laser Power System

6. __ Bolt Connection Rail 1 to Optics Table

7. __ Attach Mirror to Optics Table

8. __ Attach mirror, Focusing Lens and Cylindrical Lens to Connection Rail 2

9. __ Clamp Connection Rail 2 to Connection Rail 1

10. __ Attach Calibration Plate to Desired area of Interest

11. __ Turn on Laser at low power (Flip Power Switch on Back > Turn Key to on > Hold Down Start > press Laser 1 and Laser 2)

12. __ Angle/move mirrors to center beam on calibration plate

13. __ Angle/move lenses to achieve desired beam width and thickness

14. __ Stop Laser (Press Stop)

15. __ Open Smoke Port inside Tunnel

16. __ Put Smoke tubes through smoke port and attach tubes to smoke generator

17. __ Plug Foot Pedal into Smoke Generator and Plug Smoke Generator into power

18. __ Attach Regulator to Smoke Generator

19. __ Attach Compressed Air to Regulator

20. __ Set Regulator to 30 Psi

21. __ Attach Cameras to mounting bracket

22. __ Attach Lenses to Cameras

23. __ Connect Cameras to Power Boxes and Connect Power boxes to power

24. __ Connect Cameras to Computer with USB 3.0 port

25. __ Turn On Cameras

26. __ Open PCO Camware 64

27. __ Remove Lens Caps

28. __ Open Exposure View windows for camera 1 (View > B/W Window > Camera 1 >Image A+Image B)

29. __ Open Exposure View windows for camera 2 (View > B/W Window > Camera 2 >Image A+Image B)

30. __ Align Cameras with Stereo-PIV Calibration Plate

Data Collection

31. __ Set Image Capture to Auto Sequence (Camera Control > Camera 1/2 > Auto-Sequence > Accept > right-click image and select auto range crop)

32. __ Record Calibration Images (Red Record button to start, white square to stop)

*** Note that Calibration Plate should fill the Image Field of View**

33. __ Export Camera 1 Recorder Sequence (File > Export Recorder Sequence > select desired save destination > Select Split doubleshutter > Save > Select Yes)

34. __ Export Camera 2 Recorder Sequence (File > Export Recorder Sequence > select desired save destination > Select Split doubleshutter > Save > Select Yes)

35. __ Write down/Remember which camera is Left Camera and which camera is Right Camera

36. __ Open Calibration Images and check focus and alignment (Move Cameras and recapture images as necessary)

37. __ **ONCE FOCUSED CALIBRATION IMAGES ARE CAPTURED:** Measure Pixels Per Inch on Calibration Card and write down result (pixels appear as an AAA x BBB at the top of the image)

38. __ Use Pixels per Inch and desired tunnel run speed to calculate the time for something to move 20 pixels in the image

39. __ Attach Laser to Quantum Composer (Fire Lamp 1 to T1, Fire Lamp 2 to T4, Fire Q-Sw 1 to T6, Fire Q-Sw 2 to T7)

40. __ Attach Cameras to Quantum Composer (Control In Exp Trig on both cameras to T8)

41. __ Turn On Quantum Composer

42. __ Set Laser and camera Timings (T6 delay = T1 + 190 µs, T7 Delay = T4 + 190 µs, T8 delay = T0 + 0 s)

43. __ Set time between laser pulses to the time for something to move 20 pixels with the Quantum Composer (T4 delay= T1 + X seconds)

44. __ Set time between laser pulse cycles (T1 delay = T0 + X sec)*

This step Varies based on the exposure time set in PCO Camware64. This time must be less than the exposure time in PCO Camware 64, but greater than the exposure time minus T4.* *(AKA: PCO Exposure Time - T4 < T1 < PCO Exposure Time)***

45. __ In PCO Camware64: Set Image Capture to External Exposure start (Camera Control > External Exp. Start > Accept)

46. __ Start Laser firing (hold start > press Laser 1 and Laser 2)

47. __ Turn Laser to external control (press Q-SW and Flashlamp buttons to illuminate EXT)

48. __ Turn Laser To High Power (Toggle Low/High Button, Turn Energy Dial to display 999)

49. __ Put on Laser Safety Goggles

50. __ **TURN ON LASER WARNING LIGHT!!! DO NOT PROCEED WITHOUT DOING THIS STEP!**

51. __ Turn on Smoke Generator (On Switch and on button on foot pedal)

52. __ Once Ready light on smoke generator foot pedal is illuminated, Start the tunnel

53. __ Generate Smoke until smoke is sufficiently dense by hitting start on pedal (no measurement for this, just use best judgement)

54. __ Turn all lights in the ready room, control room, and test section off

55. __ Press Run on Quantum Composer (if laser doesn't turn on, hit Laser 1 and Laser 2 Buttons on Laser Power Box)

56. __ Press Record in PCO Camware64

57. __ Once 168 image pairs have been recorded by each camera, press stop in PCO Camware64

58. __ Export Camera 1 Recorder Sequence (File > Export Recorder Sequence > select desired save destination > Select Split doubleshutter > Save)

59. __ Export Camera 2 Recorder Sequence (File > Export Recorder Sequence > select desired save destination > Select Split doubleshutter > Save)

Data Analysis

60. __ Open DaVis 8.4.0

61. __ Start a new PIV Project (New button in top left > type of project is PIV)

62. __ Click Import in top Left

63. __ Use Directory on left to navigate to the Left Camera images and select image A of the first image pair

64. __ Define time between frames as T4 and time between images as 20,000 µs

65. __ Click Add to List

66. __ Select the image from the import list in the bottom left

67. __ Verify the file range to be imported is 1 - 168

68. __ Click Import Data

69. __ Click Exit

70. __ Click Import in top Left

71. __ Use Directory on left to navigate to the Right Camera images and select image A of the first image pair

72. __ Define time between frames as T4 and time between images as PCO Exposure Time

73. __ Click Add to List

74. __ Select the image from the import list in the bottom left

75. __ Verify the file range to be imported is 1 - 168

76. __ Click Import Data

77. __ Click Exit

78. __ Select Left Camera data set, then click processing

79. __ Add Group copy and reorganize data sets, operation merge data sets to multi frame

80. __ Click Parameters, then use search on the right to select the corresponding right camera dataset

81. __ Start Processing

82. __ Click Exit when processing is finished

83. __ Select the new MergeDatasets and click Processing

84. __ Add Group attributes, Operation add Default Attributes

85. __ Click Parameters, and change number of cameras to 2, set 2. Camera to camera 2, and select overwrite existing attributes

86. __ Start Processing

87. __ Click Exit when processing is finished

88. __ Select the new AddDefaultAttributes and click Processing

89. __ Add Group vector calculation - double frames, Operation PIV (particle image velocimetry)

90. __ Click Vector calculation parameter, and select Stereo Cross Correlation without changing other settings

91. __ Click Test Processing verify result matches expected flow characteristics

92. __ Repeat steps 56-59 for remainder of test

93. __ Once All Points have been Captured, Shut Down Tunnel

94. __ Press Stop on Quantum Composer

95. __ To Process all data follow steps 62-91, but select Start processing on step 91 instead of test processing

1.

Frame should be bolted in at each corner, with 1/4-20 bolts.

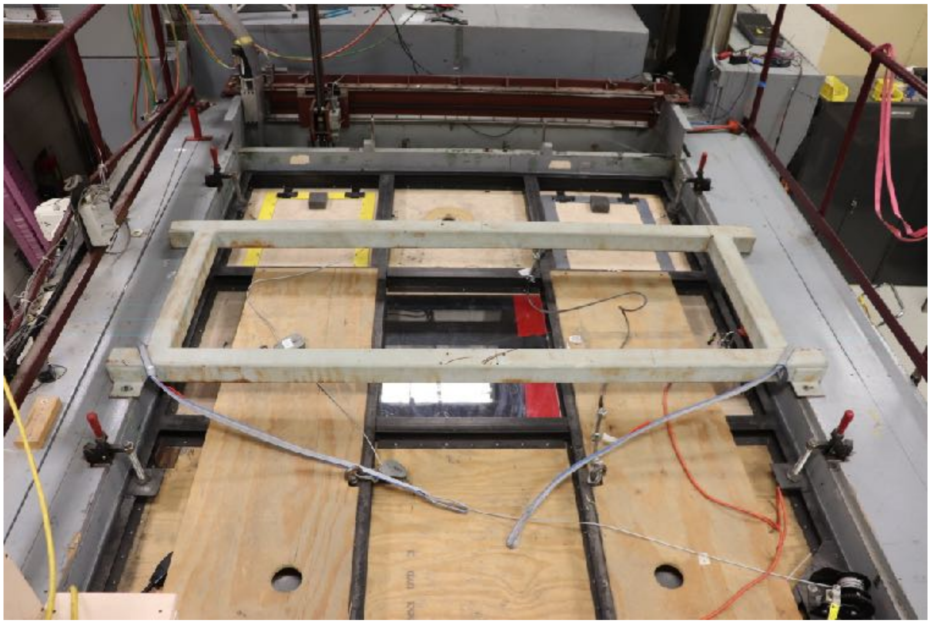

2.

Frame is bolted into the 6 steel mounting blocks on the side of the test section. A close-up of the mounting bracket can be seen below:

3.

The optics table should be clamped to the PIV frame on the roof of the tunnel in such a way that it will not vibrate or move independently from the frame.

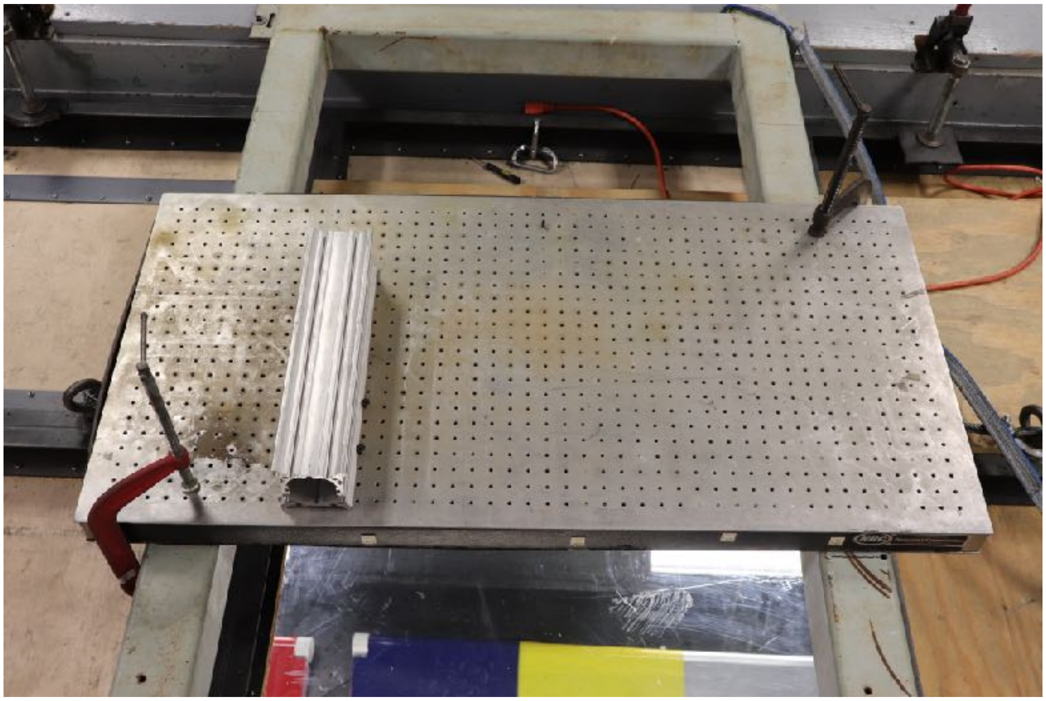

4.

Laser head should be bolted into a corner position such that it minimizes the area of the mounting table occupied.

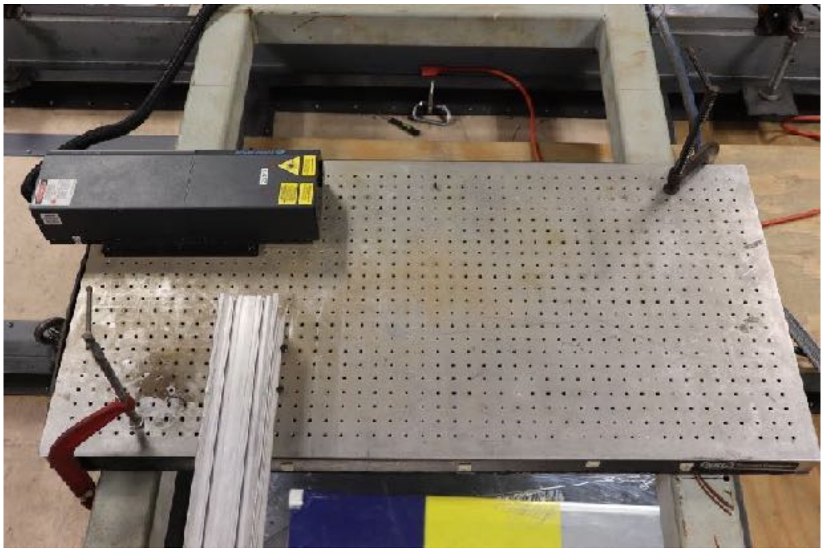

5.

The laser head has 4 connections which must be made to ensure proper operation. The water routing is color coded to ensure proper flow direction.

6.

Connection rail 1 should be bolted onto the laser table with at least 3” of overhang to facilitate the attachment of Connection rail 2. Connection rail 1 can be shifted as needed to accommodate connection rail 2 during the installation step.

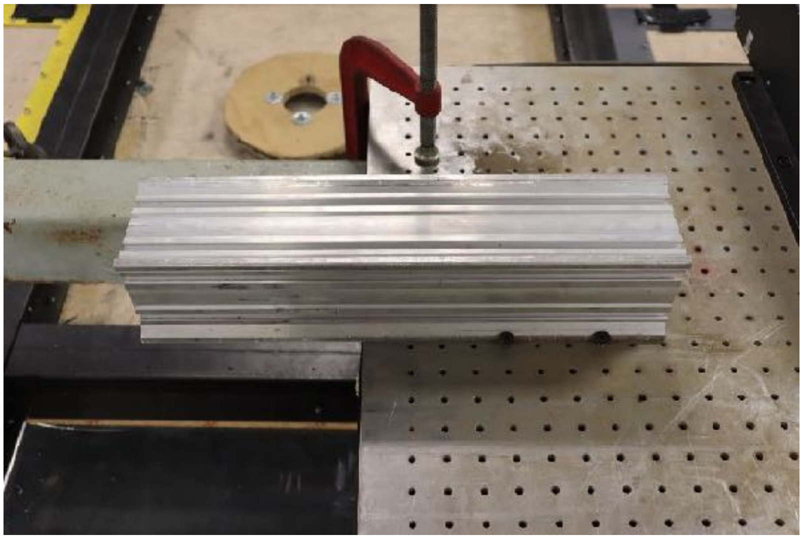

7.

The first mirror should be attached directly to the optics table with a 1” tall aluminum post using an insert that screws directly into the holes on the optics table. Be sure to align the mirror with the laser such that the beam can be turned at a 90 degree angle to run parallel with connection rail 1.

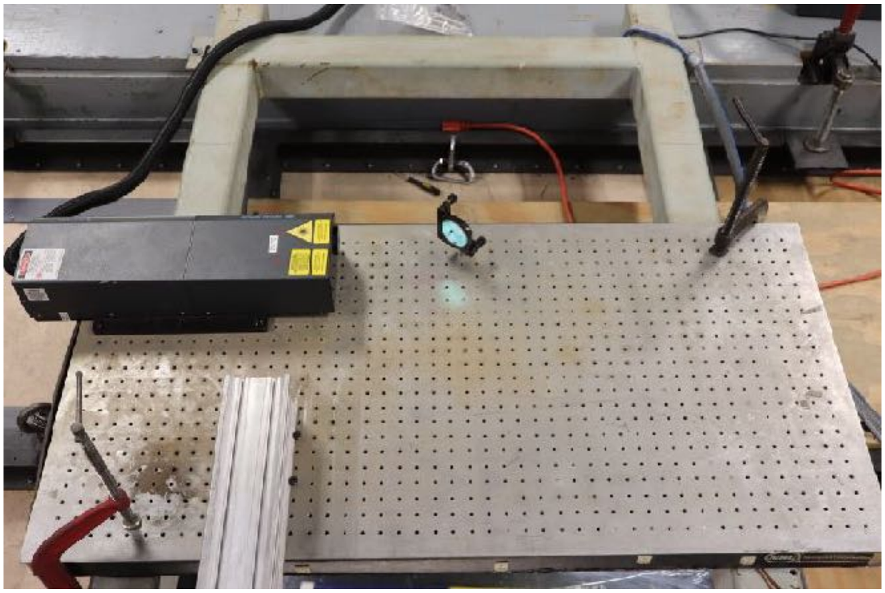

8.

The mirror, focusing lens, and cylindrical lens must be spaced such that the mounts will not interfere with one another, and the beam will be as focused as possible going into the cylindrical mirror. The exact distance changes depending on the lens used, but the distance between the focusing lens and the cylindrical lens should be equal the focal length of the focusing lens. Be sure the flat side of the cylindrical lens points towards the focusing lens. Exact placement of the mirror can be changed to angle the laser into the focusing lens.

9.

Connection rail 2 should be clamped to connection rail 1 in such a way that the mirror will angle the beam off the laser table and down into the focusing lens.

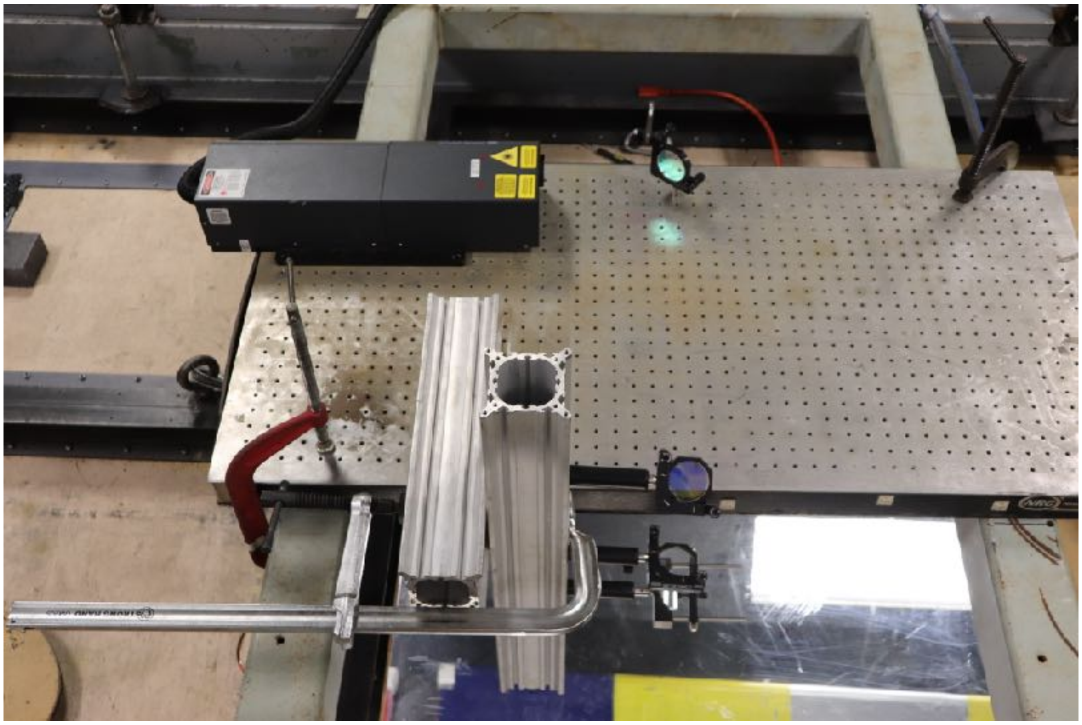

10.

The calibration plate should be set at the region of interest in the tunnel. For freestream tests and/or measurements around a model, this requires the use of a tripod or other support structure to locate the calibration plate in the desired area. For model tests, the plate can be placed directly on the model in the region of interest. It is highly recommended to secure the plate with a strip of aluminum tape on the back side so that it does not fall through gaps in the floor plate and into the balance room.

11.

When powering the laser on, it takes a few seconds after hitting start before the lasers will actually be able to turn on. There is a change in the frequency of the sound made by the laser which tells the user it is ready to be activated.

12.

Coarse movements of the beam can be made by moving the mirror and its optical post within the mount. Fine movements can be made using the knobs on the lens holder, with the target being the front edge of the calibration plate.

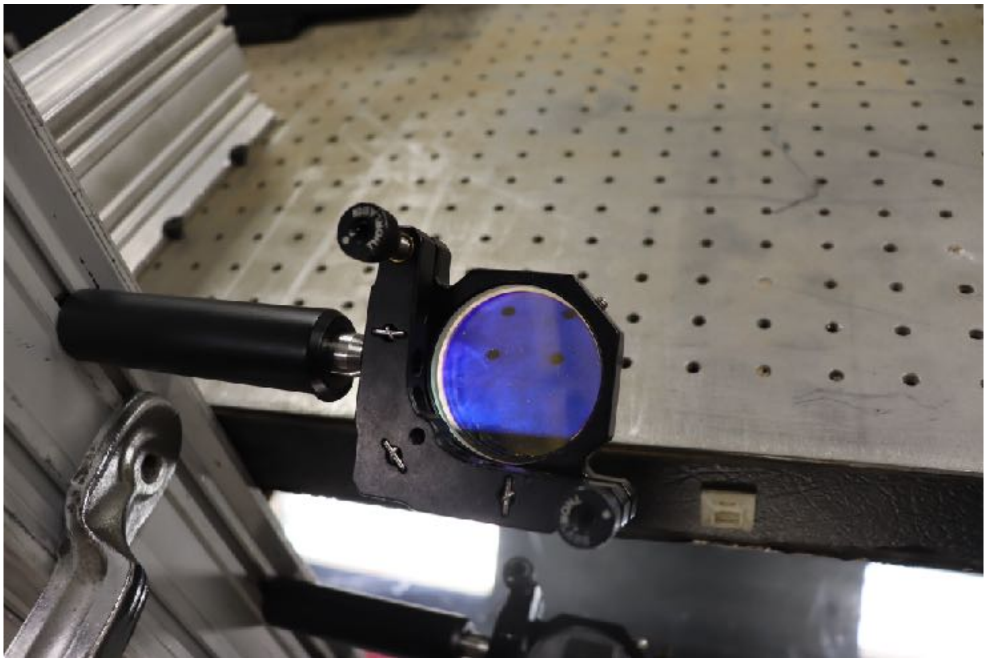

13.

The focusing lens may be moved up and down connection rail 2 to change the width and thickness of the laser sheet. For 2-D PIV, the sheet should be made as thin as possible.

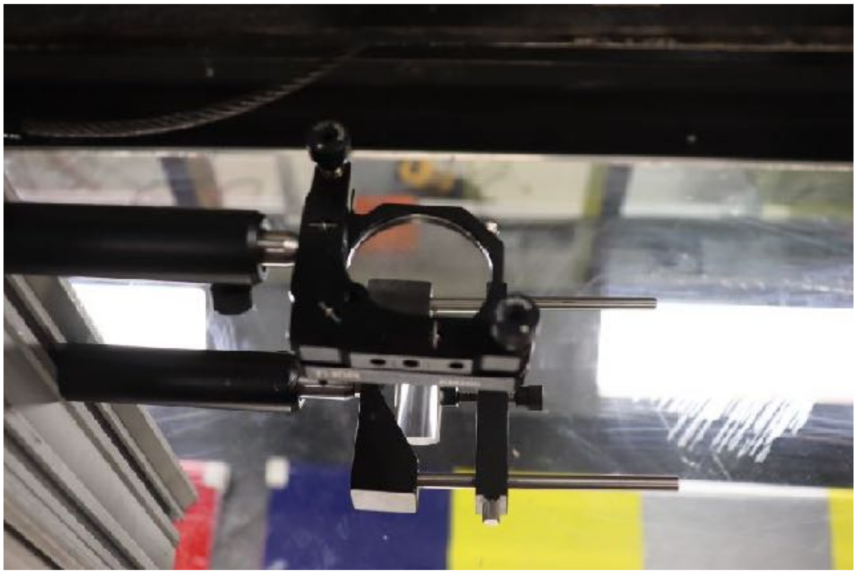

14.

This step is self explanatory. To stop the laser, press the stop button on the control box.

15.

Remove the smoke port by unscrewing the two bolts holding the plate into the wall of the tunnel.

16.

The smoke tubes are friction fit to slide together, and should not require tightening. If excess smoke is being released from the system during operation, slightly tighten the tubing using the screws located at each joiner.

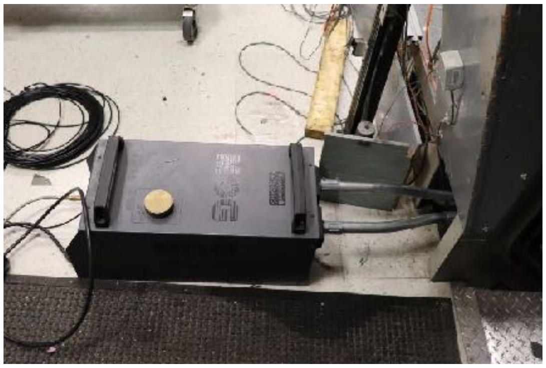

17.

The foot pedal plugs into the back of the smoke generator, and the smoke generator power plugs into an extension cord that runs into the corresponding plug below the 208V AC power switch on the left side of the ready room.

18.

The regulator can be attached to the smoke generator with a wrench. Be sure to tighten the connection with one wrench on the regulator input and one on the smoke generator input port to seal the connection as fully as possible.

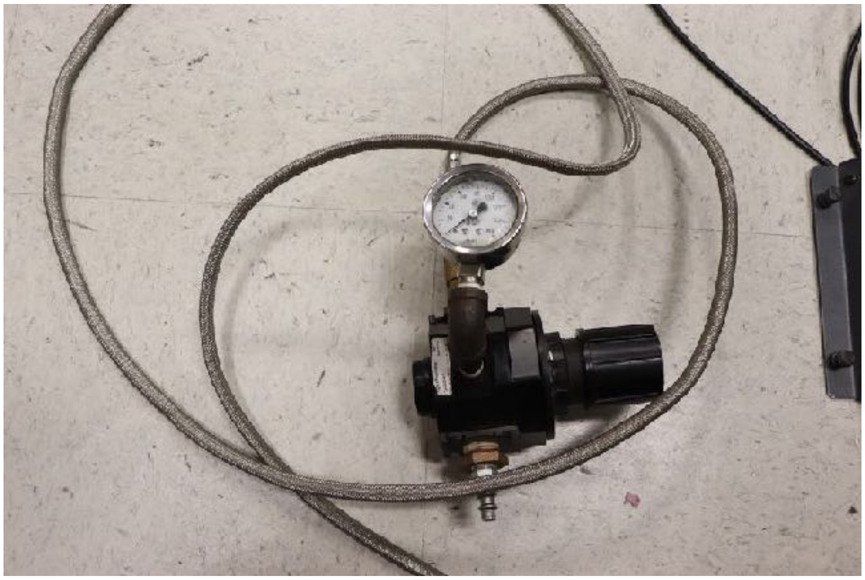

19.

A compressed air line can be pulled from next to the tunnel entry door and attached to the regulator.

20.

Depending on the regulator used, exact operation will vary, but setting the regulator to 30 psi is vital to the successful operation of the smoke generator. If the pressure is too low, the fog fluid will not be released into the heating element of the system, failing to produce any smoke. If the pressure is too high, the fluid will not spend enough time near the heating coil, shooting fog liquid into the test section of the tunnel without ever producing smoke.

21.

Each camera should fit into the mounting bracket such that the back of the camera is flush with the back side of the mounting bracket, and the bottom of the camera mates flush with the inside surface of the mounting bracket.

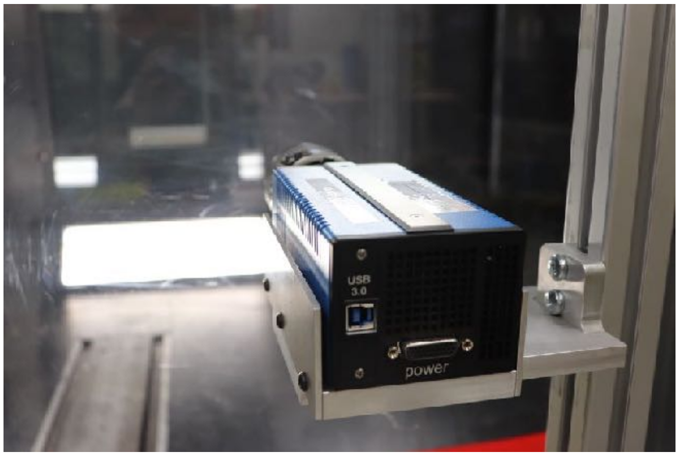

22.

If pulling the cameras out from storage, attach the lens to the front of each camera by lining up the grooves on the lens and camera base and twisting the lens until it clicks into place.

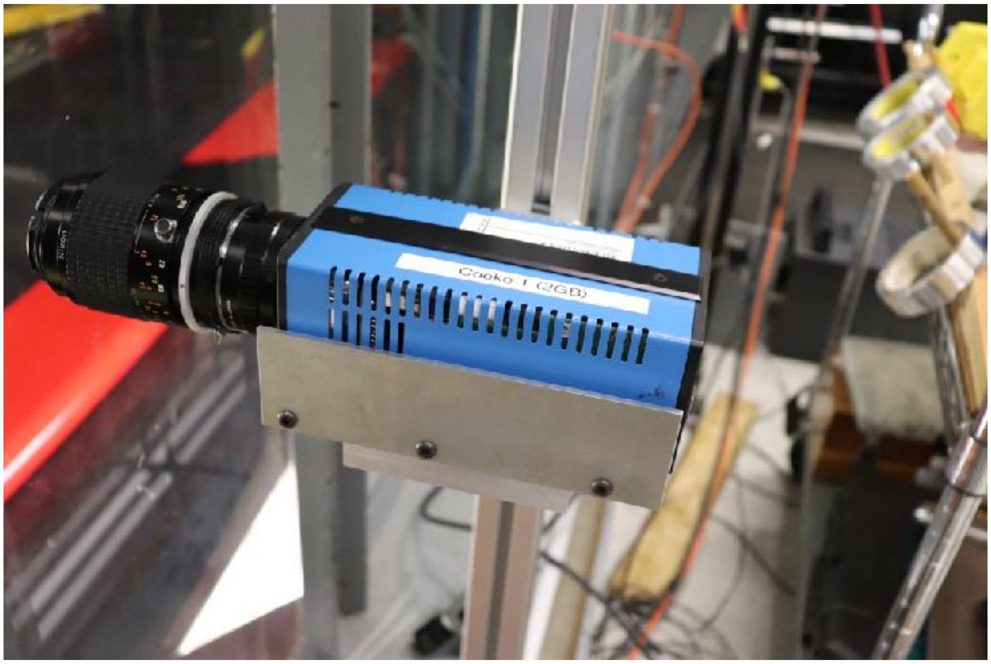

23.

The camera and power box are connected with a specific pinned adapter that must be screwed in with a flathead screwdriver. The camera power box is powered with a standard plug that is included in the yellow storage case.

24.

Each yellow storage case also includes a USB 3.0 cord that can be used to plug the cameras into the computer. This allows for data transfer between the cameras and the computer, and is necessary for the images to show up in the PCO camware64 software.

25.

Each camera is powered on by flipping the power switch on the front of the power box. Once both lights on the front of the box have a steady green light, proceed to the next step.

26.

Use the start menu or desktop shortcut to navigate to PCO camware64. This program is what we use to capture all PIV image pairs, and is critical for all PIV data collection.

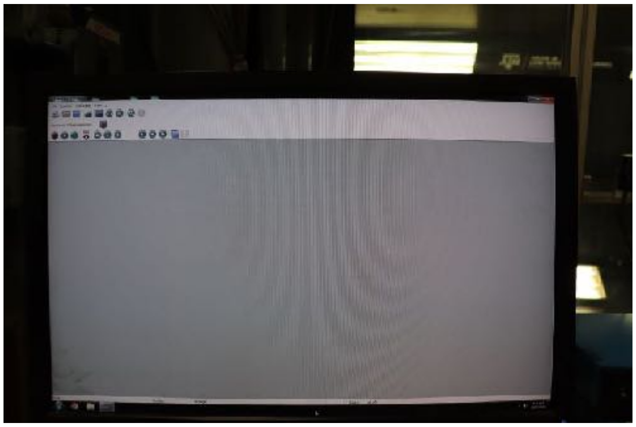

27.

Remove the lens cap on the camera to allow proper imaging of the region of interest.

28.

Exposure view windows can be opened by selecting the view tab, then selecting B/W window and clicking on image A + image B. Then select camera 1 to open the viewing windows for image A and image B of camera 1.

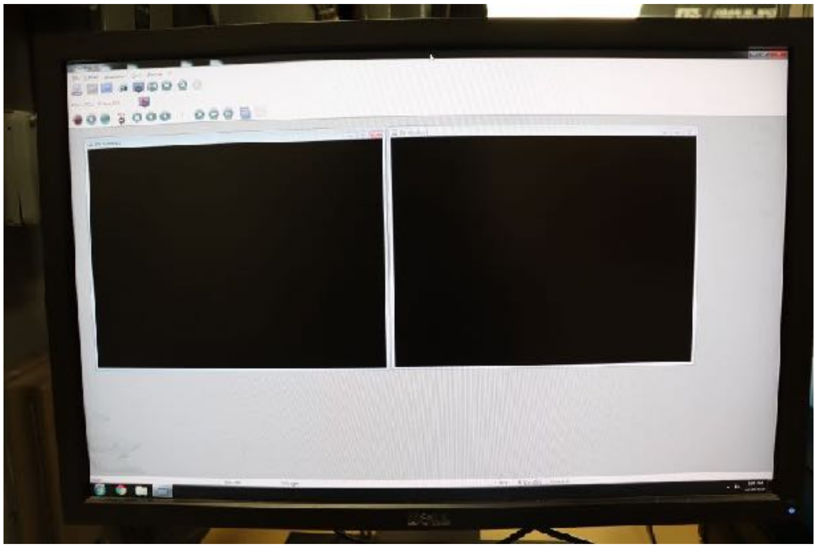

29.

Exposure view windows can be opened by selecting the view tab, then selecting B/W window and clicking on image A + image B. Then select camera 2 to open the viewing windows for image A and image B of camera 2.

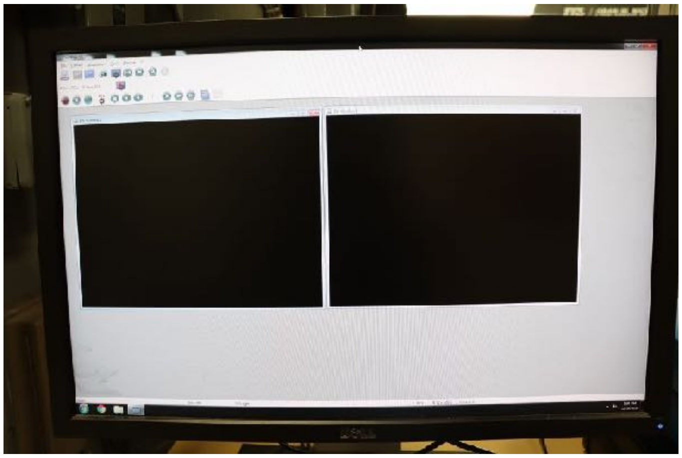

30.

Align the camera with the calibration plate by moving the vertical support of the mounting frame in the streamwise direction and moving the mounting bracket up and down on the vertical support. It is important to note that the calibration plate must fill the majority of the image frame in order for DaVis to produce a good calibration, so the zoom might need to be adjusted depending on the lens being used. A good camera placement can be seen below:

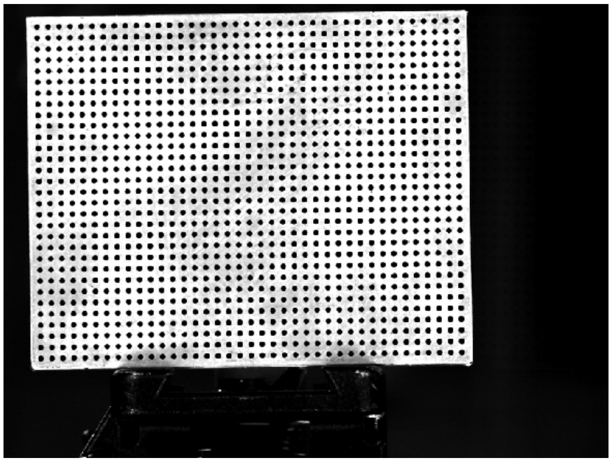

31.

Image capture settings can be changed by selecting Camera control, then clicking auto sequence in the new window and accept. If done correctly, the window should look like the picture below:

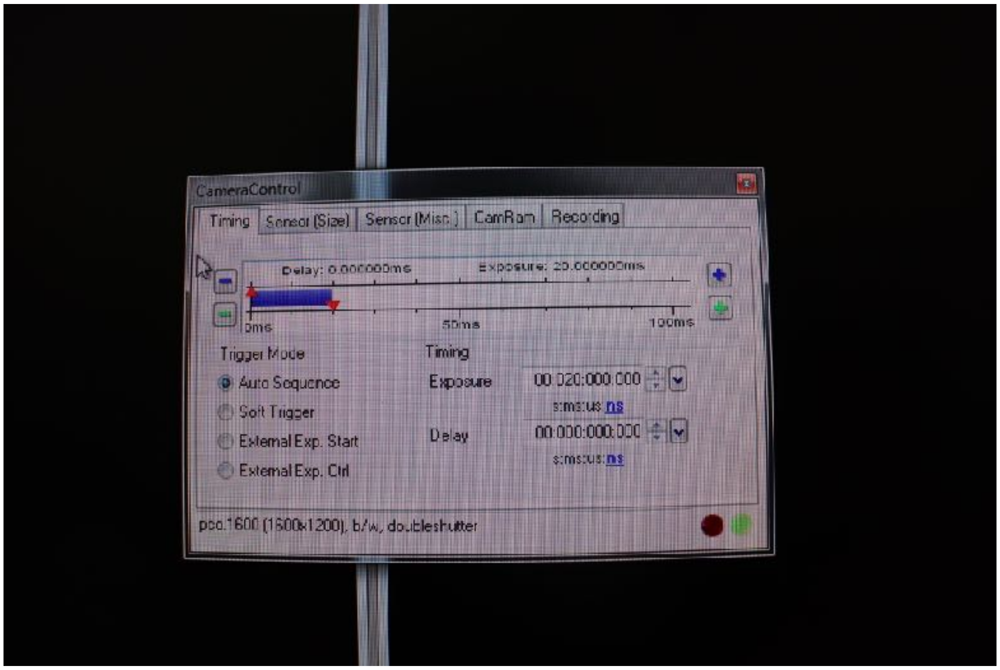

Delay: 0.000000ms

Exposure: 20.000000ms

● Auto Sequence

○ Soft Trigger

○ External Exp. Start

○ External Exp. Ctrl

Exposure 00:020:000:000

Delay 00:000:000:000

pco.1600 (1600x1200), b/w, doubleshutter

32.

To record images, click the red record button in the top left corner of the screen. The progress bar in the bottom left will begin to turn green, and the recorder sequence can be stopped at any point with the white square next to the record button.

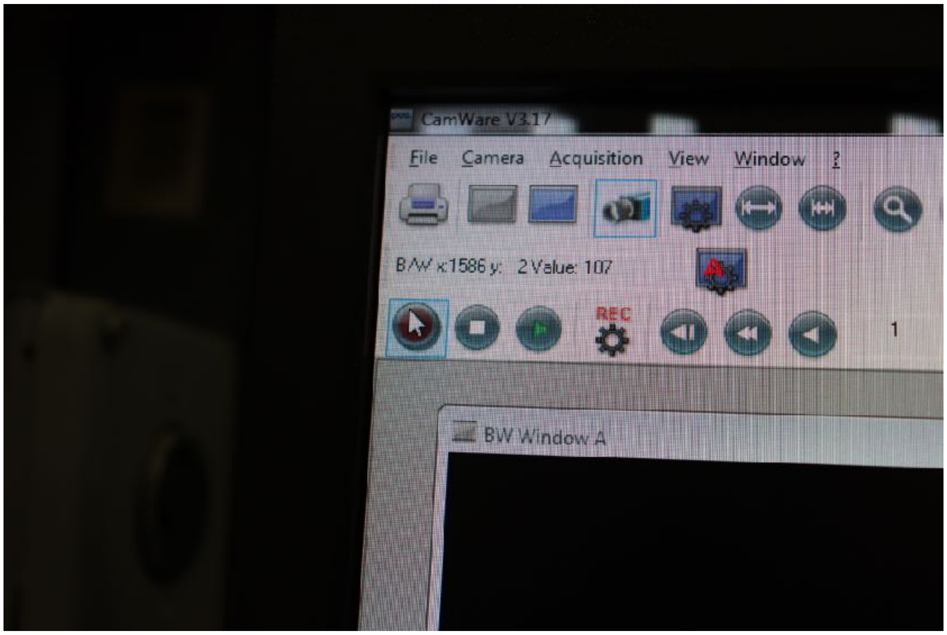

B/W x:1586 y: 2 Value: 107

33.

To export the images, click one of the frames corresponding to the left camera, then file, then export recorder sequence. Use the navigation menu to select the desired save destination, check the split double shutter box and click save.

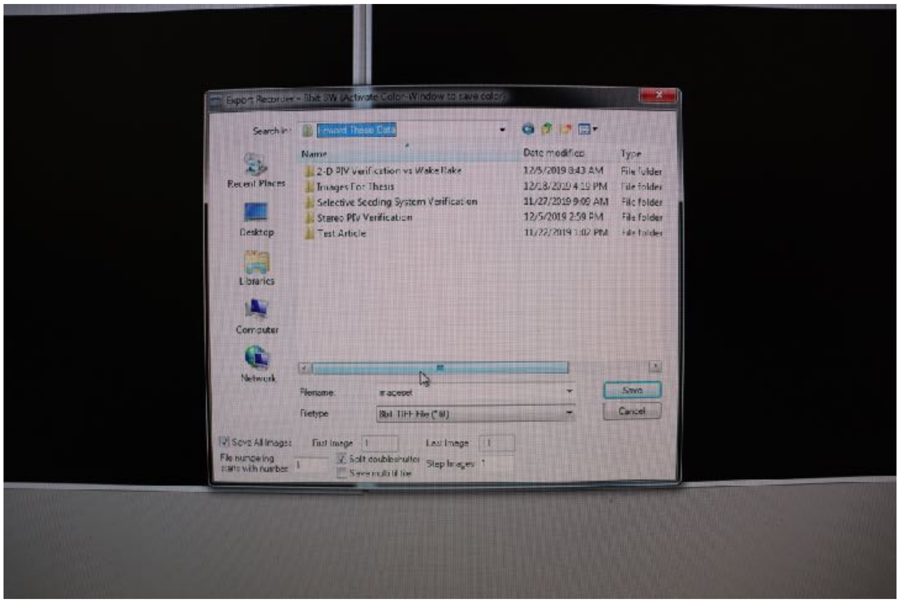

Name	Date modified	Type
2-D PIV Verification vs Wake Rake	12/5/2019 8:43 AM	File folder
Images For Thesis	12/18/2019 4:19 PM	File folder
Selective Seeding System Verification	11/27/2019 9:09 AM	File folder
Stereo PIV Verification	12/5/2019 2:59 PM	File folder
Test Article	11/22/2019 1:02 PM	File folder

Filetype: 8bit TIFF File (*.tif)

☑ Save All Images First Image 1 Last Image 1

File numbering starts with number 1

☑ Split doubleshutter

☐ Save multi tif file

Step Images 1

34.

To export the images, click one of the frames corresponding to the right camera, then file, then export recorder sequence. Use the navigation menu to select the desired save destination, check the split double shutter box and click save.

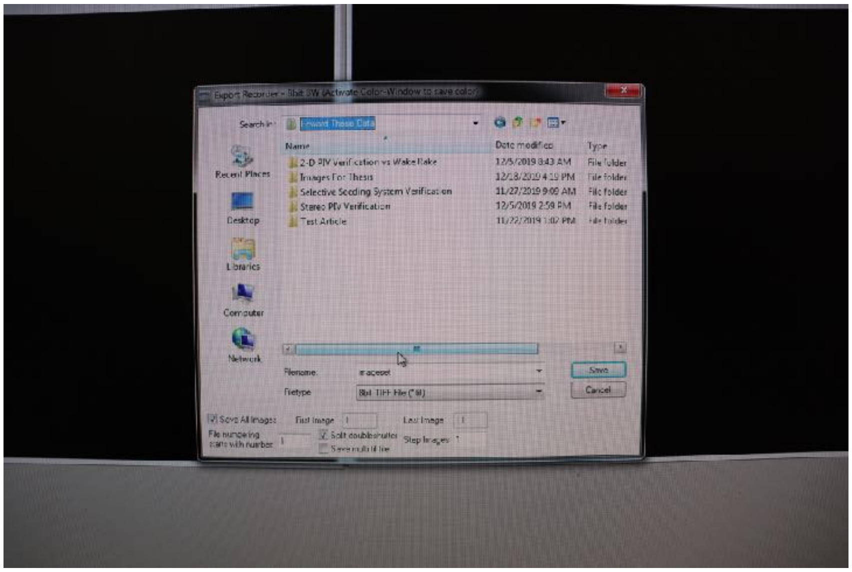

Name	Date modified	Type
2-D PIV Verification vs Wake Rake	12/5/2019 8:43 AM	File folder
Images For Thesis	12/18/2019 4:19 PM	File folder
Selective Seeding System Verification	11/27/2019 9:09 AM	File folder
Stereo PIV Verification	12/5/2019 2:59 PM	File folder
Test Article	11/22/2019 1:07 PM	File folder

Filetype: 8bit TIFF File (*.tif)

☑ Save All Images First Image: 1 Last Image: 1

File numbering starts with number: 1 ☑ Split doubleshutter ☐ Save multi tif file Step Images: 1

35.

In PCO camware64, the cameras used are displayed as camera 1 and camera 2. In DaVis, it is very helpful to have things labeled as left and right camera to make data importing and processing simpler. Thus, it is very helpful to know which camera number corresponds to left and right camera respectively.

36.

Navigate to the save destination of the calibration images and open one of the images to check the focus and alignment of the image. It is vital that the image is well-focused, otherwise the particles will not be easily identified by DaVis during image processing, resulting in incorrect measurements. Below is an example of a well-focused and aligned calibration image. You don't have to worry about any in-plane rotations of the plate, as these will be corrected during the calibration regime in DaVis.

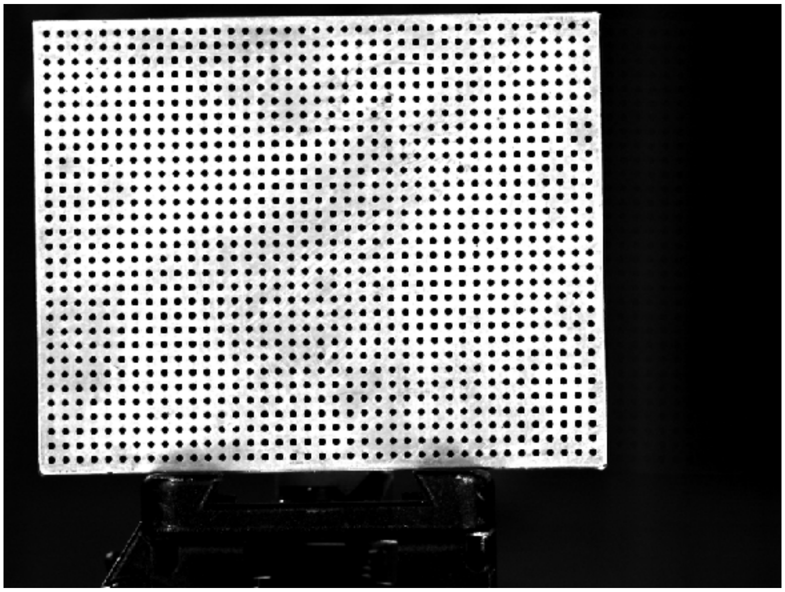

37.

To measure the pixels per inch, draw a volume from one side of the calibration plate to the other, with the corners of the box as close to the edges of the plate as possible. This will produce a pixel measurement for the calibration plate, which can be used to determine the conversion for pixels to inches. This will become relevant during setup of the quantum composer, so write the pixels per inch value down.

38.

To calculate the time for a particle to move 20 pixels in the image, one must determine a desired run speed in inches per second, and then use the pixels per inch value obtained in step 34 to convert the run speed into pixels per second. From there, calculate the time for each particle to move 20 pixels in the image with the following formula:

$$20 \div (\text{pixels per second}) = \text{Time for a particle to move 20 pixels}$$

39.

Use BNC cables to attach the laser power system to the quantum composer, attaching Fire Lamp 1 to T1, Fire Lamp 2 to T4, Fire Q-Sw 1 to T6, and Fire Q-Sw 2 to T7. It helps to have the cables color coded to make setup easier.

40.

The camera can be attached to the quantum composer with another BNC cable, running camera external exp trig to T8.

41.

Turning on the quantum composer is as simple as hitting the power button on the quantum composer. If it doesn't turn on, ensure that it is plugged in.

42 - 44.

To set the laser and camera timings, use the next button to navigate to the time delay for a given channel, and use the arrow keys on the quantum composer to change the time delay and reference time for that channel. For the reference time, T0 refers to the moment the run button is pressed, while all other TX values set the reference to another channel. To shift between channels (T1 to T2, etc.), press function and then channel.

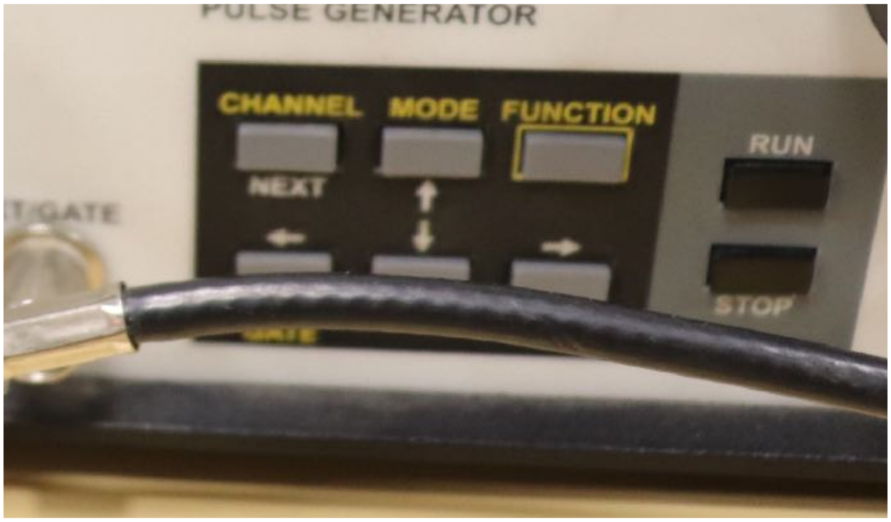

45.

To set the camera control to external control in PCO camware64, select camera control, then click external exposure start and then accept.

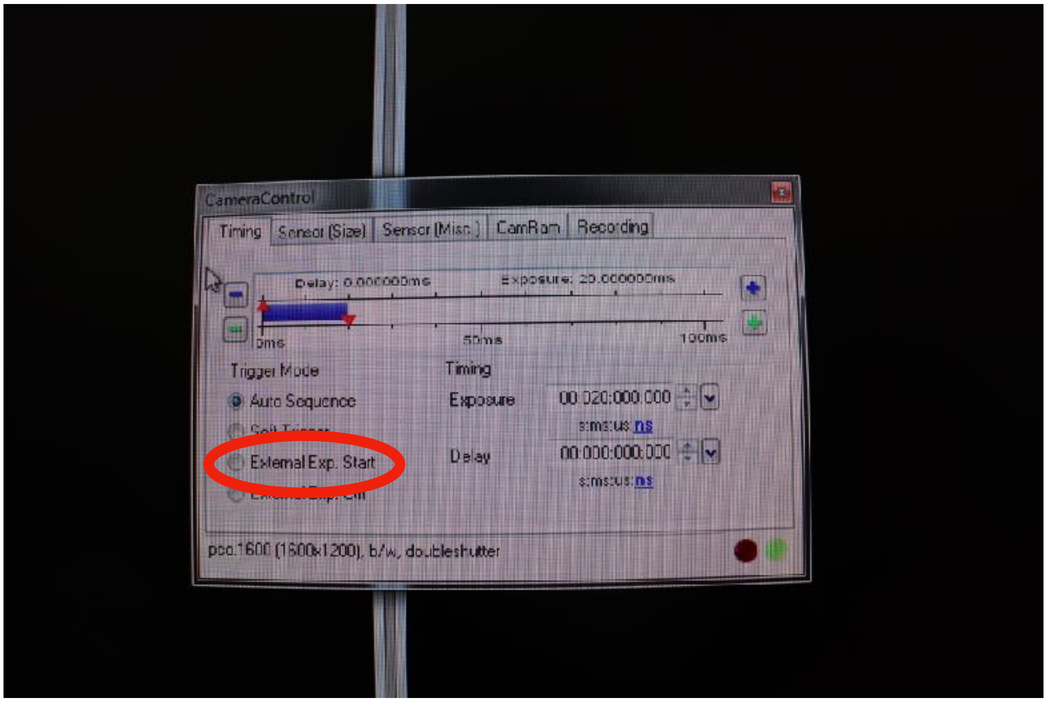

Delay: 0.000000ms

Exposure: 20.000000ms

- ● Auto Sequence
- ○ Soft Trigger
- ○ External Exp. Start
- ○ External Exp. Ctrl

Exposure 00:020:000:000 s:ms:us:ns

Delay 00:000:000:000 s:ms:us:ns

pco.1600 (1600x1200), b/w, doubleshutter

46.

To start the laser firing, press and hold start on the laser for approximately 2 seconds. Once the whirring of the laser decreases in frequency (clear audio cue), then press the laser 1 and laser 2 buttons to start the laser firing.

47.

Switch the laser to external control by pressing the Flashlamp and Q-SW buttons so that the light under EXT is illuminated.

48.

Turn the laser to high power by pressing the pressing the low/high button so that the light under high is illuminated, and turn the energy dial clockwise until the digital readout displays 999.

49.

Before proceeding, it is imperative that all personnel that will be in the ready room while conducting PIV are wearing laser safety goggles. The LSWT has multiple pairs that can be worn, including two that can be worn over normal glasses. At high power, this laser can do permanent damage to the naked eye, so it is vital that you are wearing proper safety attire prior to use of the laser at high power.

50.

It is also vital that you turn on the laser warning light. The switch may be found on the shelf in the front right corner of the control room on the shelf. This will illuminate the red lights above each entry to the ready room so that everyone in the facility will know the laser is in use and will take the necessary safety precautions.

51.

Turn on the smoke generator by flipping the switch on the generator and then pressing the on button on the foot pedal.

52.

This step is fairly self explanatory, there is a light on the foot pedal of the smoke generator that is labeled ready. When the generator is sufficiently warm, the ready light will turn green. When this happens, start the tunnel and get up to the desired speed.

53.

To generate smoke sufficiently dense for PIV measurements, press the start button on the foot pedal and allow the system to generate smoke until you see smoke coming from the settling chamber and into the test section. When that occurs, press the start button again and move to the next step.

54.

This step is also self explanatory. Turn off all lights in the ready room, control room, and test section. The goal is to eliminate as much light as possible to maximize the contrast between the particles illuminated by the laser sheet and the background of the image. Thus, making the room as dark as possible is ideal.

55.

Press the run button on the quantum composer to start the laser. Sometimes the laser will not start up on the first press of Run for reasons unknown. If this happens, leave the quantum composer running and press the laser 1 and laser 2 buttons on the laser power box.

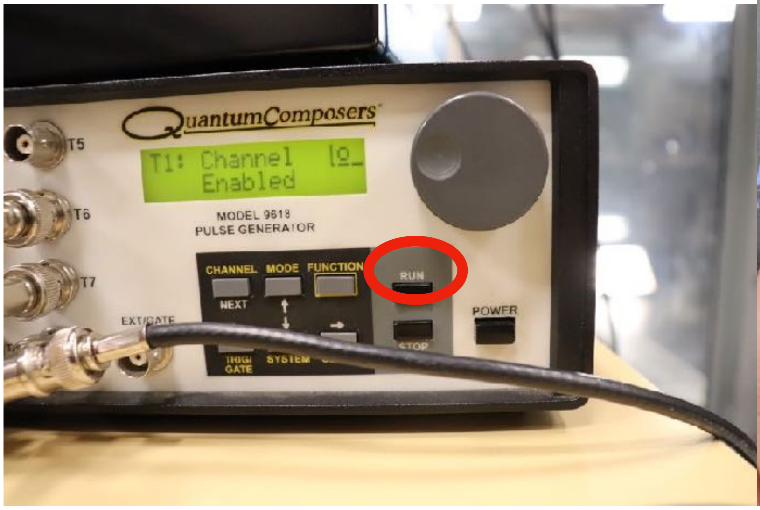

56.

To record image pairs, click the red record button in the top left corner of PCO camware64.

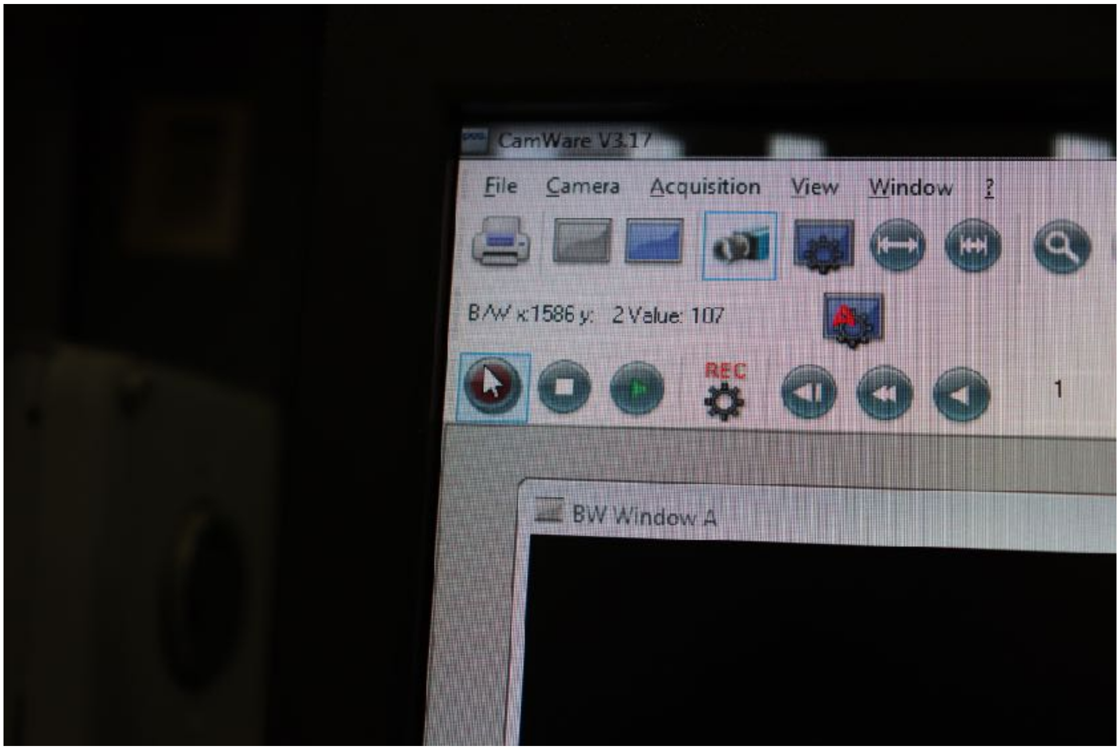

57.

Once the blue progress bar in the lower left portion of the screen is full, press stop in the upper left corner of PCO camware 64.

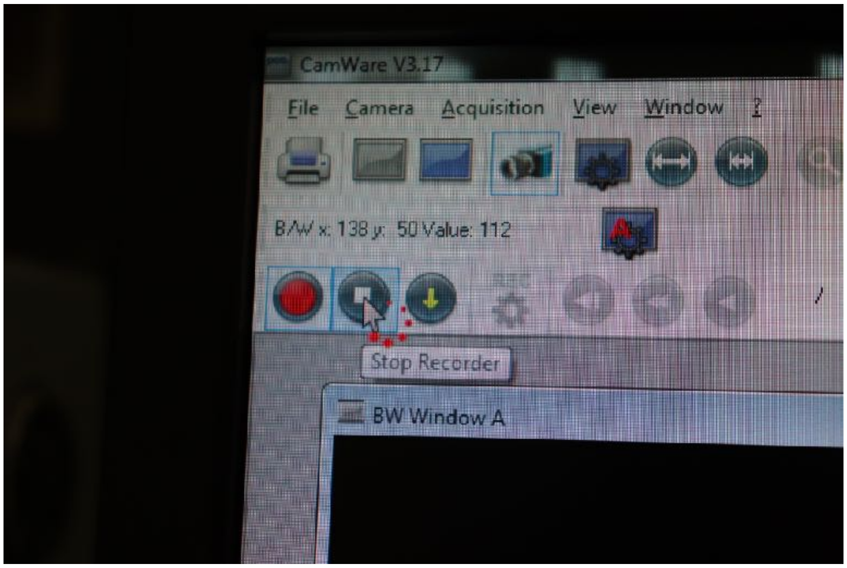

58.

To export the images click one of the frames corresponding to camera 1, then file, then export recorder sequence. Use the navigation menu to select the desired save destination, check the split double shutter box and click save.

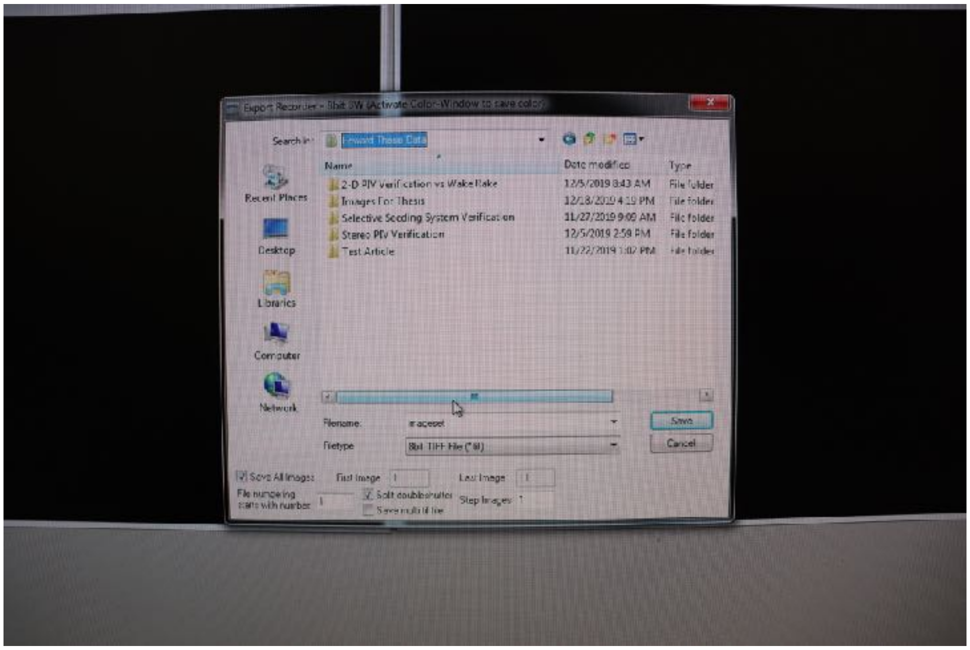

Name	Date modified	Type
2-D PIV Verification vs Wake Rake	12/5/2019 8:43 AM	File folder
Images For Thesis	12/18/2019 4:19 PM	File folder
Selective Seeding System Verification	11/27/2019 9:09 AM	File folder
Stereo PIV Verification	12/5/2019 2:59 PM	File folder
Test Article	11/22/2019 1:02 PM	File folder

Filetype: 8bit TIFF File (*.tif)

☑ Save All Images First Image: 1 Last Image: 1

File numbering starts with number: 1

☑ Split doubleshutter

☐ Save multi tif file

Step Images: 1

59.

To export the images click one of the frames corresponding to camera 2, then file, then export recorder sequence. Use the navigation menu to select the desired save destination, check the split double shutter box and click save.

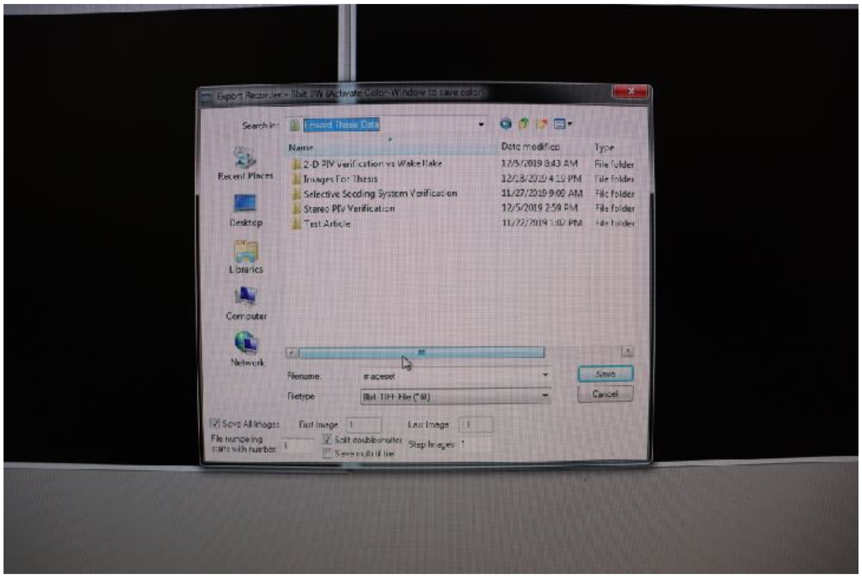

Name	Date modified	Type
2-D PIV Verification vs Wake Rake	12/5/2019 8:43 AM	File folder
Images For Thesis	12/18/2019 4:19 PM	File folder
Selective Seeding System Verification	11/27/2019 9:09 AM	File folder
Stereo PIV Verification	12/5/2019 2:59 PM	File folder
Test Article	11/22/2019 1:02 PM	File folder

Filetype: 8bit TIFF File (*.tif)

☑ Save All Images First Image: 1 Last Image: 1

File numbering starts with number: 1

☑ Split doubleshutter

☐ Save multi tif file

Step Images: 1

60.

Now that a dataset has been captured, it must be analyzed to ensure the image pairs captured produce reasonable data. To do this, DaVis 8.4.0 must be opened. It is important to note that the license dongle must be inserted into one of the USB ports on the computer in order for the program to open.

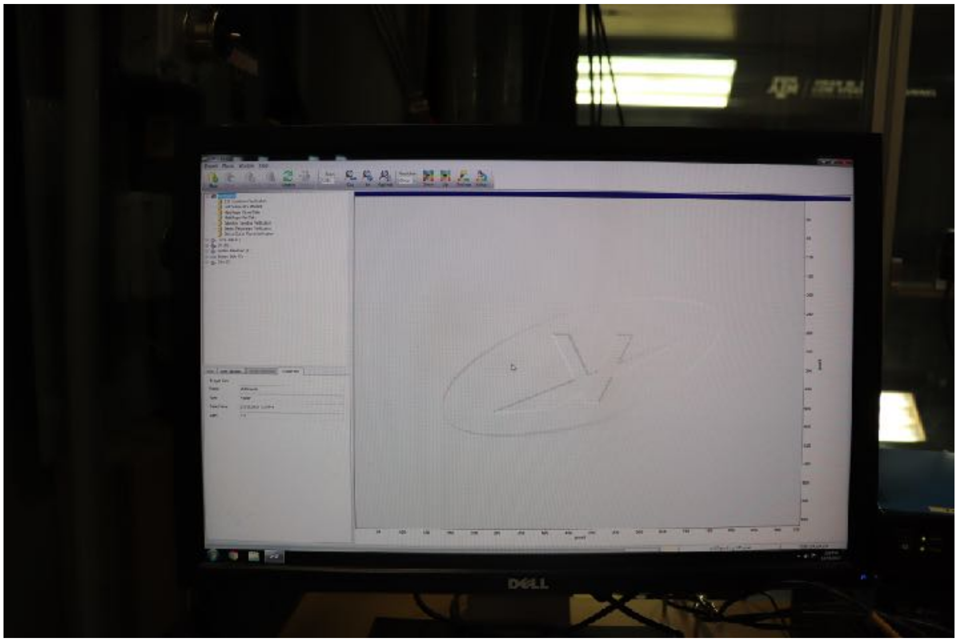

61.

To start a new PIV project, select the new icon in the top left corner of the screen. Select specify and input the desired project name, and be sure to designate the type of project as PIV before hitting ok.

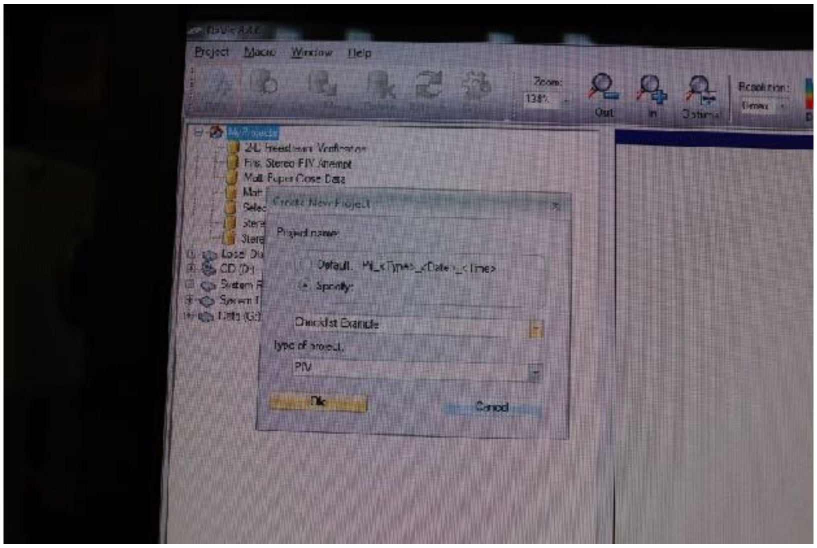

Create New Project

Project name:

○ Default: PIV_<Type>_<Date>_<Time>

● Specify:

Checklist Example

Type of project:

PIV

62.

To import the desired image pairs, select the import icon in the top left corner of the screen. This should send you to the screen shown below:

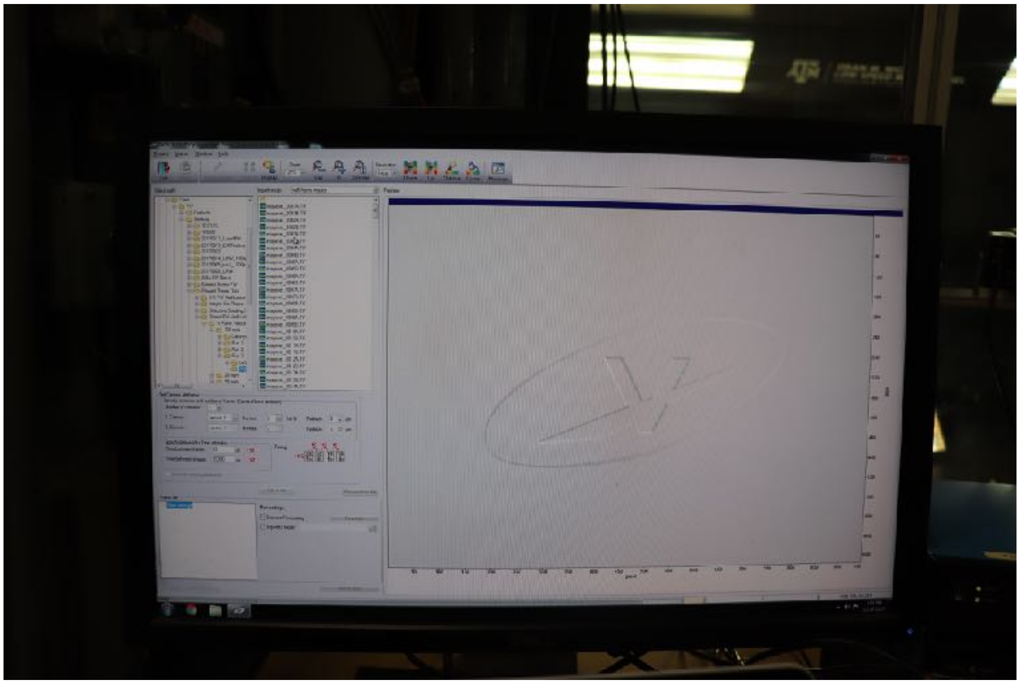

63.

Use the directory to navigate to the desired set of images for importing, and select image A from the first image pair of the dataset.

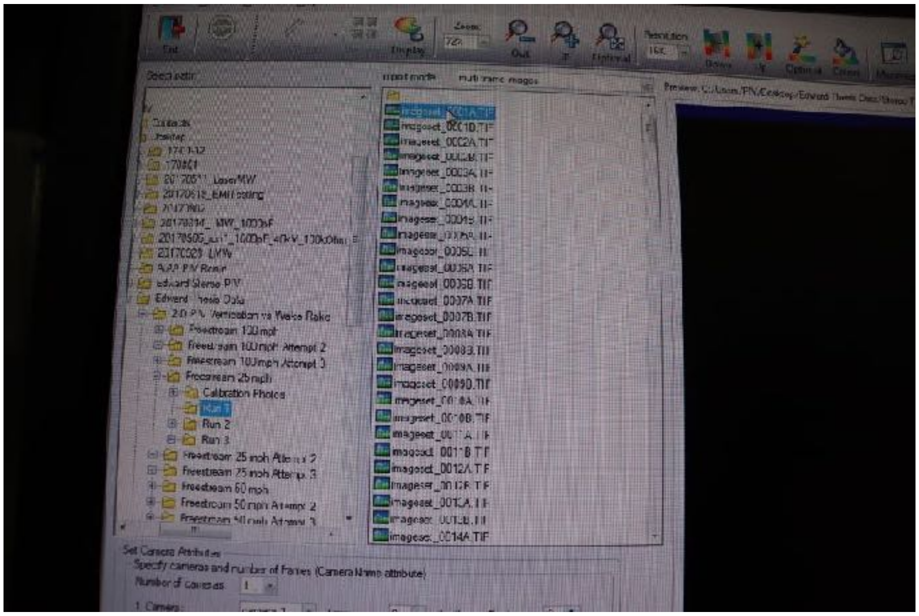

64.

In the import menu, define the time between frames as the delay on T4 in the quantum composer and the time between images as the exposure time defined in PCO camware64.

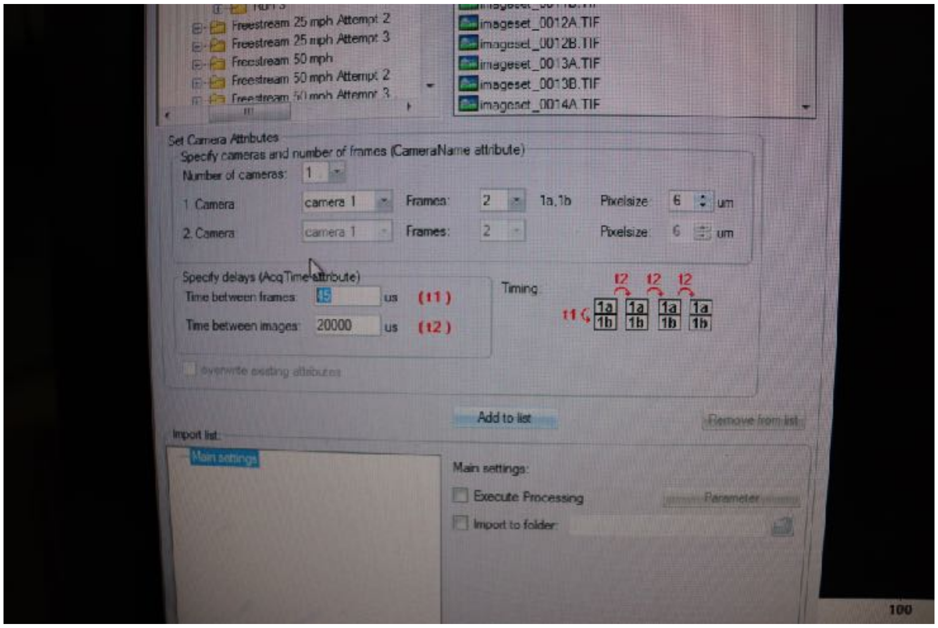

Specify cameras and number of frames (CameraName attribute)

Number of cameras: 1

1 Camera: camera 1 Frames: 2 1a,1b Pixelsize: 6 um

2 Camera: camera 1 Frames: 2 Pixelsize: 6 um

Specify delays (AcqTime attribute)

Time between frames: 45 us (t1)

Time between images: 20000 us (t2)

☐ overwrite existing attributes

Main settings:

☐ Execute Processing

☐ Import to folder:

65.

Click the add to list button on the left side of the screen to prepare the images for importing.

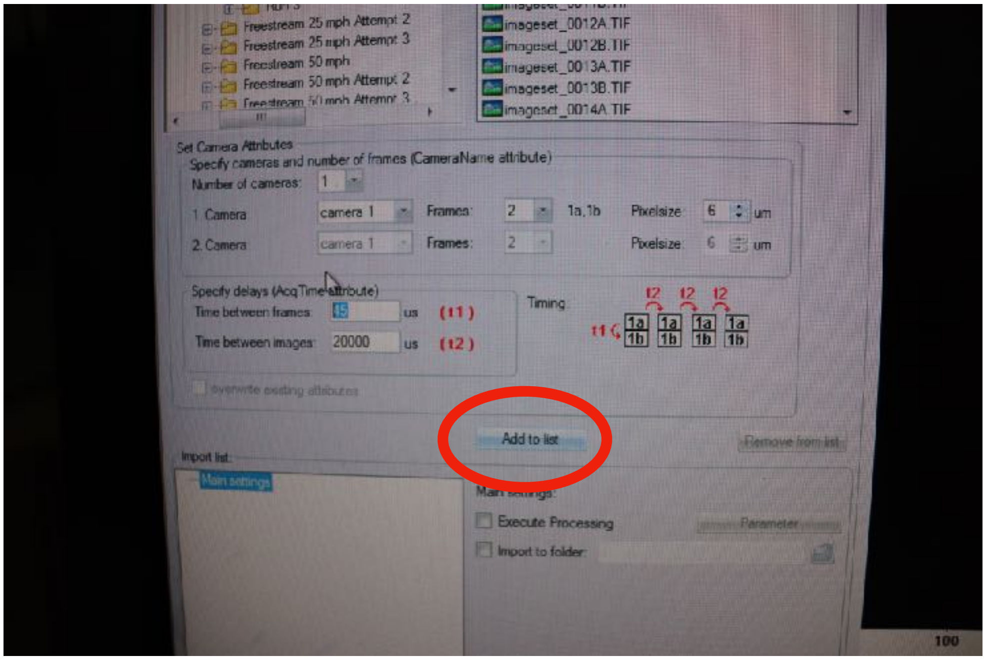

Specify cameras and number of frames (CameraName attribute)

Number of cameras: 1

1 Camera: camera 1 Frames: 2 1a,1b Pixelsize: 6 um

2 Camera: camera 1 Frames: 2 Pixelsize: 6 um

Specify delays (AcqTime attribute)

Time between frames: 45 us (t1)

Time between images: 20000 us (t2)

☐ overwrite existing attributes

Main settings:

☐ Execute Processing

☐ Import to folder:

66.

Now that Add to list has been clicked, the desired image should appear in the import list on the lower left corner of the screen. To view the import details for the desired dataset, select the image from the import list.

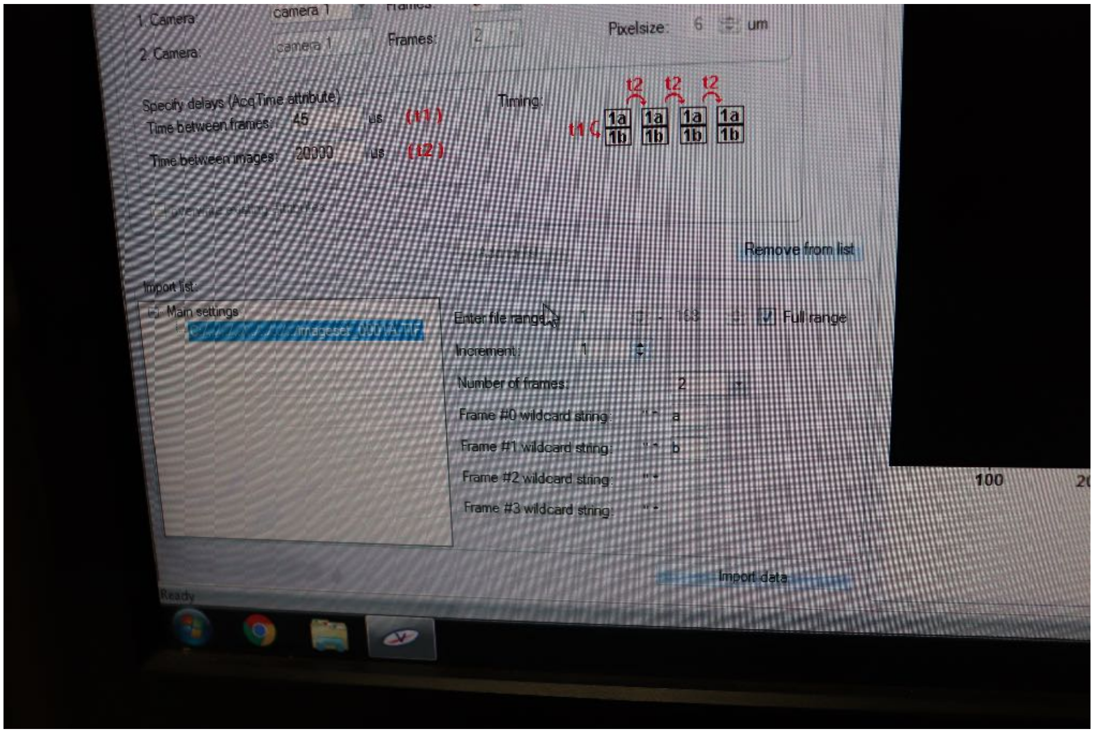

1. Camera: camera 1
2. Camera: camera 1

Frames: 2

Pixelsize: 6 um

Specify delays (AcqTime attribute)

Time between frames: 45 us (t1)

Time between images: 20000 us (t2)

Enter file range: 1 - 168 ☑ Full range

Increment: 1

Number of frames: 2

Frame #0 wildcard string: a

Frame #1 wildcard string: b

Frame #2 wildcard string:

Frame #3 wildcard string:

67.

Verifying the full range of images is imported by verifying the range listed under the import details for the desired dataset is 1-168. This range is located on the bottom left side of the screen, next to the import list.

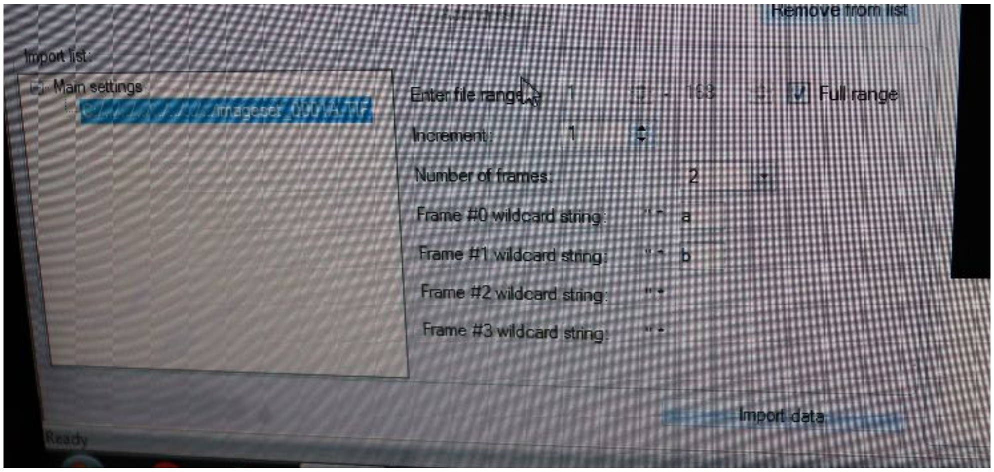

Enter file range: 1 - 168 ☑ Full range

Increment: 1

Number of frames: 2

Frame #0 wildcard string: a

Frame #1 wildcard string: b

Frame #2 wildcard string:

Frame #3 wildcard string:

68.

The import data button can also be found on the lower left side of the screen, beneath the import details and import list prompts. Clicking this button will import all image pairs from the import list into DaVis for processing.

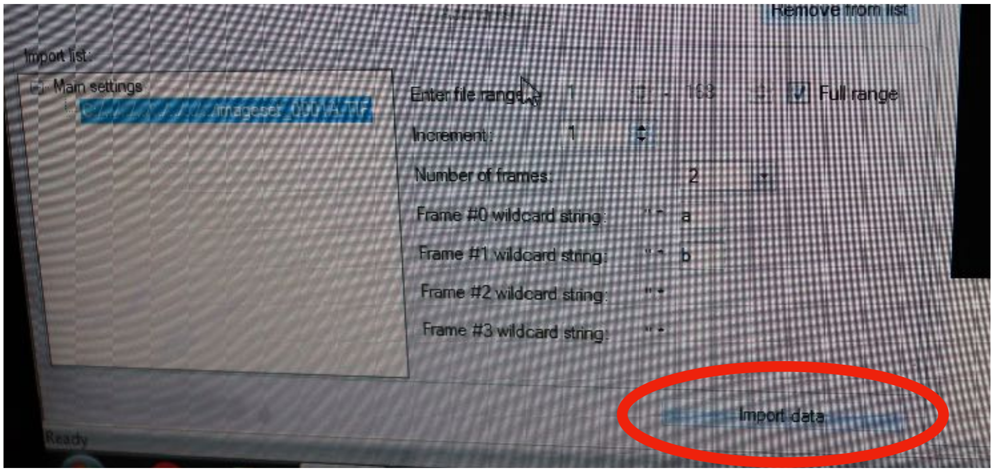

Enter file range: 1 - 163 ☑ Full range
Increment: 1
Number of frames: 2
Frame #0 wildcard string: a
Frame #1 wildcard string: b
Frame #2 wildcard string:
Frame #3 wildcard string:

69.

Once the exit icon in the top left corner becomes selectable, click exit to return to the project home screen.

70.

To import the desired image pairs, select the import icon in the top left corner of the screen. This should send you to the screen shown below:

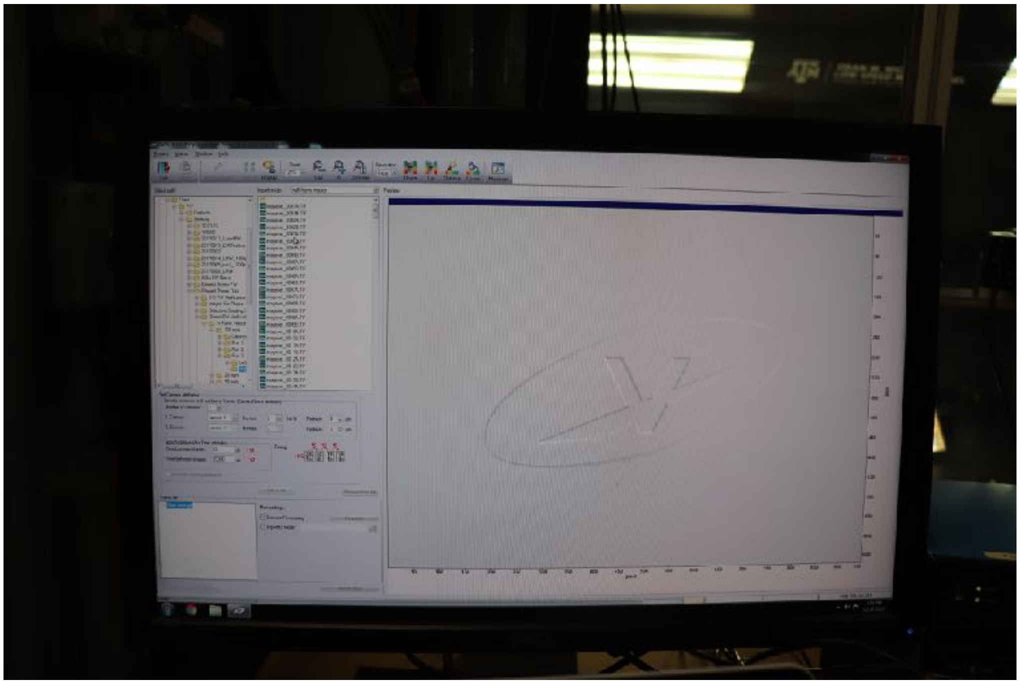

71.

Use the directory to navigate to the desired set of images for importing, and select image A from the first image pair of the dataset.

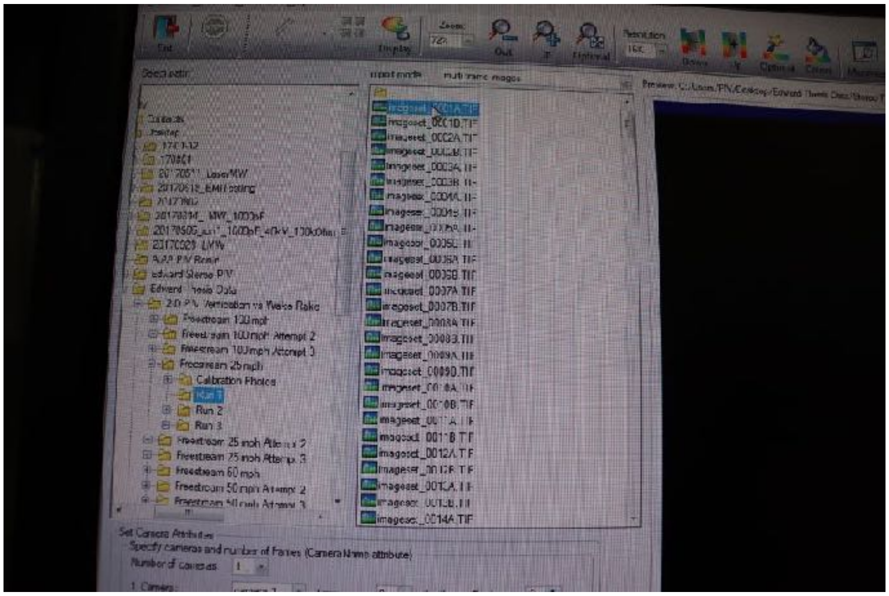

72.

In the import menu, define the time between frames as the delay on T4 in the quantum composer and the time between images as the exposure time defined in PCO camware64.

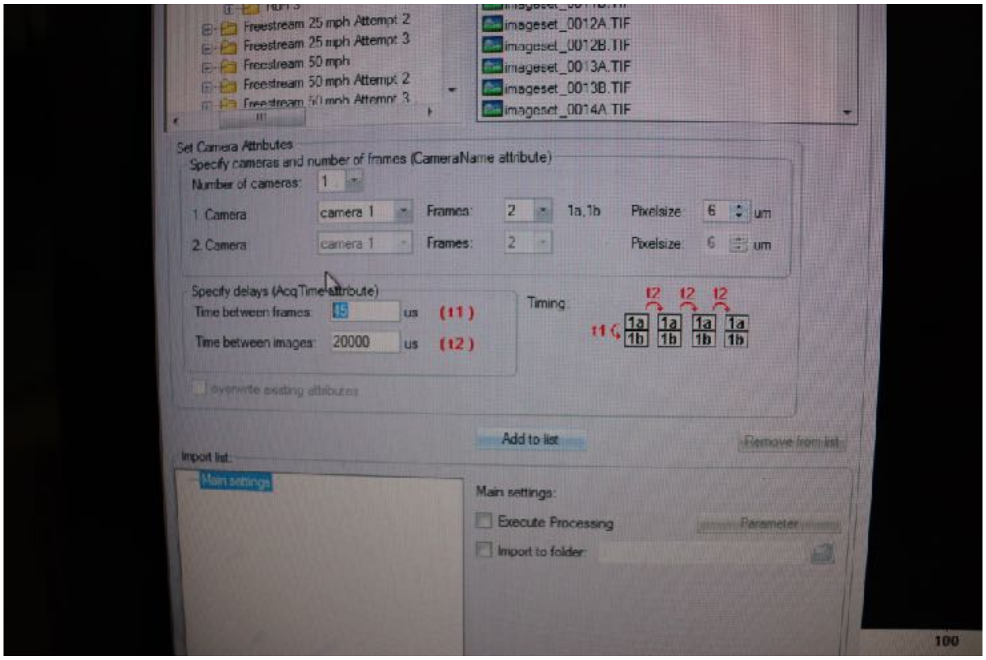

Number of cameras: 1

1 Camera: camera 1 Frames: 2 1a,1b Pixelsize: 6 um

2 Camera: camera 1 Frames: 2 Pixelsize: 6 um

Time between frames: 15 us (t1)

Time between images: 20000 us (t2)

73.

Click the add to list button on the left side of the screen to prepare the images for importing.

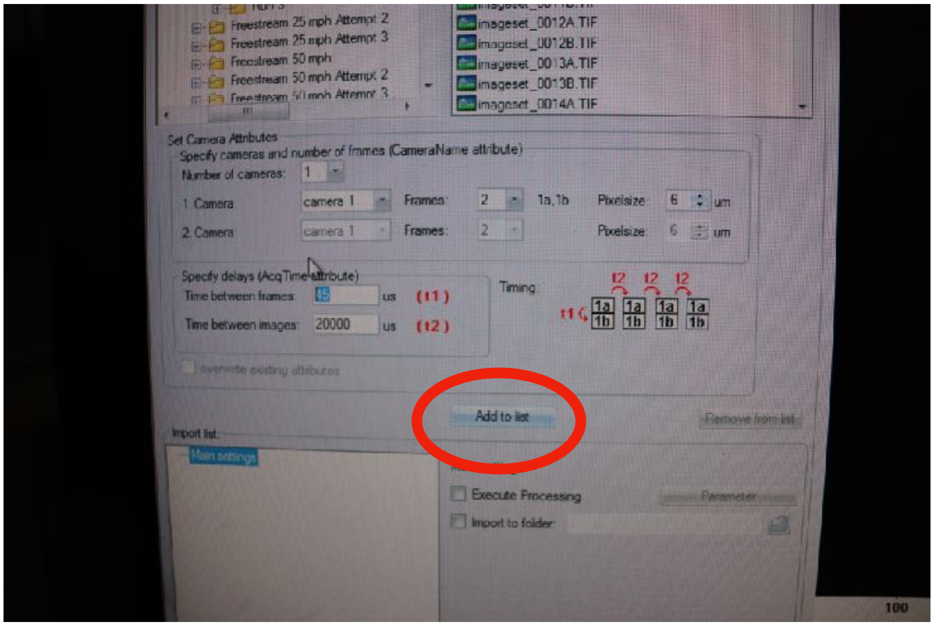

Number of cameras: 1

1 Camera: camera 1 Frames: 2 1a,1b Pixelsize: 6 um

2 Camera: camera 1 Frames: 2 Pixelsize: 6 um

Time between frames: 15 us (t1)

Time between images: 20000 us (t2)

74.

Now that Add to list has been clicked, the desired image should appear in the import list on the lower left corner of the screen. To view the import details for the desired dataset, select the image from the import list.

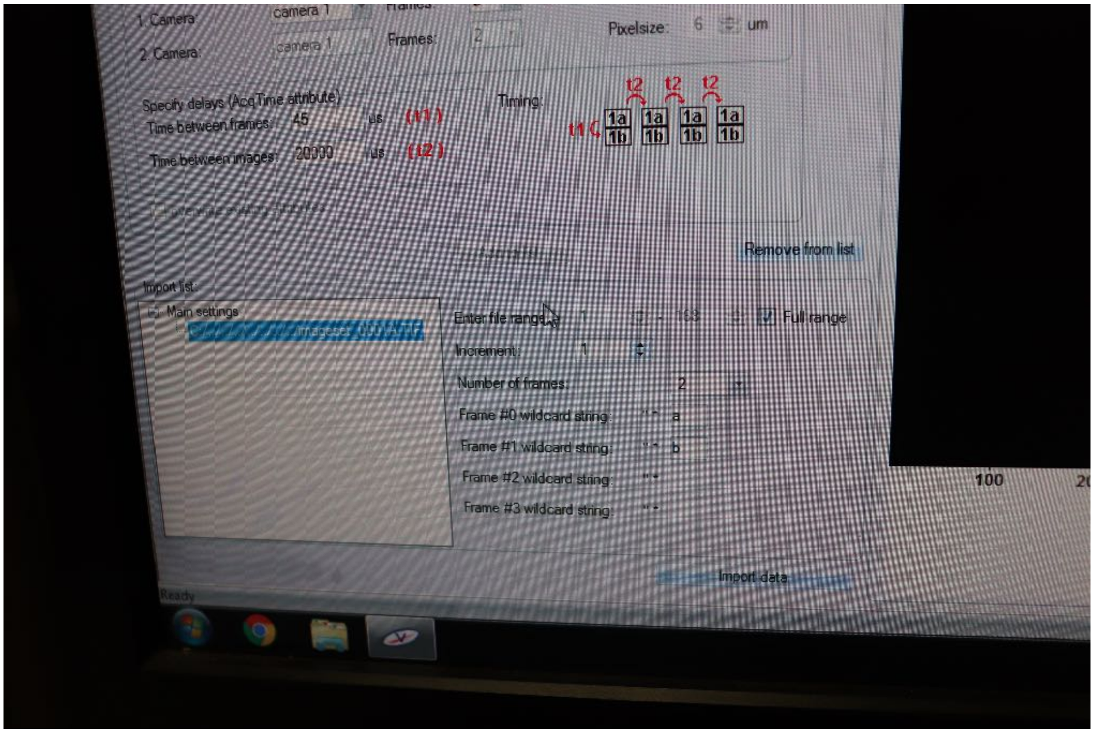
1. Camera: camera 1

2. Camera: camera 1

Frames: 2

Pixelsize: 6 um

Specify delays (AcqTime attribute)

Time between frames: 45 us (t1)

Time between images: 20000 us (t2)

Enter file range: 1 - 168 ☑ Full range

Increment: 1

Number of frames: 2

Frame #0 wildcard string: "*" a

Frame #1 wildcard string: "*" b

Frame #2 wildcard string: "*"

Frame #3 wildcard string: "*"

75.

Verifying the full range of images is imported by verifying the range listed under the import details for the desired dataset is 1-168. This range is located on the bottom left side of the screen, next to the import list.

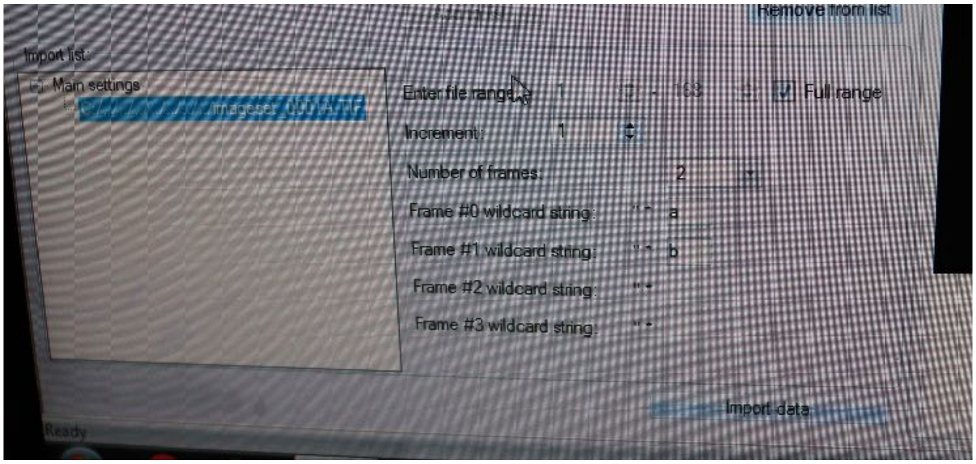
Enter file range: 1 - 168 ☑ Full range

Increment: 1

Number of frames: 2

Frame #0 wildcard string: "*" a

Frame #1 wildcard string: "*" b

Frame #2 wildcard string: "*"

Frame #3 wildcard string: "*"

76.

The import data button can also be found on the lower left side of the screen, beneath the import details and import list prompts. Clicking this button will import all image pairs from the import list into DaVis for processing.

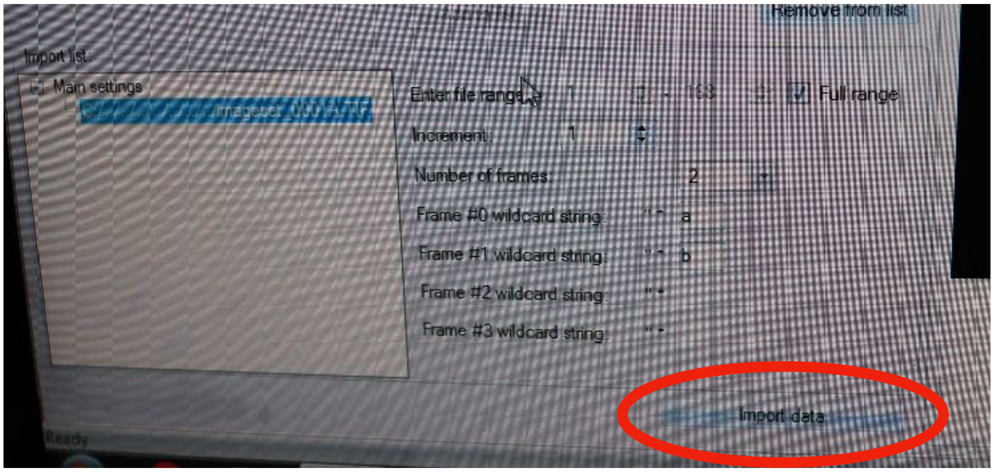

Enter file range: 1 - [illegible] ☑ Full range
Increment: 1
Number of frames: 2
Frame #0 wildcard string: "*" a
Frame #1 wildcard string: "*" b
Frame #2 wildcard string: "*"
Frame #3 wildcard string: "*"

77.

Once the exit icon in the top left corner becomes selectable, click exit to return to the project home screen.

78.

To process data, select the newly imported left camera data and click processing in the top toolbar. This will navigate you to the data processing screen.

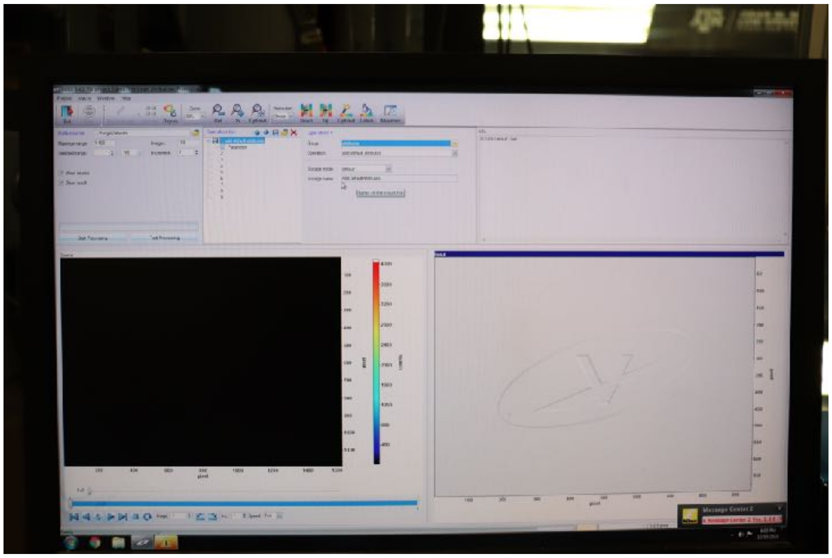

79.

To add a new processing step, clear the operation list with the red x in the upper right corner of the list, and then add a new operation. Under group, select copy and reorganize data sets, and under operation select merge data sets to multi frame. Storage mode and storage name should be left alone.

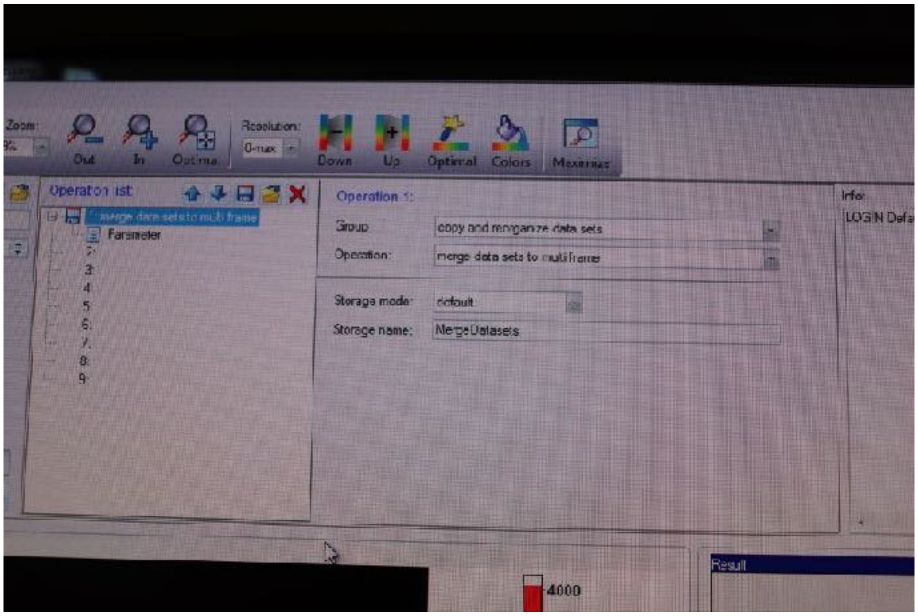

Operation 1:

Group: copy and reorganize data sets

Operation: merge data sets to multi frame

Storage mode: default

Storage name: MergeDatasets

80.

Clicking the parameters option in the operation list brings up the ability to select data sets. Using the open folder icon, you can navigate to the imported right camera data and select it. If done properly, it should look like the following image:

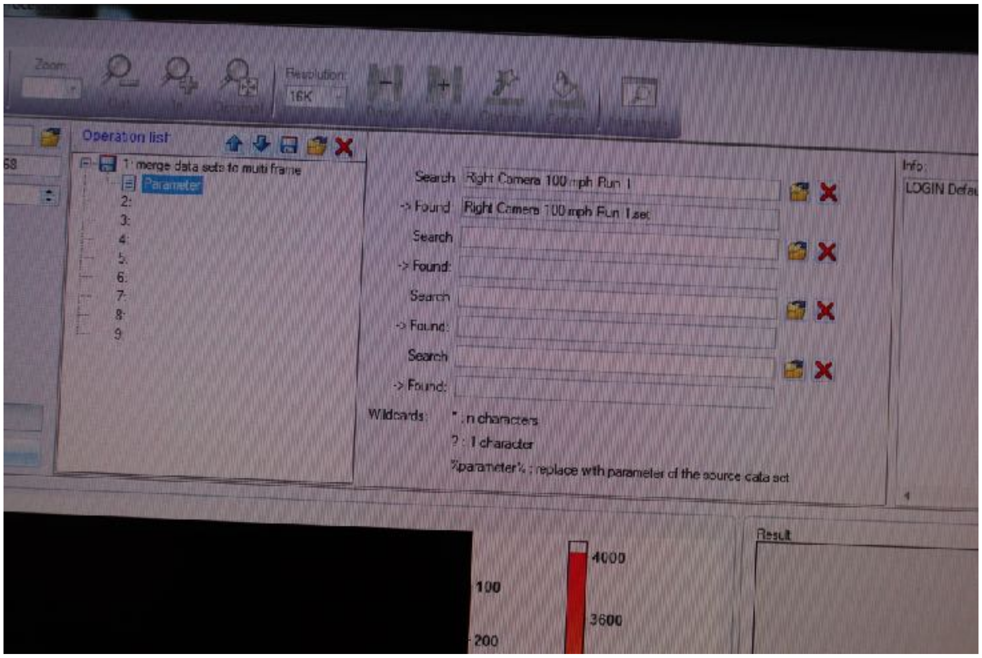

1: merge data sets to multi frame
Parameter
2:
3:
4:
5:
6:
7:
8:
9:

Search: Right Camera 100 mph Run 1
-> Found: Right Camera 100 mph Run 1.set
Search:
-> Found:
Search:
-> Found:
Search:
-> Found:

Wildcards: * : n characters
? : 1 character
%parameter% : replace with parameter of the source data set

81.

Select start processing and allow DaVis to complete its processing.

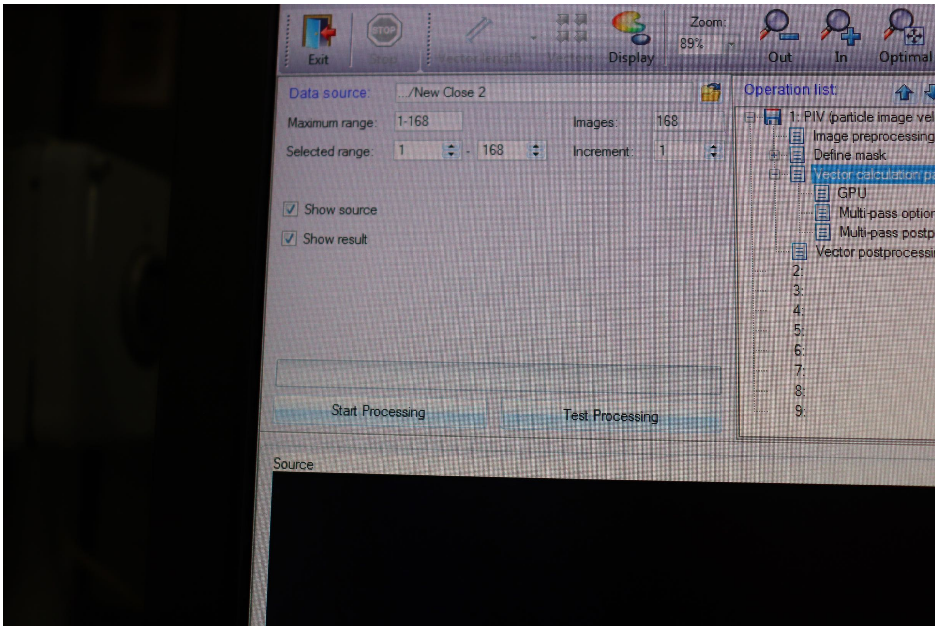

Data source: ../New Close 2
Maximum range: 1-168
Images: 168
Selected range: 1 - 168
Increment: 1
☑ Show source
☑ Show result

1: PIV (particle image vel
Image preprocessing
Define mask
Vector calculation pa
GPU
Multi-pass optior
Multi-pass postp
Vector postprocessi
2:
3:
4:
5:
6:
7:
8:
9:

82.

Once the exit icon in the top left corner becomes selectable, click exit to return to the project home screen.

83.

To process data, select the plus next to the left camera data set, select the newly produced merge datasets and click processing in the top toolbar. This will navigate you to the data processing screen for the merged data.

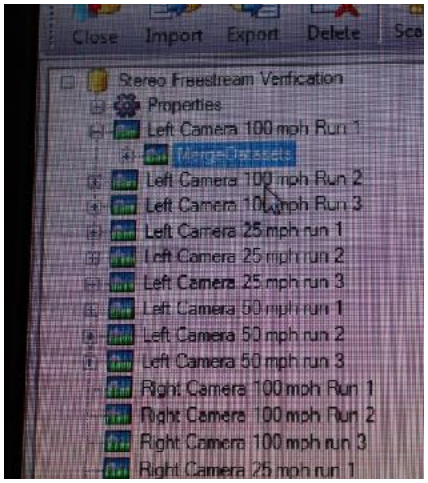

Stereo Freestream Verification
Properties
Left Camera 100 mph Run 1
MergeDatasets
Left Camera 100 mph Run 2
Left Camera 100 mph Run 3
Left Camera 25 mph run 1
Left Camera 25 mph run 2
Left Camera 25 mph run 3
Left Camera 50 mph run 1
Left Camera 50 mph run 2
Left Camera 50 mph run 3
Right Camera 100 mph Run 1
Right Camera 100 mph Run 2
Right Camera 100 mph run 3
Right Camera 25 mph run 1

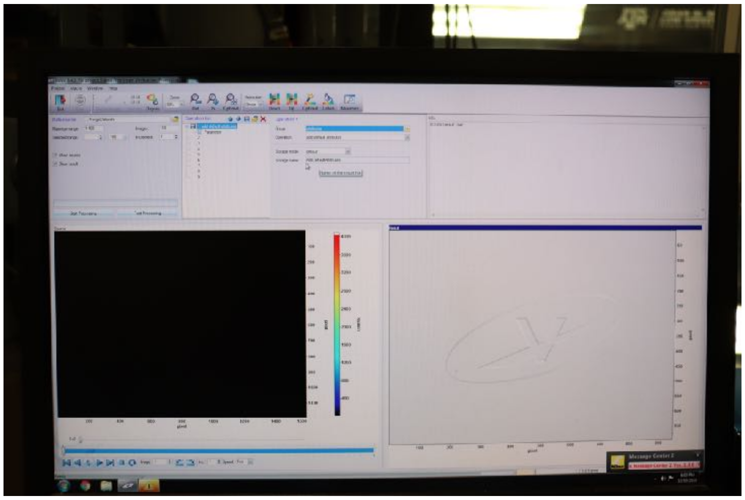

84.

To add a new processing step, clear the operation list with the red x in the upper right corner of the list, and then add a new operation. Under group, select attributes, and under operation select add default attributes. Storage mode and storage name should be left alone.

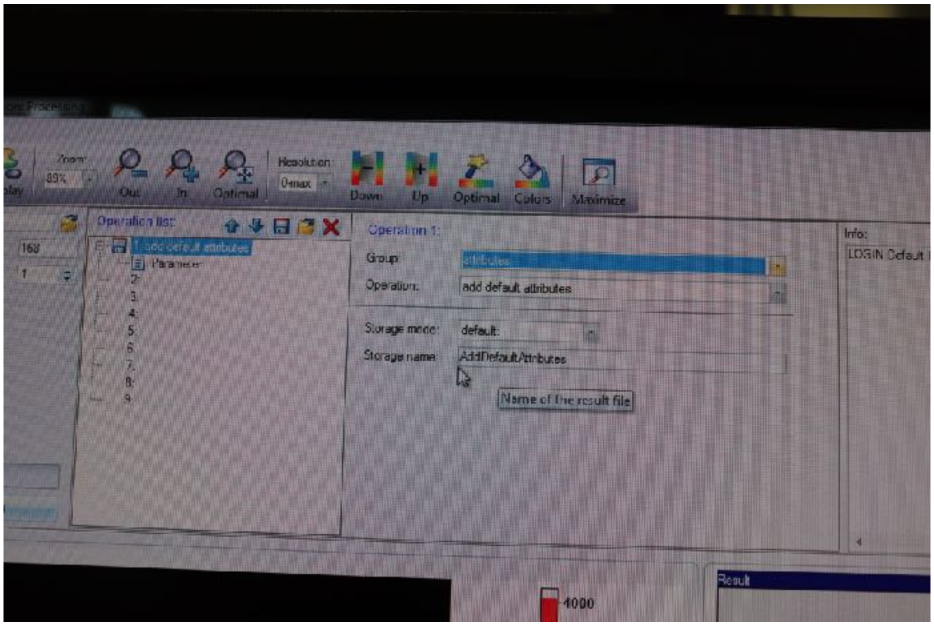

Operation 1:

Group: attributes

Operation: add default attributes

Storage mode: default:

Storage name: AddDefaultAttributes

Name of the result file

85.

Clicking the parameters option in the operation list brings up the ability to change data settings. Change the number of cameras to 2, change the 2. camera: to camera 2, and check the overwrite existing attributes box. If done properly, it should look like the following image:

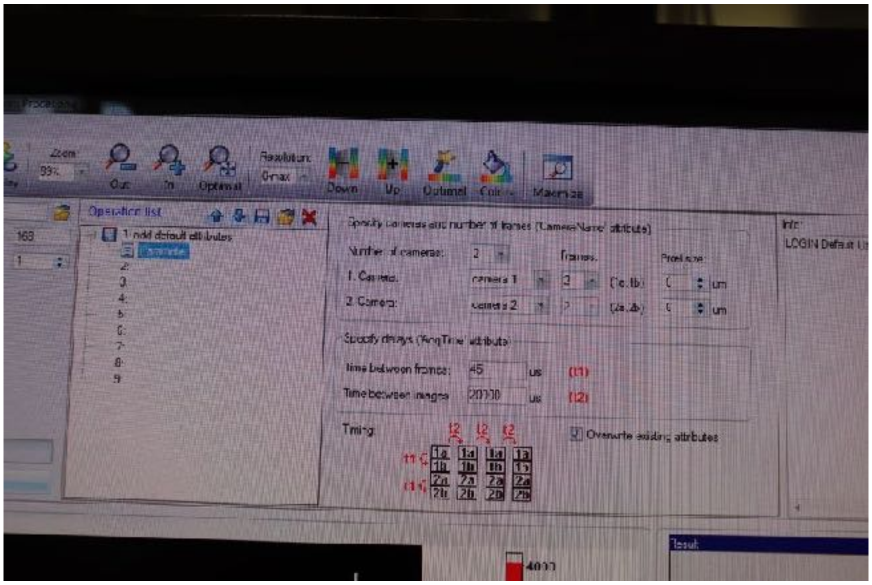

Specify cameras and number of frames ('CameraName' attribute)

Number of cameras: 2

		Frames:		Pixel size:
1. Camera:	camera 1	2	(1a,1b)	0 um
2. Camera:	camera 2	2	(2a,2b)	0 um

Specify delays ('AcqTime' attribute)

Time between frames: 45 us (t1)

Time between images: 20000 us (t2)

☑ Overwrite existing attributes

86.

Select start processing and allow DaVis to complete its processing.

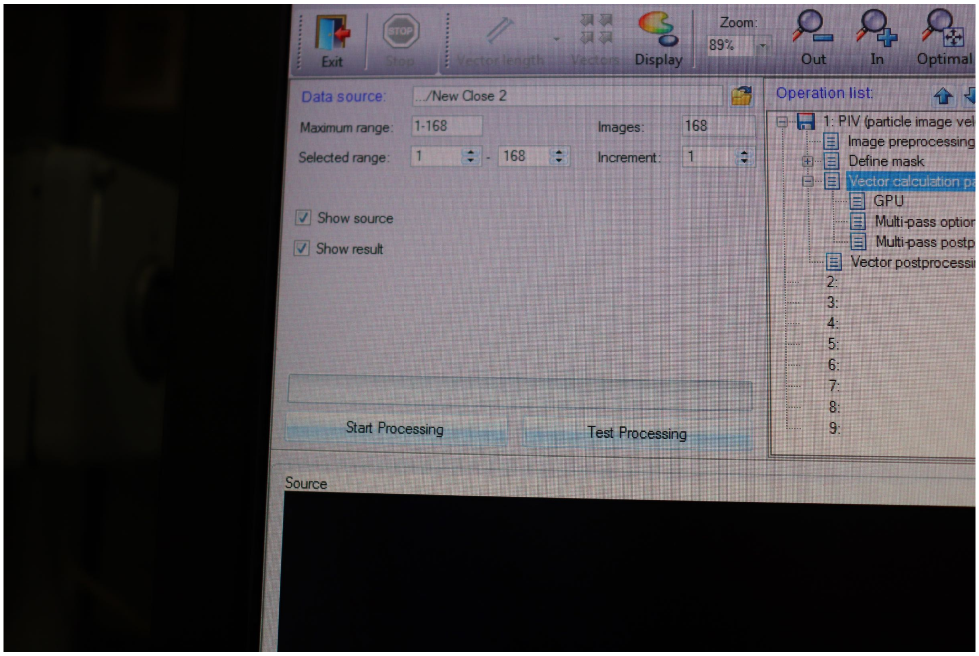

Data source: .../New Close 2

Maximum range: 1-168

Images: 168

Selected range: 1 - 168

Increment: 1

☑ Show source

☑ Show result

87.

Once the exit icon in the top left corner becomes selectable, click exit to return to the project home screen.

88.

To process data, select the plus next to the left camera data set, and the plus next to MergeDatasets, and select the newly produced AddDefaultAttributes. Next, click processing in the top toolbar. This will navigate you to the data processing screen for the merged data.

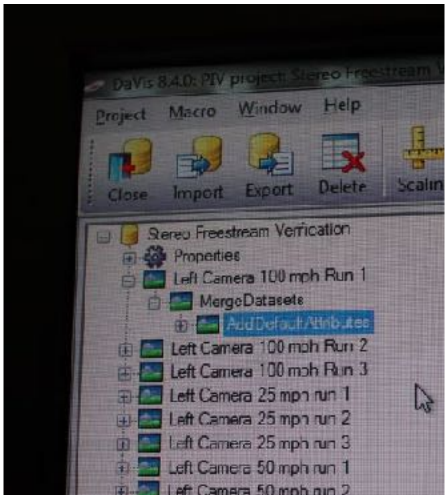

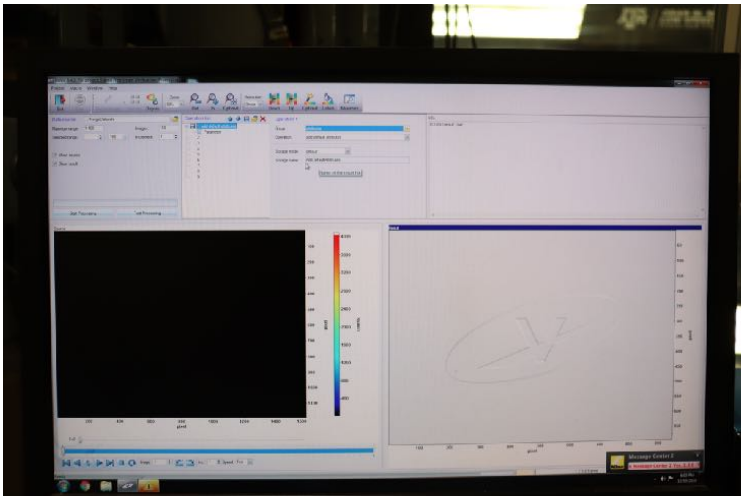

89.

To add a new processing step, clear the operation list with the red x in the upper right corner of the list, and then add a new operation. Under group, select Vector Calculation - Double Frames, and under operation select PIV (particle image velocimetry). Storage mode and storage name should be left alone.

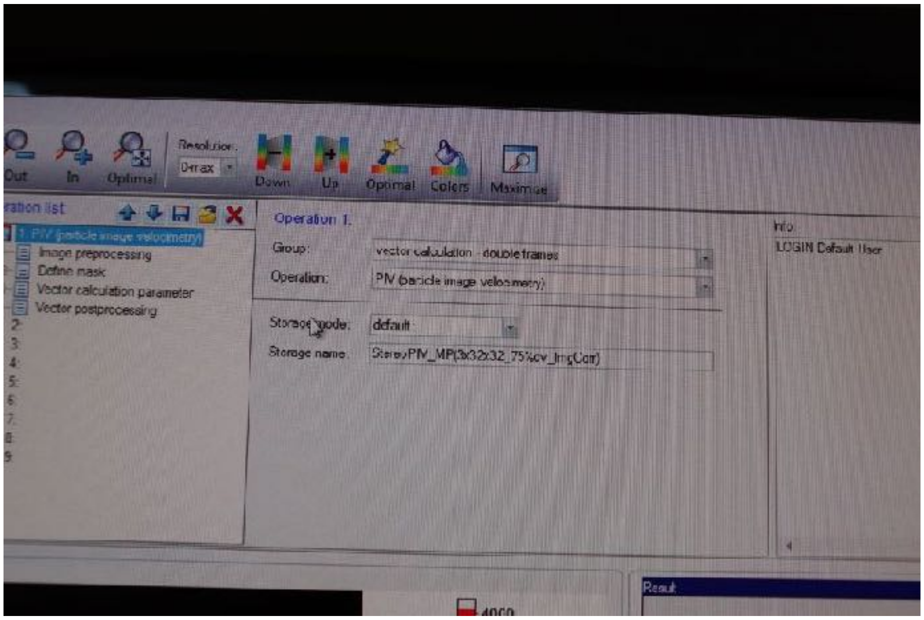

Operation 1.

Group: vector calculation - double frames

Operation: PIV (particle image velocimetry)

Storage mode: default

Storage name: StereoPIV_MP(3x32x32_75%ov_ImgCorr)

LOGIN Default User

90.

Select Vector calculation parameter in the operation list, and then click cross correlation. All other settings should be left in their defaults. You can verify that the settings match the image shown below:

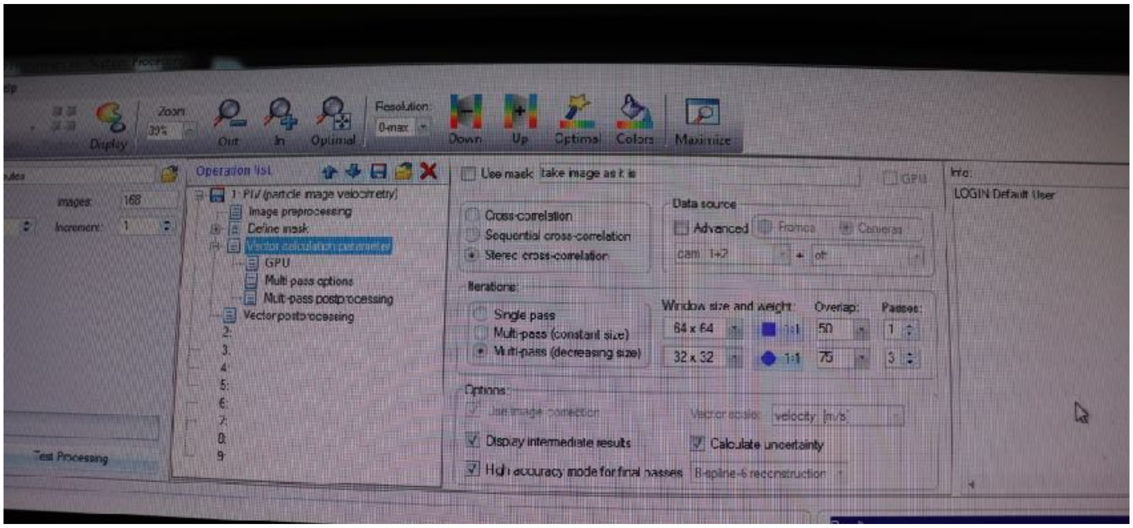

Images: 168

Increment: 1

Operation list:

- 1: PIV (particle image velocimetry)
  - Image preprocessing
  - Define mask
  - Vector calculation parameter
    - GPU
    - Multi-pass options
    - Multi-pass postprocessing
  - Vector postprocessing
- 2:
- 3:
- 4:
- 5:
- 6:
- 7:
- 8:
- 9:

☐ Use mask: take image as it is

☐ GPU

Info: LOGIN Default User

○ Cross-correlation
○ Sequential cross-correlation
● Stereo cross-correlation

Data source: ☐ Advanced ○ Frames ● Cameras
cam 1+2 + of

Iterations:

○ Single pass
○ Multi-pass (constant size)
● Multi-pass (decreasing size)

Window size and weight		Overlap:	Passes:
64 x 64	■ 1:1	50	1
32 x 32	● 1:1	75	3

Options:

☑ Use image correction

Vector scale: velocity [m/s]

☑ Display intermediate results

☑ Calculate uncertainty

☑ High accuracy mode for final passes: B-spline-6 reconstruction

91.

Select test processing and allow DaVis to process the first image pair. The results will show up in the results box on the lower right side of the screen. Once this is complete, verify the flow directions and values are reasonable by using the relevant vector filters under the vector length option in the upper toolbar. The test processing button can be seen in the lower portion of the image below, and the vector length selection can be seen greyed out in the top center of the image below.

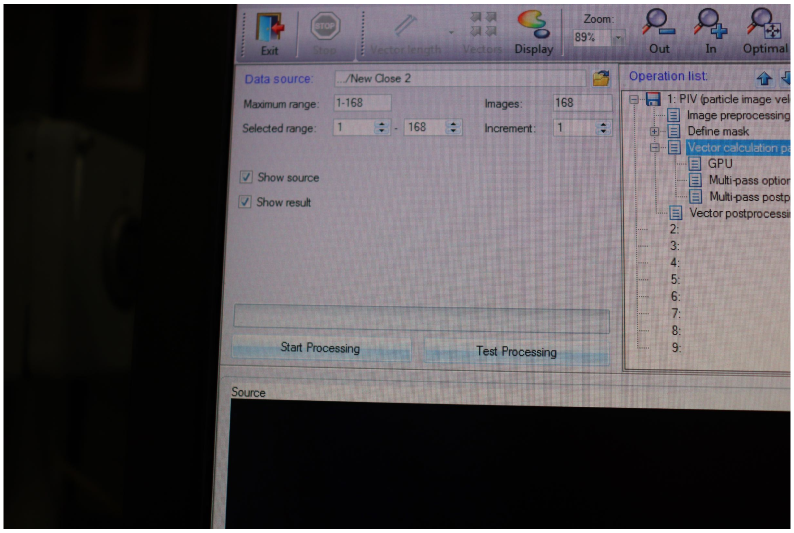

Data source: .../New Close 2

Maximum range: 1-168

Images: 168

Selected range: 1 - 168

Increment: 1

☑ Show source

☑ Show result

Operation list:

- 1: PIV (particle image vel
  - Image preprocessing
  - Define mask
  - Vector calculation pa
    - GPU
    - Multi-pass optior
    - Multi-pass postp
  - Vector postprocessi
- 2:
- 3:
- 4:
- 5:
- 6:
- 7:
- 8:
- 9:

92.

Repeat steps 56-59 as many times as necessary to capture all requested data for the test. Depending on the customer, you may want to capture multiple datasets at each point, this is something that is by no means required, and only affects the amount of data that is taken.

93.

Once all data has been captured for a given run, shut down the tunnel.

94.

Press stop on the quantum composer to stop the laser pulses in the tunnel. This is imperative before removing safety glasses or turning off the laser warning light.

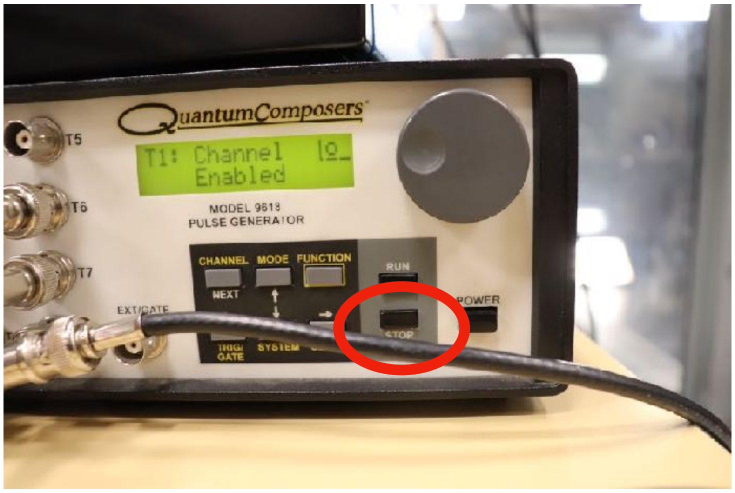

95.

To process all data for a specified point, follow steps 62-91, but select Start processing instead of test processing to batch process all the image pairs for that run.

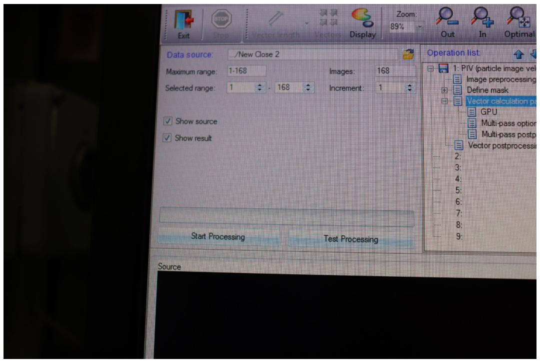

Data source: .../New Close 2
Maximum range: 1-168
Images: 168
Selected range: 1 - 168
Increment: 1
☑ Show source
☑ Show result